STATIONARY WAVE AMPLITUDES IN ROTATING DISCS

BY

AYODELE OLAMIGOKE

A DISSERTATION PRESENTED FOR

THE DEGREE OF DOCTOR OF PHILOSOPHY

DEPARTMENT OF MECHANICAL ENGINEERING

UNIVERSITY OF SHEFFIELD

MARCH, 1981

ACKNOWLEDGMENT

The author sincerely thanks Professor D. S. Dugdale for inspiring and guiding the progress of this investigation.

Many thanks are also due to his wife Bukie for her constant support.

To God be the glory for great things he has done.

SUMMARY

This research was carried out to evaluate the stationary wave amplitudes that can occur in fast spinning centrally-clamped discs, and to investigate the effect of frequency separation "between principal orthogonal modes on the wave amplitudes. The wave amplitudes were determined for the modes with two and three nodal diameters. The methods used in generating the frequency splitting are (i) the clamping of a disc at a number of positions, and (ii) the use of discs with diametrically opposite holes. The work involved both experimental and theoretical analyses.

The experimental work included the determining of the natural frequencies of the discs, of the wave response frequencies of the discs at different rotational speeds, of the damping values, of the stationary wave amplitudes due to constant values of applied transverse force, and of wave amplitudes in discs with known amounts of frequency separation. The theoretical work included evaluating values corresponding to the experimental results, the determining of the mode shapes and the membrane stresses in the vibrating discs. The calculations were computerised as far as possible.

Comparison of the response frequencies determined by using the different theoretical methods showed that disc mode shape is not significantly affected by the rotational speed or by vibration amplitude. The in-plane membrane stresses, which are important in determining the effects of internal stresses and of vibration amplitude, consist of the axisymmetric and harmonic components. The harmonic stresses were found to be less significant than the axisymmetric membrane stresses.

Stationary waves amplitudes were found to be greater at the smaller clamping ratios and for the lower modes of vibration. Higher side-rubbing forces, equivalent to applying higher transverse forces, are also possible in rotating discs at the smaller clamping ratios, because of the longer arc of cutting.

Small values of frequency separation, less than 2 percent., did not significantly affect the stationary wave amplitudes. Higher values of frequency separation led to reasonable reduction in the wave amplitudes.

To obtain reliable experimental values of natural frequencies, a suitable furnace was built and residual stresses in the discs were reduced by heat treatment. The stress-relieving led to closer agreement between the experimental and theoretical values.

CONTENTS

1. INTRODUCTION 1

1. Literature Survey 1
2. Vibration in Circular Saw Processes 7
3. Work done 15

2. THEORETICAL ANALYSIS 22

1. Equations of Plate Vibration 22
2. Energy Methods 37
3. Internal Stresses 46
4. Nonlinear Vibrations 55
5. Stationary Waves 74
6. Side-rubbing in Circular Saws 83

3. EXPERIMENTAL METHODS 84

1. Disc Specimens 84
2. Stress Relieving 86
3. Natural Frequencies 88
4. Travelling Waves 90
5. Damping Values 92
6. Stiffness Coefficient 93
7. Stationary Wave Amplitudes 94

4. RESULTS 99

1. Membrane Stresses 100
2. Energy Constants 101
3. Natural Frequencies 102
4. Mode Shapes 102
5. Compliance Coefficients 103
6. Nonlinearity Ratio 104
7. Damping 104
8. Frequency Separation 105
9. Standing Wave Amplitudes 106
10. Pulsating Wave Amplitudes 107

5. DISCUSSIONS AND CONCLUSIONS 108

1. Membrane Stresses 108
2. Internal Stresses 111
3. Natural Frequencies 112
4. Wave Frequencies 114
5. Frequency Separation 115
6. Damping Values 117
7. Standing Wave Amplitudes 119
8. Pulsating Waves 121
9. Summary 124

LIST OF SYMBOLS

a - outside radius of disc

b - clamping radius of disc

c - central hole radius of disc

e - strain

f - frequency

h - thickness

m - number of nodal circles

n - number of nodal diameters

p - frequency of forcing function

r - radius

$\bar{r}$ - radius ratio, $\frac{r}{a}$

s - percentage frequency separation

t - time

u_b - bending energy constant

u_i - interaction energy constant

u_k - kinetic energy constant

u_m - membrane energy constant

w - transverse component of displacement

$\dot{w}$ - velocity of transverse displacement, $\frac{\partial w}{\partial t}$

$\bar{w}$ - rim transverse displacement amplitude

D - flexural rigidity, $\frac{Eh^3}{12(1-\nu^2)}$

E - Young's modulus

F - stress function

N - membrane force per unit length

N' - axisymmetric component of membrane force/length

N" - harmonic component of membrane force/length

$\overline{N}$ - nondimensional membrane force/length, $\frac{Na^2}{Eh\overline{w}^2}$

$\hat{N}$ - total in-plane force/length

N_r - radial membrane force/length

N_θ - tangential membrane force/length

$N_{r\theta}$ - shear membrane force/length

P - applied force

R - radial displacement function

T - kinetic energy

U - strain energy

α - clamping radius ratio, $\frac{b}{a}$

γ - ratio of central hole radius to outside hole radius, $\frac{c}{a}$

ε - nonlinearity ratio

ζ - damping ratio

θ - angular position

λ - frequency ratio

ν - Poisson's ratio

ρ - material density

σ - stress

$\overline{\sigma}$ - in-plane stress

σ_r - radial stress

σ_θ - tangential stress

$\sigma_{r\theta}$ - shear stress

ϕ - phase angle

χ - frequency parameter, $\frac{\omega a^2}{h}\sqrt{\frac{12\rho(1-\nu^2)}{E}}$

ω - frequency

Ω - rotational speed

Ω_0 - speed parameter, $\frac{h}{a^2}\sqrt{\frac{E}{12\rho(1-\nu^2)}}$

$\overline{\Omega}$ - speed ratio, $\frac{\Omega}{\Omega_0}$

LIST OF TABLES

1. Response frequencies for different values of rim amplitudes

2. Natural frequencies of discs by the exact and the two energy methods

3. Natural frequencies of discs by the finite element method

4. Relative displacement, slope and curvature values in a freely-vibrating disc

5. Curvature values in discs

LIST OF FIGURES

1.1 Waves in a rotating disc

2.1 Response curves for large amplitude vibration

2.2 4-position clamping of a disc

2.3 A disc with 2 holes

2.4 Stationary waves in rotating discs

3.1 Stress-relieving furnace

3.2 Testing of a vibrating stationary disc

3.3 Frequency test rig for a stationary disc

3.4 A sand pattern for the mode n=2

3.5 A sand pattern in a disc with 2 holes

3.6 Frequency test rig for a rotating disc

3.7 Travelling wave frequencies

3.8 Calibration curve for the capacitive probe readings

3.9 Pattern of a decaying oscillation

3.10 Determining the point-load stiffness of a disc

3.11 Stationary wave rim displacement of a disc

4.1 Membrane forces/length for the mode n=0

4.2 Membrane forces/length for the mode n=1

4.3 Membrane forces/length for the mode n=2

4.4 Membrane forces/length for the mode n=3

4.5 Membrane forces/length for the mode n=4

4.6 Energy constants for the mode n=0

4.7 Energy constants for the mode n=1

4.8 Energy constants for the mode n=2

4.9 Energy constants for the mode n=3

4.10 Energy constants for the mode n=4

4.11 Curves for locating critical speeds

4.12 Frequency values for different clamping ratios

4.13 Values of modal compliance coefficients, c_n

4.14 Values of compliance coefficients, C

4.15 Values of nonlinearity ratio for the stationary disc

4.16 Decaying oscillation amplitudes in a stationary disc for the mode n=2

4.17 Decaying oscillation amplitudes in a stationary disc for the mode n=3

4.18 Frequencies in a disc clamped at 6 positions

4.19 Frequencies in a disc clamped at 4 positions

4.20 Frequencies in a disc clamped at 2 positions

4.21 Frequencies in a disc with 2 holes ($n=2, \alpha=0.226$)

4.22 Frequencies in a disc with 2 holes ($n=2, \alpha=0.339$)

4.23 Frequencies in a disc with 2 holes ($n=3, \alpha=0.226$)

4.24 Frequencies in a disc with 2 holes ($n=3, \alpha=0.339$)

4.25 Standing wave amplitudes in a disc ($\alpha=0.226$)

4.26 Standing wave amplitudes in a disc ($\alpha=0.339$)

4.27 Theoretical standing wave amplitudes (α=0.1)

4.28 Theoretical standing wave amplitudes (α=0.3)

4.29 Theoretical standing wave amplitudes (α=0.5)

4.30 Wave amplitudes and the envelope curve for the occurence of stationary waves

4.31 Maximum wave amplitudes in a disc for different values of percent. frequency separation

Chapter 1

INTRODUCTION

1.1 Literature Survey

1.1.1 Linear Vibrations

The earliest study of flexural motion of circular plates is probably that of Poisson(1). He based his investigation on the classical(Lagrange) theory of plates, obtaining the lower frequencies of the axially symmetric flexural motions of a circular disc with traction free boundary(2). Later, Kirchoff(3) gave the general solution of the free vibration equation(4) and calculated the natural frequencies and modes of vibration of an unconstrained uniform disc(5). Notable contributions were also made by Rayleigh(6). Southwell(7) gave a table of natural frequencies for centrally-clamped discs. A fuller table of frequencies for centrally-clamped flat discs was given by Vogel and Skinner(8). Natural frequencies were given by McLeod and Bishop(4) for plates restrained at the rim; they also compiled tables giving the boundary conditions, and the mode shapes for circular plates undergoing linear vibration. A number of approximate methods have been used to determine natural frequencies and mode shapes of vibrating circular plates. Most of the approximate methods, as used in references (7),(9),(10)

are based on energy principle. Recently, the finite element method has come to be used. It makes the analysis of plates, especially those with irregular boundaries, by numerical methods relatively easy.

1.1.2 Initial Stresses

Much of the early study of the vibration of rotating discs was considered by Lamb and Southwell(9) and Southwell(7). Southwell proposed, using the Rayleigh method, that the square of the lower limit frequency is equal to the sum of the squares of the separate frequencies of a plate in static flexure and a rotating membrane. More comprehensive studies of the effects of rotation in vibrating discs were conducted by Tobias and Arnold(11). Dugdale(12) discussed the methods by which frequencies of rotating discs could be determined. He(13) also examined the effect of rotation on the stiffness of the plate. Rotational stresses are in-plane stresses and the effects of other in-plane stresses have also to be studied. Dugdale(14), writing on the measurement of internal stress values, described methods for estimating the values of initial stresses present in the discs. Introduction of initial in-plane stresses in discs by hammering(tensioning) has been used for quite a long time to increase the stiffness and improve the flatness of the plate. Dugdale(15) gave a theoretical analysis of circular

saw tensioning. Mote(5) gave an analysis of the free vibration of initially stressed circular discs. In his analysis of centrally-clamped variable thickness discs, using the Rayleigh-Ritz technique, he found frequencies of transverse vibration of plates having rotational and thermal in-plane stresses, as well as induced initial stresses. Dugdale(16) had earlier carried out a study of the effect of internal stress on the flexural stiffness of discs. He gave an analysis of the effect of transverse loading and of initial stresses, introduced by hammering, on the stiffness of discs and got fair agreement between experimental and calculated values. Dugdale(17) later carried out a study of the flexure of thin discs having initial stresses introduced by rolling over a narrow annulus. The control of disc stability using thermal stresses has been studied by Mote. Mote(10,18,19) studied the effects of heat in discs, and also, using the finite element method(20), considered the transient and steady-state conduction of heat in rotating discs. Mote and Nieh(21) theoretically and experimentally investigated the relationship between the state of membrane stresses, critical rotation speed, and the frequency spectrum in radially symmetric discs. In a report(22), on the residual stresses and tensioning in discs, Szymani discussed the effects and measurements of residual stresses.

1.1.3 Nonlinear Vibration

The differential equations governing the nonlinear motion of plates, most often, have to be solved by approximate methods. There is a theory for large static deflection of plates due to Foppl, von Karman, and Timoshenko. To solve the problems of large deflections of plates, an estimate of the membrane stresses must be made(23). Way(24) solved the differential equations for static circular plates by substituting a power series into the equations and, using variational methods, determined the coefficients in the series. Berger(23), to decouple the differential equations, neglected the strain energy due to a second invariant of the middle surface strains. Dugdale and Squires(25) and Dugdale(17,26) gave methods for deriving values of membrane stresses in plates. Several writers(27,28,29) have used the Berger hypothesis in analysing nonlinear behaviour of plates. Tobias(30) analysed the nonlinear vibrations of imperfect discs. He derived the equations of motion by substituting the strain and kinetic energies of the plate into the Lagrange equation.

1.1.4 Forced Vibration

Forced vibration very often yields nonlinear behaviour in the plates being excited. Reisman(31) considered the forced vibration of a clamped plate. He employed a 'singularity solution' in conjuction with the classical theory and found cross receptances for arbitrarily placed exciting force. McLeod and Bishop(4) gave a theoretical analysis of the forced vibration of circular plates, giving tables of values for receptances of circular plates under various forms of excitation. These methods are an extension of the statically-loaded plate based on the linear vibration analysis of plates. Dugdale(26) extended the approach of Tobias(30), i.e. applying Lagrange equations, to consider the forced vibration of imperfect discs. Tobias and Arnold(11) presented a study of the forced vibration of circular plates in linear and nonlinear zones.

1.1.5 Stationary Waves

The formation of stationary waves is a dreaded phenomenon in circular saw operation. The great danger about these waves is that they can be excited by time-constant stationary force. The linear theory suggests that stationary waves are excitable only at the critical speeds for a plate; however, experiment shows, and the nonlinear theory confirms, that these waves can be maintained over a

wide speed range depending on the magnitude of the applied force and the characteristics of the plate(11,26). A stationary wave is the reverse travelling wave component in a disc rotating beyond its minimum critical speed. Dugdale(32) gave a method for finding the speeds of circular saw rotation at which self excitation of the travelling waves occur.

The practice is often to try and increase the disc stiffness, and therefore the critical speeds, and work with disc speeds well below the minimum critical speed. Methods such as tensioning, thermal control(21), feedback control(33) using externally applied electromagnetic forces can be used to increase the disc stiffness.

The effect of disc imperfection on the natural frequencies and vibration modes as indicated by Tobias and Arnold(11) was first published by Zenneck(34). He pointed out how frequency separation could be caused between two principal orthogonal modes of vibration by having certain configurations of disc imperfection. Tobias and Arnold(11) recognised that disc imperfections have some effect on the magnitude and behaviour of stationary waves. They described the phenomenon of large amplitude stationary waves and stated that the magnitude of disc vibration is reduced by the introduction of imperfection. Their experiments show that the stationary wave amplitude is

much smaller for the higher modes. Frequency separation between orthogonal modes is generated by imposing conditions which disturb the symmetry between the patterns of the two modes. Dugdale(35) examined the effect of geometrical variables on the natural frequencies of the saw disc. The generation of frequency separation between principal modes of vibration involves causing the plate to lose its symmetry. The analysis of such plates, therefore, requires numerical computation, as the usual governing equations become impossible to solve. The finite element method has emerged as an invaluable method in this respect. This method has been used by Mote(36) in the study of rotating discs, having holes and slots, and subjected to in-plane temperature variation.

1.2 Vibration in Circular Saw Processes

Circular saws are usually made of flat thin plates of steel with cutting teeth round the outside edge. The saws are made from alloy steel ingots. The ingots are heated in a furnace, hammered or cog-rolled to slabs, and cross-rolled to plates. They are then sheared to size and put through a flattening process. The blanks are toothed and the centre and pin holes bored out. The steel is then hardened and tempered. The saw is partially tensioned and the surface ground. Final tension is put in by hammering or rolling and the centre hole is reamed to size. The

teeth are then sharpened and set(37).

A circular saw, when used for cutting, is firmly bolted to the rotating spindle while it is held between a pair of centrally located circular clamping discs(flanges). The clamping discs are many times thicker than the saw and are held together very tightly against the saw in order to maintain high saw stiffness. The inside surface of a clamping disc is usually recessed, leaving an outside annulus for effective clamping. The width of the clamping annulus on the disc is made small in order to give high clamping pressure but large enough to prevent rotation of the saw plate at the clamped surface. The ratio of the clamping disc diameter to that of the saw is termed the clamping ratio. Values of clamping ratio are required to be small in order to provide a considerable depth of cut. The clamping ratio, however, needs to be large enough to ensure an appreciable stiffness in the saw.

The thickness of the saw depends on the material being cut, the diameter of the saw, the running speed of the saw and the accuracy of the cut required. If power depends on volume rate of removal of material, a thin saw will require less power for the same area rate of sawing. It also wastes less material. However, a thin saw has less transverse stiffness and can be more easily deflected.

Such bending of a saw leads to poor cutting and could result in the damage of the saw in the case of excessive bending. There are some circular saws with non-uniform thickness along a radius. The thickness usually tapers down from the clamping edge to the free outside edge. This is to ensure reasonable saw stiffness while keeping down kerf waste and cutting power requirement. Such saws would more readily suffer from side-rubbing because of the reduced clearance at the thicker part of the saws. The manufacture of 'taper' saws is more complicated than that of flat saws.

Another important parameter in saw cutting operation is the speed of rotation of the circular plate. The running speed of the saw depends on the mechanical properties of the material being cut, the thickness of the material or the depth of cut, and the dimensions of the circular saw. The rotation of a circular plate induces tensile stresses in the plate, which add to the stiffness of the plate. The natural frequencies would therefore be increased as shown in equation (1.1)

$$\omega'^2 = \omega^2 + a'\Omega^2 \qquad (1.1)$$

where ω' is the speed corrected frequency,

ω is the frequency of the stationary disc,

Ω is the rotational speed,

a' is a vibration mode constant.

The rotation of the plate, however, sets up travelling waves. Each mode of vibration sets up two travelling waves, forward and reverse waves. Exciting a rotating plate at a frequency equal to the speed of a travelling wave also excites the wave component for that mode of vibration. When the speed of the reverse travelling wave is zero, a stationary wave would be set up. That steady state vibration motion can be caused by a small stationary force means, by the linear theory, that the stiffness of the plate is zero when a stationary wave is formed. This is not strictly true when finite deflections are considered when the behaviour of the plate ceases to be linear and becomes nonlinear.

1.2.1 Materials, Speeds and Feeds

Circular saws are used for cutting materials ranging from wood to steel, and diameters range from 100mm to 3000mm. The resistance to cutting of wood materials is relatively low, and we find rim speeds up to 4000m/min and in-feed rates up to 80m/min. Saws used for cutting metal often have tungsten carbide teeth. They also have much lower rim speeds and lower feed rates, e.g. 100m/min and 0.5m/min for cutting steel. Non-ferrous metals require rim speeds intermediate between those for steel and wood.

However, friction saws for cutting light sections often run at high rim speeds, around 7000m/min.

1.2.2 Saw Dimensions

The thickness of a saw very much depends on the diameter of the saw. The thickness of wood-saws is usually below 3mm and could be as small as 1mm for plates with diameters less than 200mm. The ratio of thickness to diameter is usually slightly higher for steel cutting saws than for wood cutting saws. Values of clamping ratio usually encountered range from 0.2 to about 0.4. for sawing wood, about 0.3 for the cutting of non-ferrous metals, and about 0.35 for sawing steel.

1.2.3 Vibration at Initial Engagement

At initial contact of the saw teeth with material being cut, transient vibration of saw plate occurs. This vibration causes a widening of cut and a roughening of the edge of the material being cut . It could also alter the line of cut if the component workpiece is not tightly clamped. The impact and the resulting vibration could have adverse effects on the bearings of the rotating shaft. This form of vibration persists until more than one tooth is engaged on the arc of cutting. The severity of the vibration depends on the feed rate, the tooth pitch, the mechanical properties of the material being cut, the tooth thickness, and the diameter of the saw.

1.2.4 Self-excited Vibrations

Self-excited vibration is autonomous, drawing its energy from an external source by its own periodic motion. Such vibration in circular plates, is commonly generated by the rotation of a plate against static deflection. The vibration could, therefore, be classified as displacement excitation vibration. Displacement under a static force is moved round the plate due to the rotation of a plate. The excitation may be represented by a Fourier series of the rotational speed and its harmonics. Response to such excitation could become significant when one of the speeds of the travelling waves possible in the plate coincides with the rotational speed or one of its harmonics. The effect of such self-excited vibrations depends on the damping present and the mode of vibration excited, the harmonic of the speed causing resonance and the displacement generating the excitation.

1.2.5 Stationary Waves

When a rotating circular plate vibrates in resonance, the motion excited can be detected as two travelling waves, a forward and a reverse travelling wave, the forward wave travelling in the direction of rotation of the plate and the reverse wave travelling in the direction opposed to rotation. When the speed of the reverse wave, relative to a stationary observer, is zero, a stationary

wave exists.

A mode of vibration can usually be excited by applying a forcing function whose frequency is equal to the speed of either of the travelling waves for that mode. Consequently, a constant force can excite a stationary wave if the circular plate is spinning at the critical speed for the formation of a stationary wave for the mode excited.

Stationary waves are particularly undesirable in circular saw cutting processes because they are excitable by time-constant force functions. Such forces are always present in cutting processes. The vibration amplitude generated can be very considerable, especially for modes of vibration with smaller numbers of nodal diameters. Such vibration could easily cause damage to the saws. Circular saws, therefore, run at speeds away from the critical speeds; that is, at speeds lower than the minimum critical speed.

1.2.6 Noise

Rotating discs, even when not cutting, may generate noise. The noise generated increases with increasing rim speed. Much of the noise produced is caused by the teeth on the saws: and the number, size, shape, and arrangement of the teeth do play an important role in the noise caused during rotation. During saw cutting operation, further

noise is produced by the cutting action of the teeth, and may be emitted by the saw disc or by the workpiece or the machine structure.

1.2.7 Thermal Effects

Much of the energy required during a cutting process is dissipated as heat. Heat is absorbed by the cutting teeth and conducted radially inwards toward the spindle, and is simultaneously removed by a radial flow of air. The steady-state temperature distribution depends on the material being cut, the size of the saw, the number and shape of the cutting tooth, the speed of the saw, and the feedrate.

The heating of a saw rim produces compressive stresses at the outside edge of the saw. Such compressive stresses lower the stiffness of the saw. Tensile hoop stresses are therefore introduced at the rim of a circular saw, a process termed tensioning, before they are used for cutting, in order to counteract the effect of the compressive thermal stresses that develop during cutting. A further motive for arranging that rim stresses are tensile and not compressive is that this helps to keep the blade flat during manufacturing processes.

1.3 Work done

This work is primarily the study of the effect of time-constant transverse forces on the vibration of rotating thin discs. The work is particularly concerned with plate problems as they exist in circular saws and circular saw operation.

The research has been carried out as a combination of experimental tests and theoretical analyses. In most cases, observed results are compared with expected results derived from the relevant theory. These analyses are usually based on some specific assumptions; and these assumptions should correspond with conditions that exist in the plate being tested, for the results from both to be comparable.

1.3.1 Stress Relieving

Often, an indeterminate distribution of initial stress is present which significantly affects the dynamic properties of a plate, especially in very thin plates. This makes the comparison of experimental and theoretical values difficult. Stress-relieving of plates was carried out by heat-treatment. A furnace, specially built for this purpose, was used to heat plates to a stress-relieving temperature, and the plates were then slowly and evenly cooled.

1.3.2 Frequencies and Mode Shapes

The dynamic analysis of an elastic body requires the determination of the natural frequencies of the body. Natural frequencies of the plates used, centrally-clamped discs, were determined by exciting each plate at the rim. The natural frequencies were determined for modes of vibration that are most often met with in circular saw operation. These frequencies were determined by exciting the plate using either a small vibrator or an electromagnet connected to an oscillator. The amplitude was kept small so as to approximate linear vibration. The occurrence of a resonance was determined by the movement of the sand particles spread on the plate during excitation of the plate. The sand pattern formed identifies the mode shape.

Theoretical calculations were made for values of natural frequency using various methods. These include the exact method and various energy methods, such as a modified Rayleigh method, the Rayleigh-Ritz method, the finite element method. The values derived by these methods are compared with one another and are also compared with the experimental values. The use of these methods required the development of the relevant theories that the methods are based upon. The computation of the results by these methods was carried out with the aid of digital computing;

although, in some cases, results of fair accuracy could be attained by longhand calculation. The results of these calculations, as with other calculations, are given as dimensionless parameters.

1.3.3 In-plane Stresses

Theoretical analyses, concerning the effect of internal stresses, are given. The forms of internal stresses considered are the types resulting from symmetric loading of the plates. The internal stresses are rotational, temperature, and rolling stresses. The analyses are used to show the effects of these stresses on the frequency response of the plate. Membrane stresses, which are stresses resulting from nonlinear bending of thin plates, are also in-plane stresses. The stresses interact with internal stresses to give the interaction strain energy of the plate. The stresses also contribute the membrane strain energy of the plate, which is the energy quantity that accounts for the nonlinear effect in the plate. Expressions for membrane stresses are given, using approximate methods.

1.3.4 Damping Values

Experimental damping values for the plate material and plate assembly were found. The values were determined by getting the decay pattern of the plate vibration, on a storage oscilloscope, over reasonable periods of time. These tests were conducted for different clamping ratios, speeds, and for the relevant modes of plate vibration. Equivalent viscous damping ratio values were then found. The effects of clamping configuration and plate vibration amplitude, if any, on the damping values were also investigated.

1.3.5 Frequency Separation

Frequency separation between principal orthogonal modes of a plate vibrating with a particular mode shape can be effected by imposing conditions which cause dissimilarity between the mode shapes obtained in the plate. The greater the amount of dissimilarity between the principal mode shapes, the greater the amount of frequency separation. Two methods were used to generate frequency separation between the modes; cutting equally spaced holes with centres at the same radius, and clamping the plate at a number of equally spaced positions at a common clamping radius. Experimental and theoretical values of frequency separation values are given for the two methods.

1.3.6 Forced Vibration

Response curves, showing displacements against plate speed, were plotted. The values are derived from tests performed on plates rotating about and above the minimum critical speeds. The tests were repeated for plates with different clamping ratio values and for differing modes of vibration with two, three, and four modal diameters. The vibration response parameters being measured were those of the standing waves that could be excited, and maintained over certain speed ranges, by applying a constant force. The measurements taken were repeated for different values of applied lateral force. A theoretical analysis of the forced vibration problem of rotating discs is developed, using energy quantities previously determined in the Lagrange equation. Equivalent theoretical displacement curves are compared with the response curves determined from the experiments.

1.3.7 Suppression of Stationary Waves

The focus of the work done is the reduction of the effects of stationary waves in spinning discs. Deflection amplitudes of stationary waves in plates can be very high and the speed range over which the waves can be maintained is usually large, especially for standing waves corresponding to the modes with smaller number of nodal diameters. In a rotating, otherwise initial stresses-free

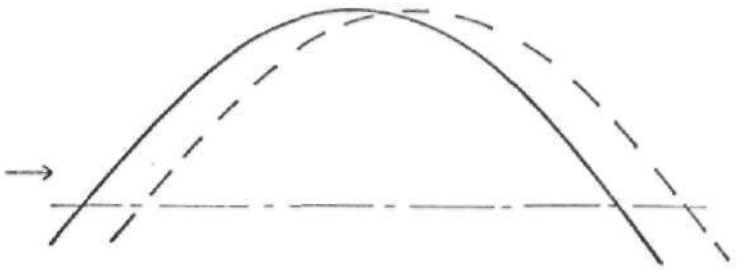
disc, stationary waves exist for number of nodal diameters from two upwards. For plate assemblies with clamping ratio under 0.5, wave amplitudes are much more considerable for modes with the smaller number of nodal diameters. Methods were therefore sought to reduce wave amplitudes, especially in the modes with two and three nodal diameters.

The method used in effecting the reduction in wave amplitudes is the introduction of frequency separation between orthogonal modes. A standing stationary wave is only possible in a disc without significant frequency separation but wave amplitudes could still be large even when there is appreciable frequency separation. When there is frequency separation, a pulsating stationary wave may exist. Fig. 1.1 shows sketches of a travelling wave, a standing stationary wave, and a pulsating stationary wave.

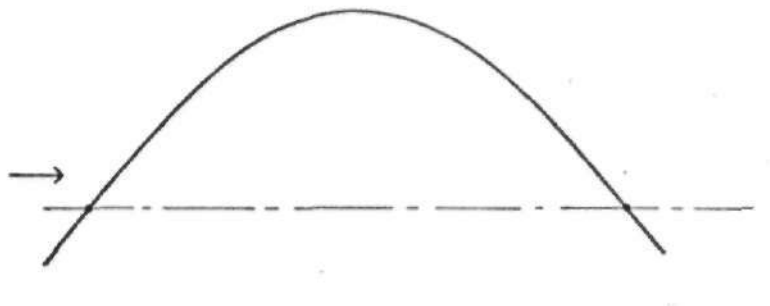
Tests were carried out to determine the wave amplitudes, and speed ranges over which large wave amplitudes were maintained using plate assemblies with known frequency separation values. These tests were performed using the two methods of generating frequency separation. Response curves are plotted showing maximum deflection values against plate speed for varying clamping ratios and for different values of force. Defining accepted levels of plate deflection, values of frequency

separation necessary to keep within such levels were determined for different values of applied force. Using an extension of the theory of forced vibration of plates without frequency separation, equivalents of the values got from the experiments were derived and compared with the experimental values. The analysis was used to give more specific relationships between frequency separation and vibration response values.

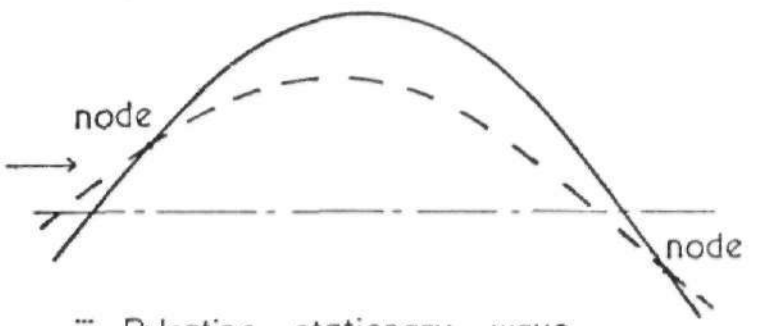
A description of waves in rotating discs is given in appendix IV.



i. Travelling wave



ii. Standing stationary wave



iii. Pulsating stationary wave

Fig. 1.1 WAVES IN A ROTATING DISC.

Chapter 2

THEORETICAL ANALYSIS

2.1 Equations of Plate Vibration

2.1.1 Elasticity Equations

In a plate, the thickness is small compared to the dimensions of the "faces". The plane, normally, between the faces is termed the "middle-surface" of the plate. The following analysis is carried out with the middle-surface lying in the x-y plane of the fixed rectangular coordinates (x,y,z).

The displacement of an arbitrary point (x,y,z) in the plate is represented by (u,v,w) and the displacement of a point on the middle-surface (x,y,0) is given by $(\bar{u},\bar{v},\bar{w})$. Similarly the components of strain at (x,y,z) are denoted by $(e_{xx},e_{yy},....,e_{xy})$ and those at (x,y,0) are denoted by $(\bar{e}_{xx},\bar{e}_{yy},.....,\bar{e}_{xy})$.

Strain-displacement Relations

When an elastic body is deformed, the following are the relations between the strains and the displacements(38).

$$e_{xx} = \frac{\partial u}{\partial x} + \frac{1}{2}[(\frac{\partial u}{\partial x})^2 + (\frac{\partial v}{\partial x})^2 + (\frac{\partial w}{\partial x})^2] \quad (2.1a)$$

$$e_{yy} = \frac{\partial v}{\partial y} + \frac{1}{2}[(\frac{\partial u}{\partial y})^2 + (\frac{\partial v}{\partial y})^2 + (\frac{\partial w}{\partial y})^2] \quad (2.1b)$$

$$e_{zz} = \frac{\partial w}{\partial z} + \frac{1}{2}[(\frac{\partial u}{\partial z})^2 + (\frac{\partial v}{\partial z})^2 + (\frac{\partial w}{\partial z})^2] \quad (2.1c)$$

$$e_{zy} = \frac{1}{2}(\frac{\partial w}{\partial y} + \frac{\partial v}{\partial z} + \frac{\partial u \partial u}{\partial y \partial z} + \frac{\partial v \partial v}{\partial y \partial z} + \frac{\partial w \partial w}{\partial y \partial z}) \quad (2.1d)$$

$$e_{xz} = \frac{1}{2}(\frac{\partial u}{\partial z} + \frac{\partial w}{\partial x} + \frac{\partial u \partial u}{\partial z \partial x} + \frac{\partial v \partial v}{\partial z \partial x} + \frac{\partial w \partial w}{\partial z \partial y}) \quad (2.1e)$$

$$e_{yx} = \frac{1}{2}(\frac{\partial v}{\partial x} + \frac{\partial u}{\partial y} + \frac{\partial u \partial u}{\partial y \partial x} + \frac{\partial v \partial v}{\partial y \partial x} + \frac{\partial w \partial w}{\partial y \partial x}) \quad (2.1f)$$

It is characteristic of thin plates that transverse deflection w may be of a larger order of magnitude than the in-plane displacements u and v. This means that in these plates, the strain term w^2 may not be negligible, and may be of the same order of magnitude as u or v. Therefore, quadratic terms $(\frac{\partial w}{\partial x})^2$, $(\frac{\partial w}{\partial y})^2$, $\frac{\partial w \partial w}{\partial x \partial y}$ are retained in equations 2.1 while the other quadratic terms are discarded. The following assumptions, though not compatible with the stress-strain relations for a general three-dimensional body are reasonable in the analysis of of the transverse vibration of thin plates.

$$e_{yz} = 0; \; e_{zx} = 0; \; e_{zz} = 0 \quad (2.2)$$

The relations of equation 2.2 signify that lines normal to the middle surface remain straight and normal to the surface under the deformation(39). The assumptions also

yield the following;

$$u = \bar{u} - z\frac{\partial w}{\partial x}; \quad v = \bar{v} - z\frac{\partial w}{\partial y}; \quad w = \bar{w} \tag{2.3}$$

$$\begin{aligned} \text{and } e_{xx} &= \bar{e}_{xx} - z\frac{\partial^2 w}{\partial x^2}; \\ e_{yy} &= \bar{e}_{yy} - z\frac{\partial^2 w}{\partial y^2}; \\ e_{xy} &= \bar{e}_{xy} - z\frac{\partial^2 w}{\partial x \partial y}; \end{aligned} \tag{2.4}$$

$$\begin{aligned} \text{where } \bar{e}_{xx} &= \frac{\partial \bar{u}}{\partial x} + \frac{1}{2}\left(\frac{\partial w}{\partial x}\right)^2, \\ \bar{e}_{yy} &= \frac{\partial \bar{v}}{\partial y} + \frac{1}{2}\left(\frac{\partial w}{\partial y}\right)^2, \\ \bar{e}_{xy} &= \frac{1}{2}\left(\frac{\partial \bar{v}}{\partial x} + \frac{\partial \bar{u}}{\partial y} + \frac{\partial w}{\partial x}\frac{\partial w}{\partial y}\right). \end{aligned} \tag{2.5}$$

Stress-strain Relations

In isotropic, linearly elastic plates, the stress-strain relations can be approximated by the following relations, which are for a state of plane stress.

$$\begin{aligned} (\sigma_{xx} + \bar{\sigma}_{x0}) &= \frac{E}{1-\nu^2}(e_{xx} + \nu e_{yy}) \\ (\sigma_{yy} + \bar{\sigma}_{y0}) &= \frac{E}{1-\nu^2}(e_{yy} + \nu e_{xx}) \\ (\sigma_{xy} + \bar{\sigma}_{xy0}) &= \frac{E}{1+\nu} \cdot e_{xy} \end{aligned} \tag{2.6}$$

where E is the Young's modulus,

ν is the Poisson's ratio,

$\bar{\sigma}_{x0}$, $\bar{\sigma}_{y0}$, $\bar{\sigma}_{xy0}$ are internal stresses.

2.1.2 Energy Equations

At any instant the energy of a vibrating conservative system is partly kinetic and partly potential. The potential energy, V, is the difference between the strain energy, U, in the system and the work W done on the system.

$$V = U - W \tag{2.7}$$

Strain Energy

In a thin plate, the strain energy density, U_δ , is as follows;

$$U_\delta = \frac{1}{2}\left[(\sigma_{xx} + \bar{\sigma}_{x0})e_{xx} + (\sigma_{yy} + \bar{\sigma}_{y0})e_{yy} + 2(\bar{\sigma}_{xy} + \bar{\sigma}_{xy0})e_{xy}\right] \tag{2.8}$$

This can be written as as follows;

$$U_\delta = \frac{E}{2(1-\nu^2)}\left[(e_{xx}+e_{yy})^2 - 2(1-\nu)(e_{xx}e_{yy}-e_{xy}^2)\right] + \left[\bar{\sigma}_{x0}e_{xx}+\bar{\sigma}_{y0}e_{yy}+2\bar{\sigma}_{xy0}e_{xy}\right] \tag{2.9}$$

The strain energy of the entire plate is

$$U = \int\int\int U_\delta . dzdxdy \tag{2.10}$$

When the relations in equation 2.4 and 2.9 are substituted into equation 2.10, the strain energy separates into the following;

$$U = U_b + U_m + U_i \tag{2.11}$$

where U_b is the bending energy,

U_m is the membrane energy,

and U_i is the interaction energy.

The result of the integration with respect to z is

$$U_b = \frac{E}{24(1-\nu^2)} \int\int h^3 \left[\left(\left(\frac{\partial^2 w}{\partial x^2} + \frac{\partial^2 w}{\partial y^2} \right)^2 - 2(1-\nu)\left[\frac{\partial^2 w}{\partial x^2} \cdot \frac{\partial^2 w}{\partial y^2} - \left(\frac{\partial^2 w}{\partial x \partial y} \right)^2 \right] dx dy \right] \right] \tag{2.12}$$

$$U_m = \frac{1}{2} \int\int \left[N_x \bar{e}_{xx} + N_y \bar{e}_{yy} + 2N_{xy} \bar{e}_{xy} \right] dx dy \tag{2.13}$$

$$U_i = \int\int h \left[\bar{\sigma}_{x0} \bar{e}_{xx} + \bar{\sigma}_{y0} \bar{e}_{yy} + 2\bar{\sigma}_{xy0} \bar{e}_{xy} \right] dx dy \tag{2.14}$$

where the membrane forces per unit length, N, can be found from the following expressions.

$$\begin{aligned} N_x &= \frac{Eh}{1-\nu^2} \left[\bar{e}_{xx} + \nu \bar{e}_{yy} \right] \\ N_y &= \frac{Eh}{1-\nu^2} \left[\bar{e}_{yy} + \nu \bar{e}_{xx} \right] \\ N_{xy} &= \frac{Eh}{1+\nu} \cdot \bar{e}_{xy} \end{aligned} \tag{2.15}$$

It can be shown, by integration by parts, that the

expressions for U_m and U_i reduce to the forms given in equations 2.16 and 2.17(40).

$$U_m = \frac{1}{4}\int\int\left[N_x\left(\frac{\partial w}{\partial x}\right)^2 + N_y\left(\frac{\partial w}{\partial y}\right)^2 + 2N_{xy}\frac{\partial w}{\partial x}\frac{\partial w}{\partial y}\right]dxdy \qquad (2.16)$$

$$U_i = \frac{1}{2}\int\int h\left[\bar{\sigma}_{x0}\left(\frac{\partial w}{\partial x}\right)^2 + \bar{\sigma}_{y0}\left(\frac{\partial w}{\partial y}\right)^2 + 2\bar{\sigma}_{xy0}\frac{\partial w}{\partial x}\frac{\partial w}{\partial y}\right]dxdy \qquad (2.17)$$

Kinetic Energy

The kinetic energy, T, in vibrating plates is given as shown below.

$$T = \frac{\rho}{2}\int\int h\left(\frac{\partial w}{\partial t}\right)^2 dxdy \qquad (2.18)$$

where ρ is the plate density.

Hamiltonian Integral

The lagrangian of a system is defined as follows;

$$L = T - V \qquad (2.19)$$

The hamiltonian integral, I, is the integral of the lagrangian, L, within two arbitrary time intervals.

$$I = \int_{t_1}^{t_2} L.dt \tag{2.20}$$

The motion of a body would be such as to render the hamiltonian integral I an extremum(41).

Energy Equations in Polar Coordinates

Analysis of circular plates is more readily carried out using polar coordinates.

Strain energy: As earlier stated, the strain energy expression is as follows;

$$U = U_b + U_m + U_i \tag{2.11}$$

$$U_b = \frac{E}{24(1-\nu^2)} \int\int h^3 \left[(\nabla^2 w)^2 - 2(1-\nu)\left[\frac{\partial^2 w}{\partial r^2}\left(\frac{1}{r}\frac{\partial w}{\partial r} + \frac{1}{r^2}\frac{\partial^2 w}{\partial \theta^2}\right) - \left(\frac{\partial}{\partial r}\left(\frac{1}{r}\frac{\partial w}{\partial \theta}\right)\right)^2 \right] \right] .rdrd\theta \tag{2.21}$$

$$U_m = \frac{1}{4} \int\int \left[N_r \left(\frac{\partial w}{\partial r}\right)^2 + \frac{N_\theta}{r^2}\left(\frac{\partial w}{\partial \theta}\right)^2 + \frac{2N_{r\theta}}{r}\frac{\partial w}{\partial r}\frac{\partial w}{\partial \theta} \right] rdrd\theta \tag{2.22}$$

$$U_i = \frac{1}{2} \int\int h \left[\bar{\sigma}_{rO}\left(\frac{\partial w}{\partial r}\right)^2 + \frac{\bar{\sigma}_{\theta O}}{r^2}\left(\frac{\partial w}{\partial \theta}\right)^2 + 2\frac{\bar{\sigma}_{r\theta O}}{r}\frac{\partial w}{\partial r}\frac{\partial w}{\partial \theta} \right] rdrd\theta \tag{2.23}$$

$$\text{where } N_r = \frac{Eh}{1-\nu^2}\left[\bar{e}_{rr} + \nu\bar{e}_{\theta\theta}\right]$$
$$N_\theta = \frac{Eh}{1-\nu^2}\left[\bar{e}_{\theta\theta} + \nu\bar{e}_{rr}\right] \qquad (2.24)$$
$$N_{r\theta} = \frac{Eh}{1+\nu}.\bar{e}_{r\theta}$$

$$\text{and } \bar{e}_{rr} = u_r + \frac{1}{2}\left(\frac{\partial w}{\partial r}\right)^2$$
$$\bar{e}_{\theta\theta} = \frac{u}{r} + \frac{1}{r}\frac{\partial v}{\partial \theta} + \frac{1}{2r^2}\left(\frac{\partial w}{\partial \theta}\right)^2 \qquad (2.25)$$
$$\bar{e}_{r\theta} = \frac{1}{2}\left(\frac{\partial v}{\partial r} - \frac{v}{r} + \frac{1}{r}\frac{\partial u}{\partial \theta} + \frac{1}{r}\frac{\partial w}{\partial r}\frac{\partial w}{\partial \theta}\right)$$

Kinetic energy: The kinetic energy expression is as follows;

$$T = \frac{\rho}{2}\iint h\left(\frac{\partial w}{\partial t}\right)^2 .r\,dr\,d\theta \qquad (2.26)$$

2.1.3 Equilibrium Conditions

The equations of motion are derivable from the energy equations, by the use of the calculus of variations. The principle of Hamilton states that the motion of a system is such as to render the hamiltonian integral I, as given in equation 2.20, where t_1 and t_2 are arbitrary instants of time, an extremum with respect to continuously twice differentiable functions of the integral(41). The lagrangian can be expressed as follows;

$$L = L\left(u, \frac{\partial u}{\partial x}, \frac{\partial u}{\partial y}, v, \frac{\partial v}{\partial x}, \frac{\partial v}{\partial y}, w, \frac{\partial w}{\partial x}, \frac{\partial w}{\partial y}, \frac{\partial^2 w}{\partial x^2}, \frac{\partial^2 w}{\partial x \partial y}, \frac{\partial^2 w}{\partial y^2}\right) \qquad (2.27)$$

The integral of equation 2.20 is extremized with respect to the functions of the lagrangian which describe the actual plate configuration at $t = t_1$ and $t = t_2$ by the particular functions which describe the actual motion for all t. The process yields the following conditions within the plate region.

$$\frac{\partial \hat{N}_x}{\partial x} + \frac{\partial \hat{N}_{xy}}{\partial y} = 0 \tag{2.28a}$$

$$\frac{\partial \hat{N}_{xy}}{\partial x} + \frac{\partial \hat{N}_y}{\partial y} = 0 \tag{2.28b}$$

$$\frac{\partial}{\partial x}\left[\hat{N}_x \frac{\partial w}{\partial x} + \hat{N}_{xy} \frac{\partial w}{\partial y}\right] + \frac{\partial}{\partial y}\left[\hat{N}_{xy} \frac{\partial w}{\partial x} + \hat{N}_y \frac{\partial w}{\partial y}\right] = \frac{Eh^3}{12(1-\nu^2)} \nabla^4 w + \rho h \frac{\partial^2 w}{\partial t^2} \tag{2.28c}$$

The following conditions should also hold along the boundaries.

$$u.\left[\hat{N}_{xy}.dx - \hat{N}_x.dy\right] = 0 \tag{2.29a}$$

$$v.\left[\hat{N}_y.dx - \hat{N}_{xy}.dy\right] = 0 \tag{2.29b}$$

$$w.\left[\left[\frac{\partial^3 w}{\partial x^3} + (2-\nu)\frac{\partial^3 w}{\partial y^2 \partial x}\right]dy - \left[\frac{\partial^3 w}{\partial y^3} + (2-\nu)\frac{\partial^3 w}{\partial y \partial x^2}\right]dx - \left(\hat{N}_x \frac{\partial w}{\partial x} + \hat{N}_{xy} \frac{\partial w}{\partial y}\right)dy + \left(\hat{N}_y \frac{\partial w}{\partial y} + \hat{N}_{xy} \frac{\partial w}{\partial x}\right)\right] = 0 \tag{2.29c}$$

$$\frac{\partial w}{\partial x}\cdot\left[\frac{\partial^2 w}{\partial x^2} + \nu\frac{\partial^2 w}{\partial y^2}\right] = 0 \qquad (2.29d)$$

$$\frac{\partial w}{\partial y}\cdot\left[\frac{\partial^2 w}{\partial y^2} + \nu\frac{\partial^2 w}{\partial x^2}\right] = 0 \qquad (2.29e)$$

$$\text{where } \hat{N}_x = h\bar{\sigma}_{xO} + N_x$$
$$\hat{N}_y = h\bar{\sigma}_{yO} + N_y$$
$$\hat{N}_{xy} = h\bar{\sigma}_{xyO} + N_{xy} \qquad (2.30)$$
$$\nabla^4 w = \nabla^2(\nabla^2 w) = \frac{\partial^4 w}{\partial x^4} + 2\frac{\partial^4 w}{\partial x^2 \partial y^2} + \frac{\partial^4 w}{\partial y^4}$$

Equations of Motion

The relations in equations 2.28 are the equations of motion and those in equation 2.29 are the boundary conditions. Introducing stress function F such that

$$\hat{N}_x = \frac{\partial^2 F}{\partial y^2}\ ;\quad \hat{N}_y = \frac{\partial^2 F}{\partial x^2}\ ;\quad \hat{N}_{xy} = -\frac{\partial^2 F}{\partial x \partial y}\ ; \qquad (2.31)$$

the equations of motion reduce to the following;

$$\frac{\partial^2 F \partial^2 w}{\partial y^2 \partial x^2} - 2\frac{\partial^2 F}{\partial x \partial y}\frac{\partial^2 w}{\partial x \partial y} + \frac{\partial^2 F \partial^2 w}{\partial x^2 \partial y^2} = D\nabla^4 w + \rho h\frac{\partial^2 w}{\partial t^2} \qquad (2.32)$$

$$\text{and } \nabla^4 F = Eh\left[\left(\frac{\partial^2 w}{\partial x \partial y}\right)^2 - \frac{\partial^2 w \partial^2 w}{\partial x^2 \partial y^2}\right] \qquad (2.33)$$

Boundary Conditions

The conditions that should be satisfied at the boundaries of a vibrating plate primarily depend on the constraints imposed on the plate at such boundaries. The common types of physical constraints on plates are (i) rigid clamping, (ii) simple support, and (iii) no restraints(free edge). The relations in equation 2.29 give the various boundary conditions. The following conditions are given assuming that the edge lies on a line parallel to the x-axis.

Rigid clamping(built-in edge): The conditions to be satisfied at the built-in edge are as follows;

$$u = v = 0 \; ; \quad w = 0 \; ; \quad \frac{\partial w}{\partial y} = 0 \; . \tag{2.34}$$

Simple support: The boundary conditions at the simply supported edge are as follows;

$$\hat{N}_y = \hat{N}_{xy} = 0 \; ; \quad w = 0 \; ; \quad \frac{\partial^2 w}{\partial y^2} + \nu \frac{\partial^2 w}{\partial x^2} = 0. \tag{2.35}$$

Free edge: Conditions to satisfied at the free edge are as follows;

$$\begin{aligned} &\hat{N}_y = \hat{N}_{xy} = 0, \\ &\frac{\partial^3 w}{\partial y^3} + (2-\nu)\frac{\partial^3 w}{\partial y \partial x^2} = 0, \\ &\frac{\partial^2 w}{\partial y^2} + \nu \frac{\partial^2 w}{\partial x^2} = 0. \end{aligned} \tag{2.36}$$

Linear vibrations: When a plate is vibrating with small amplitudes, the equations of motion as in equations 2.32 and 2.33 become decoupled, with the membrane stresses being neglected. The equations reduce to the following;

$$\nabla^4 w + \frac{\rho h}{D}\frac{\partial^2 w}{\partial t^2} - \frac{h}{D}\left[\bar{\sigma}_{x0}\frac{\partial^2 w}{\partial x^2} + 2\bar{\sigma}_{xy0}\frac{\partial^2 w}{\partial x\,\partial y} + \bar{\sigma}_{y0}\frac{\partial^2 w}{\partial y^2}\right] = 0 \qquad (2.37)$$

In the absence of initial stresses, the equation of motion further reduces to the following;

$$\nabla^4 w + \frac{\rho h}{D}\cdot\frac{\partial^2 w}{\partial t^2} = 0 \qquad (2.38)$$

Equation 2.38 is the classical differential equation for linear vibration of plates.

The boundary conditions compatible with equation 2.38 are the same as those earlier given, but with in-plane displacements u and v, and the membrane stresses neglected.

Equations in Polar Coordinates

The relations of equation 2.38 are given in polar coordinates in equation 2.39.

$$\frac{\partial \hat{N}_r}{\partial r} + \frac{1}{r}\frac{\partial \hat{N}_{r\theta}}{\partial \theta} + \frac{1}{r}(\hat{N}_r - \hat{N}_\theta) = 0 \qquad (2.39a)$$

$$\frac{\partial \hat{N}_{r\theta}}{\partial r} + \frac{1}{r}\frac{\partial \hat{N}_\theta}{\partial \theta} + \frac{2}{r}\hat{N}_{r\theta} = 0 \qquad (2.39b)$$

$$\hat{N}_r\frac{\partial^2 w}{\partial r^2} + 2\hat{N}_{r\theta}\frac{\partial}{\partial r}\left(\frac{1}{r}\frac{\partial w}{\partial \theta}\right) + \hat{N}_\theta\left(\frac{1}{r}\frac{\partial w}{\partial r} + \frac{1}{r^2}\frac{\partial^2 w}{\partial \theta^2}\right) = D\nabla^4 w + \rho h\frac{\partial^2 w}{\partial t^2} \tag{2.39c}$$

where $\hat{N}_r = h\bar{\sigma}_{r0} + N_r$

$\hat{N}_\theta = h\bar{\sigma}_{\theta 0} + N_\theta$

$\hat{N}_{r\theta} = h\bar{\sigma}_{r\theta 0} + N_{r\theta}$

The stress function introduced in equation 2.31 is defined in polar coordinates as follows;

$$\begin{aligned}\hat{N}_r &= \frac{1}{r}\frac{\partial F}{\partial r} + \frac{1}{r^2}\frac{\partial^2 F}{\partial \theta^2}\\ \hat{N}_\theta &= \frac{\partial^2 F}{\partial r^2}\\ \hat{N}_{r\theta} &= -\frac{\partial}{\partial r}\left(\frac{1}{r}\frac{\partial F}{\partial \theta}\right)\end{aligned} \tag{2.40}$$

The relations in equation 2.39 become as follows;

$$\left[\frac{1}{r}\frac{\partial F}{\partial r} + \frac{1}{r^2}\frac{\partial^2 F}{\partial \theta^2}\right]\frac{\partial^2 w}{\partial r^2} - 2\frac{\partial}{\partial r}\left(\frac{1}{r}\frac{\partial F}{\partial \theta}\right)\frac{\partial}{\partial r}\left(\frac{1}{r}\frac{\partial w}{\partial \theta}\right) + \frac{\partial^2 F}{\partial r^2}\left(\frac{1}{r}\frac{\partial w}{\partial r} + \frac{1}{r^2}\frac{\partial^2 w}{\partial \theta^2}\right) = D\nabla^4 w + \rho h\frac{\partial^2 w}{\partial t^2} \tag{2.41a}$$

$$\nabla^4 F = Eh\left[\left[\frac{\partial}{\partial r}\left(\frac{1}{r}\frac{\partial w}{\partial \theta}\right)\right]^2 - \frac{\partial^2 w}{\partial r^2}\cdot\left[\frac{1}{r}\frac{\partial w}{\partial r} + \frac{1}{r^2}\frac{\partial^2 w}{\partial \theta^2}\right]\right] \tag{2.41b}$$

Linear vibrations: The governing equation for linear vibrations of stress-free discs is as given in equation 2.38. The boundary conditions for the boundary constraints are given below.

Clamped edge

$$w = \frac{\partial w}{\partial r} = 0 \tag{2.42}$$

Simply-supported edge

$$w = \frac{\partial^2 w}{\partial r^2} + \nu\left(\frac{1}{r}\frac{\partial w}{\partial r} + \frac{1}{r^2}\frac{\partial^2 w}{\partial \theta^2}\right) = 0 \tag{2.43}$$

Free edge

$$\begin{aligned} &\frac{\partial^2 w}{\partial r^2} + \nu\left(\frac{1}{r}\frac{\partial w}{\partial r} + \frac{1}{r^2}\frac{\partial^2 w}{\partial \theta^2}\right) = 0 \\ &\frac{\partial}{\partial r}(\nabla^2 w) + \frac{1-\nu}{r}\left[\frac{\partial}{\partial r}\left(\frac{1}{r}\frac{\partial^2 w}{\partial \theta^2}\right)\right] = 0 \end{aligned} \tag{2.44}$$

Free Vibrations of Circular Plates

The natural modes are solutions of the type

$$w = f(r,\theta).g(t)$$

Substituting this into equation 2.38, then

$$\frac{D}{\rho h}.\frac{\nabla^4 f}{f} = -\frac{1}{g}\frac{\partial^2 g}{\partial t^2} = \bar{\omega}^2 \tag{2.45}$$

$$\text{or } \nabla^4 f = \frac{\rho h}{D}\bar{\omega}^2 f = 0 \tag{2.45a}$$

$$\text{and } \frac{\partial^2 g}{\partial t^2} + \bar{\omega}^2 g = 0 \tag{2.45b}$$

The solution of equation 2.45b is as follows;

$$g = g_0 \sin(\bar{\omega}t + \phi), \quad (g_0 = \text{const.}) \tag{2.46}$$

Equation 2.46 shows that $\bar{\omega}$ is the natural frequency of the plate. Equation 2.45a is solved assuming

$$f(r,\theta) = R(r).s(\theta)$$

Substituting the expression for f in equation 2.45a and solving, yields the following

$$s(\theta) = s_0 \cos n(\theta-\phi) , \quad (s_0 = \text{const.}) \tag{2.47}$$

where the constant n denotes the number of nodal diameters, and

$$R(r) = A_n J_n(kr) + B_n Y_n(kr) + C_n I_n(kr) + D_n K_n(kr) \tag{2.48}$$

where $k^4 = \frac{\bar{\omega}^2 \rho h}{D}$,

$J_n(kr)$, $Y_n(kr)$, $I_n(kr)$, $K_n(kr)$ are Bessel functions as defined in reference (4).

and A_n, B_n, C_n, D_n are constants.

Particular values of natural frequencies and mode shapes are derived by solving the eigenvalue problem, involving satisfying the boundary conditions(4).

2.2 Energy Methods

The vibration problem of a disc reduces in each case to that of finding a function w of r and θ that satisfies the given boundary conditions and makes the hamiltonian integral I a minimum(41). The use of the calculus of variations leads to the set of partial differential equations, which are the equations of motion earlier given. The hamiltonian integral can, however, be used directly in the approximate analysis of plate vibrations. The problem is reduced to that of minimising an energy integral by assuming the deflection w in the following form;

$$R(r) = a_1 f_1(r) + a_2 f_2(r) + \ldots\ldots\ldots + a_N f_N(r)$$
$$\text{and } w(r,\theta) = R(r)\cos(n\theta) \qquad (2.49)$$

The coefficients a_1, a_2 ,....., a_N , are chosen to make the energy integral minimum and therefore,

$$\frac{\partial I}{\partial a_1} = \frac{\partial I}{\partial a_2} = \ldots\ldots = \frac{\partial I}{\partial a_N} = 0 \qquad (2.50)$$

2.2.1 Rayleigh's Method

Rayleigh's method is a procedure used in estimating the fundamental frequency of a system for any specified θ-function without solving the associated eigenvalue problem. Rayleigh's principle states that "the estimated frequency of vibration of a conservative system, oscillating about the equilibrium position, has a stationary value in the neighbourhood of a natural mode"(42). The Rayleigh's method can be used to obtain an estimate for the lowest eigenvalue $\bar{\omega}^2$, where $\bar{\omega}$ is the system natural frequency. As Rayleigh's method gives a minimum value in the neighbourhood of a fundamental mode, to obtain an estimate for $\bar{\omega}^2$, we must choose and insert in the energy equations a trial deflection function resembling as closely as possible the deflection function of the system in its fundamental mode. Estimates obtained by Rayleigh's method are higher than the actual fundamental frequency.

Suitable Displacement Function

A close approximation to the exact value of $\bar{\omega}^2$ is by using as approximating functions the functions representing the deflection of a disc under uniform loading. These functions are as follows;

$$R_0(r) = A_0 + B_0 r^2 + C_0 \ln r + D_0 r^2 \ln r$$
$$R_1(r) = A_1 r + B_1 r^3 + \frac{C_1}{r} + D_1 r \ln r \qquad (2.51)$$
$$R_n(r) = A_n r^n + B_n r^{n+2} + \frac{C_n}{r^n} + \frac{D_n}{r^{n-2}}$$

A fifth term is added to each of these functions so that the functions can satisfy the necessary boundary conditions. The approximating function then becomes

$$R'_n(r) = R_n + E_n r^l \qquad (2.52)$$

The value of the index l can be chosen to give lower approximation for the frequency value for the mode of vibration of the plate being considered. The minimisation role of the fifth term introduces an improvement over the usual Rayleigh method and since the functions are made to satisfy all the necessary boundary conditions, the computed frequency values, compared to similar values by the exact method, are very good indeed.

Computation Procedure

The unrestrained radial portion of the plate is divided into a number of segments and the energy densities are computed, using the displacement profile whose coefficients have been determined by satisfying the four boundary conditions, at each point between the segments. Energy values are computed over the plate region by

numerical integration. The frequency value ϖ^2 is found as the ratio of the strain energy to the kinetic energy. If the computation of the effects of internal stresses is to be considered, such stresses are calculated independently of the deflection values and the stress values are used with the displacement values in computing the interaction energy. To obtain the effects of membrane stresses, the derived displacement functions are used to compute the membrane stresses using the method earlier given, and the stresses can then be used in getting the membrane energy. For any particular situation, the frequency values can be found for varying values of the index, l, of the fifth term in equation 2.52. The value that would give the minimum frequency value could then be used for getting improved frequency value and displacement profile.

The accuracy of the computed values was found to depend on the index value l, the number and distributions of subdivisions, and the precision of the digital computer used.

2.2.2 Rayleigh-Ritz Method

The Rayleigh-Ritz method is an extension of the Rayleigh method. It is a procedure for lowering the estimate of the frequency parameter $\bar{\omega}^2$. The method has a further edge on the Rayleigh method as it gives estimates of a finite number of higher eigenvalues. The admissible functions $f_i(r)$ as used in equation 2.49 are only required to satisfy the geometric boundary conditions in the plate system. It is also necessary that the chosen functions be twice differentiable in the energy equations. If a generating set with N functions is used, the problem can be reduced to the matrix form

$$\left[k \right]\{a\} = \bar{\omega}^2 \left[m \right]\{a\} \qquad (2.53)$$

where $\left[k \right]$ and $\left[m \right]$ are NxN constant symmetric matrices, and are the stiffness and mass matrices respectively.

The solution of equation 2.53 yields N eigenvalues $\bar{\omega}_i^2$ and associated eigenvectors $\{a_i\}$, (i=1,2,....,N). The eigenvalues $\bar{\omega}_i^2$ represent estimates of the first N frequency parameters of the plate system and they provide upper bounds for the actual frequency parameters(42).

Suitable Displacement Functions

A convenient admissible function is of the form

$$f_i(r) = r^A(r-b)^B \tag{2.54}$$

where A and B are constants and b is the clamping radius.

The generating set used in the various computation is

$$R(r) = \sum_{i=1}^{i=N} (r-b)^{i+1} \tag{2.55}$$

Computation Procedure

The plate radius between the flanges and the free edge is discretised into a number of subdivisions and component energy densities for each of the N functions are found at each of these points. The minimising procedure is carried out with respect to each of the N functions, resulting in N equations. The eigenvalue problem is then solved using a suitable routine. The accuracy of the method is improved with increase in the number of functions in the generating set. The derived frequency values are also improved when the number of points at which energy densities are computed are increased. The largest number of functions in the assumed profile is often restricted by the precision of the digital computer used. The Ritz method, unlike the Rayleigh method, can be

used in analysing plates with radius dependent thickness. It is also better suited for the analysis of plates with internal stresses. In the analysis of plates with large deflections, the Ritz method can be used iteratively to get improved frequency and displacement values. The Ritz method, however, requires much more computation time and storage space than the modified Rayleigh method.

2.2.3 Finite Element Method

The finite element method relates the primary unknown function to the individual element rather than to the total system. Derivation of the element stiffness matrix follows from the chosen function and the variational principle governing the problem. As the element stiffness matrix is based on a derivation that is essentially unchanged irrespective of the constraints of the problem, it becomes the foundation for applying the finite element method as a method of approximate solution for boundary-value problem(43).

Linear Vibrations

The transverse deflections are interpolated as follows;

$$\underline{w}(x,y) = \underline{L}(x,y) \cdot \underline{w}_e(x,y) \qquad (2.56)$$

where $\underline{L}$ is the set of interpolation functions

$\underline{w}$ is the displacement at any point

$\underline{w}_e$ is the vector of element nodal displacement

The strain-displacement relation becomes the following;

$$\underline{e} = z\begin{bmatrix} \frac{\partial^2 w}{\partial x^2} \\ \frac{\partial^2 w}{\partial y^2} \\ \frac{\partial^2 w}{\partial x \partial y} \end{bmatrix} = \underline{B}.\underline{w}_e \qquad (2.57)$$

The stress-strain relation is the following;

$$\underline{\sigma} = \underline{D}.\underline{e} = \underline{D}.\underline{B}.\underline{w}_e \qquad (2.58)$$

From strain energy considerations, the element stiffness matrix is of the form

$$\underline{K} = \int_V \underline{B}^T \underline{D}\underline{B} dV \qquad (2.59)$$

The mass matrix is formed by assembling mass matrices for all the the elements.

$$\underline{M} = \int_V \underline{L}^T \rho \underline{L} dV \qquad (2.60)$$

The vibration problem then becomes the characteristic-value problem given by the following equation(43);

$$\left[\underline{K} - \bar{\omega}^2 \underline{M}\right] \underline{w}_s = 0 \qquad (2.61)$$

where $\underline{w}_s$ is the vibration mode shape

$\underline{K}$ is the stiffness matrix for the plate

$\underline{M}$ is the mass matrix for the plate

$\bar{\omega}$ is the angular frequency of vibration

Computation Procedure

PAFEC 75, of which copyright is held by PAFEC Ltd., was used for the determination of the plate natural frequencies. The eight-noded facet shell element(44210) was, mainly, used in the analyses. The program requires the plate to be suitably discretised and nodal coordinates given. Coordinates of midside nodes can be omitted if such nodes lie half-way between the adjacent end nodes. The program can be used to generate more elements, although with straight edges, within the defined elements. The restraints on the plate are required to be defined and so are the number of modes for which frequencies and modes shapes are to found. The program has plotting routines for drawing the plate geometry and displacements.

2.3 Internal Stresses

Internal stresses in a vibrating disc are defined as stresses not primarily caused by the vibratory motion of the plate. These stresses are due to to the straining of the plate material by external means. The common forms of internal stresses encountered in circular saw operations are (i) initial stresses, (ii) rotational stresses, and (iii) thermal stresses.

2.3.1 Equilibrium Conditions

It is assumed that the total internal stress system in a disc is the sum of the stresses due to the individual effects of "prestressing", rotation, and temperature variation within the plane of the disc. The equation of equilibrium of a symmetrically stressed rotating disc is as follows;

$$\frac{\partial}{\partial r}(r\bar{\sigma}_{r0}) - \bar{\sigma}_{\theta 0} + \rho\Omega^2 r^2 = 0 \qquad (2.62)$$

where Ω is the rotational speed

$\bar{\sigma}_{r0}$, $\bar{\sigma}_{\theta 0}$ are the internal stresses

The displacement-stress relations are the following;

$$\bar{u}_r = \frac{1}{E}\left[\bar{\sigma}_{r0} - \nu\bar{\sigma}_{\theta 0}\right] + \alpha_1 q$$

$$\frac{\bar{u}}{r} = \frac{1}{E}\left[\bar{\sigma}_{\theta 0} - \nu\bar{\sigma}_{r0}\right] + \alpha_1 q \qquad (2.63)$$

where α_1 is the coeff. of linear expansion

q is the temperature rise

Combining equations 2.62 and 2.63 yields the following;

$$\frac{d}{dr}\left[\frac{1}{r}\frac{d}{dr}(ur)\right] = (1+\nu)\alpha_1 q_r - \frac{1-\nu^2}{E}\rho\Omega^2 r \qquad (2.64)$$

Solving equation 2.64 yields the following;

$$\bar{u} = C_1 r + \frac{C_2}{r} - \frac{1-\nu^2}{8E}\rho\Omega^2 r^3 + \frac{1+\nu}{r}\alpha_1 \int qrdr \qquad (2.65)$$

where C_1, C_2 are constants of integration.

From equation 2.63 and 2.65, the internal stresses can be expressed as follows;

$$\bar{\sigma}_{r0} = \frac{E}{1-\nu}C_1 - \frac{E}{r^2(1+\nu)}C_2 - \frac{E\alpha_1}{r^2}\int qrdr - \frac{3+\nu}{8}\rho\Omega^2 r^2 \qquad (2.66)$$

$$\bar{\sigma}_{\theta 0} = \frac{E}{1-\nu}C_1 + \frac{E}{r^2(1+\nu)}C_2 + \frac{E\alpha_1}{r^2}\int qrdr - E\alpha_1 q - \frac{1+3\nu}{8}\rho\Omega^2 r^2 \qquad (2.67)$$

The appropriate boundary conditions allow the integration constants C_1 and C_2 to be determined. It may, however, be necessary to use different sets of boundary conditions for the different states of stresses; initial, rotational, thermal.

2.3.2 Initial Stresses

"Tensioning" stresses are often introduced in circular saws to increase the stiffness of the saws. Tensioning is carried out by hammering or rolling of the plate surface. The increase in plate stiffness due to tensioning is expected to offset any possible reduction in stiffness that may be be due to thermal stressing. Much of the tensioning in saws is by the pressure rolling method and the initial stresses imposed by this method can be derived using the equations derived in section 2.3.1.

When a circular plate is subjected to axisymmetric rolling at a radius d, the imposed condition can be approximated by a shrink-fit pressure p dependent on rolling pressure(5). The initial stresses, radial and tangential, are given by the following;

$$\bar{\sigma}_{ri} = A_1 + \frac{A_2}{r^2}$$
$$\bar{\sigma}_{\theta i} = A_1 - \frac{A_2}{r^2} \qquad (2.68)$$

Two stress functions are necessary to determine the stress distribution along a radius of the plate. The conditions are the following;

$$\text{(i)}\ \bar{\sigma}_{ri}(a) = 0$$
$$\text{(ii)}\ \bar{\sigma}_{ri}(d+) = \bar{\sigma}_{ri}(d-) = p \qquad (2.69)$$
$$\text{(iii)}\ \bar{\sigma}_{ri}(c) = 0$$

where a is the outside radius

c is the central hole radius

d is the rolling radius

p is dependent on the "rolling" pressure

With $\bar{r} = \frac{r}{a}$, $\gamma = \frac{c}{a}$, $\varepsilon = \frac{d}{a}$, the stresses in the two regions are given below.

(i) In the region $\gamma < \bar{r} < \varepsilon$

$$\begin{aligned} \bar{\sigma}_{ri} &= \frac{-p\varepsilon^2}{\varepsilon^2-\gamma^2}\left(1 - \frac{\gamma^2}{\bar{r}^2}\right) \\ \bar{\sigma}_{\theta i} &= \frac{-p\varepsilon^2}{\varepsilon^2-\gamma^2}\left(1 + \frac{\gamma^2}{\bar{r}^2}\right) \end{aligned} \tag{2.70}$$

(ii) In the region $\varepsilon < \bar{r} < 1$

$$\begin{aligned} \bar{\sigma}_{ri} &= \frac{p\varepsilon^2}{1-\varepsilon^2}\left(1 - \frac{1}{\bar{r}^2}\right) \\ \bar{\sigma}_{\theta i} &= \frac{p\varepsilon^2}{1-\varepsilon^2}\left(1 + \frac{1}{\bar{r}^2}\right) \end{aligned} \tag{2.71}$$

2.3.3 Rotational Stresses

Rotational stresses are always present in circular saws during cutting, as in any rotating body. The rotational stresses are found from the following relations.

$$\begin{aligned} \bar{\sigma}_r &= \rho\Omega^2\left[A_1 + \frac{A_2}{r^2} - \frac{3+\nu}{8}r^2\right] \\ \bar{\sigma}_\theta &= \rho\Omega^2\left[A_1 - \frac{A_2}{r^2} - \frac{1+3\nu}{8}r^2\right] \end{aligned} \tag{2.72}$$

where A_1, A_2 are arbitrary constants determined from the

following boundary conditions.

$$\begin{aligned} &(i)\ \bar{\sigma}_r(a) = 0 \\ &(ii)\ \bar{\sigma}_r(c) = 0 \end{aligned} \qquad (2.73)$$

where a and c are the outside radius and the central hole radius respectively, of the disc.

The determination of the constants in equation 2.72 leads to the following expressions for the radial and tangential rotational stresses.

$$\begin{aligned} \bar{\sigma}_r &= \frac{3+\nu}{8}\rho\Omega^2\left[1 + \gamma^2 - \frac{\gamma^2}{\bar{r}^2} - \bar{r}^2\right] \\ \bar{\sigma}_\theta &= \frac{3+\nu}{8}\rho\Omega^2\left[1 + \gamma^2 + \frac{\gamma^2}{\bar{r}^2} - \frac{1+3\nu}{3+\nu}.\bar{r}^2\right] \end{aligned} \qquad (2.74)$$

where $\gamma = \frac{c}{a}$, $\bar{r} = \frac{r}{a}$

2.3.4 Thermal Stresses

If the internal stress state is only temperature dependent, the stresses are given by the following expressions.

$$\begin{aligned} \bar{\sigma}_r &= A_1 + \frac{A_2}{r^2} - \frac{E\alpha_1}{r^2}\int qrdr \\ \bar{\sigma}_\theta &= A_1 - \frac{A_2}{r^2} + \frac{E\alpha_1}{r^2}\int qrdr - E\alpha_1 q \end{aligned} \qquad (2.75)$$

The constants A_1 , A_2 in equation 2.75 are determined using the the conditions given in equation 2.76. Considering a plate, with outside radius a and central

hole radius c, clamped up to radius b, then the necessary conditions are the following;

$$\begin{aligned} &\text{(i) } \bar{\sigma}_r(a) = 0; \quad \text{(ii) } \bar{\sigma}_r(b+) = \bar{\sigma}_r(b-) \\ &\text{(iii) } \bar{\sigma}_\theta(b+) = \bar{\sigma}_\theta(b-); \quad \text{(iv) } \bar{\sigma}_r(c) = 0 \end{aligned} \tag{2.76}$$

Two stress functions will be determined, one for the region within the clamping radius and the other for the region outside the clamping radius. It will be necessary to know the temperature distribution across the plate radius in order to be able write explicit expressions for thermal stresses.

2.3.5 Effects of Internal Stresses

The presence of internal stresses in discs affects the bending characteristics by introducing an additional strain energy term, the interaction energy, U_i.

$$U_i = \frac{1}{2}\int\int h\left[\bar{\sigma}_r\left(\frac{\partial w}{\partial r}\right)^2 + \frac{\bar{\sigma}_\theta}{r^2}\left(\frac{\partial w}{\partial \theta}\right)^2 + 2\frac{\bar{\sigma}_{r\theta}\partial w \partial w}{r\ \partial r \partial \theta}\right] r dr d\theta \tag{2.77}$$

In a circular plate with axially symmetric internal stress distribution, the shear stress $\bar{\sigma}_{r\theta}$ is zero. Assuming a mode shape of the form

$$w(r,\theta) = R(r)\cos n\theta \tag{2.78}$$

The interaction energy for symmetrically stressed plates is as follows;

$$U_i = \frac{\pi k}{2} \int\int h \left[\overline{\sigma}_r . R^2 + \frac{n^2 \overline{\sigma}_\theta}{r^2} . \left(\frac{dR}{dr}\right)^2 \right] r dr \qquad (2.79)$$

where k = 1 for n = 1,2,.....

and k = 2 for n =0.

From equation 2.79, the effect of internal stresses on the plate stiffness will depend, especially for higher modes, on whether the tangential stresses are tensile or compressive.

Initial Stresses

The expressions for symmetrically generated initial stresses in section 2.3.2 is only approximate and more rigorous consideration is required depending on the geometry of the rolling mechanism. The analysis given serves adequately to show that for higher modes (n >2), symmetrical "rolling" tensioning generates increases in modal stiffness. As pointed out by Dugdale(13), stressing in this form is only advantageous when the plate is rotated at high speeds. Stationary waves are normally encountered for modes with number of nodal diameters n>2, therefore tensioning by symmetric rolling will serve to increase the minimum critical speeds at which these waves are formed.

Analysis of initial stresses due to tensioning by

hammering is different(44). Such initial stresses would be asymmetric, as are most stresses encountered in practice. Manufacture of saw discs introduces non-symmetric initial stresses and such stresses are usually unknown in value and distribution. Consequently, the effect of the stresses on the plate modal compliances is unknown. It is therefore necessary to reduce the initial stresses before performing natural frequency tests, especially in the thinner plates.

Rotational Stresses

Rotational stresses, as given in the relations of equation 2.74, are tensile all over the plate. Consequently, rotation leads to increase in the natural frequencies in all modes of vibration of a disc. The variation of frequency values with rotational speed is given by the following expression.

$$\bar{\omega}^2 = \bar{\omega}_0^2 + a_n^2\Omega^2 \qquad (2.80)$$

where $\bar{\omega}$ is the speed-corrected frequency

$\bar{\omega}_0$ is the frequency of the stationary disc

Ω is the disc angular velocity

a_n^2 is a positive-valued energy constant

Thermal Stresses

Circumferential heating of a circular plate around the rim yields tensile radial stresses but predominantly compressive tangential stresses. This state of stress will cause an increase in the natural frequency in the mode with n=0 and reduction in the natural frequencies of the higher modes(n > 2). Heating of the plate around the centre will have the reverse effects to those for heating around the rim.

2.3.6 Stress Relieving Method

The fundamental mechanism of stress relaxation and the conditions under which it can occur are not yet fully known, but it is known that relaxation is particularly marked at high temperature(45). Relaxation curves obtained experimentally(45) all exhibit two clearly defined sections; the first characterised by a rapid fall in stress, and the second by a slower fall.

Relieving of initial stresses can be carried by the procedure given below(46).

(i) A temperature of about 700^{o}C is usually satisfactory for the relieving of initial stresses.

(ii) The soaking time should be long enough to enable every part of the plate to attain the heat treatment temperature.

(iii) The cooling should be such as to avoid temperature

gradients, and the furnace doors should not be opened before the temperature has dropped to about 200°C.

2.4 Nonlinear Vibrations

The vibration of a thin plate, as can be seen from the derived equations of motion, is nonlinear. While the plate amplitude $\bar{w}$ is small, $\bar{w} < \frac{h}{2}$, the problem can be considered linear and the nonlinear effects ignored. There is no classical solution to the nonlinear problem and approximate solutions have to be devised. A reliable approximation to the nonlinear problem can be deduced by the use of energy methods. It is then necessary to derive the expressions for the membrane stresses in terms of plate displacements.

2.4.1 Membrane Stresses

The relations governing membrane forces/length, as described in section 2.1, are restated below. Assuming the membrane forces/length are expressed in terms of the stress function F as follows;

$$N_r = \frac{1}{r}\frac{\partial F}{\partial r} + \frac{1}{r^2}\frac{\partial^2 F}{\partial \theta^2} \; ; \quad N_\theta = \frac{\partial^2 F}{\partial r^2} \; ; \quad N_{r\theta} = -\frac{\partial}{\partial r}\left(\frac{1}{r}\frac{\partial F}{\partial \theta}\right) \quad (2.81)$$

The membrane stresses are obtained from strains by elasticity equations;

$$N_r = \frac{Eh}{1-\nu^2}\left[\frac{\partial u}{\partial r} + \frac{1}{2}\left(\frac{\partial w}{\partial r}\right)^2 + \nu\left[\frac{1}{r}\frac{\partial v}{\partial \theta} + \frac{u}{r} + \frac{1}{2r^2}\left(\frac{\partial w}{\partial \theta}\right)^2\right]\right] \quad (2.82a)$$

$$N_\theta = \frac{Eh}{1-\nu^2}\left[\frac{1}{r}\frac{\partial v}{\partial \theta} + \frac{u}{r} + \frac{1}{2r^2}\left(\frac{\partial w}{\partial \theta}\right)^2 + \nu\left[\frac{\partial u}{\partial r} + \frac{1}{2}\left(\frac{\partial w}{\partial r}\right)^2\right]\right] \quad (2.82b)$$

$$N_{r\theta} = \frac{Eh}{2(1+\nu)}\left[\frac{\partial v}{\partial r} + \frac{1}{r}\frac{\partial u}{\partial \theta} - \frac{v}{r} + \frac{1}{r}\frac{\partial w}{\partial r}\frac{\partial w}{\partial \theta}\right] \quad (2.82c)$$

Eliminating the in-plane displacements u and v from the expressions of equation 2.82; and using the relations of equation 2.81, these lead to the following differential equation.

$$\nabla^4 F = Eh\left[\left[\frac{\partial}{\partial r}\left(\frac{1}{r}\frac{\partial w}{\partial \theta}\right)\right]^2 - \frac{\partial^2 w}{\partial r^2}\left(\frac{1}{r}\frac{\partial w}{\partial r} + \frac{1}{r^2}\frac{\partial^2 w}{\partial \theta^2}\right)\right] \quad (2.83)$$

If the mode shape of a vibrating circular plate is expressed as following;

$$w_n = R(r)\cos n\theta\ , \quad (2.84)$$

it is found that the stress function takes the form of the following expression;

$$F_n = Q(r) + P(r)\cos 2n\theta \quad (2.85)$$

Substituting equations 2.84 and 2.85 into equation 2.83 yields the following;

$$\frac{1}{r}\frac{d}{dr}\left[r\frac{d}{dr}\left(\frac{1}{r}\frac{d}{dr}\left[r\frac{dQ}{dr}\right]\right)\right] = G_1(r) \quad (2.86)$$

and

$$r^{2n-1}\frac{d}{dr}[\frac{1}{r^{4n-1}dr}(r^{4n-1}\frac{d}{dr}[\frac{1}{r^{4n-1}dr}(r^{2n}P)])] = G_2(r) \tag{2.87}$$

where

$$G_1(r) = -\frac{Eh}{2}\left[\frac{d^2R}{dr^2}(\frac{1dR}{rdr} - \frac{n^2}{r^2}R) - \frac{n^2}{r^2}[(\frac{dR}{dr})^2 - \frac{2RdR}{r\,dr} + \frac{R^2}{r^2}]\right]$$

$$G_2(r) = -\frac{Eh}{2}\left[\frac{d^2R}{dr^2}(\frac{1dR}{rdr} - \frac{n^2}{r^2}R) + \frac{n^2}{r^2}[(\frac{dR}{dr})^2 + \frac{2RdR}{r\,dr} - \frac{R^2}{r^2}]\right]$$

The forces/length, given in terms of P and Q, are as follows;

$$\begin{aligned} N_r &= \frac{1dQ}{rdr} + (\frac{1dP}{rdr} - \frac{4n^2}{r^2}P)\cos 2n\theta \\ N_\theta &= \frac{d^2Q}{dr^2} + \frac{d^2P}{dr^2}\cos 2n\theta \\ N_{r\theta} &= -\frac{2n}{r}(\frac{P}{r} - \frac{dP}{dr})\sin 2n\theta \end{aligned} \tag{2.88}$$

Symmetric Stress Function,Q

The relation of equation 2.86 can be integrated to give the following expression.

$$\frac{d}{dr}[\frac{1}{rdr}\frac{d}{dr}(r\frac{dQ}{dr})] = -\frac{Eh}{4r}\left[(\frac{dR}{dr})^2 - \frac{n^2}{r}R(2\frac{dR}{dr}\ \frac{R}{r})\right] = f_1(r) \tag{2.89}$$

Further integrations with respect to r leads to the following;

$$\frac{d}{dr}(r\frac{dQ}{dr}) = r\int f_1.dr + A_1 r$$
$$= f_2(r) + A_1 r$$
$$\frac{dQ}{dr} = \frac{1}{r}\int f_2.dr + \frac{A_1 r}{2} + \frac{A_2}{r} \qquad (2.90)$$
$$= f_3(r) + \frac{A_2}{r} + \frac{A_1 r}{2}$$
$$Q = \int f_3.dr + A_3 + A_2 \ln r + \frac{A_1 r^2}{4}$$

The membrane forces/length derivable from the symmetric part, Q, of the stress function F are given in equation 2.91.

$$N_r' = \frac{1}{r^2}\int f_2.dr + \frac{A_2}{r^2} + \frac{A_1}{2}$$
$$N_\theta' = \int f_1.dr - \frac{1}{r^2}\int f_2.dr - \frac{A_2}{r^2} + \frac{A_1}{2} \qquad (2.91)$$
$$N_{r\theta}' = 0$$

Harmonic Stress Function,P

Following a procedure similar to that for the symmetric stress function, the harmonic function is given in equation 2.92.

$$P = \frac{1}{r^{2n}}\int g_3.dr + \frac{B_3}{r^{2n}} + \frac{B_2 r^{2n}}{4n} - \frac{B_1}{4(2n-1)r^{(2n-2)}} \qquad (2.92)$$
$$+ \frac{B_0 r^{2n+2}}{16n(2n+1)}$$

where

$$g_3 = r^{4n-1}\int g_2.dr$$

$$g_2 = \frac{1}{r^{4n-1}}\int g_1.dr$$

$$g_1 = r^{4n-1}\int \frac{G_2(r)}{r^{2n-1}}.dr$$

The forces/length derivable from the harmonic part of the stress function F are as follows;

$$N_r'' = \frac{1}{r^{2n+1}}\left[g_3 - \frac{2n(2n+1)}{r}\int g_3.dr\right] - B_3\frac{2n}{r^{2n+2}} + B_2\frac{(1-2n)r^{2n-2}}{2} + B_1\frac{n-1+2n^2}{2(2n-1)r^{2n}} + B_0\frac{(n+1-2n^2)r^{2n}}{8n(2n+1)} \qquad (2.93a)$$

$$N_\theta'' = r^{2n-1}g_2 - \frac{1}{r^{2n+1}}g_3 + \frac{2n(2n+1)}{r^{2n+2}}\int g_3.dr + B_3\frac{2n(2n+1)}{r^{2n+2}} + B_2\frac{(2n-1)}{2}r^{2n-2} - B_1\frac{(n-1)}{2r^{2n}} + B_0\frac{(n+1)}{8n}r^{2n} \qquad (2.93b)$$

$$N_{r\theta}'' = 2n\left[\frac{g_3}{r^{2n+1}} - \frac{(2n+1)}{r^{2n+2}}\int g_3.dr - B_3\frac{(2n+1)}{r^{2n+2}} + B_2\frac{(2n-1)}{4n}r^{2n-2} + \frac{B_1}{4r^{2n}} + B_0\frac{r^{2n}}{16n}\right] \qquad (2.93c)$$

Boundary Conditions

The constants of integration in equations 2.91 and 2.93 are determined by applying the conditions prevaling at the boundaries of the disc. The membrane forces/length are given fully as follows;

$$\begin{aligned} N_r &= N_r' + N_r'' \cos 2n\theta \\ N_\theta &= N_\theta' + N_\theta'' \cos 2n\theta \\ N_{r\theta} &= N_{r\theta}'' \sin 2n\theta \end{aligned} \qquad (2.94)$$

Considering a circular plate with outside radius a, central hole radius c, the boundary conditions used for evaluating the membrane forces/length are as follows;

$$\begin{aligned} &\text{(i)}\ N_r'(a) = N_r'(c) = 0 \\ &\text{(ii)}\ N_r''(a) = N_r''(c) = 0 \\ &\text{(iii)}\ N_{r\theta}''(a) = N_{r\theta}''(c) = 0 \end{aligned} \qquad (2.95)$$

These conditions yield the following expressions for the membrane forces/length.

$$N_r' = \frac{1}{r^2}\left[\int_\gamma^{\bar{r}} f_2.dr + \frac{1}{1-\gamma^2}\int_\gamma^1 f_2.\left(\frac{\gamma^2}{r^2} - 1\right).dr\right] \qquad (2.96a)$$

$$N_\theta' = \int_\gamma^{\bar{r}} f_1.dr - \frac{1}{r^2}\left[\int_\gamma^{\bar{r}} f_2.dr + \frac{1}{1-\gamma^2}\int_\gamma^1 f_2.\left(\frac{\gamma^2}{r^2}+1\right)dr\right] \qquad (2.96b)$$

Similar, though more lengthy, expressions can be deduced

from the conditions given in equation 2.95.

2.4.2 Nonlinear Frequencies

The membrane forces/length as given in subsection 2.4.1 are only dependent on the transverse displacement, w, and its derivatives. The relations given for the membrane forces/length can be used to derive the response frequency values for given values of plate displacement. The nonlinear problem can be solved using the Rayleigh-Ritz method in an iterative manner. The eigenvalue problem is solved, initially, neglecting the nonlinear effect. The derived eigenvectors are used to derive the membrane energy. The net energy integral is minimised and the resulting eigenvectors are used to generate new membrane forces/length. The iterative procedure is continued until the change in the nonlinear frequency is below an acceptable level. The modified Rayleigh method described in subsection 2.2.2, in which the index of the fifth term in the assumed displacement function can be varied to minimise the plate frequency values, can also be used for deriving nonlinear displacement-dependent frequencies.

Natural frequency values in plates were found not to be sensitive to minor changes in mode shapes. The mode shape for linear vibration can therefore be used in deriving values for membrane stresses, even when the vibration amplitude is of the order of the plate

thickness. This assumption leads to considerable reduction in computation time and it allows more general nonlinearity relations to be given. Table 1. shows values of nonlinear frequency against amplitude for a particular configuration, in which the values were derived using a minimising method, and similar values derived by assuming that the mode shape is not significantly affected by amplitude values.

2.4.3 Forced Vibration

The equation of motion for the forced vibration of discs is, here, derived from the energy quantities, using the Lagrange equation stated in equation 2.97.

$$\frac{\partial}{\partial t}\left(\frac{\partial T}{\partial \dot{w}_i}\right) - \left(\frac{\partial T}{\partial w_i}\right) + \left(\frac{\partial U}{\partial w_i}\right) = R_i \qquad (2.97)$$

where T is the kinetic energy

U is the strain energy

R_i is the i^{th} component of the generalised force

Perfect Stationary Discs

In vibrating discs, the energy quantities, T, U, are expressed as follows;

$$T = \pi\rho h a^2 . \dot{w}^2 . u_k$$
$$U = \pi\left[D\frac{w^2}{a^2}.u_b + \frac{Eh}{a^2}w^4.u_m\right] \qquad (2.98)$$

where D is the flexural rigidity, $\frac{Eh^3}{12(1-\nu^2)}$

u_b is the bending strain energy constant

u_m is the nonlinear membrane energy constant

u_k is the kinetic energy constant

Substituting for T and U in equation 2.97 yields the following;

$$\frac{\partial^2 w}{\partial t^2} + \bar{\omega}_0^2 . w + \bar{\omega}_0^2 \varepsilon_0 \frac{w^3}{h^2} = \frac{R}{2\rho h a^2 u_k \pi} \qquad (2.99)$$

where

$$\bar{\omega}_0^2 = \frac{Eh^2}{12\rho a^4(1-\nu^2)} \cdot \frac{u_b}{u_k}$$

$$\varepsilon_0 = 24(1-\nu^2) \cdot \frac{u_m}{u_b}$$

If the applied force is of period p, such that R = P cos pt, the equation 2.99 becomes the following;

$$\frac{\partial^2 w}{\partial t^2} + \bar{\omega}_0^2 w\left(1 + \varepsilon_0 \frac{w^2}{h^2}\right) = \bar{\omega}_0^2 . w_{fn} \cos pt \qquad (2.100)$$

where w_{fn} is the static deflection component for the mode considered

and

$$w_{fn} = \frac{Pa^2}{2\pi D u_b} \qquad (2.101)$$

Taking into consideration the effect of damping within the vibrating system, the equation of motion can be modified by including an equivalent dissipative force/mass term, to give the following;

$$\frac{\partial^2 w}{\partial t^2} + 2\zeta p \frac{\partial w}{\partial t} + \bar{\omega}_0^2 w\left(1+\varepsilon_0 \frac{w^2}{h^2}\right) = \bar{\omega}_0^2 w_{fn} \cos pt \qquad (2.102)$$

where $\zeta = \frac{1}{pt_c}$

and t_c is the time required for the vibration amplitude to drop to 0.368 of an initial value (assuming viscous damping).

Equation 2.102 is known as Duffing's equation for a damped system. Writing $x = \frac{w}{h}$, and $y = \frac{w_{fn}}{h}$, equation 2.102 becomes the following;

$$\frac{\partial^2 x}{\partial t^2} + 2\zeta p\frac{\partial x}{\partial t} + \bar{\omega}_0{}^2 x(1+\varepsilon_0 x^2) = \bar{\omega}_0{}^2 y \cos pt \qquad (2.103)$$

Assuming that $\tau = pt$ and $\beta = \frac{\bar{\omega}_0}{p}$, equation 2.103 can be expressed as follows;

$$x'' + 2\zeta x' + \beta^2 x(1+\varepsilon_0 x^2) = \beta^2 y \cos \tau \qquad (2.104)$$

Periodic solutions are derived for equations 2.104 using the perturbation technique. Neglecting the higher order terms, the approximate solution to equation 2.104 is as follows;

$$x(t) = A_0\cos(pt-\phi) + \frac{\varepsilon}{32\lambda^2} A_0{}^3\cos 3(pt-\phi) \qquad (2.105)$$

where

$$A_0{}^2[(2\zeta\lambda)^2 + (1+\frac{3}{4}\varepsilon A_0{}^2-\lambda^2)^2] = y^2 \qquad (2.106)$$

$$\lambda = \frac{1}{\beta} = \frac{p}{\bar{\omega}_0}$$

$$\phi = \tan^{-1}\left[\frac{2\zeta\lambda}{1+\frac{3}{4}\varepsilon A_0{}^2-\lambda^2}\right] \qquad (2.107)$$

Imperfect Stationary Discs

In perfect discs, the response frequencies of the two principal orthogonal modes for a particular mode shape are the same and there is no frequency separation. When there is significant frequency separation, exciting the disc at any arbitrary position could result in resonant vibration of the disc at one of its principal orthogonal response frequencies. Therefore, for each mode shape, two sets of response characteristics are possible, and the possible energy quantities can be expressed as follows;

$$T_1 = \pi \rho h a^2 \dot{w}_1^2 . u_{k1}$$

$$U_1 = \pi D \frac{w_1^2}{a^2} . u_{b1} + \frac{\pi E h}{a^2} w_1^4 . u_{m1} \qquad (2.108)$$

or

$$T_2 = \pi \rho h a^2 \dot{w}_2^2 . u_{k2}$$

$$U_2 = \pi D \frac{w_2^2}{a^2} . u_{b2} + \frac{\pi E h}{a^2} w_2^4 . u_{m2} \qquad (2.109)$$

In imperfect discs, a pure sinusoidal wave profile is no longer possible but the resulting mode shape will be the sum of a sinusoidal shape and its harmonics. In many practical cases, the resulting mode shape can be approximated as sinusoidal. With a small amount of frequency separation, the nodal lines for one normal mode

will be displaced angularly by approximately one quarter of a wavelength relative to the nodal lines of the other mode. The analysis for the possible equations of motion is similar to that for the perfect stationary disc. The possible equations of motion are as follows;

$$\frac{\partial^2 w_1}{\partial t^2}+2\zeta_1 p\frac{\partial w_1}{\partial t}+\bar{\omega}_{01}{}^2 w_1\left(1+\varepsilon_{01}\frac{w_1{}^2}{h^2}\right) = \bar{\omega}_{01}{}^2 w_{f1}\cos pt \tag{2.110}$$

or

$$\frac{\partial^2 w_2}{\partial t^2}+2\zeta_2 p\frac{\partial w_2}{\partial t}+\bar{\omega}_{02}{}^2 w_2\left(1+\varepsilon_{02}\frac{w_2{}^2}{h^2}\right) = \bar{\omega}_{02}{}^2 w_{f2}\sin pt \tag{2.111}$$

The vibration amplitude does not significantly affect the mode shape(table 1) and therefore the following assumption can be made.

$$u_{m1} = u_{m2} = u_m \tag{2.112}$$

The natural frequencies for linear vibrations at the two principal orthogonal modes are related as given in the following equation.

$$\frac{\bar{\omega}_{02}{}^2}{\bar{\omega}_{01}{}^2} = \frac{u_{b2}}{u_{k2}}\cdot\frac{u_{k1}}{u_{b1}} \tag{2.113}$$

Following the assumption of equation 2.112, the nonlinearity ratios for the two principal modes are related as given in the following equation;

$$\frac{\varepsilon_{01}}{\varepsilon_{02}} = \frac{u_{b1}}{u_{b2}} \tag{2.114}$$

The expression of equation 2.113 is directly related to the amount of frequency separation between the principal orthogonal modes. The effects of the frequency separation method on the energy constants u_b and u_k will depend on the location and type of the dynamic imperfection.

Position clamping: The effect of the kinetic energy is concentrated close to the rim but the strain energy distribution is more widespread over the disc. Therefore, it can be assumed that the kinetic energy constant is relatively unaffected by position clamping, and the relationship in equation 2.113 can be expressed as follows;

$$\frac{\bar{\omega}_{02}^{\,2}}{\bar{\omega}_{01}^{\,2}} = \frac{u_{b2}}{u_{b1}} \tag{2.115}$$

Assuming that $\bar{\omega}_{02} > \bar{\omega}_{01}$ and that $\bar{\omega}_{02} = \bar{\omega}_{01} + \Delta\bar{\omega}$, where $\Delta\bar{\omega}$ is small ($\Delta\bar{\omega} \ll \bar{\omega}_{01}$), the following approximations can be made.

$$\begin{aligned} u_{b2} &= u_{b1}(1 + 2s) \\ \varepsilon_{02} &= \varepsilon_{01}(1 + 2s) \\ w_{f2} &= \frac{w_{f1}}{1+2s} \end{aligned} \tag{2.116}$$

where $s = \dfrac{\Delta\bar{\omega}}{\bar{\omega}_{01}}$

The possible equations of motion can then be expressed as follows;

$$\frac{\partial^2 w_1}{\partial t^2} + 2\zeta_1 p \frac{\partial w_1}{\partial t} + \bar{\omega}_{01}^2 w_1 \left(1 + \varepsilon_{01} \frac{w_1^2}{h^2}\right) = \bar{\omega}_{01}^2 w_{f1} \cos pt \quad (2.117)$$

or

$$\frac{\partial^2 w_2}{\partial t^2} + 2\zeta_2 p \frac{\partial w_2}{\partial t} + \bar{\omega}_{01}^2 (1+2s) w_2 \left[1 + \varepsilon_{01} (1+2s) \frac{w_2^2}{h^2}\right] = \bar{\omega}_{01}^2 w_{f1} \sin pt \quad (2.118)$$

The approximate solutions to equations 2.117 and 2.118 are similar to that given in equation 2.107. If the damping ratios are assumed similar for the two orthogonal modes, the maximun vibration amplitude will be higher for the lower response frequency.

Disc with holes: The relative effects of having holes close to the rim of a disc on the kinetic and strain energy values can be evaluated by using a procedure similar to that employed by Dugdale(35). The kinetic and strain energy densities for the perfect disc are found and contributions by the regions of the disc corresponding to the hole areas are subtracted from the total kinetic and strain energy values for the mode patterns corresponding to the two principal modes. These are (i) when the nodal lines pass through the hole area, and (ii) when the hole areas are midway between the nodal lines (in the antinodal position). The frequency separation and its

effects on the energy constants will depend on the area, and radial location of the holes. This method is only valid for holes with small areas. It is not used in determining the amount of frequency separation but to estimate the relative effects of the holes on the energy constants.

The analysis of a disc with holes will be similar to that for position-clamped discs, except for the differences in the relative magnitudes of the kinetic and strain energy constants. Assuming, in the extreme situation, that the strain energy values in the two principal modes are relatively unaffected by the presence of the holes, the relationship of equation 2.113 can then be expressed as follows;

$$\frac{\bar{\omega}_{02}^2}{\bar{\omega}_{01}^2} = \frac{u_{k1}}{u_{k2}} \tag{2.120}$$

Using the same assumptions as in equation 2.116, we have the following;

$$\begin{aligned} u_{k2} &= u_{k1}(1-2s) \\ \varepsilon_{02} &= \varepsilon_{01} \\ w_{f2} &= w_{f1} \end{aligned} \tag{2.121}$$

The possible equations of motion can then be expressed as follows;

$$\frac{\partial^2 w_1}{\partial t^2} + 2\zeta_1 p \frac{\partial w_1}{\partial t} + \bar{\omega}_{01}^2 w_1 \left(1 + \varepsilon_{01} \frac{w_1^2}{h^2}\right) = \bar{\omega}_{01}^2 w_{f1} \cos pt \quad (2.122)$$

or

$$\frac{\partial^2 w_2}{\partial t^2} + 2\zeta_2 p \frac{\partial w_2}{\partial t} + \bar{\omega}_{01}^2 (1+2s) w_2 \left(1 + \varepsilon_0 \frac{w_2^2}{h^2}\right) = \bar{\omega}_{01}^2 (1+2s) w_{f1} \sin pt \quad (2.123)$$

The approximate solutions to equations 2.122 and 2.123 are similar to that given in equation 2.107.

Equation Constants

The determination of forced vibration response as given in equations 2.105 to 2.107 requires that the equations' constants be known. These "equation" constants are the damping ratio ζ, the nonlinearity ratio ε, the force displacement ratio y, and the frequency ratio λ .

Damping ratio: Damping values were found to consist mainly of three types. These are (i) the hysteretic damping in the disc material, (ii) air damping of the oscillation of the disc, (iii) other external damping caused by effects such as clamping and rotation. Hysteretic damping is always present during bending of a disc and air damping is present during oscillation of the disc. Air damping has been found to increase with increase in vibration amplitude(47). Damping resulting from clamping effects was found to be higher for the lower modes of vibration. There

is no reliable theoretical evaluation of damping values in general real structures, and the damping values used were obtained experimentally.

Nonlinearity ratio: This is a measure of how nonlinear the vibration problem is. The value actually is not a constant but does vary with vibration amplitude. As shown in table 1, the nonlinear frequency values for the amplitude ratio $\frac{w_i}{h}$ up to 2.5 are not significantly affected by assuming that the mode shape of the disc is identical to that for linear vibration. It therefore follows that the nonlinearity ratio ε evaluated using the displacement profile for linear vibration is a good approximation, for values of vibration amplitude up to 2.5 times the disc thickness.

Force displacement ratio: The force displacement ratio, y, is the ratio of the equivalent displacement w_{fn} for the mode excited, of the applied force to the plate thickness h. The applied force is the sum of the modal forces for all possible modes.

Frequency ratio: The frequency ratio λ is the ratio of the forcing frequency p to the natural frequency ω of the mode being excited. The natural frequency can be found by using one of the methods given in section 2.2.

Displacement response curves: The response curves for the forced vibration, according to the relations of equations 2.106 and 2.107, are of the form shown in fig. 2.1. The amplitude curve shows a backbone curve. Maintaining the applied force and steadily increasing the speed ratio, the amplitude increases from O through B to C. At C a collapse occurs as the tangent to the response curve becomes vertical. On the other hand, if the frequency is reduced from beyond the collapse frequency, the amplitude increases from Z through E to point D, where again the tangent to the response curve is vertical and the amplitude jumps to point B on the upper limb, from which point it decreases along the curve to O with decreasing frequency. Similar changes occur in the phase angles at the same frequencies as the jumps occur in the amplitude curve.

2.5 Stationary Waves

Stationary waves in rotating discs are defined as such waves that occur that have no motion in the plane of the discs; i.e. in the direction of rotation of the discs. A standing wave is a stationary wave that has no motion in the transverse direction and appears stationary in space, and a pulsating wave is a stationary wave that is formed from more than one pure wave and has relative motion in the transverse direction of the discs. Fig. 2.4 shows sketches of stationary waves in rotating discs.

Due to the nonlinearity effect present in plate bending at finite amplitudes, a stationary wave, once generated, can be maintained with increasing amplitude over a large speed range. A stationary wave is generated by loading a disc rotating at about one of its critical speeds with a constant force and the response amplitude of the generated wave can be very large, depending on the applied force. Since a stationary wave can be maintained over a large speed range, discs have to be run at speeds below the minimum critical speed if large amplitude stationary waves are to be avoided.

In real discs there are two principal orthogonal modes of vibration, (except in the case with zero nodal diameters,) having the same number of nodal diameters n. The occurrence of two distinct orthogonal modes, usually

with some amount of detectable amount of response frequency difference between the two modes, is due to either material or geometric imperfection in the centrally-clamped disc. Large values of frequency separation between two orthogonal modes with similar mode shapes can be effected by imposing conditions that destroy the axial symmetry in the assembled disc. Tobias and Arnold(11) showed that such methods could be used to reduce the amplitudes of stationary waves.

The analysis presented was found to, reasonably, approximate the wave amplitudes and phase angles. The damping values, which are very important in determining the maximum wave amplitudes and the speed range over which a stationary wave is maintained, have been chosen to make the computed values of speed range correspond to equivalent experimental values.

2.5.1 Frequency Separation Methods

Two methods were used to achieve frequency separation the orthogonal modes. These are (i) clamping at a number of finite positions on a common circumference, (ii) having discs with a pair of diametrically opposite holes. Significant separation in the frequencies of orthogonal modes with 2 and 3 nodal diameters were sought.

Position Clamping

Fig. 2.2 shows a sketch of the clamping of a disc at four positions. Position clamping with the number of clamping pads of 2,3,4,6 were considered. According to the Zenneck rule, significant frequency separation occurred for modes with n nodal diameters when 2n is a multiple of the number of clamping positions. Therefore, clamping at 2 positions should lead to frequency separation in all modes except for the mode with zero nodal diameters. It is, however, not practical to clamp a disc at only 2 positions.

Asymmetric Holes

Fig. 2.3 shows a sketch of a centrally-clamped disc with a pair of opposite holes. The Zenneck rule, as earlier defined but replacing the number of clamping positions with the number of holes, applies. Experimental values of frequency separation in circular plates with drilled holes were obtained by Dugdale(35). The number of circular holes considered in this study was restricted to 2. This number is suitable for achieving significant frequency separation in the modes with 2 and 3 nodal diameters.

2.5.2 Stationary Wave Amplitudes

The energy quantities, in terms of the displacements of the two principal orthogonal modes, can be expressed approximately as follows;

$$T = \pi\rho h a^2(\dot{w}_1^2 u_{k1} + \dot{w}_2^2 u_{k2}) \tag{2.124a}$$

$$U = \frac{\pi D}{a^2}\left[w_1^2(u_{b1}+\bar{\Omega}^2 u_{i1}) + w_2^2(u_{b2}+\bar{\Omega}^2 u_{i2})\right] + \frac{\pi E}{2a^2}(u_{m1}+u_{m2})(w_1^2+w_2^2)^2 \tag{2.124b}$$

where u_{k1}, u_{k2} are the kinetic energy constants
u_{b1}, u_{b2} are the bending energy constants
u_{i1}, u_{i2} are the rotational energy constants
u_{m1}, u_{m2} are the membrane energy constants
w_1, w_2 are the wave amplitudes
$\bar{\Omega}$ is the speed ratio

In a stationary disc, the two orthogonal modes with the same number of nodal diameters can be excited separately. In a rotating disc, at and beyond the critical speed, the two modes are excited almost simultaneously. The equations of motion, similar to equation 2.102 become the following;

$$\frac{\partial^2 w_1}{\partial t^2} + 2\zeta p\frac{\partial w_1}{\partial t} + \bar{\omega}_1^2 w_1[1+\frac{\varepsilon_1}{h^2}(w_1^2+w_2^2)] = \bar{\omega}_1^2 w_{fn1}\cos pt$$
$$\frac{\partial^2 w_2}{\partial t^2} + 2\zeta p\frac{\partial w_2}{\partial t} + \bar{\omega}_2^2 w_2[1+\frac{\varepsilon_2}{h^2}(w_1^2+w_2^2)] = \bar{\omega}_2^2 w_{fn2}\sin pt \qquad (2.125)$$

where

$$\varepsilon_1 = 24(1-\nu^2)\frac{\bar{\omega}_{01}^2}{\bar{\omega}_1^2}\cdot\frac{u_{m1}}{u_{b1}},\quad \varepsilon_2 = 24(1-\nu^2)\frac{\bar{\omega}_{02}^2}{\bar{\omega}_2^2}\cdot\frac{u_{m2}}{u_{b2}} \qquad (2.126)$$

$$\bar{\omega}_1^2 = \frac{\bar{\omega}_{01}^2}{1-\frac{\bar{\omega}_{01}^2 u_{i1}}{n^2\Omega_0^2 u_{b1}}},\quad \bar{\omega}_2^2 = \frac{\bar{\omega}_{02}^2}{1-\frac{\bar{\omega}_{02}^2 u_{i2}}{n^2\Omega_0^2 u_{b2}}} \qquad (2.127)$$

$$w_{fn1} = \frac{Pa^2}{2\pi D(u_{b1}+\bar{\Omega}_1^2 u_{i1})};\quad w_{fn2} = \frac{Pa^2}{2\pi D(u_{b2}+\bar{\Omega}_2^2 u_{i2})} \qquad (2.128)$$

Writing $x_1 = \frac{w_1}{h}$, $x_2 = \frac{w_2}{h}$, $y_1 = \frac{w_{fn1}}{h}$, $y_2 = \frac{w_{fn2}}{h}$, $\tau = pt$, $\beta_1 = \frac{\bar{\omega}_1}{p}$, $\beta_2 = \frac{\bar{\omega}_2}{p}$, the relations in equation 2.125 become the following;

$$x_1''+2\zeta x_1'+\beta_1^2 x_1+\varepsilon_1\beta_1^2(x_1^3+x_1x_2^2) = \beta_1^2 y_1\cos\tau$$
$$x_2''+2\zeta x_2'+\beta_2^2 x_2+\varepsilon_2\beta_2^2(x_1^2x_2+x_2^3) = \beta_2^2 y_2\sin\tau \qquad (2.129)$$

Seeking approximate solutions of the form

$$x_1 = a_1\cos\tau + b_1\sin\tau$$
$$x_2 = a_2\cos\tau + b_2\sin\tau \qquad (2.130)$$

requires solving the following set of simultaneous equations.

$$a_1(1-\lambda_1^2)+2\zeta\lambda_1 b_1+\frac{\varepsilon_1}{4}[3a_1^3+3a_1b_1^2+3a_1a_2^2 + 2b_1a_2b_2 + a_1b_2^2] = y_1 \qquad (2.131a)$$

$$b_1(1-\lambda_1^2)-2\zeta\lambda_1 a_1+\frac{\varepsilon_1}{4}[3a_1^2b_1+3b_1^3+2a_1a_2b_2 +b_1a_2^2 + 3b_1b_2^2] = 0 \qquad (2.131b)$$

$$a_2(1-\lambda_2^2)+2\zeta\lambda_2 b_2+\frac{\varepsilon_2}{4}[3a_1^2a_2+b_1^2a_1+2a_1b_1b_2 + 3a_2^3+3a_2b_2^2] = 0 \qquad (2.131c)$$

$$b_2(1-\lambda_2^2)-2\zeta\lambda_2 a_2+\frac{\varepsilon_2}{4}[a_1^2b_2+2a_1b_1a_2+3b_2b_1^2 +3a_2^2b_2 + 3b_2^3] = y_2 \qquad (2.131d)$$

Pulsating Stationary Waves

When there is no significant frequency separation between the principal orthogonal modes, a standing wave results from the relation in equation 2.131. When significant frequency separation exists, a pulsating wave develops with the pulsating frequency f_p given by

$$f_p = \frac{N}{2n} \qquad (2.132)$$

where N is the rotational speed.

To the stationary observer, the wave formed at a constant speed will not move in the plane of the disc, being stationary. The wave will, however, pulsate(fig. 2.4) between the displacements derived in equation 2.131. The nodes of the pulsating wave, often, will not occur in the plane of the disc.

Equation Constants

The equation constants are similar to those described in the analysis of standing waves.

Damping ratio: In a standing stationary wave, the damping is not affected by air resistance in the transverse direction. The damping present in a pulsating stationary wave is affected by the pulsating amplitude of the wave. The damping value will, therefore, be higher for larger values of the pulsating amplitude. Consequently, the damping in a pulsating wave will be higher than in a corressponding standing wave. The pulsating amplitude decreases with increase in frequency ratio, but it is difficult to estimate the damping present in a pulsating stationary wave. With effective central clamping, the damping present in a disc rotating with a standing wave is much lower than in an oscillating stationary disc.

Nonlinearity ratio: The nonlinearity ratio values for the two modes are estimated to vary according to the values of the two natural frequencies. The value of this ratio for the higher frequency will, usually, be lower than the corresponding value for the lower frequency.

Force displacement ratio: The displacement ratios, w_{fn1}, w_{fn2}, are determined by using the energy coefficients corresponding to the natural frequencies. The displacement ratio is usually lower for the higher frequency.

Loading Effect

Weights were used to generate the stationary waves in the rotating discs. When there was a stationary wave, the weight would be hanging down with little or no movement. The mass of the applied weight therefore had some effect on the response characteristics of the disc. The effect can be considered as being an equivalent mass added to that of the plate. A reasonable approximation is to assume that the mass has less effect on the strain energy than on the kinetic energy. The effect on the strain energy is neglected and this is compensated for by adding only half of the load's kinetic energy. The modified kinetic energy expression becomes

$$T = \pi\rho a^2\dot{w}^2\left[u_k + \frac{m_f d^2}{8\pi nha^4}\right] \qquad (2.133)$$

where m_f is the mass of applied weight

n is the number of nodal diameters(n > 2)

d is the radius of loading

This assumption means that the critical speeds are dependent on the applied weights, and so are the values of some of the equation constants of equation 2.131.

Computation Procedure

For each applied load, the critical speed is found for the plate configuration. Values of force displacement ratio and nonlinearity ratio are determined, using the relations of equations 2.126 and 2.128. The damping ratio is chosen to make the computed collapse speed correspond to that of the equivalent experimental plate assembly. The wave amplitudes and phase angles are determined by solving the set of nonlinear simultaneous relations in equation 2.131, using the Newton method. When computation is for displacements of a standing wave, the frequency separation is taken to be zero.

2.6 Side-rubbing in Circular Saws

Stationary waves, especially in wood-cutting circular saws, are usually set up due to the presence of transverse forces arising from side-rubbing between the saws and the materials being cut. A saw will cut without binding if there is clearance at all points between the saw and the workpiece. Due to possible irregularities in the workpiece material (especially in natural materials like wood), the clearance is not constant. Timber, being a resilient material, after being cut tends to spring forward, thus reducing the expected clearance(37). When cutting through knots and pockets, the hard spots will deflect the saw blade. After the tool has passed the knot, the raised spot will travel along with the sawn timber thus reducing the clearance at that point on the timber.

Deflection at any position on the saw will depend on the radius and angular displacement of the point relative to the load line. Using a particular saw to cut thinner planks will reduce the incidence of side-rubbing as this will ensure that the deflection at the leading edge is not much greater than elsewhere.

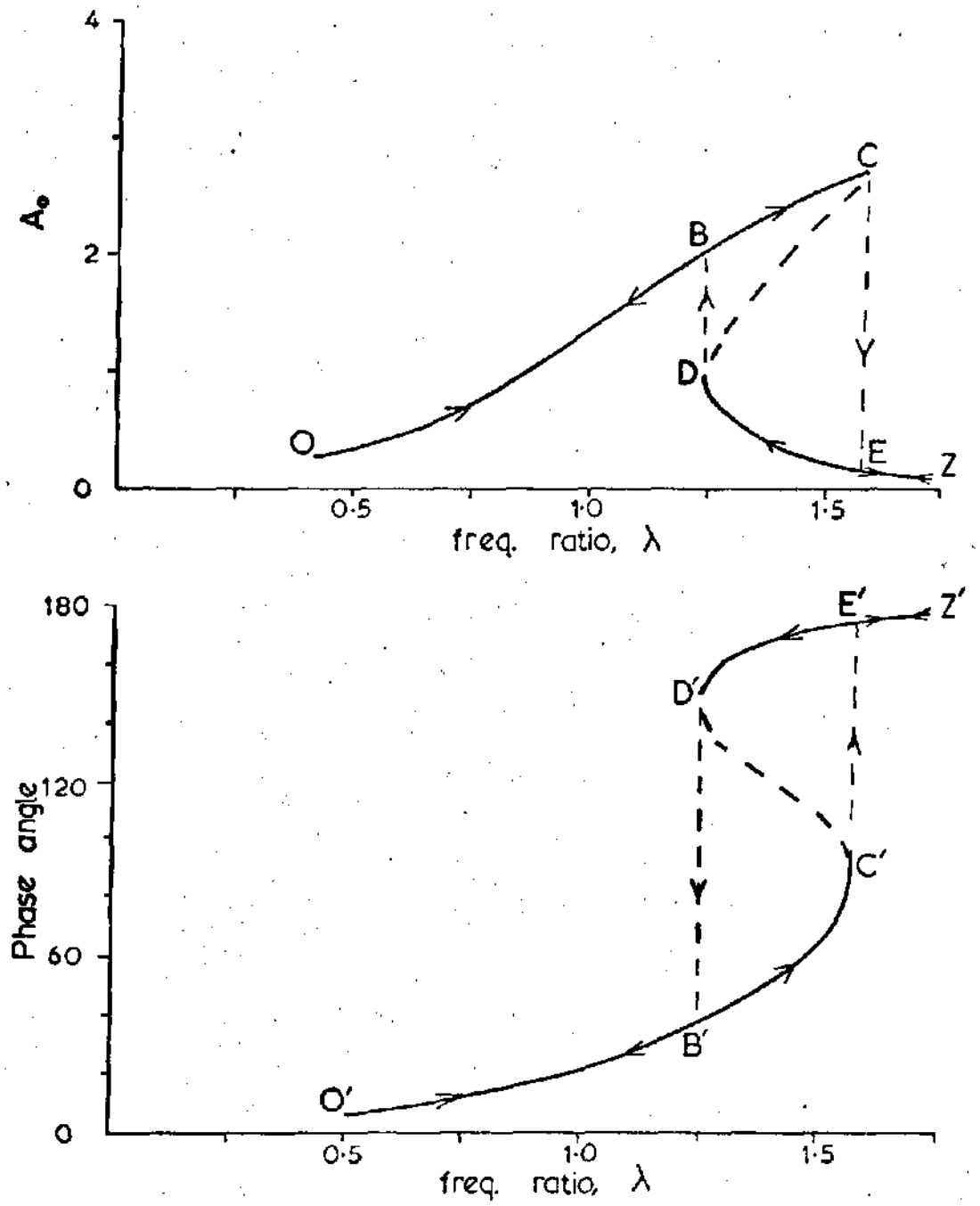


Fig. 2.1 RESPONSE CURVES FOR LARGE AMPLITUDE VIBRATION.

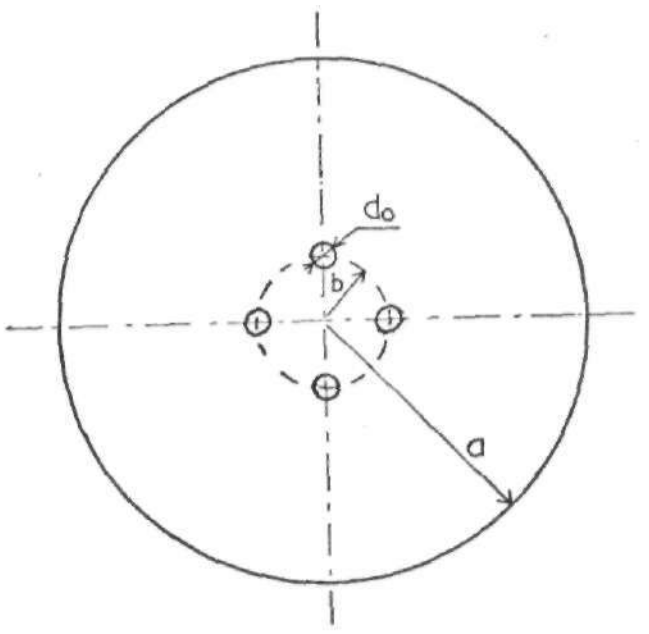


Fig. 2.2 4-POSITION CLAMPING OF A DISC, OF RADIUS a, AT RADIUS b WITH PADS HAVING DIAMETERS d_o.

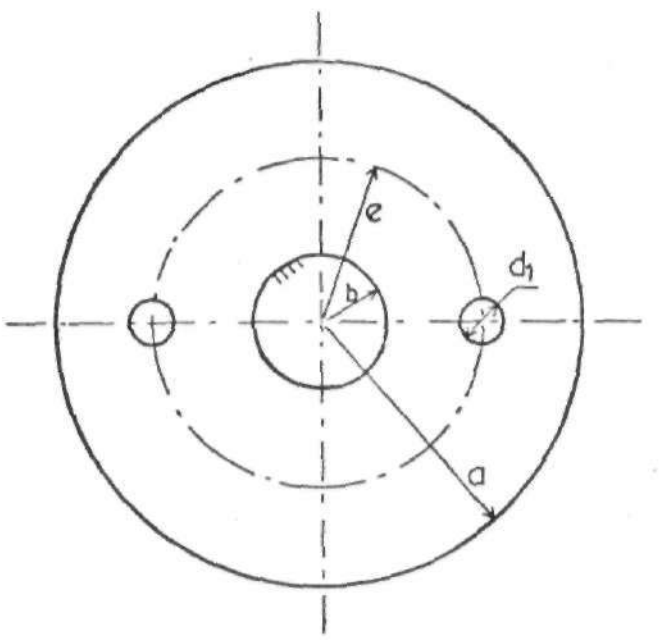
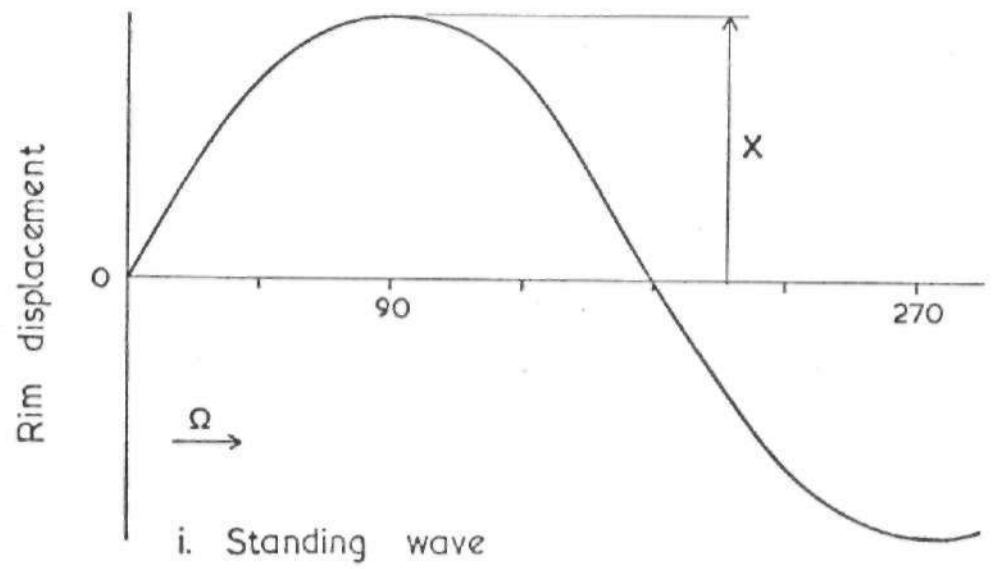


Fig. 2.3 A DISC WITH 2 HOLES OF DIAMETER d_1 AT RADIUS e, CENTRALLY CLAMPED AT RADIUS b.



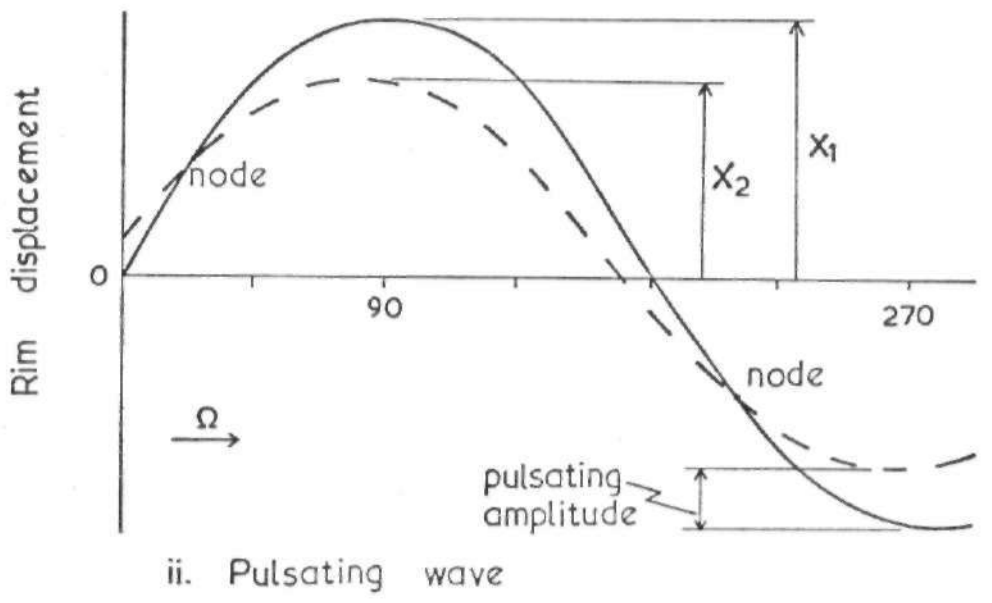


Fig. 2.4 STATIONARY WAVES IN ROTATING DISCS.

$\bar{w}/h$	Freq.[Exact]	Freq.[f*]
0.0	6.661	6.661
0.5	6.704	6.704
1.0	6.833	6.833
1.5	7.043	7.043
2.0	7.326	7.327
2.5	7.674	7.676

Table 1. RESPONSE FREQUENCIES FOR DIFFERENT VALUES OF RIM AMPLITUDES.

Chapter 3

EXPERIMENTAL METHODS

Three main types of frequency response tests were conducted. These are (i) the determining of natural frequencies of stationary discs, (ii) the determining of frequency response curves of travelling waves, and (iii) the determining of frequency response curves for large amplitude stationary waves. The experimental investigation also involved the preparation of disc specimens, the stress relieving of discs, the determination of damping values, and the determination of point-load stiffness coefficients.

3.1 Disc Specimens

The test discs were cut from flat cold-rolled mild steel sheets. The sheets had dimensions 1m by 2m. The thickness values of the various sheets were 0.95±0.03mm, 1.92±0.04mm, 3.08±0.05mm. The first set of discs, those with thickness around 3mm, were cut to outside diameter of 495mm with central hole diameter of 31.75mm. Some of the other discs were cut to outside diameter 457mm with central hole diameter of 31.75mm. The rest of the discs had outside diameter of 450mm and central hole diameter of 31.75mm.

The clamping discs were in pairs and had thickness

around 25mm. The flanges, clamping discs, had outside diameters of 101.6mm(4in), 152.4mm(6in), 203.2mm(8in), 254.0mm(10in). The central hole diameter of each of the clamping discs was 31.75mm. The clamping region on each pair of flanges is an annulus of radial width of about 12.5mm. In order to improve clamping, the flanges had threaded holes symmetrically located around their rims. The pairs of flanges with diameter 101.6mm and 203.2mm had four equally-spaced holes tapped on a circumference 12.5mm from the rim. The pair of flanges with diameters 153.6mm and 254.0mm had six holes. Some of the circular plates had corresponding holes to allow them to be assembled with flanges and bolts put through the threaded holes and tightened to improve the clamping effect.

The amount of runout present in the assembled plates depended on the clamping diameter and varied in the different plates. The maximum amount of runout occurred for the smaller flanges and the value in any of the test pieces was less than 0.60mm. A few of the discs that had too much runout were flattened by hammerring. This process would introduce some initial stress within the discs.

Some of the discs that were used for deriving frequency separation between the principal orthogonal modes each had a pair of equal-diameter diametrically opposed holes drilled. Three sets of holes were drilled,

with diameters 45.0mm, 67.5mm, and 90.0mm. The holes were centred on a circle radius of 157.5mm.

3.2 Stress Relieving

A photographic view of the furnace built for the relieving of initial stresses of plates is shown in fig. 3.1. The furnace could hold plates having outside diameter up to 500mm. The main frame of the furnace was made of angle-section steel. The furnace was covered on the outside by a 2mm thick steel casing. The inside enclosure of the furnace, made of 10mm thick heat-resistant material, had the dimensions 550X550X340mm. The space between the inside box and the outside casing was packed with refractory bricks. The top part of the furnace was removable for loading the plates into and out of the furnace.

The plates to be stress-relieved were covered in an anti-scaling paint, "Berkatekt 29". They were then packed, six together, between a 35mm thick plate on top and a 20mm thick plate at the bottom. The pack was placed on the turntable. This was in the centre of the furnace box and was operated by an electric motor. The motor turned the spindle through a belt and pulley at a speed of 9rpm. This slow rotation of the plates continued through the heating-up and cooling-down period, and was to ensure axial symmetry in the temperature distribution in the plates.

The heat in the furnace was provided by a set of 1kW electric bar heaters fitted to the top and bottom parts of the box enclosure. Power was supplied to the heaters through a number of "Variac" transformers. Temperature in the furnace box was measured using thermocouples introduced through small holes at the front part of the furnace.

With plates in the box and the lid closed down, refractory bricks were loaded lightly on top of the box. Some glass wool was then packed on the top. The supply power was switched on and was regulated to keep the furnace temperature about constant in the stress relieving temperature range for at least four hours. When the temperature was within the stress-relieving range, 650 - 750^{o}C, the variation of temperature within the furnace box was less than 10^{o}C. The cooling process could then begin. The heat input was reduced continually to achieve a cooling rate under 30^{o}C/hour. Once the furnace temperature had dropped below 100^{o}C, the cooling rate was hurried by removing part of the insulating material.

Having cooled down sufficiently, the plates were separated and soaked in a weak acid solution, one part hydrochloric acid(HCl) in twenty parts of water, to wash off the anti-scaling material. The thickness values for each of the plates were measured and so too was the amount

of runout when each of the plates was clamped between the 101.6mm diameter flanges. The natural frequencies of each plate were then determined experimentally and were compared with the values before the stress-relieving. The measured frequency was found to agree with the theoretical frequency to within 2 percent.

3.3 Natural Frequencies

The plate to be tested was clamped, at its centre between the selected pair of flanges, to the vibration bed(fig. 3.2). The excitation at varying values of frequency and amplitude, was provided by a vibrator driven by a frequency generator, through a power oscillator. Two types of exciters were used, a small vibrator and an electromagnet. When the vibrator was used, it was placed lightly in contact with plate surface. When the magnet was being used, it was about 5mm from the plate surface. The excitation frequency was shown on the frequency counter connected across the output of the power oscillator. The meter registered ten times the actual frequency. A sketch of the experimental set-up is shown in fig. 3.3.

Resonance was revealed by agitation of the sand particles initially spread over the plate. In a few tests, a capacitive probe was used to detect resonant vibration in the plate. The motion of the plate, picked up by the probe and passed through the transducer and amplifier, was

represented on the oscilloscope. This unit is shown in the dashed box in fig. 3.3. This allowed the resonant frequency to be determined more accurately, especially for modes of vibration with smaller number of nodal diameters($n<2$). The vibration amplitude was kept as small as possible when the frequency value was being measured.

Resonance in the plate occurred in a distinct mode of vibration. The mode was determined by the sand pattern on the vibrating plate. The sand particles collected in the areas around where there was no motion, that is adjacent to nodal lines. An example of the sand patterns is shown in fig. 3.4. The mode was represented by the number of nodal diameters and, if present, the number of nodal circles. It was sometimes difficult to get distinct mode patterns for modes represented by $n=0$ and $n=1$, especially when the frequencies for two modes were close.

When the excitation was set up by the electromagnet, the frequency value shown on the counter was half of the true excitation frequency, as the force is proportional to the square of the magnet current. Tests were carried out to find frequencies for each disc, clamped between different flanges, for modes of vibration having up to five nodal diameters.

3.3.1 Orthogonal Modes and Frequency Separation

In each mode, except in the mode with zero nodal diameters, the resonant vibration was excited for both orthogonal modes. The nodal diameters of the two configurations were displaced by approximately a quarter of a wavelength, with the positions of the nodal diameters of the one corresponding to the antinodal positions of the other. The frequency testing of discs with two holes showed this effect clearly(fig. 3.5), with significant frequency separation in the principal orthogonal modes n=2 and n=3. Position clamping(fig. 2.2) utilised 10mm diameter washers between the flanges and the disc. The mode shapes resulting from position clamping were, sometimes, very different to corresponding mode shapes in centrally-clamped discs.

3.4 Travelling Waves

Speed tests were conducted with the disc, between a pair of flanges, rigidly clamped on a spindle. The spindle, in ball bearings, was rotated by a d.c. motor. The drive of the motor was connected to the spindle via a belt and pulley arrangement and the spindle could be driven at speeds up to 6000rpm. The speed control was by using a "Variac" transformer. The speed was measured using a magnetic transducer and a frequency counter, and the speed was maintained within ±5rpm.

The excitation of the rotating disc was provided by an electromagnet, a force excitation similar to the one described in section 3.3. Disc motion was monitored on an oscilloscope. The signal was detected by a capacitive probe and passed through a demodulator, an amplifier and a frequency analyser, and then to the oscilloscope. Fig. 3.6 shows a sketch of the testing equipment and disc.

Resonant plate vibration occurred when the excitation frequency was equal to the frequency of the forward or reverse travelling wave. When the disc was rotating at a constant speed, the excitation frequency was varied until the oscilloscope and the frequency analyser reading indicated resonance. The wave amplitude was checked by filtering the signal, with the frequency analyser set at $\frac{1}{10}$ octave bandwidth, at the excitation frequency. When the same signal was filtered at the alternative frequency, the wave amplitude was about the same as obtained at the excitation frequency. This alternative frequency, f_a, is given by the following relation.

$$f_a = f_e \pm 2nN \qquad (3.1)$$

where f_e is the excitation frequency in Hz,

N is the disc speed in c/s,

n is the number of nodal diameters.

This was also an effective way of determining which mode of vibration was being excited. In the mode with zero number of nodal diameters, there are no travelling waves. Having found the wave frequencies corresponding to one mode of vibration, the other frequencies, below 300Hz, were found at the same speed. This procedure was repeated at other speeds to obtain data representative of the frequency-speed curves, for speeds up to 4000rpm.

The test equipment would not give reliable information below 10Hz and, therefore, wave frequencies were not determined for values below 15Hz. Speed-frequency curves were determined for modes with up to five nodal diameters. An example of speed-frequency data is shown in fig. 3.7.

3.5 Damping Values

Tests to determine damping values were carried out with the vibrating disc stationary and, separately, when rotating at different speeds. The plate deflection was picked up by the capacitive probe and displayed on the oscilloscope. The probe was set 5mm from the disc near its rim. The 'scope reading was calibrated by subjecting the position on the rim of the disc opposite the probe to known static deflections. These readings were used to obtain the calibration curve shown in fig. 3.8.

The test disc was excited at one of its resonant

frequencies and the excitation was then cut off. The decay pattern, stored on the oscilloscope, could then be photographed. This procedure was repeated with the disc clamped between different flanges. The tests were conducted for modes with number of nodal diameters up to four($n < 4$). Fig. 3.9 shows an example of the decay patterns obtained.

3.6 Stiffness Coefficient

Tests to determine disc point-load stiffness coefficient were carried out with the disc clamped, between a pair of flanges, on a rigid frame. Fig. 3.10 shows the testing equipment and set-up. The load was applied within 0.5mm of the rim of the disc. Readings of deflection against applied load were taken and more weights were added until the plate deflection got to about half of the plate thickness. Similar readings were taken while unloading the weights.

3.7 Stationary Wave Amplitudes

Tests for determining stationary wave amplitudes were carried out in an experimental set-up similar to that used in the tests for travelling wave response frequencies(section 3.4).

3.7.1 Critical Speeds

The critical speeds occurring before 5000rpm were determined by using an apparatus similar to the one described by Dugdale(13). Twelve soft brass springs were positioned, as contacts, evenly along the rim of the disc. The contacts were mounted on a perspex bracket rigidly bolted to the frame. The gap between each of the contacts and the disc was set to 1mm. Each of the contacts was connected, in an electrical circuit, to a 12 volt light bulb. The bulbs were mounted on a wooden board in the order as the corresponding contacts. The mode of the standing wave formed in the disc was determined by the pattern of lights on the board as the electrical circuit was completed by contact of the disc with any of the spring contacts. The speed-frequency response curves, already obtained, made the location of the critical speeds easier.

3.7.2 Loading Method

When the disc was rotating at a speed approaching the critical speed of the mode to be excited, a constant force was applied, acting about 8mm from the rim of the disc. An air jet from a 3mm diameter nozzle was initially used to apply the force. This method was discontinued when it was found that the force applied by the air jet was not large enough and the force magnitude was dependent on the gap between the nozzle and the disc.

The method later used involved having known weights suspended over a pulley with the force acting on the disc through a soft spring. The spring was made of a thin brass sheet with the dimensions 55.0X12.5X0.4mm. The sheet had a 4mm diameter hole drilled 10mm from one end. The sheet was then bent to a U-shape with the ends 15mm apart. The end with the hole was attached, using a bolt, to the lower end of a pendulum arrangement. The pendulum was connected, using a rigid link attached to its lower end, to the other side of the disc. The rigid link had a string attached to it, passing over a pulley, which ended in an open loop for attaching the weights.

3.7.3 Disc Displacements

The rim displacement of the disc was detected using capacitive probes, similar to the one used in the tests for determining the response frequencies of the travelling waves. Three identical probes were mounted on the perspex bracket, earlier described, with the spring contacts removed. One probe was mounted opposite the point of loading, the next was placed at an angle of 45° away from the first in the direction of rotation of the disc, and the third was placed 90° away from the first one. All the probes were mounted on the circumference of the circle, concentric with the centre of the disc, with diameter of 390mm. The probes were mounted 5mm away from the disc surface.

The probes were connected using identical screened cables of equal lengths to a selector switch box. A cable connected the selector box through the capacitive transducer oscillator to the F.M. demodulator and hence to the oscilloscope. The oscilloscope reading of the signal from the probes was calibrated against the deflection of the disc at the rim. The calibration curve is the same as earlier referred to in fig. 3.8.

The selector box was used to select the signal from any of the three probes. At any constant disc speed, the rim displacements were determined at the positions

corresponding to the locations of the probes. When a stationary wave was generated, the displacement profile would take the shape, to the stationary observer, of the wave corresponding the mode excited. The three probes were, therefore, sufficient to determine the sinusoidal profile corresponding to the stationary waves for the modes with 2 and 3 nodal diameters. The disc displacement values were taken at suitable intervals of the plate speed until collapse of the wave occurred. Fig. 3.11 shows an example of the rim displacement profiles at different speeds. The phase angle corresponds to the angular position at which the maximum displacement occurs divided by the number of nodal diameters, n.

3.7.4 Jump and Collapse Speeds

The speed at which a jump occurred from the lower to the higher stationary wave amplitude was determined by running the disc at a speed higher than the speed at which collapse of large amplitude wave occurred. The speed of the disc was then reduced steadily until the jump in the wave amplitude occurred. The wave amplitudes at the lower branch were found to be too small to measure, as they were of the order of the runout present in the disc. The collapse speed was taken as the speed at which collapse of the stationary wave started to occur.

3.7.5 Pulsating Stationary Waves

The amplitudes of a pulsating stationary wave were determined by measuring the maximum and minimum values shown on the oscilloscope for each probe. Appropriate displacement sinusoidal profiles were then drawn through the three pairs of displacement values . The amplitudes and phase angles were determined at the various test speeds. The jump and collapse speeds were determined in a manner similar to those for the standing stationary wave.

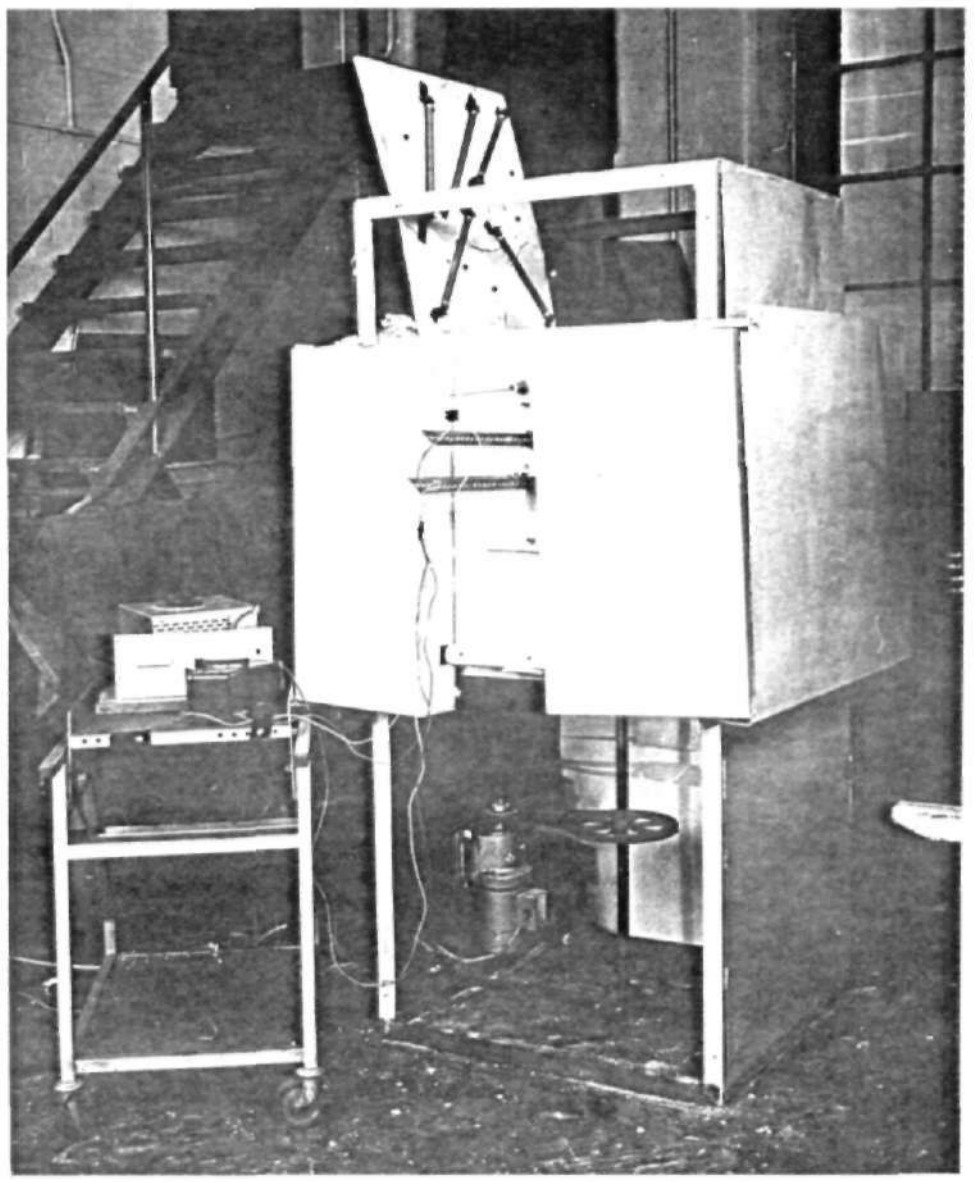


Fig. 3.1 STRESS - RELIEVING FURNACE.

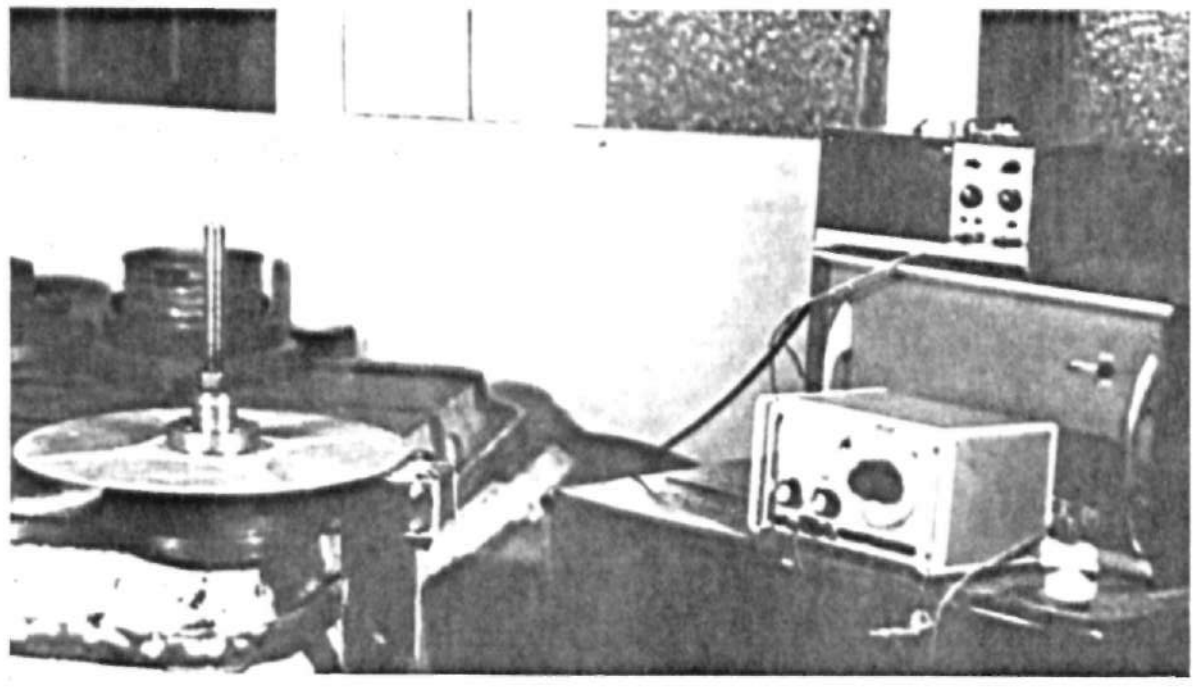
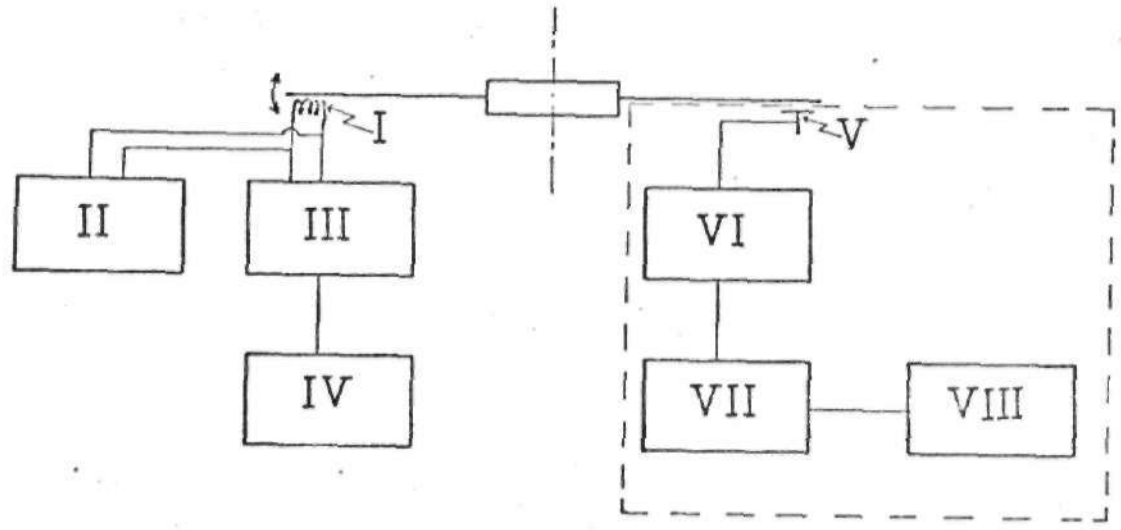


Fig. 3.2 TESTING OF A VIBRATING STATIONARY DISC.



I — Electromagnet
II — Frequency counter
III — Power oscillator
IV — Frequency generator
V — Capacitive probe
VI — Capacitive transducer oscillator
VII — F. M. demodulator
VIII — Oscilloscope
IX — Magnetic transducer
X — Frequency analyser

Fig. 3.3 FREQUENCY TEST RIG FOR A STATIONARY DISC.

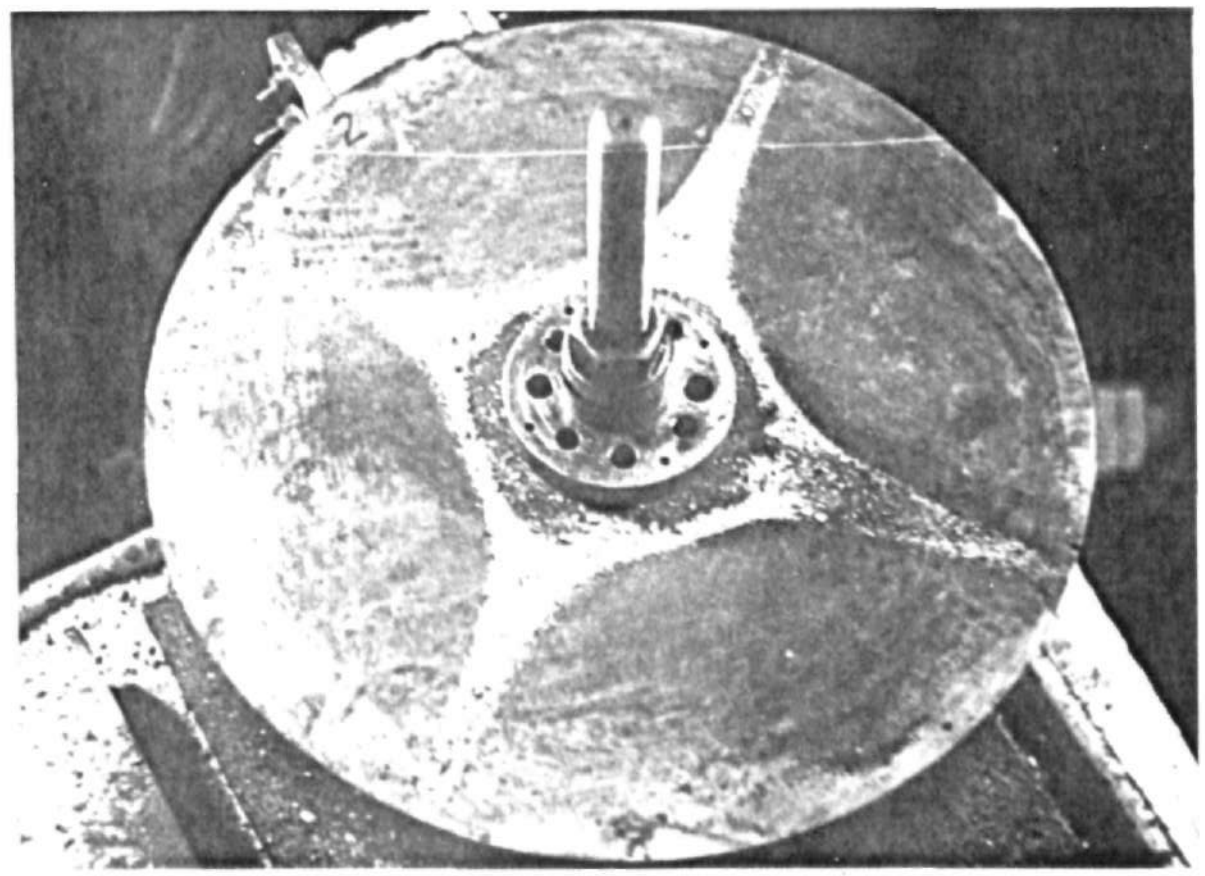


Fig. 3.4 A SAND PATTERN FOR THE MODE n = 2.

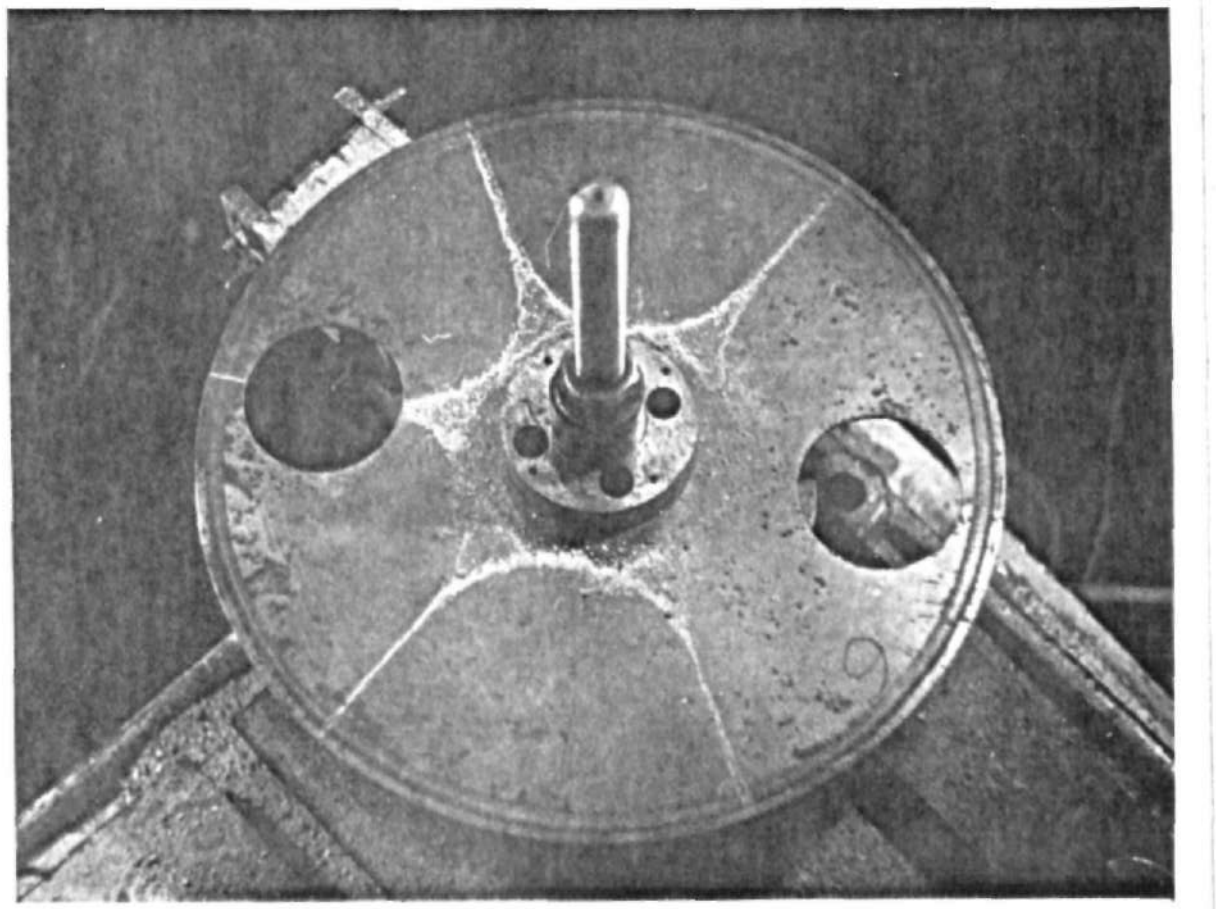
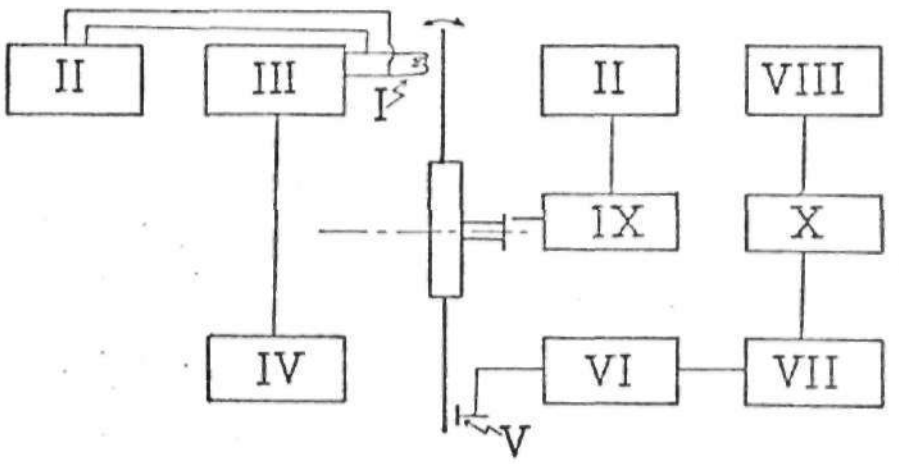


Fig. 3.5 A SAND PATTERN IN A DISC WITH TWO HOLES (n = 3).



I — Electromagnet
II — Frequency counter
III — Power oscillator
IV — Frequency generator
V — Capacitive probe
VI — Capacitive transducer oscillator
VII — F. M. demodulator
VIII — Oscilloscope
IX — Magnetic transducer
X — Frequency analyser

Fig. 3.6 FREQUENCY TEST RIG FOR A ROTATING DISC.

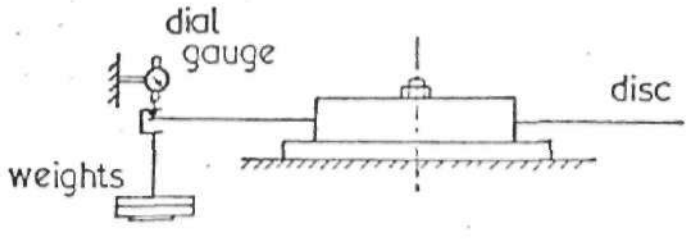


Fig. 3.10 DETERMINING THE POINT-LOAD STIFFNESS OF A DISC.

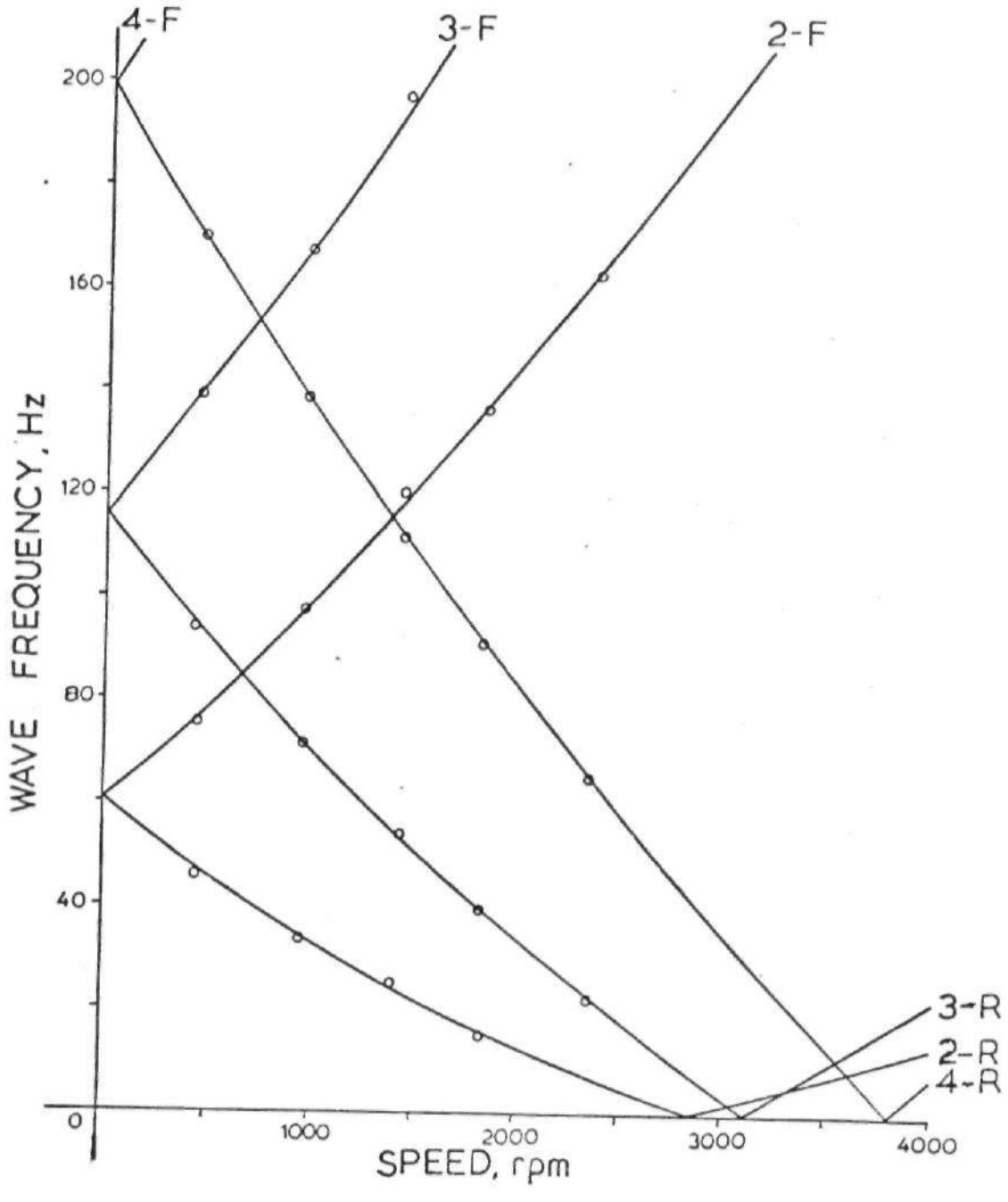


Fig. 3.7 TRAVELLING WAVE FREQUENCIES FOR A CENTRALLY CLAMPED DISC.

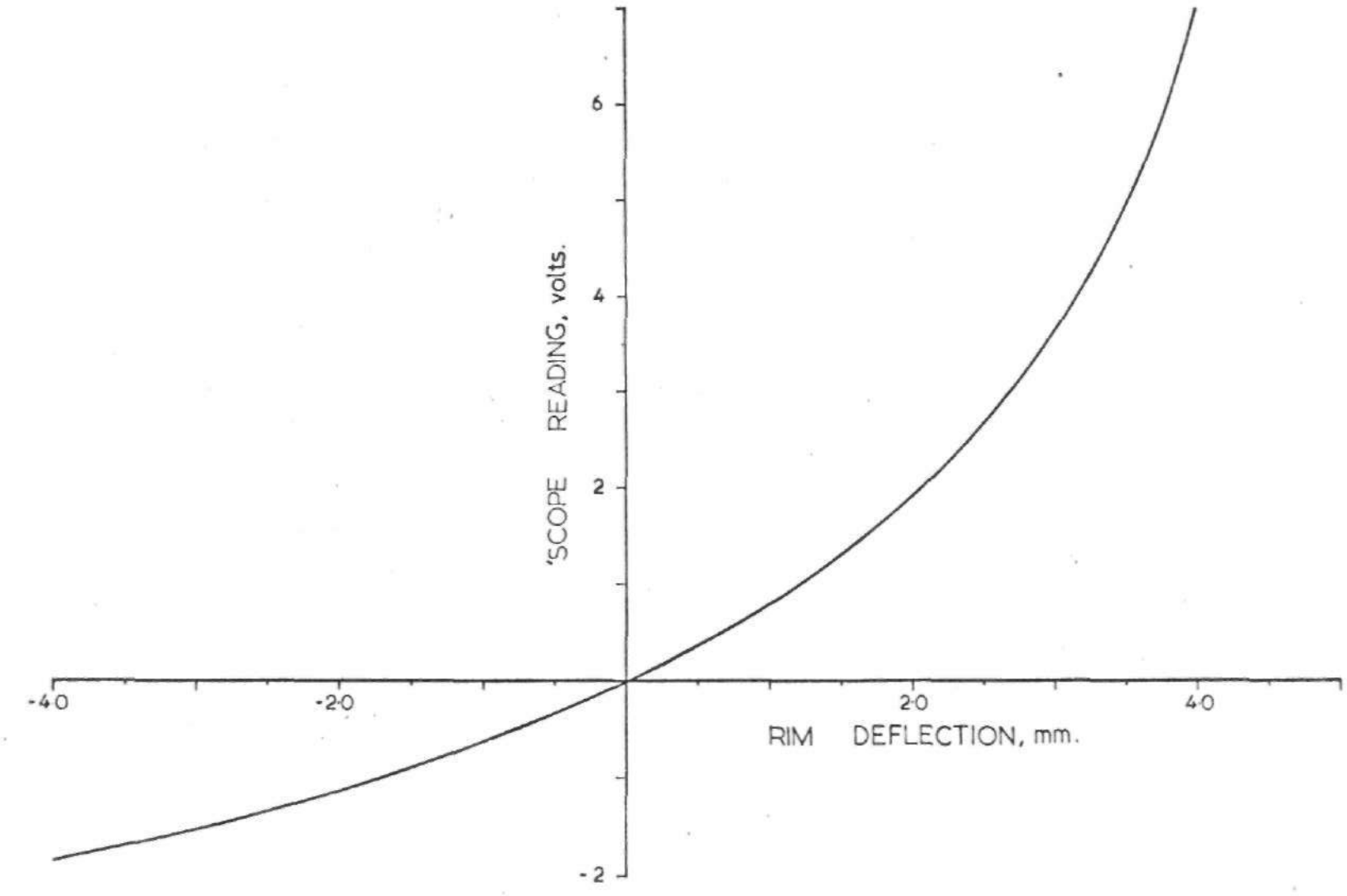


Fig. 3.8 CALIBRATION CURVE FOR THE CAPACITIVE PROBE READINGS.

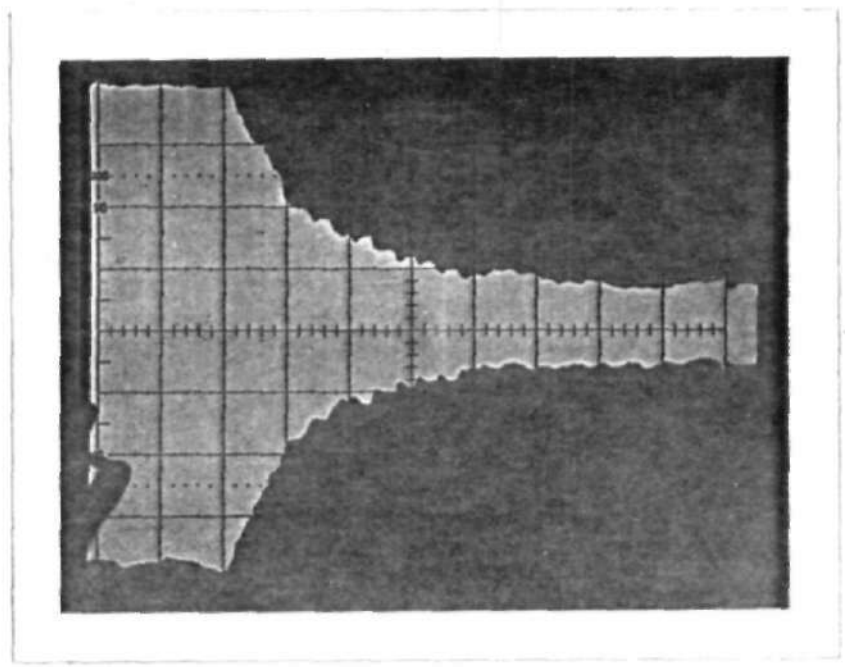


Fig. 3.9 PATTERN OF A DECAYING OSCILLATION (n = 3).

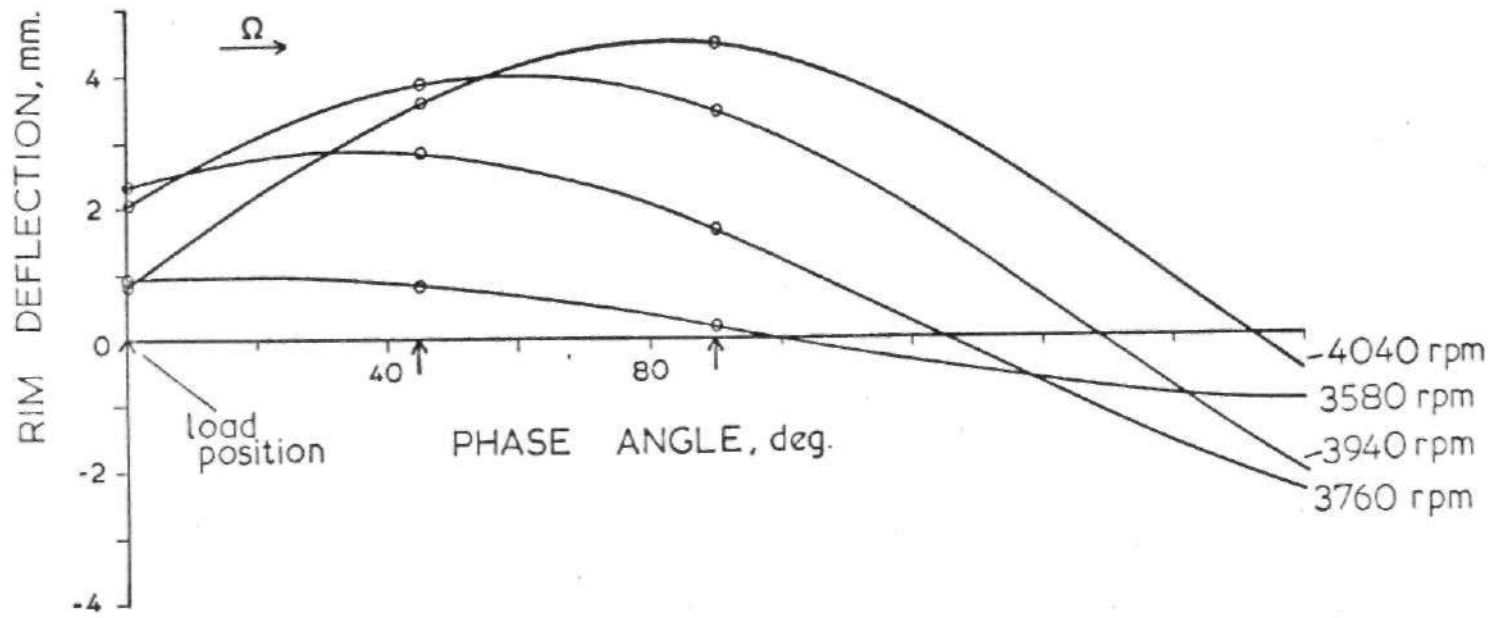


Fig. 3.11 RIM DISPLACEMENTS, AT DIFFERENT SPEEDS, OF A DISC IN WHICH A STATIONARY WAVE HAS BEEN FORMED (n = 2).

Chapter 4

RESULTS

There was variation in the dimensions of many of the discs used in the tests and, therefore, many of the results are presented in non-dimensional quantities. The majority of the experimental values were determined using the 2mm thick plates. The 1mm thick plates were found to have too much initial stress and the stress relieving method did not reduce the stresses below the level under which their effect on the vibration characteristics would be negligible. The 3mm thick plates, while relatively unaffected by the presence of initial stresses, had their critical speeds too high for the electrical motor used for driving the discs.

In many cases, only representative results have been given in this thesis. The discussion of the results and the conclusions arrived at are, however, based on the whole of the results obtained. The equivalent theoretical results were obtained using computer programs, including those in the appendix, based on the theory discussed in chapter 2.

4.1 Membrane Stresses

The membrane forces/length were derived by assuming that the relative transverse displacement values are not significantly affected by vibration amplitude, especially in the range in which the amplitude ratio y (the ratio of the maximum rim displacement to the plate thickness), is less than 2.5. The values were found by assuming that the plate is solid at the centre. Experimental evaluation of the membrane stresses was not carried out.

The stress values were calculated using subroutine MSTRE, given as part of the program MRAYL in the appendix. The transverse displacement, slope, and curvature values derived from one of the three programs BESSL, MRAYL, RRITZ, could be used as input to the subroutine. The membrane forces/length due to the symmetric and harmonic components of the stress function F are presented as separate values in figs 4.1 to 4.5 in terms of the nondimensional membrane force per length $\bar{N}$, which is defined as follows;

$$\bar{N} = \frac{N}{Eh\frac{\bar{w}^2}{a^2}} \qquad (4.1)$$

The graphs show that at points on the rim, harmonic membrane force/length in the θ-direction is positive at the nodal points and negative at the antinodal points, that is, it varies sinusoidally as $2n\theta$. A simple physical

explanation of the sign of this stress is that at the node, an element of rim is twisted out of its plane and therefore becomes increased in length, so the stress is tensile here. The graphs show the membrane forces/length due to the symmetric stress function, but only show those values due to the harmonic stress function that are significantly large.

4.2 Energy Constants

The following energy constants, u_b, bending strain energy constant, u_i, rotational interaction strain energy constant, u_m, membrane strain energy constant, and u_k, the kinetic energy constant, were found using the program MRAYL, listed in the appendix. The value of these energy constants, for values of clamping ratio between 0.1 and 0.5 are given in figs 4.6 to 4.10 for the modes n = 0,1,2,3,4. The constants are given as curves of the values of u_b, $\frac{u_b}{u_k}$, $\frac{u_i}{u_b}$, $\frac{u_m}{u_b}$. Experimental evaluation of the energy constants was not carried out. Fig. 4.11 shows the speed ratio values, $\bar{\Omega}$, at which the critical speeds occur, determined using the energy constants.

4.3 Natural Frequencies

The natural frequencies are given as the nondimensional parameter χ. Fig 4.12 shows some of the experimental values, with the continuous line representing the theoretical values.

The exact values were evaluated using program BESSL. Similar values were derived using the programs MRAYL and RRITZ, based on the modified Rayleigh and the Rayleigh Ritz methods, respectively, as described in chapter 2. Values from the three programs are given in table 2. Some of the values derived using the "PAFEC" finite element program are given in table 3. The frequencies were derived by dividing the disc into 32 isoparametric elements, each element having 8 nodes.

4.4 Mode Shapes

The plate transverse displacement and its derivatives can be derived using any of the three programs; BESSL, MRAYL, RRITZ. The "PAFEC" program could give displacements and slopes at the nodes. The second derivative of the transverse displacement, hereafter referred to as the curvature value, is the highest order derivative required in the computation of the energy values. Values of the displacement and its first derivative, the slope, can be derived from the curvature values by integration. Table 4 gives values of displacement, slope, and curvature, for a

particular plate configuration, derived from the programs BESSL, MRAYL, and RRITZ. Table 4 shows that small variations in the values of the plate displacement and slope often lead to significant variation in the curvature values. Deriving the displacement and slope values from the curvature values will, therefore, lead to more accurate results. The exact curvature values for a disc vibrating linearly, are given in table 5.

4.5 Compliance Coefficients

Compliance coefficients are presented in the forms defined by Dugdale(13), with the deflection under point load, P, at the rim being expressed as follows;

$$w(1,\theta) = Q\sum_{0}^{\infty} c_n \cos n\theta, \quad w(1,0) = QC \tag{4.2}$$

$$\text{where } Q = \frac{12(1-\nu^2)Pa^2}{\pi Eh^3}$$

The values for c_n are found from the analysis given for determining the values of the force displacement ratio in chapter 2, with the modal compliance coefficient being related to the strain energy constant by the following expression.

$$c_n = \frac{2}{u_b} \tag{4.3}$$

Fig. 4.13 shows values for the modal compliance

coefficients derived using the above relation, with values from reference (13). Fig. 4.14 shows a curve for the compliance coefficient, C, with experimentally determined values, values derived by the finite element method, and values from reference (13).

4.6 Nonlinearity Ratio

Values of the nonlinearity ratio, ε_0 , for the stationary disc, are given in fig. 4.15. Values of the nonlinearity ratio ε for a disc rotating at a known speed can be found readily from these values, providing the speed-corrected response frequency for the disc is known. Fig. 4.15 also shows equivalent values of nonlinearity ratio taken from reference (26).

4.7 Damping

Sample experimental values from the various tests for discs with similar clamping ratio and mode patterns are plotted for the modes n=2 amd n=3, in figs. 4.16 and 4.17. Values of natural logarithms of the displacement ratio $\frac{\overline{w}}{h}$ are plotted against time, in seconds, from the start of decay of disc oscillation.

4.8 Frequency Separation

Frequency separation values are presented, in terms of the nondimensional frequency parameter χ, for finite position clamping and for discs with two opposite identical circular holes. In the case of position clamping, the disc was clamped at a number of evenly spaced positions along the circumference of a circle concentric with the axis of the disc, using small diameter washers. The results presented are for discs clamped with washers having outside diameters of 10mm. The tests showed that the frequency separation could often be increased by reducing the area of the clamping pads. Figs. 4.18, 4.19, and 4.20 show experimental and finite element frequency response values, for a disc clamped at 6 positions,4 positions,and 2 positions respectively, for the mode of vibration n=2, n=3.

The natural frequencies of discs having two circular holes, with hole centre at a radius ratio to the outside radius of 0.7, were found for the different clamping ratios. Experimental and finite element frequency values against the ratio of hole area to the plate area are presented in figs. 4.21 to 4.24, for the modes n=2 and n=3, and the two clamping ratios α=0.226 and α=0.339. The hole area is the combined area of the two equal-sized opposite holes and the plate area is taken as the area of

a solid circle with the same outside radius.

4.9 Standing Wave Amplitudes

Wave amplitudes of standing waves, for the modes n=2 and n=3, for different applied forces are shown in figs. 4.25 and 4.26. The graphs show the theoretical estimates, for the different applied forces, in continuous lines and the experimental values at discrete positions. The graphs show the wave amplitudes until collapse of the wave. The theoretical values were obtained, using the nonlinearity ratio and force displacement ratio values that are dependent on the energy constants of the rotating discs. Damping ratio value of ζ=0.0013 was used in the theoretical calculations.

Figs. 4.27 to 4.29 show graphs of theoretical estimates of the square root of the displacement ratio, $\sqrt{x}$, against the speed ratio, $\bar{\Omega}$, for values of clamping ratio 0.1, 0.3, and 0.5. The standing wave amplitudes, were determined using a damping ratio value of 0.0013, and are shown for different values of the force displacement coefficient y', where y' is given as follows;

$$y' = y.u_b\left(1 + \bar{\Omega}^2\frac{u_i}{u_b}\right)^{\frac{1}{2}} \qquad (4.4)$$

4.10 Pulsating Wave Amplitudes

Fig. 4.30 shows examples of pulsating wave amplitudes in a disc with 2 holes. Fig. 4.30 also shows the envelope curve, in non-dimensional quantities determined from experimental values, for the pulsating stationary waves. Fig. 4.31 shows curves of maximum wave amplitudes for different values of percentage frequency separation, for different values of the force displcement coefficients.

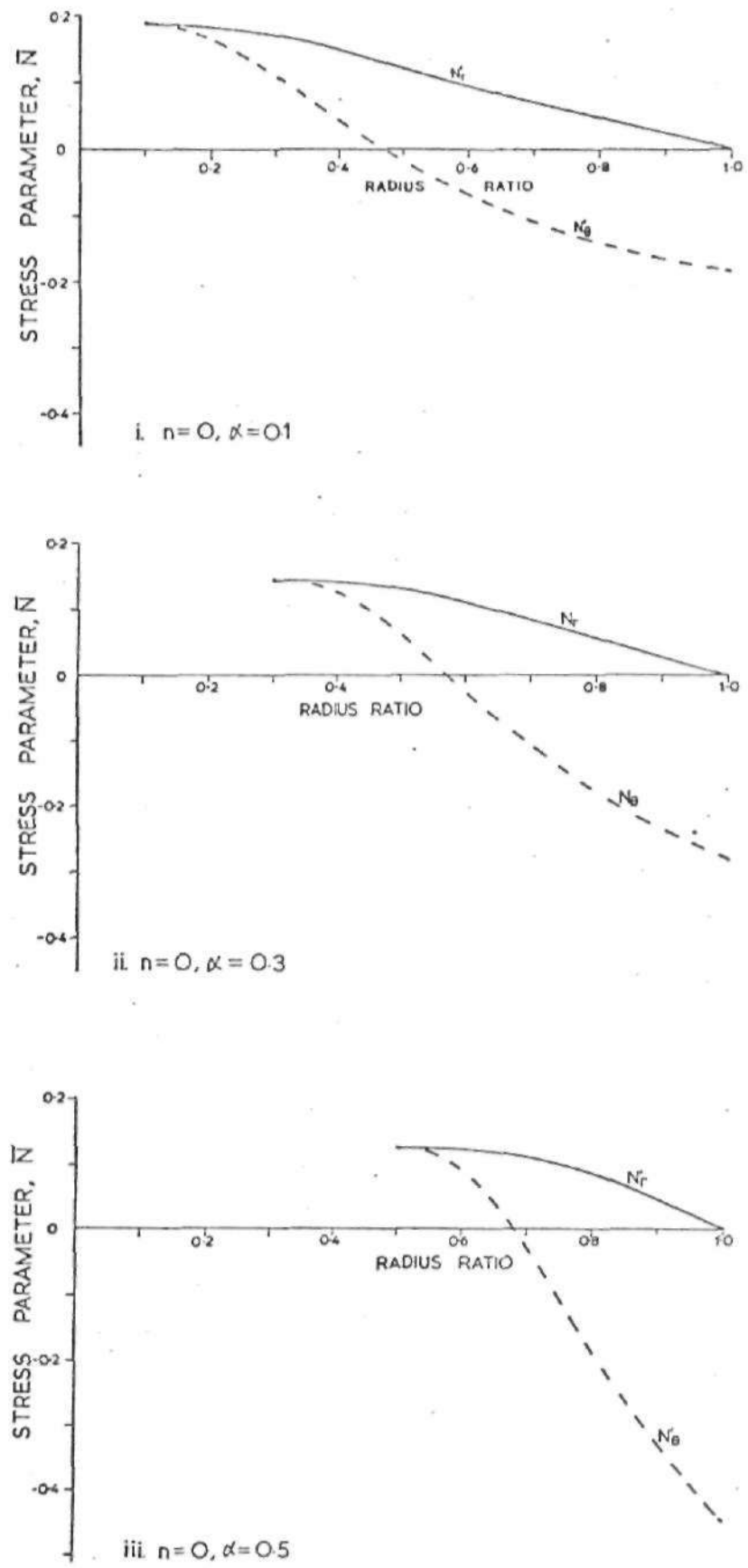
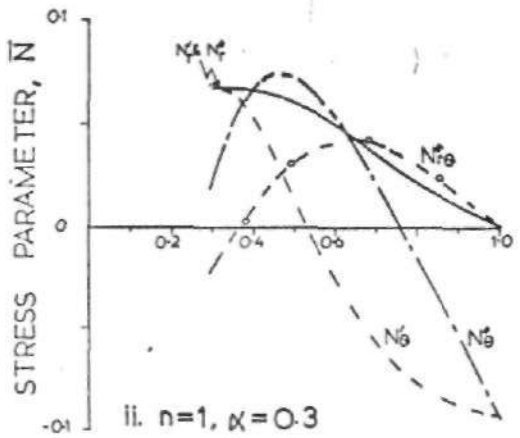
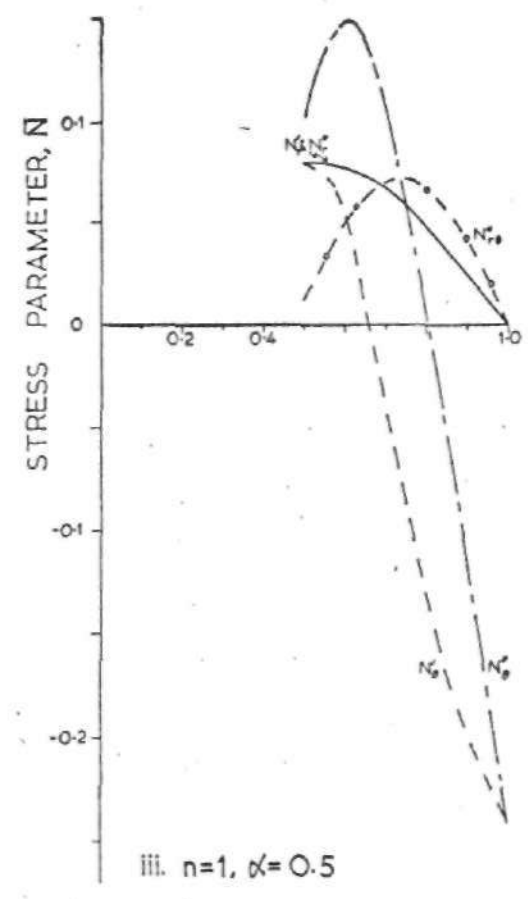


Fig. 4.1 MEMBRANE FORCES/LENGTH FOR THE MODE n = 0.





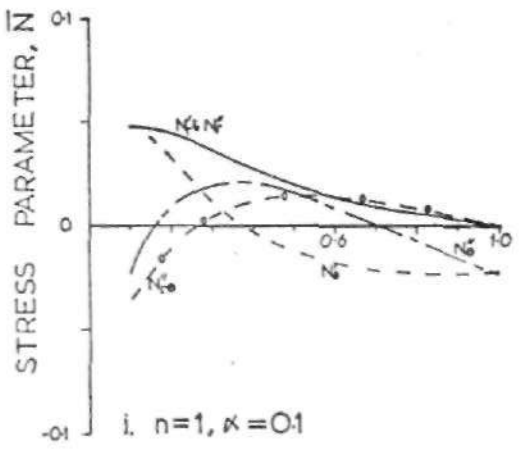


Fig. 4.2 MEMBRANE FORCES/LENGTH FOR THE MODE n = 1.

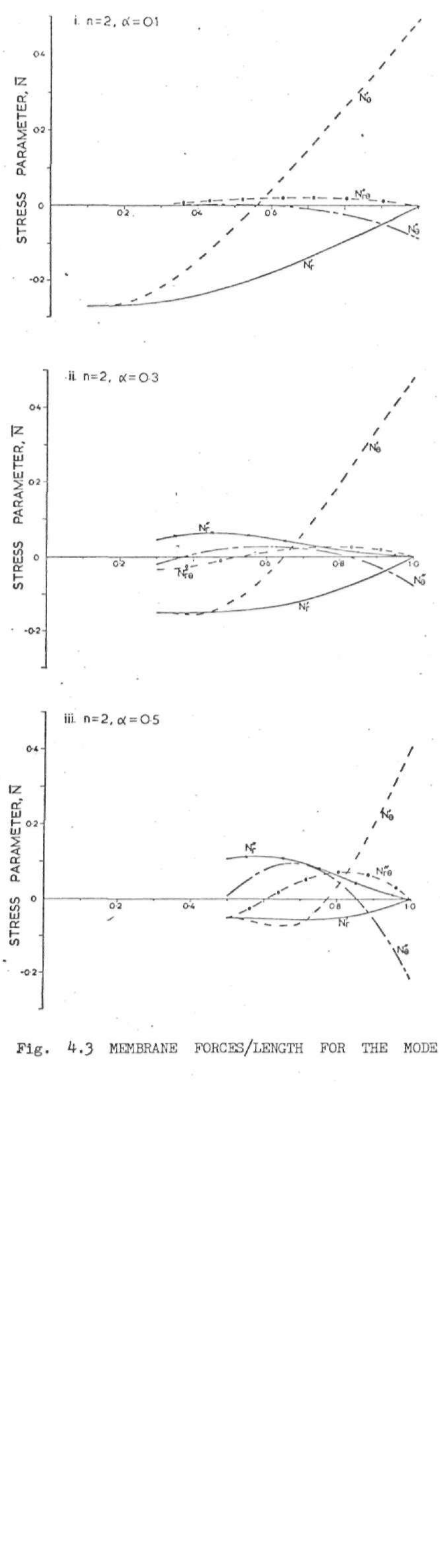
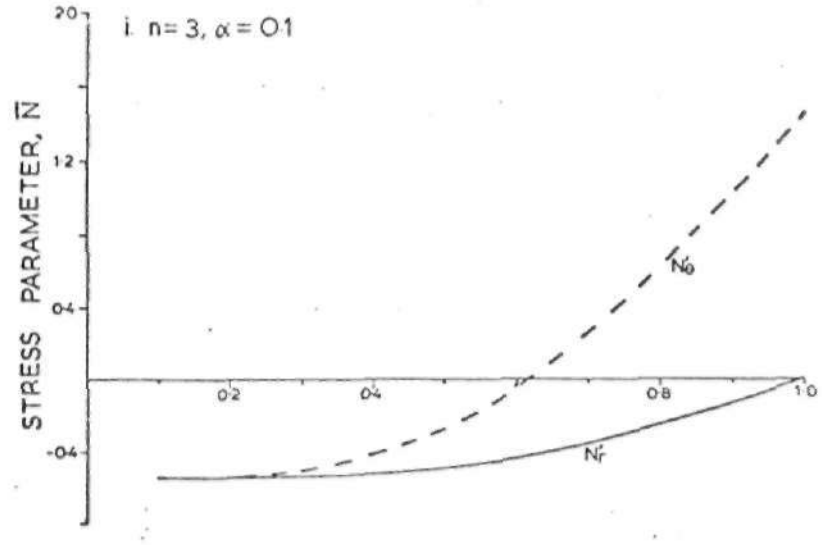
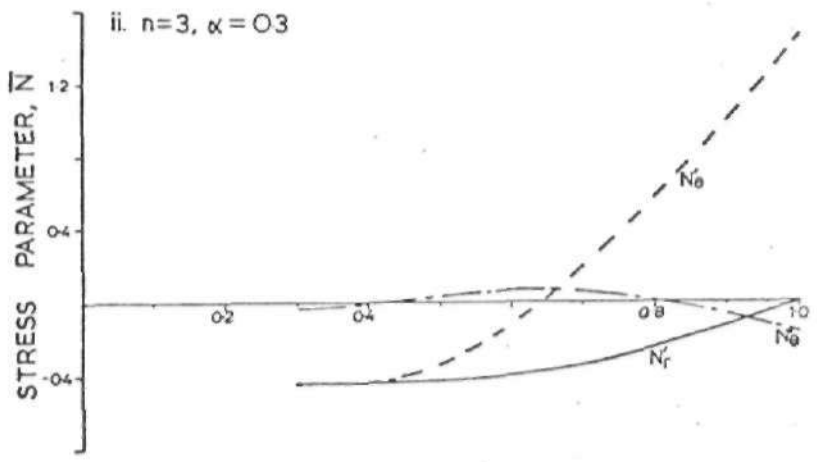


Fig. 4.3 MEMBRANE FORCES/LENGTH FOR THE MODE n.= 2.





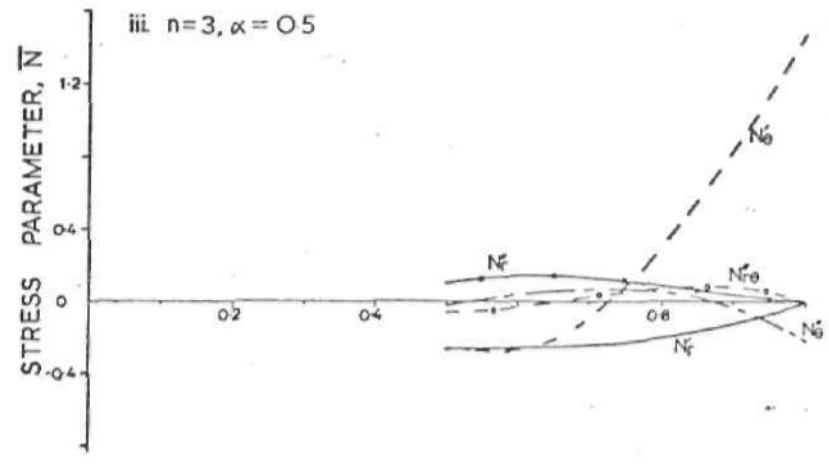


Fig. 4.4 MEMBRANE FORCES/LENGTH FOR THE MODE n = 3.

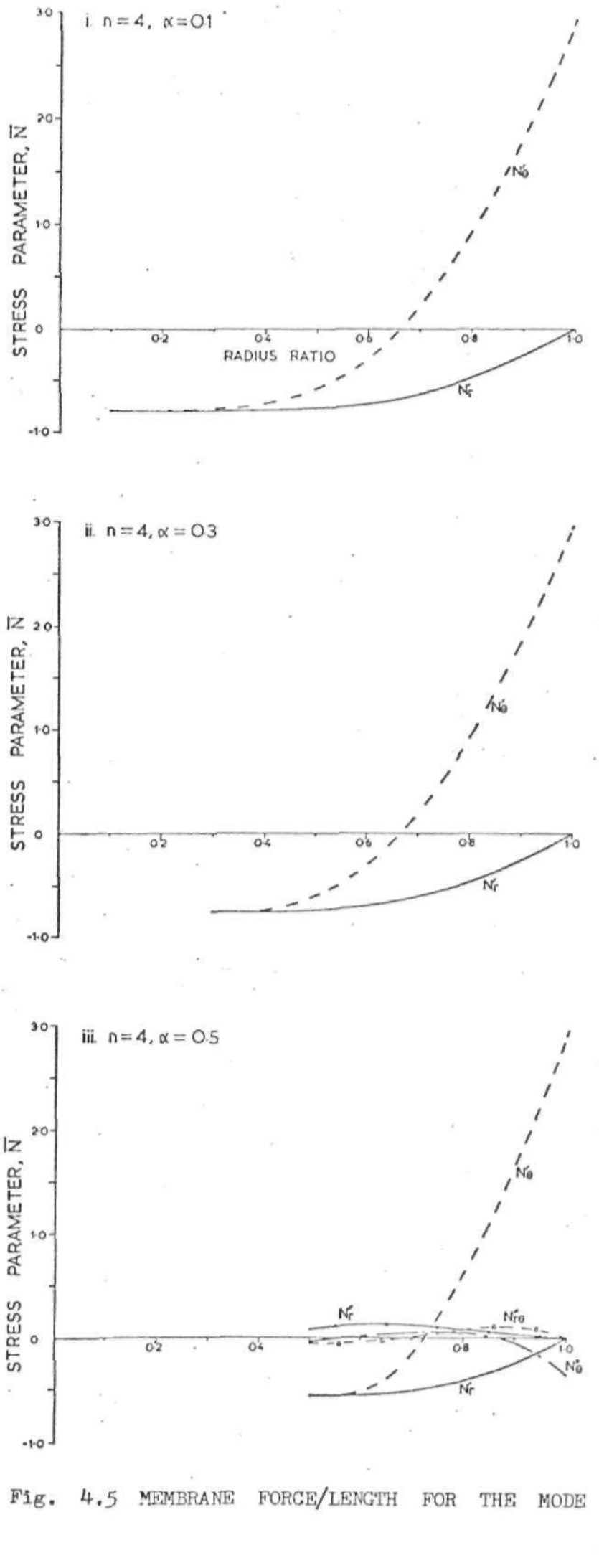


Fig. 4.5 MEMBRANE FORCE/LENGTH FOR THE MODE n = 4.

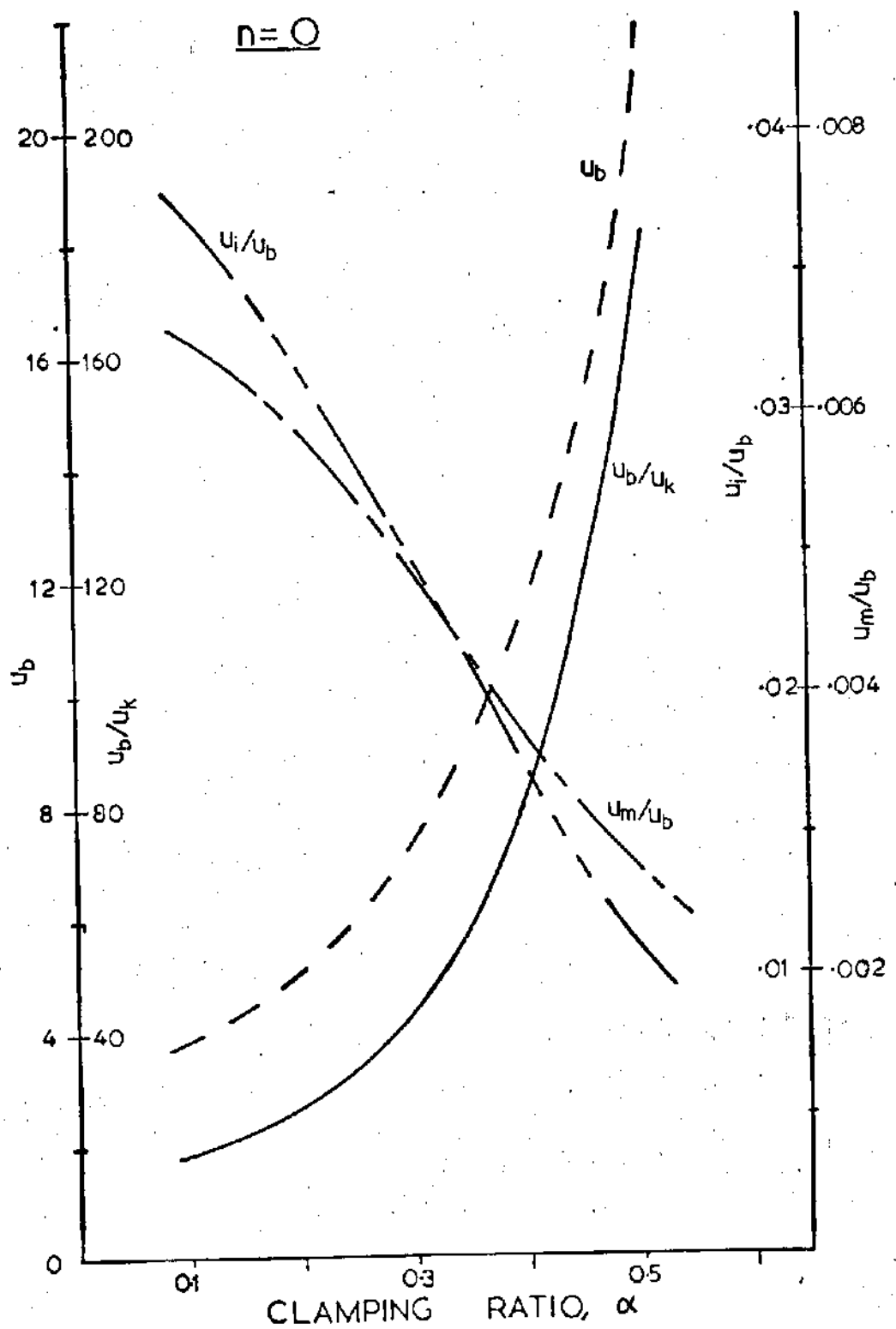


Fig. 4.6 ENERGY CONSTANTS FOR THE MODE n = 0.

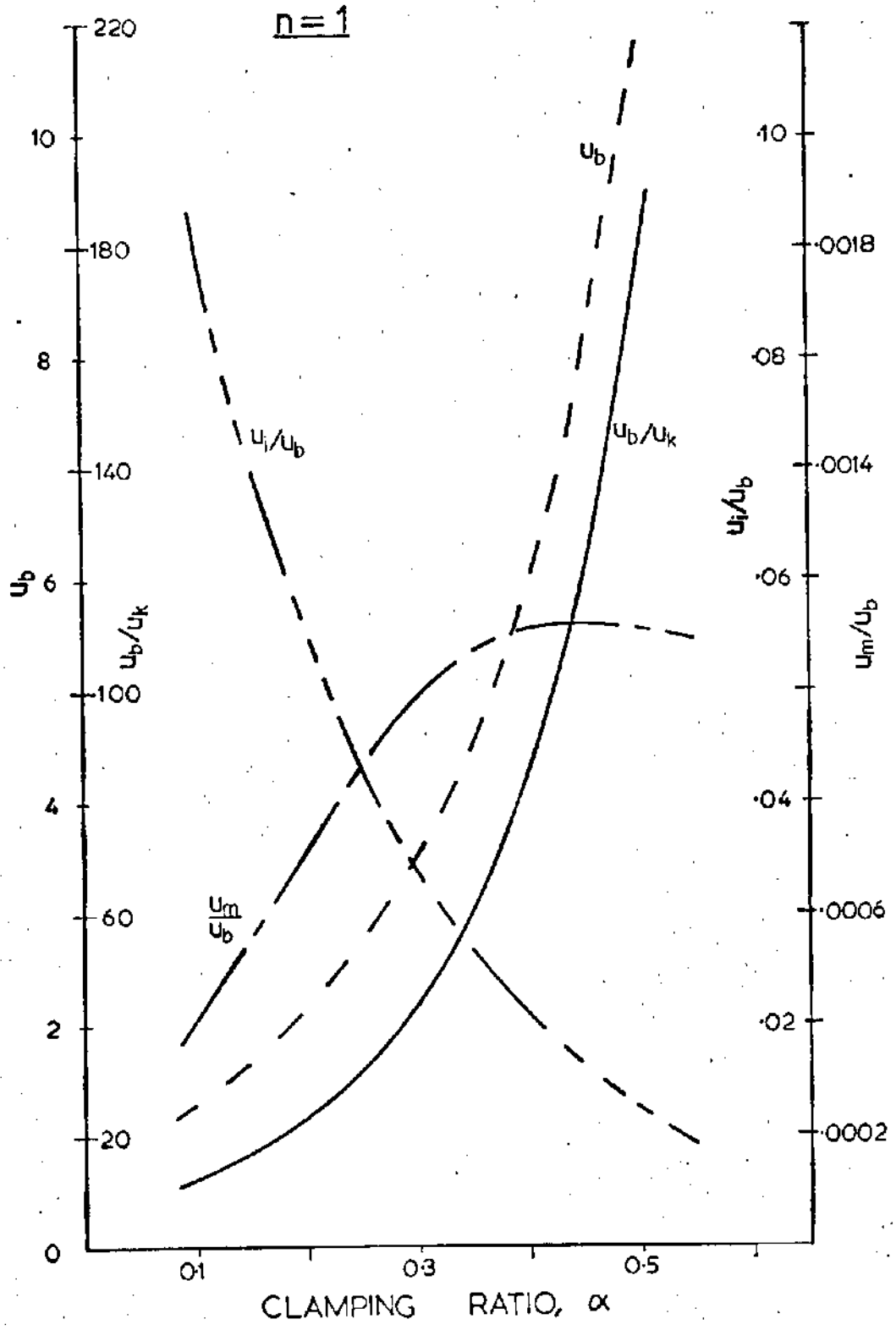


Fig. 4.7 ENERGY CONSTANTS FOR THE MODE n = 1.

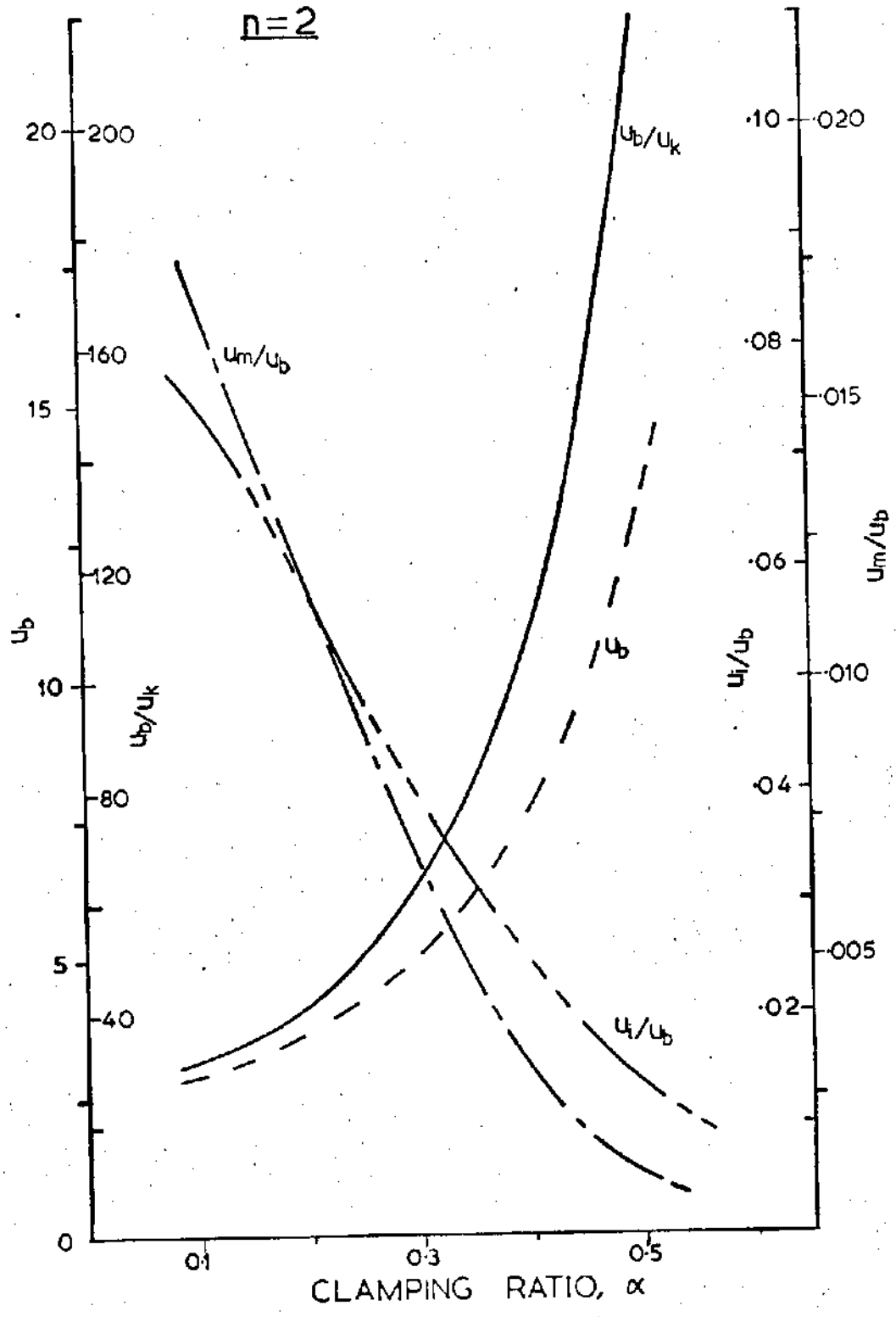


Fig. 4.8 ENERGY CONSTANTS FOR THE MODE n = 2.

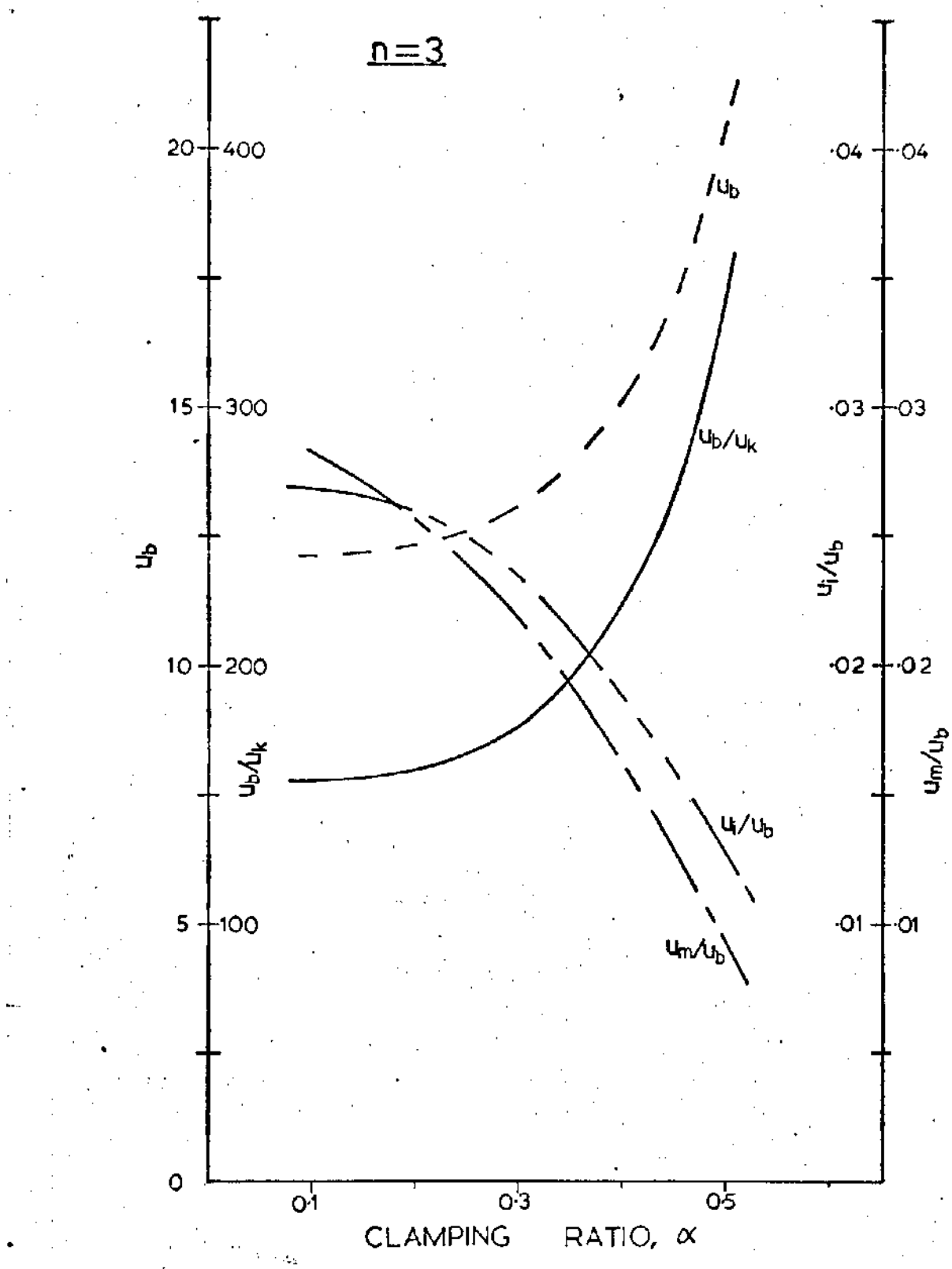


Fig. 4.9 ENERGY CONSTANTS FOR THE MODE n = 3.

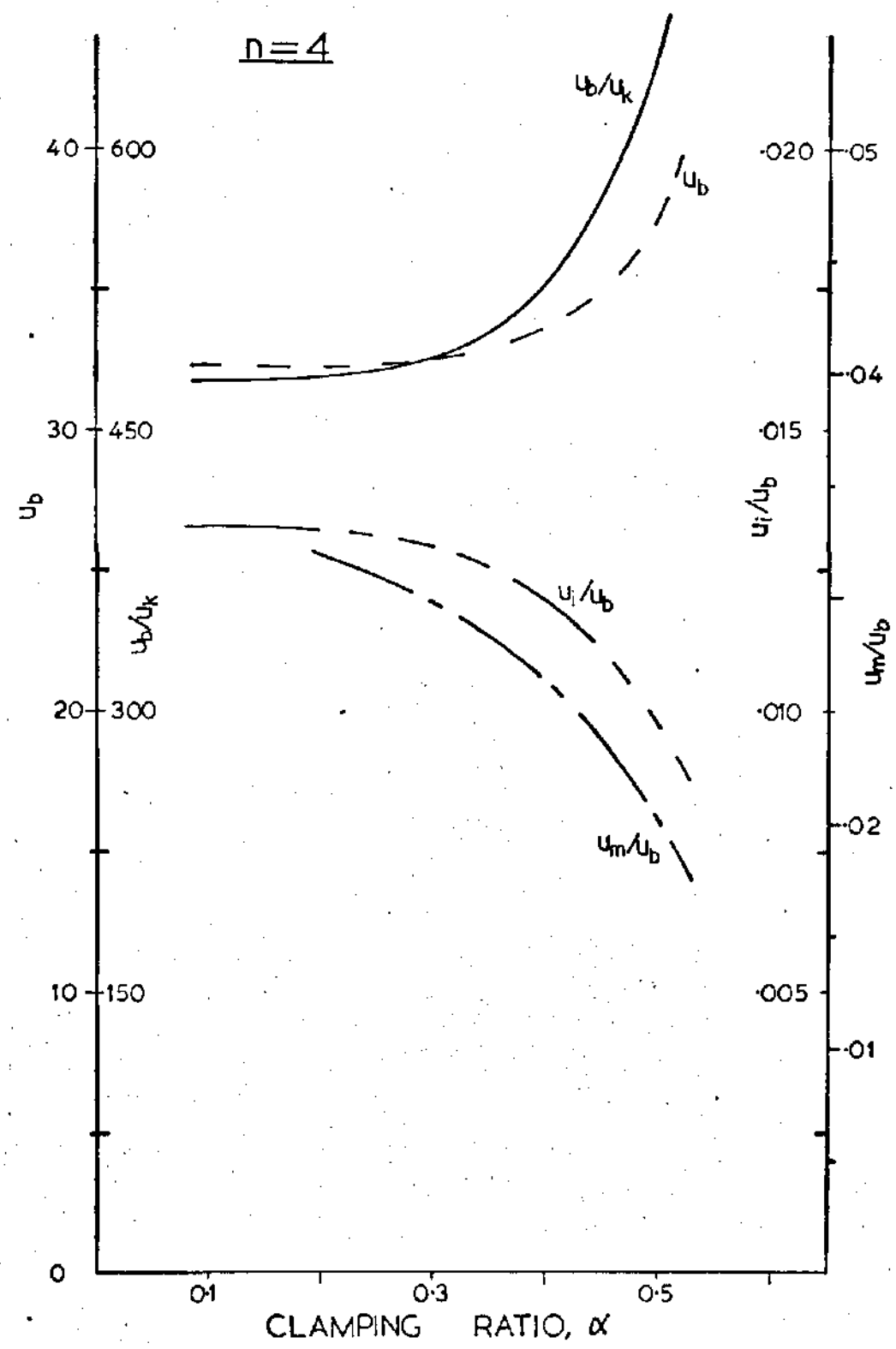


Fig. 4.10 ENERGY CONSTANTS FOR THE MODE n = 4.

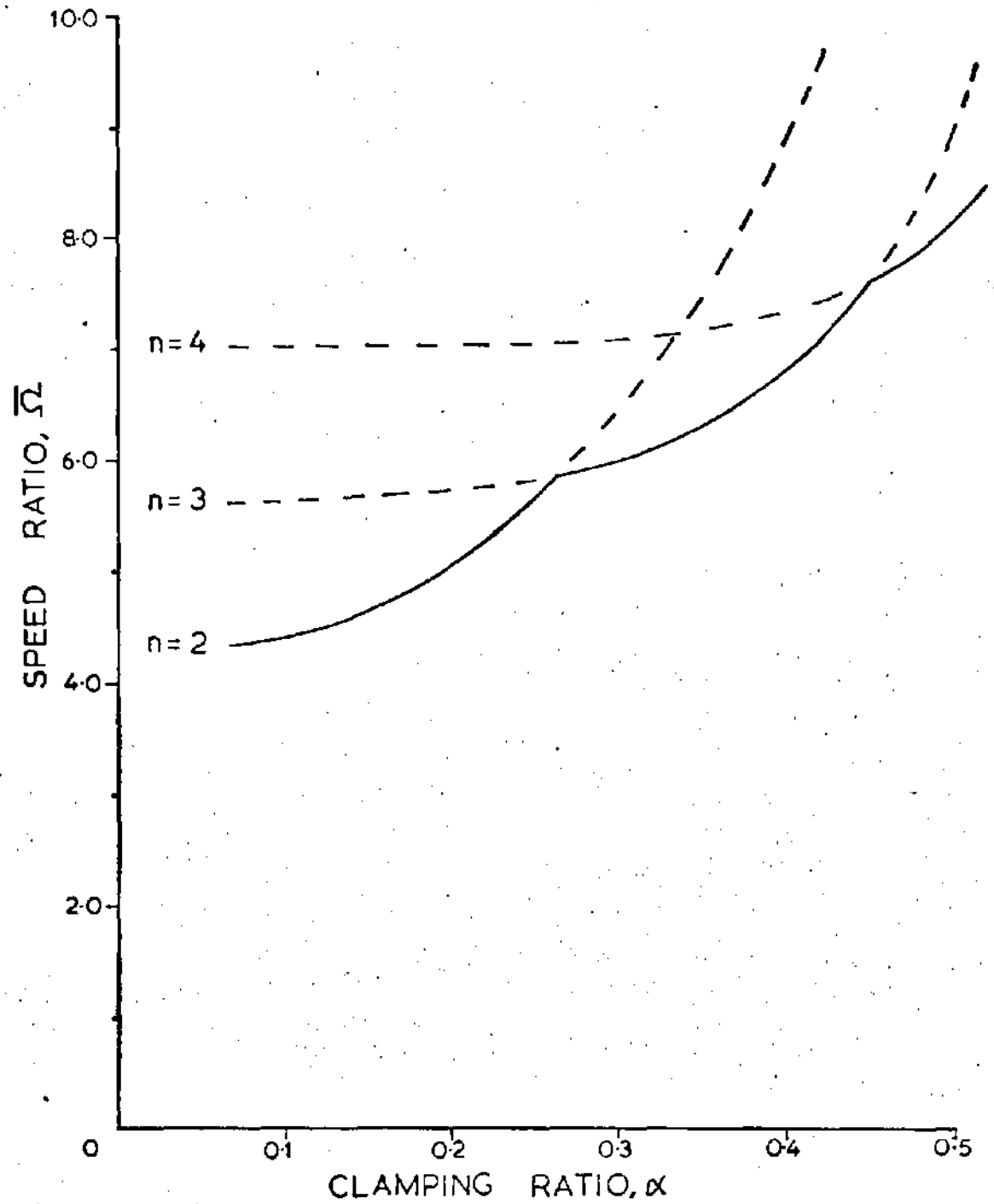


Fig. 4.11 CURVES FOR LOCATING CRITICAL SPEEDS.

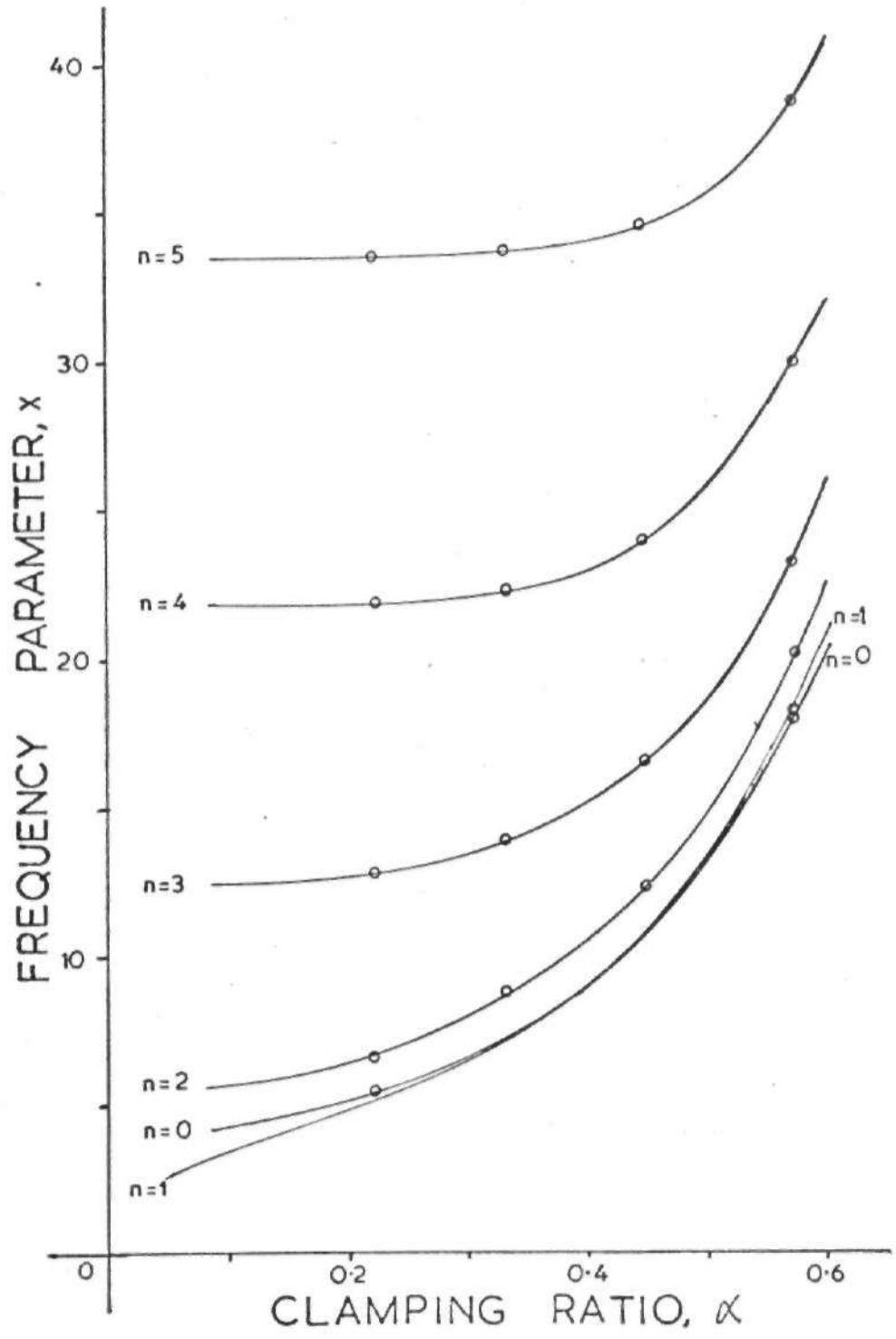


Fig. 4.12 FREQUENCY VALUES FOR DIFFERENT CLAMPING RATIOS.

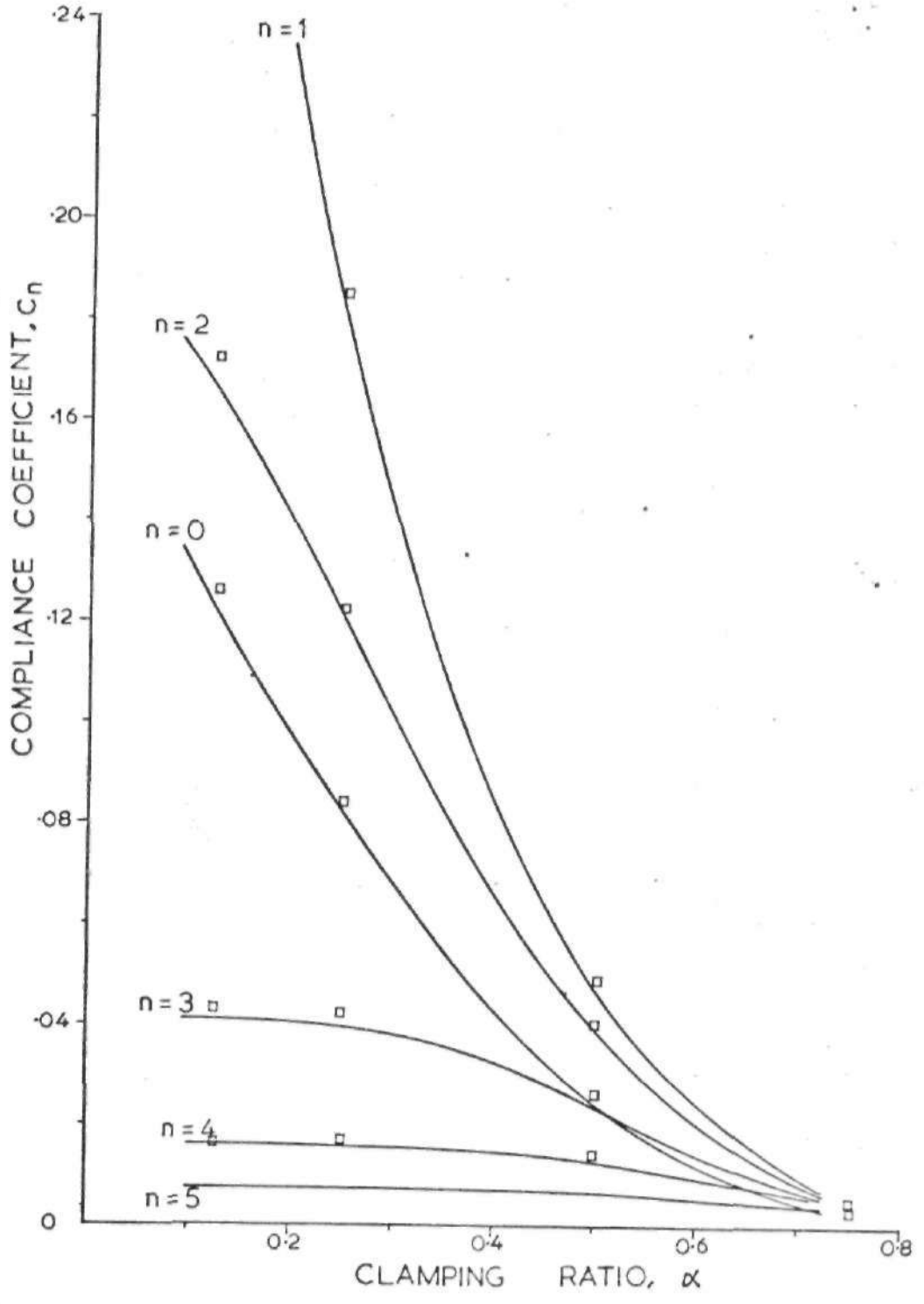


Fig. 4.13 VALUES OF MODAL COMPLIANCE COEFFICIENTS, c_n.

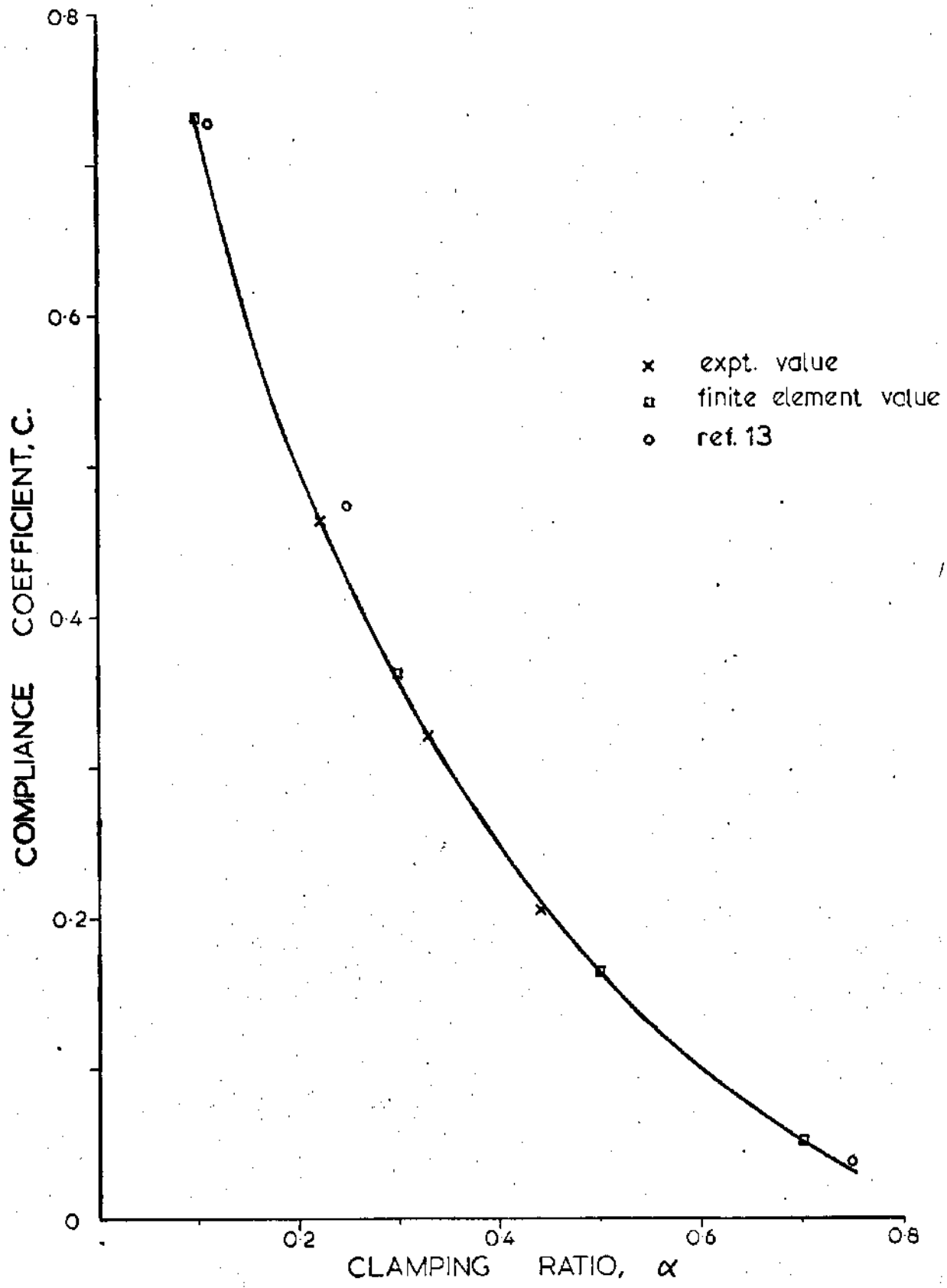


Fig. 4.14 VALUES OF COMPLIANCE COEFFICIENT, C.

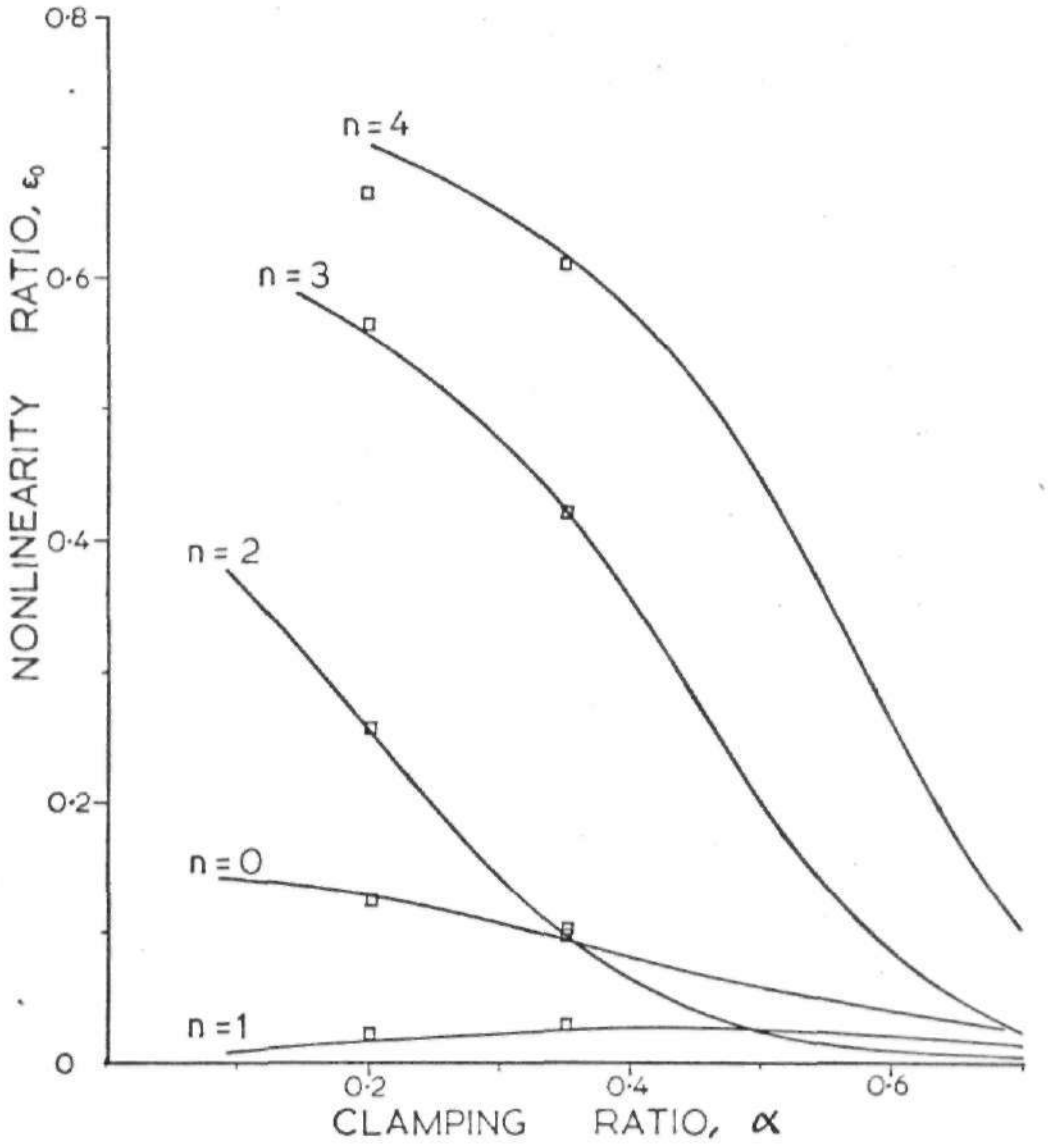


Fig. 4.15 VALUES OF DISC NONLINEARITY RATIO.

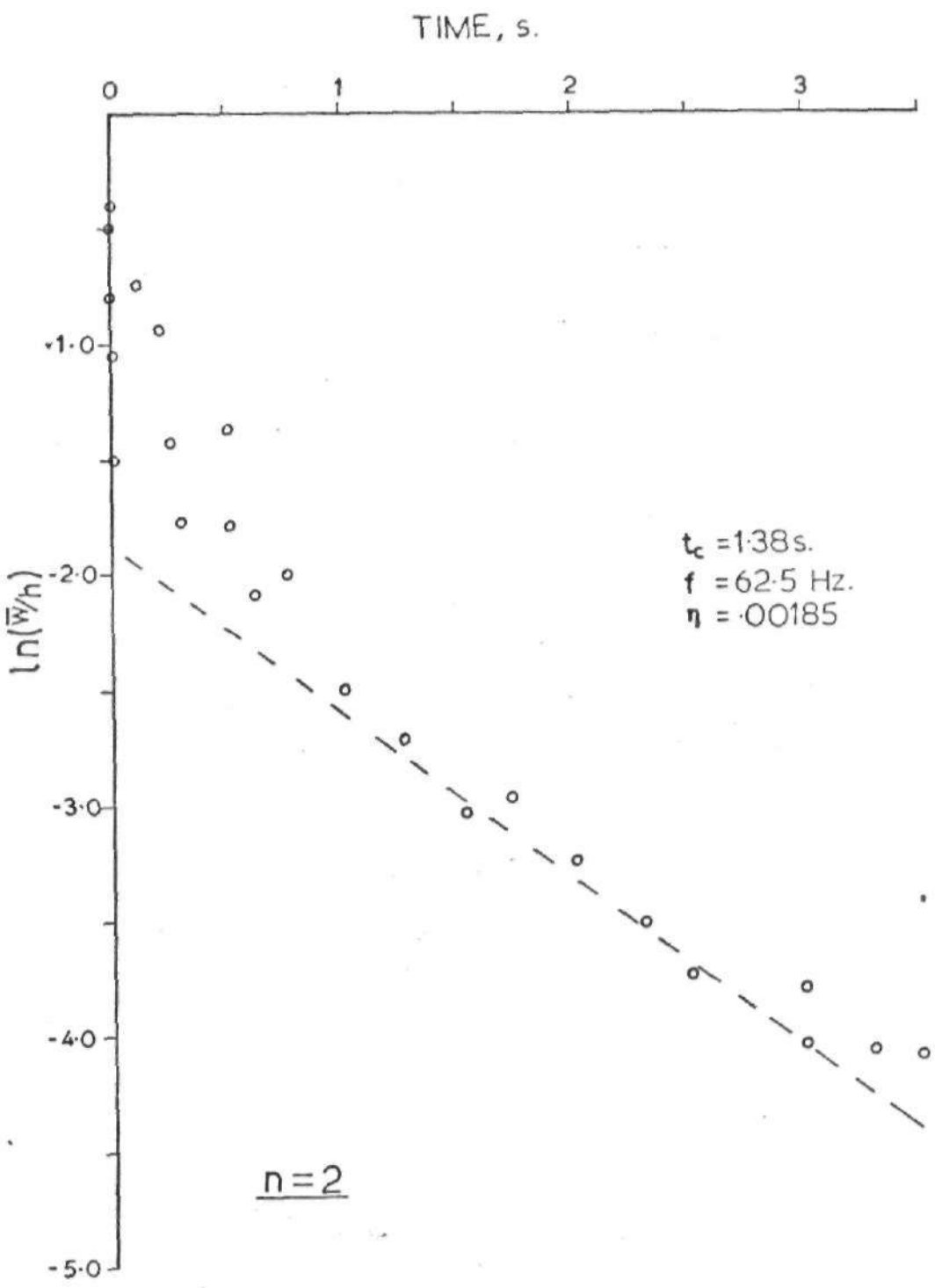


Fig. 4.16 DECAYING OSCILLATION AMPLITUDES IN A STATIONARY DISC FOR THE MODE n = 2.

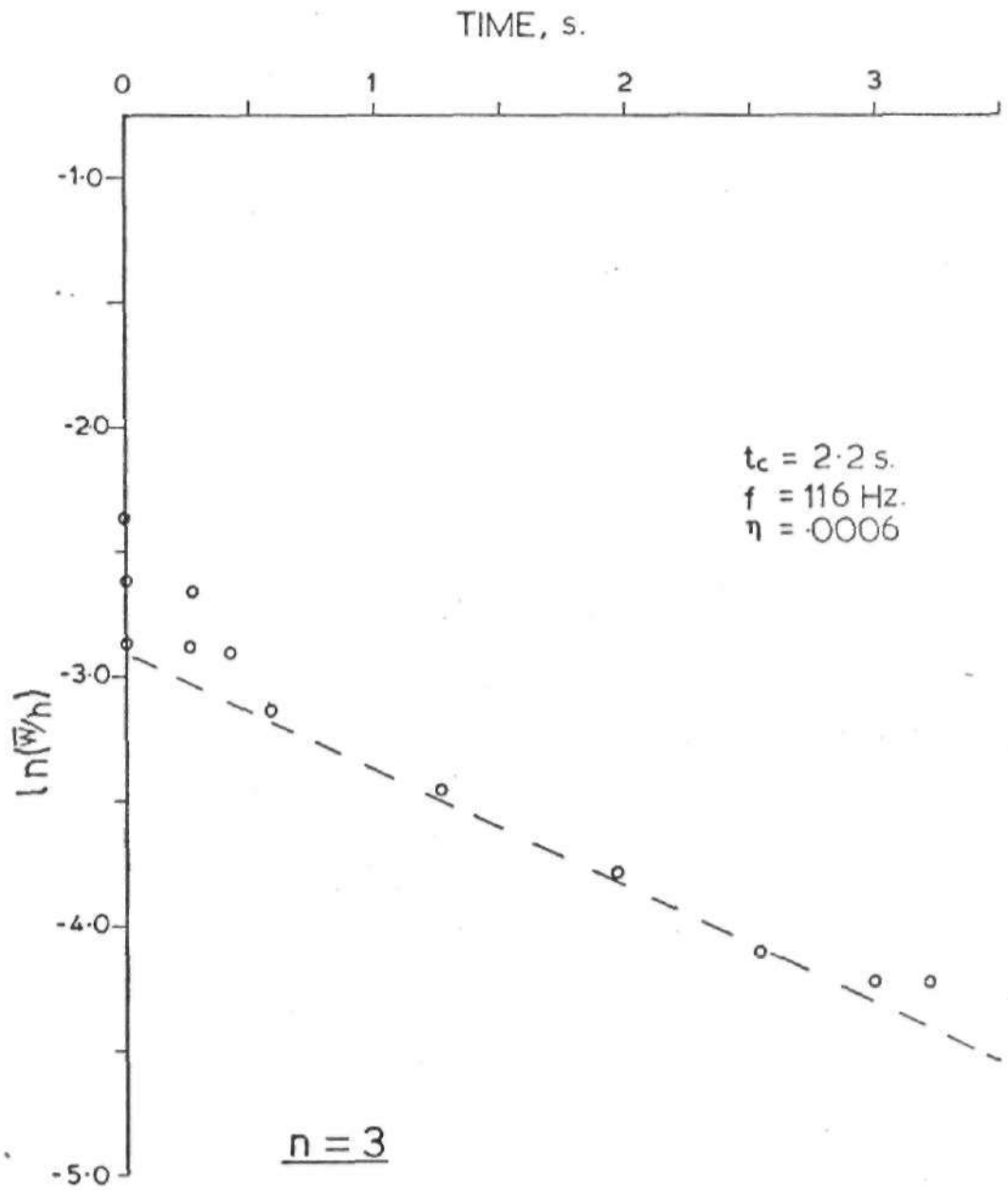


Fig. 4.17 DECAYING OSCILLATION AMPLITUDES IN A STATIONARY DISC FOR THE MODE n = 3.

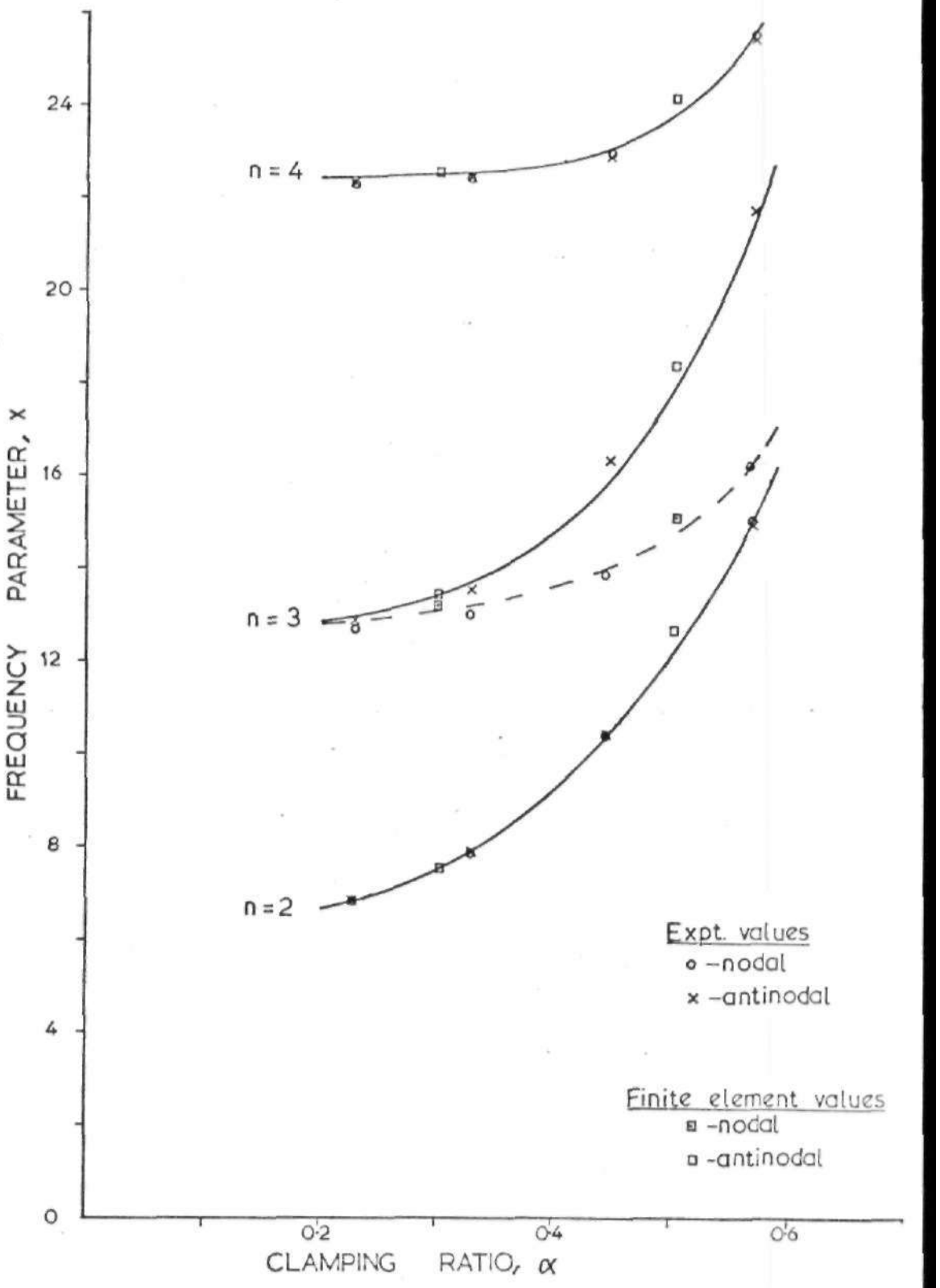


Fig. 4.18 FREQUENCIES FOR A DISC CLAMPED AT 6 POSITIONS.

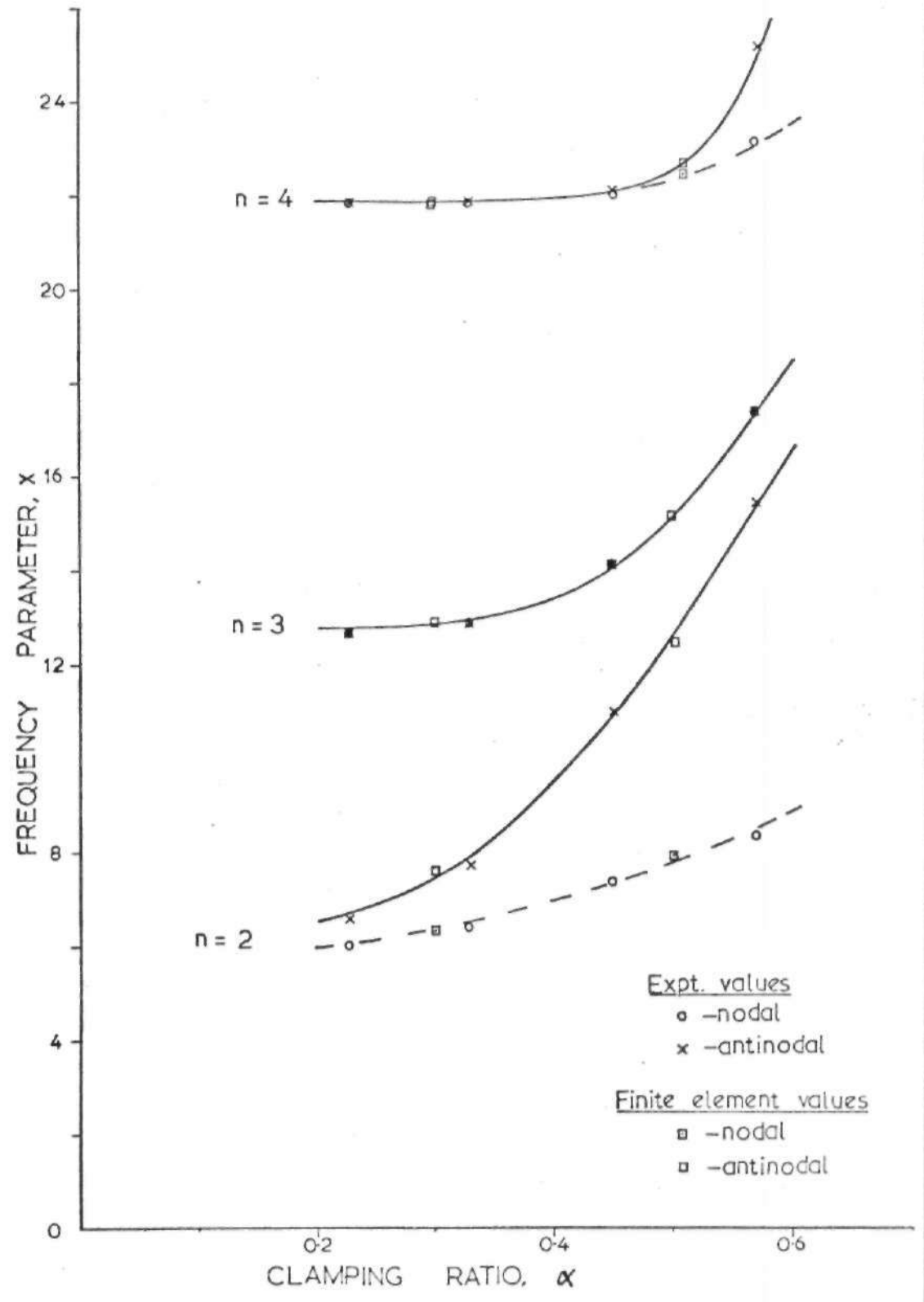


Fig. 4.19 FREQUENCIES FOR A DISC CLAMPED AT 4 POSITIONS.

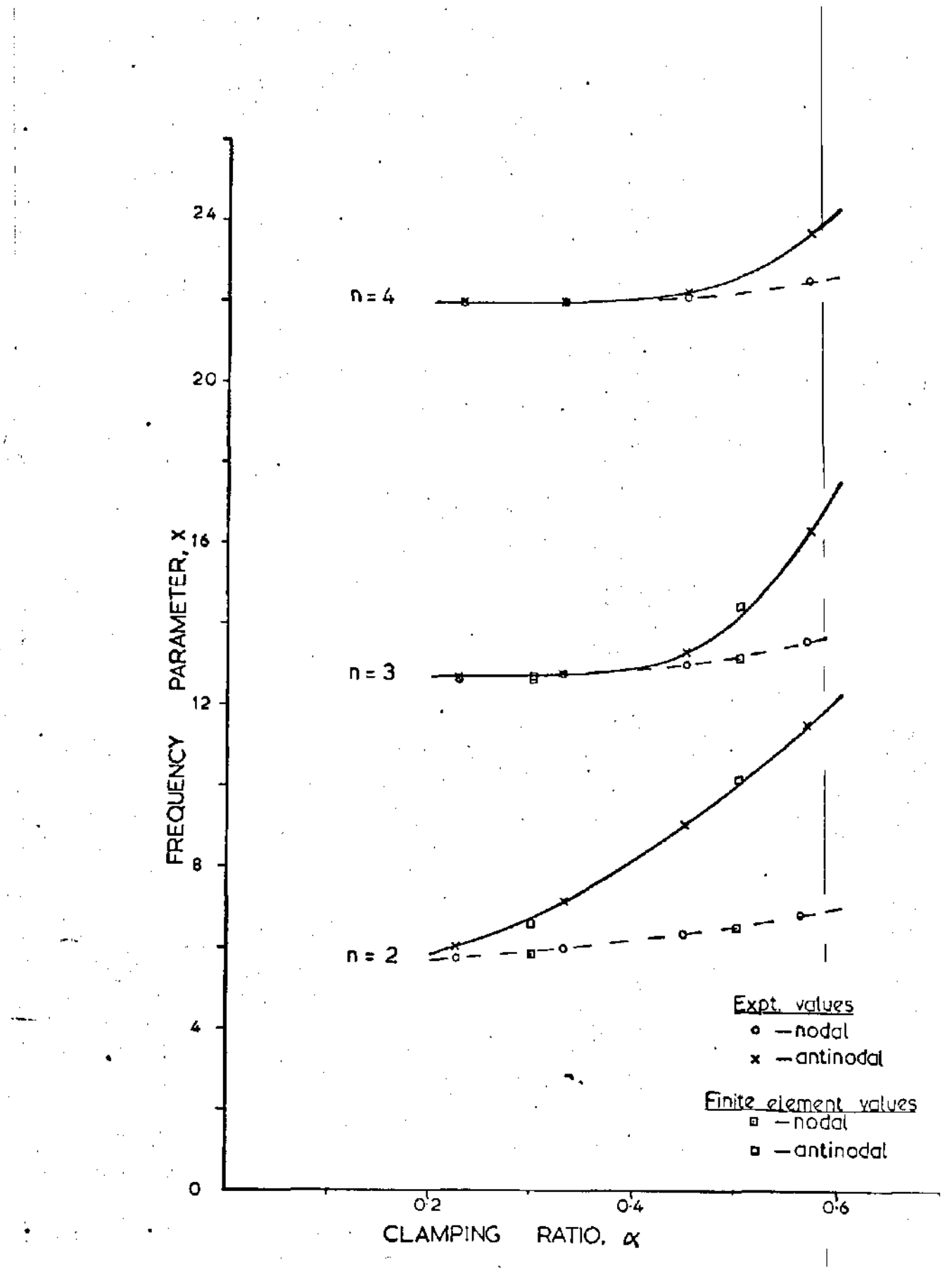


Fig. 4.20 FREQUENCIES FOR A DISC CLAMPED AT 2 POSITIONS.

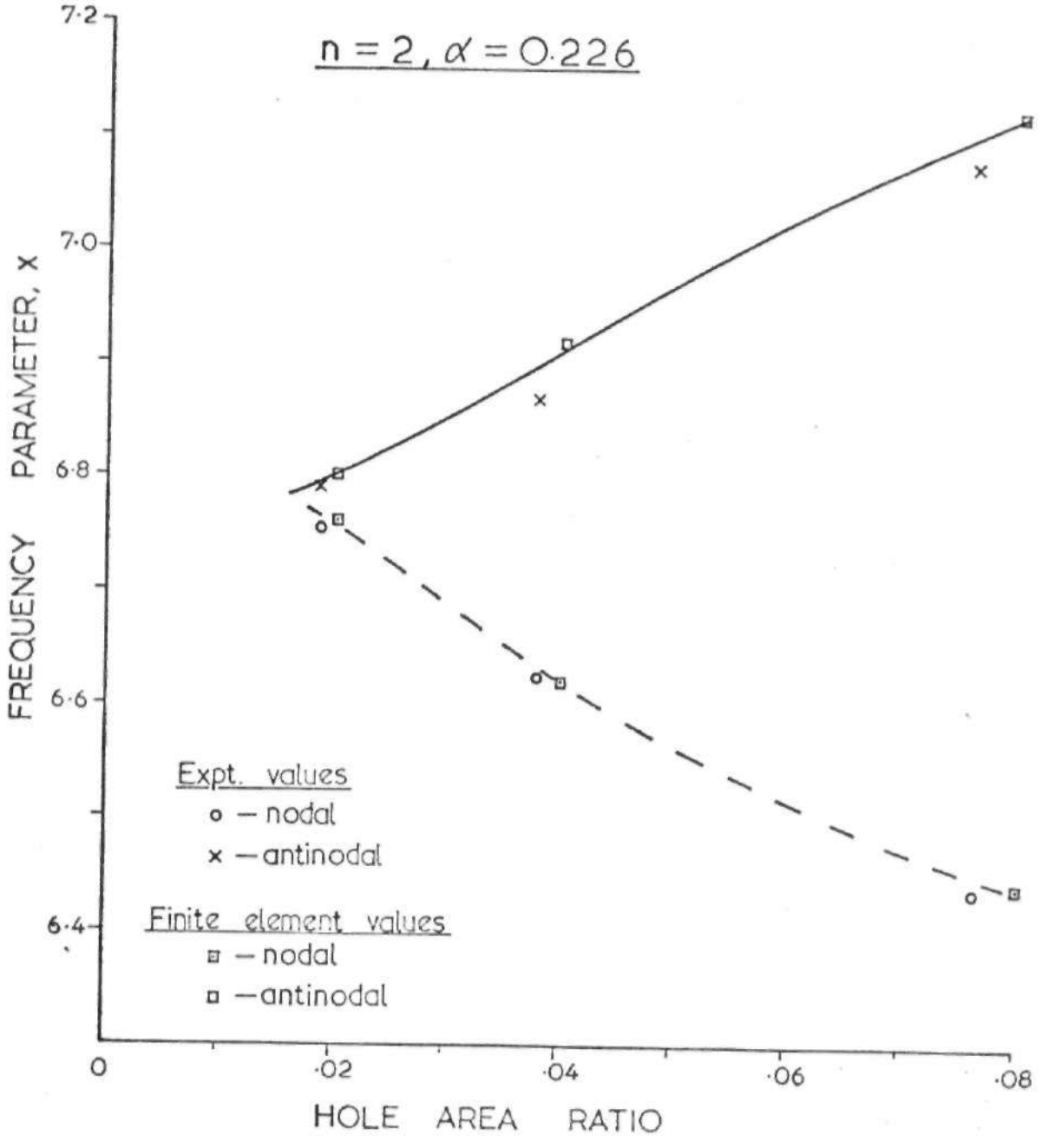


Fig. 4.21 FREQUENCIES FOR A DISC WITH 2 HOLES.

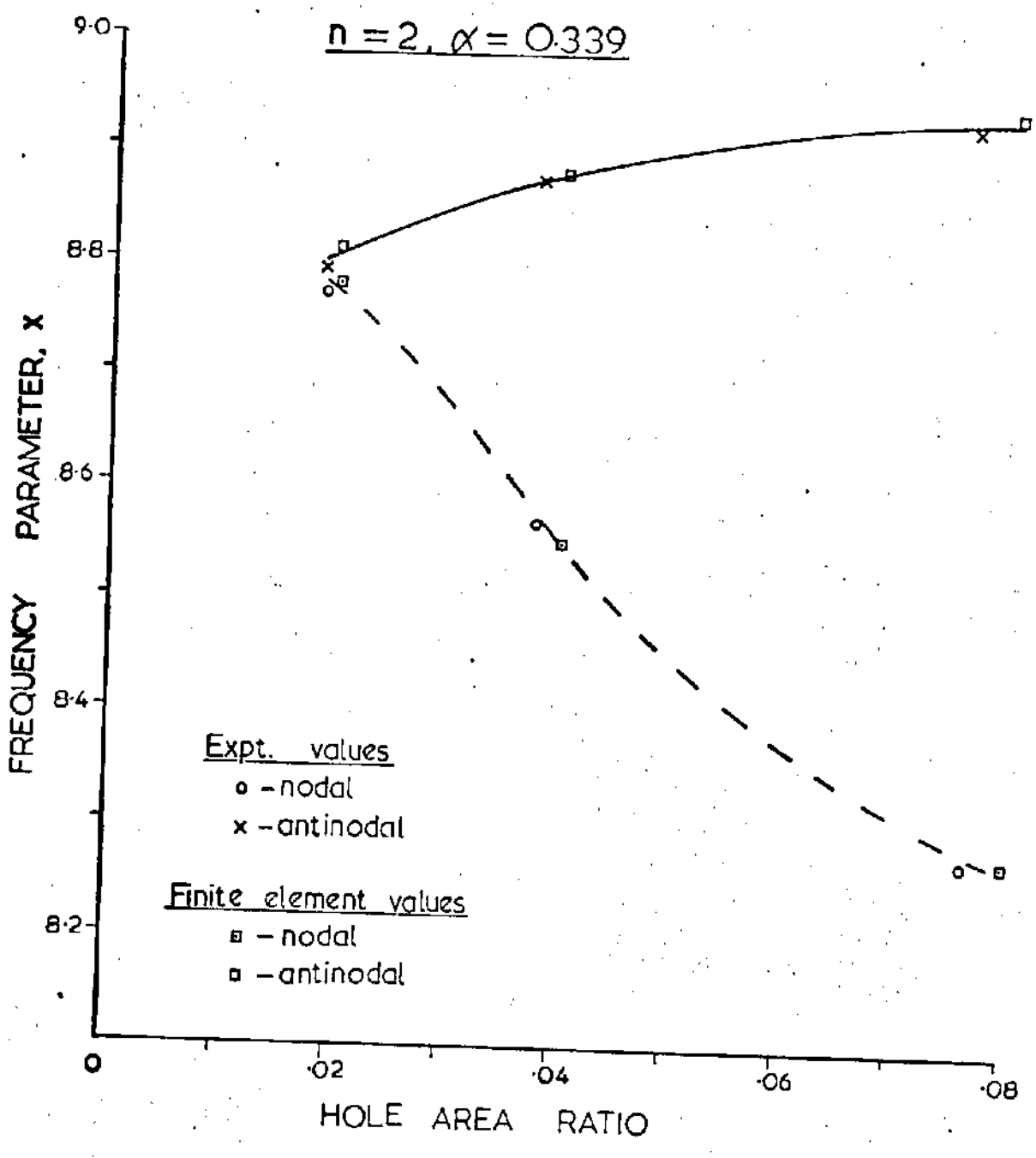


Fig. 4.22 FREQUENCIES FOR A DISC WITH 2 HOLES.

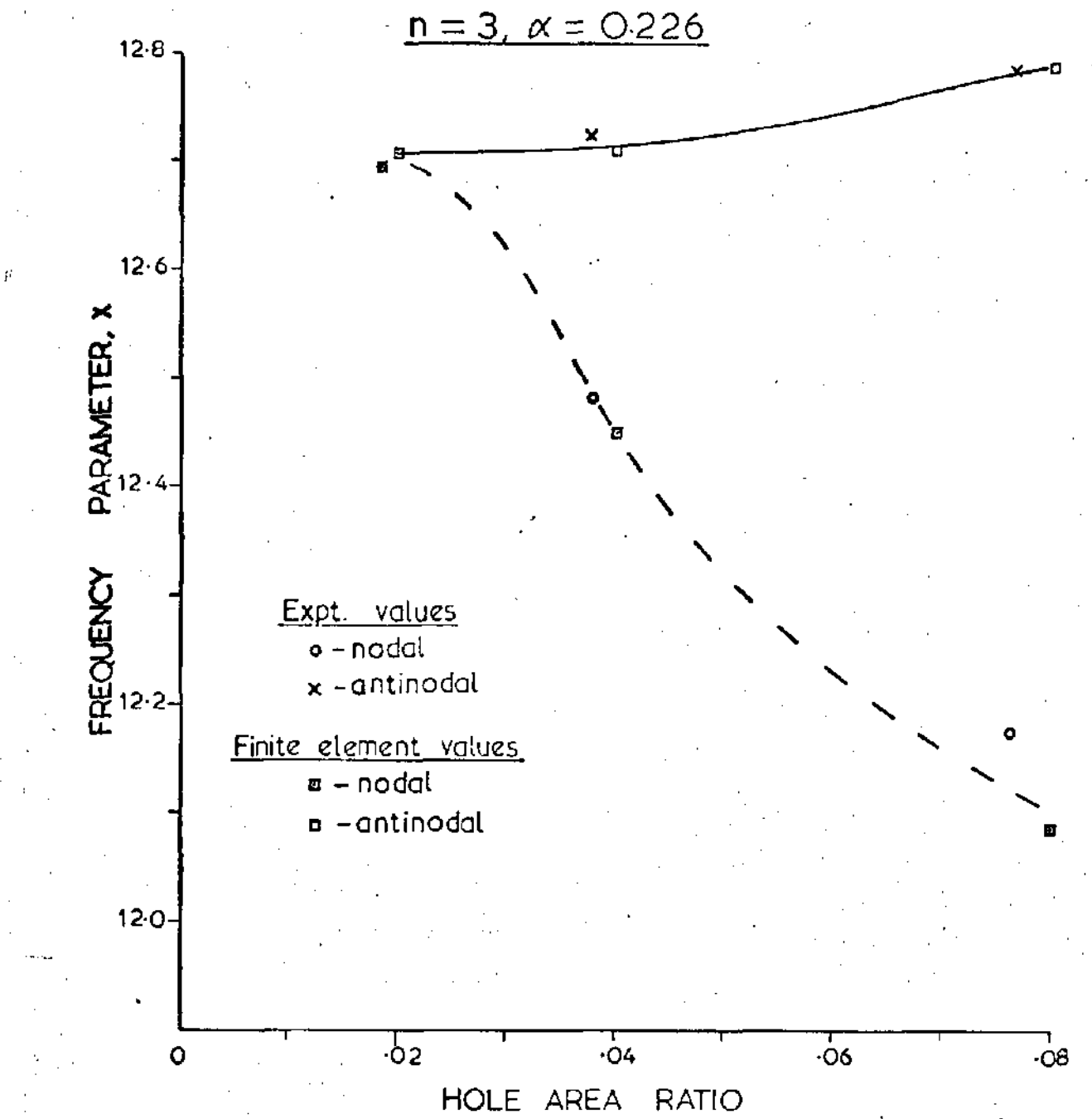


Fig. 4.23 FREQUENCIES FOR A DISC WITH 2 HOLES.

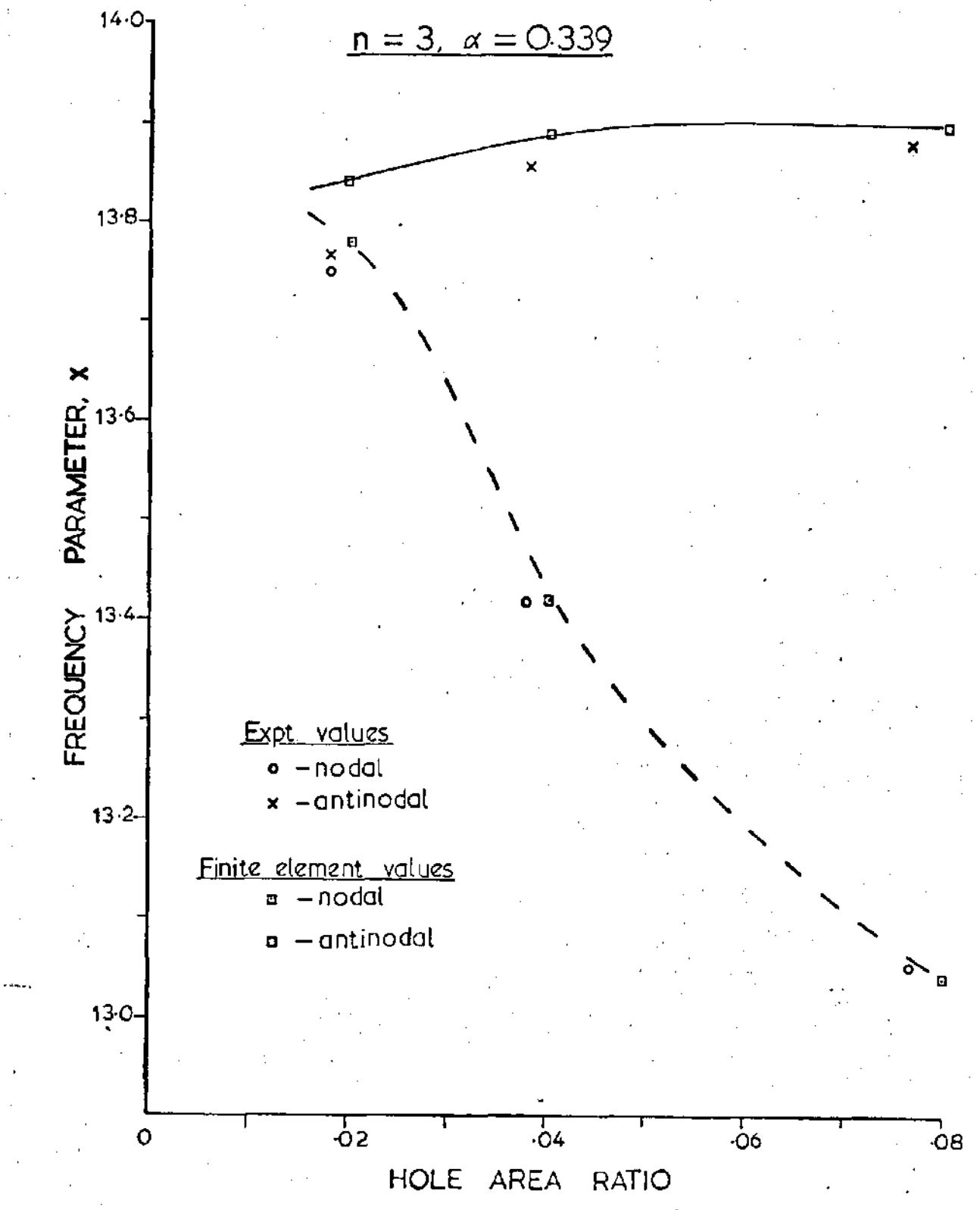


Fig. 4.24 FREQUENCIES FOR A DISC WITH 2 HOLES.

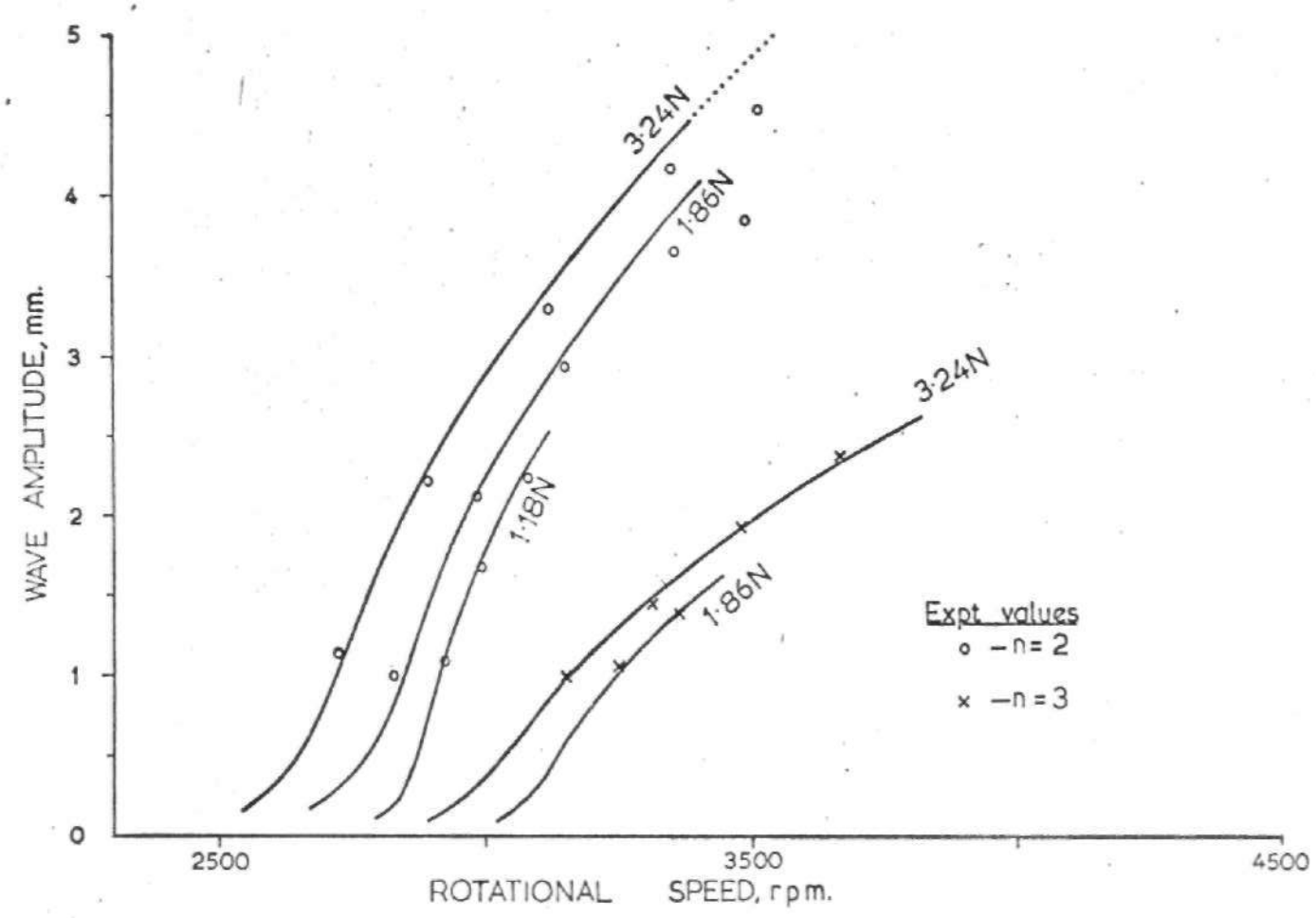


Fig. 4.25 STANDING WAVE AMPLITUDES IN A DISC (α = 0.226).

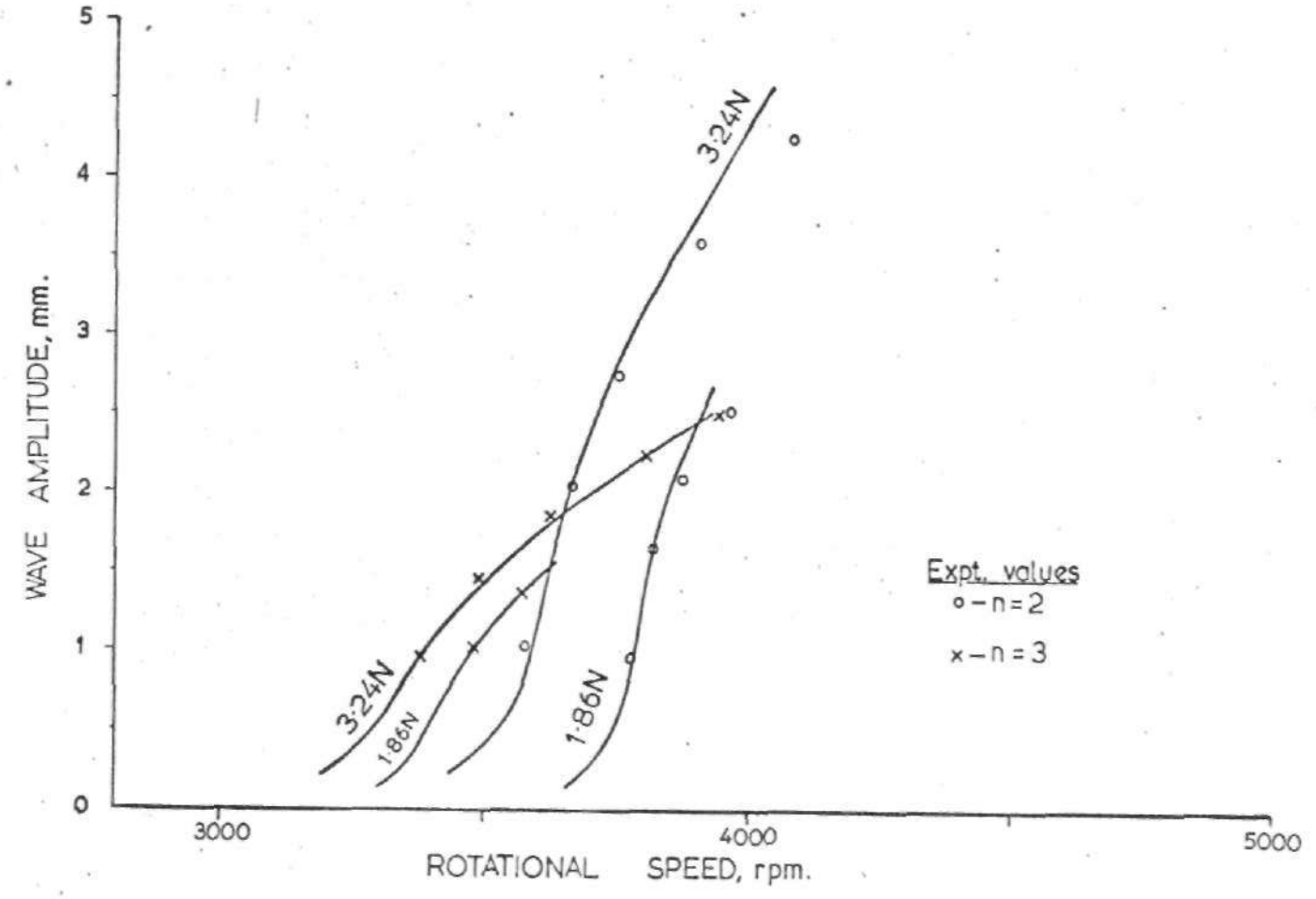


Fig. 4.26 STANDING WAVE AMPLITUDES IN A DISC (α = 0.339).

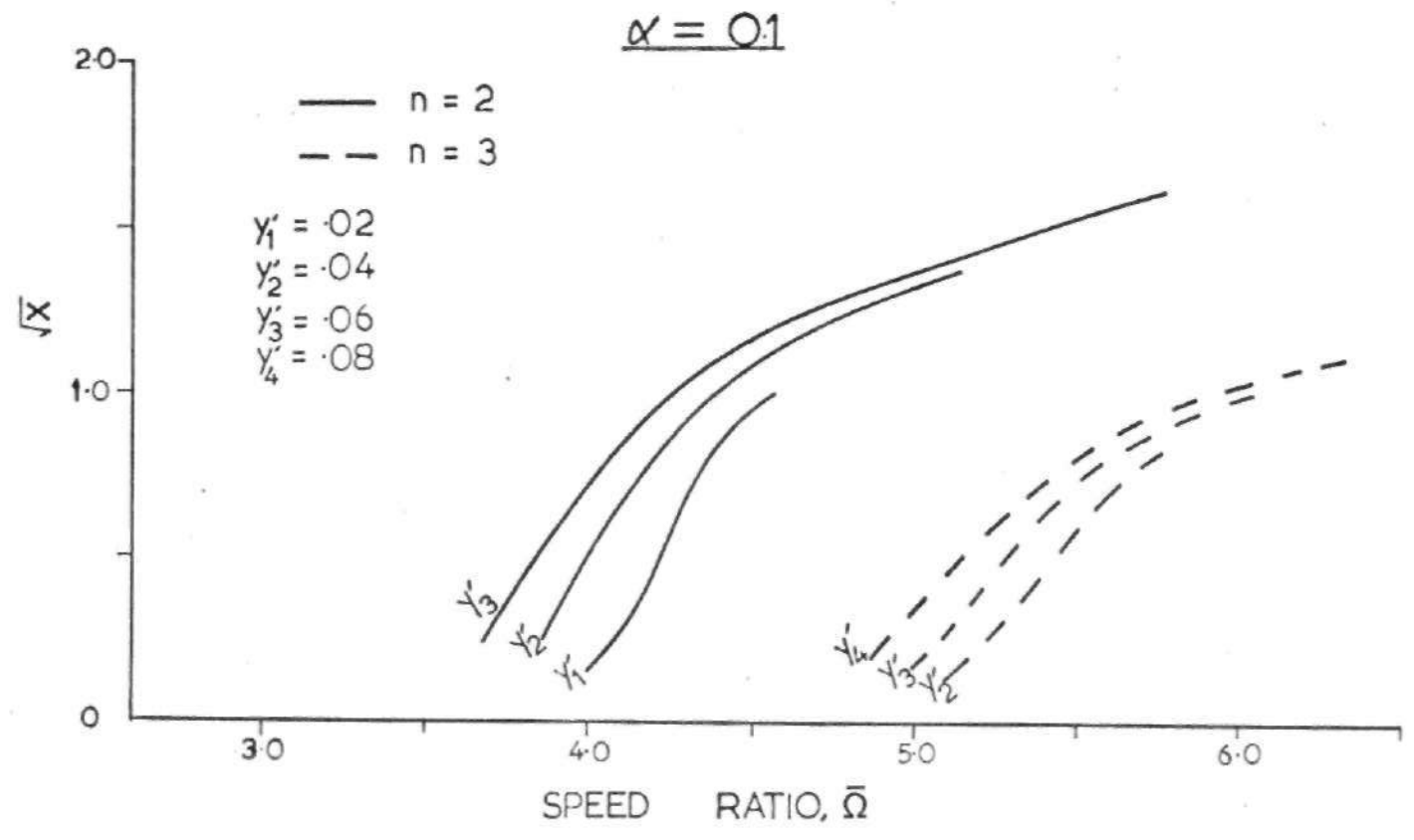


Fig. 4.27 THEORETICAL STATIONARY WAVE AMPLITUDES (α = 0.1).

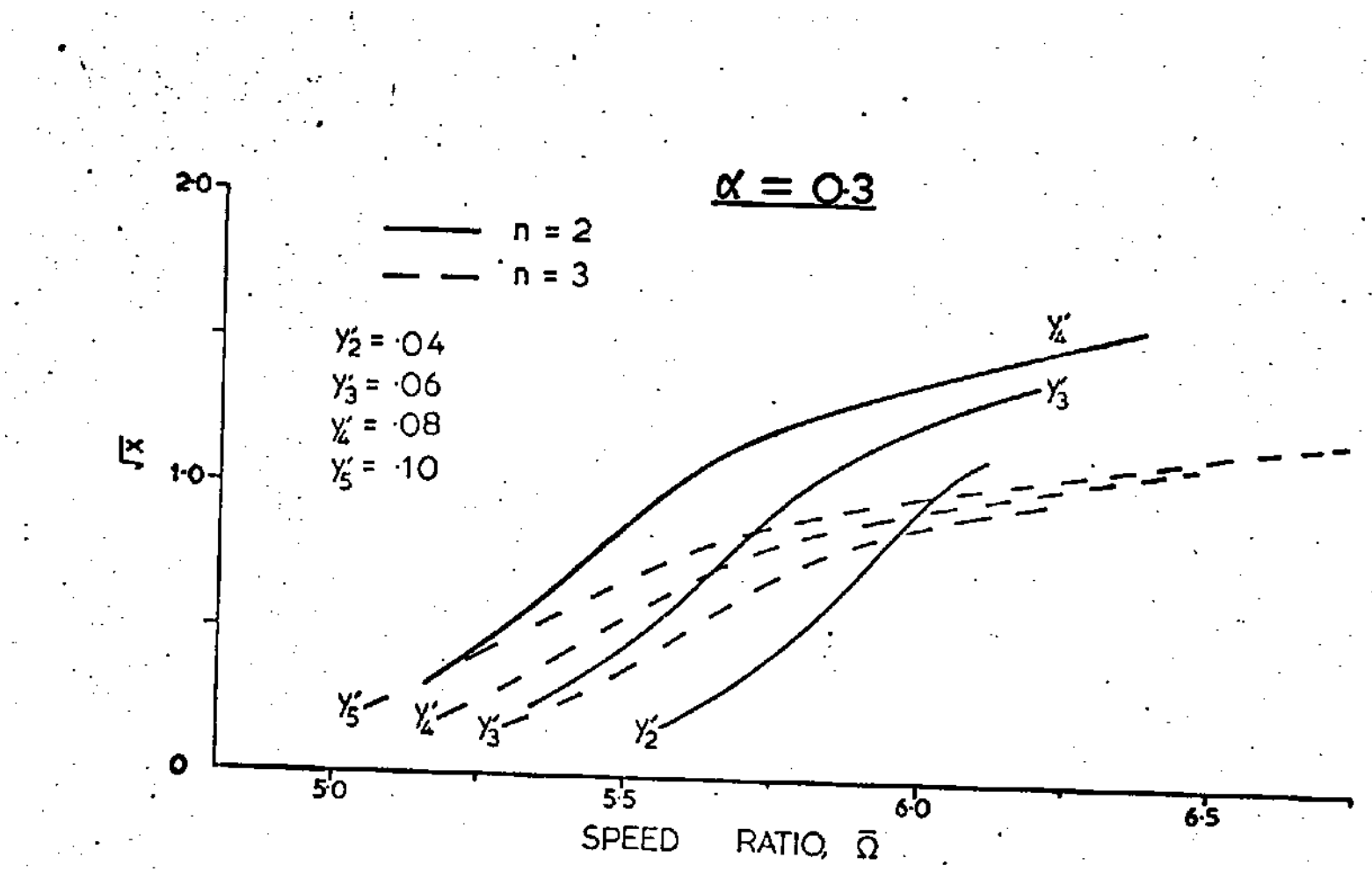


Fig. 4.28 THEORETICAL STATIONARY WAVE AMPLITUDES ($\alpha = 0.3$).

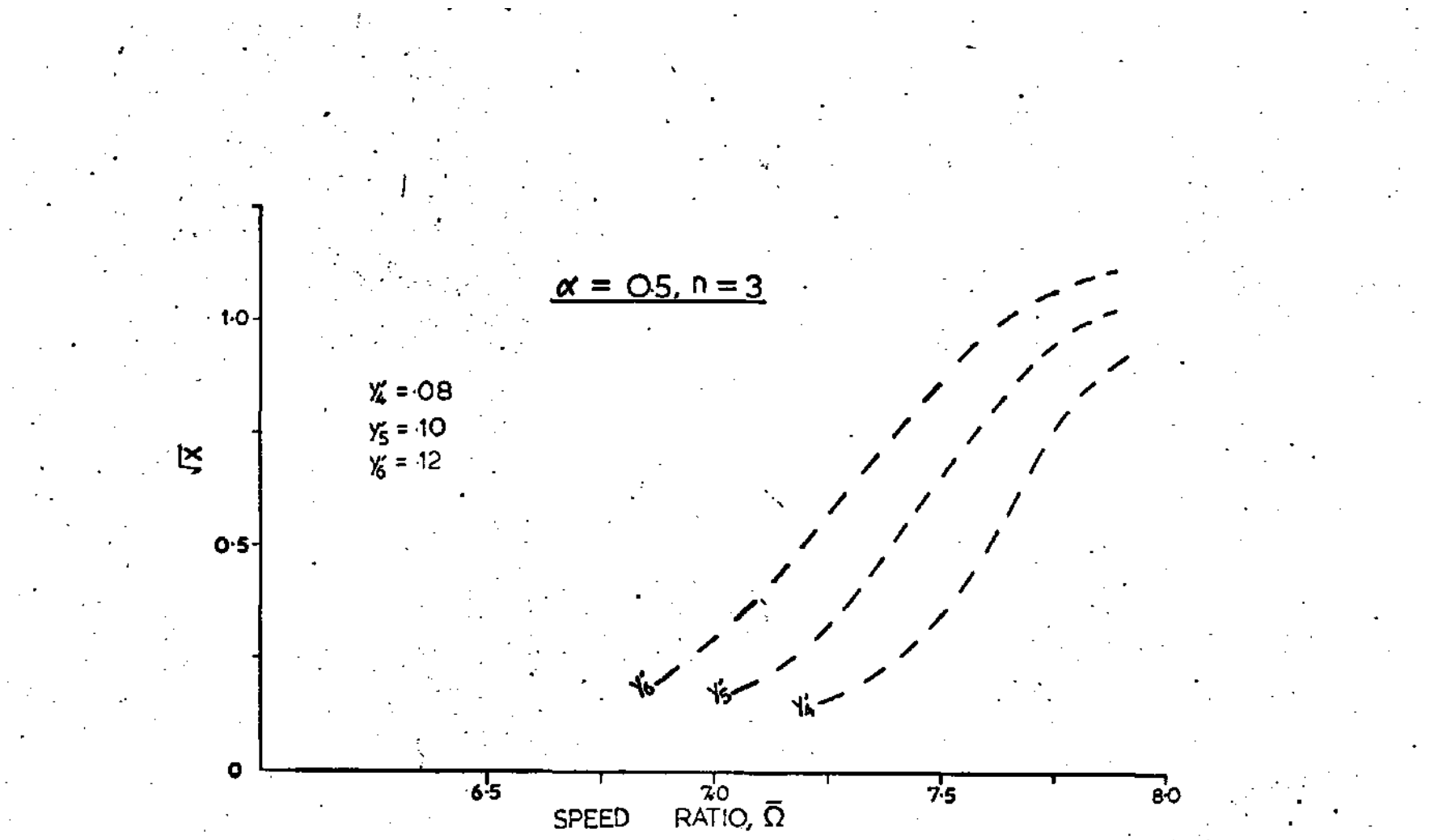


Fig. 4.29 THEORETICAL STATIONARY WAVE AMPLITUDES ($\alpha = 0.5$).

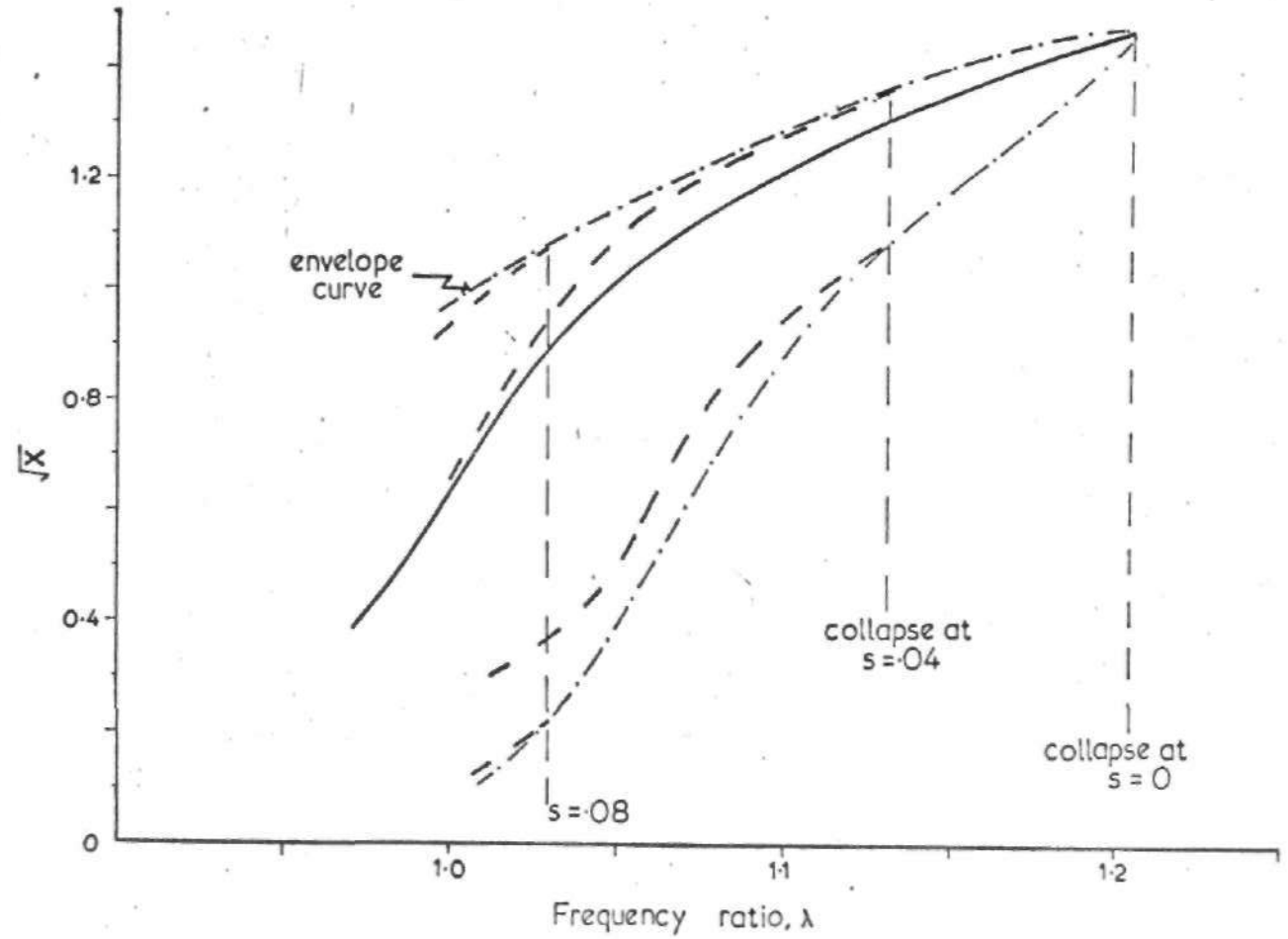


Fig. 4.30 WAVE AMPLITUDES FOR DIFFERENT VALUES OF PERCENT. FREQUENCY SEPARATION, AND THE ENVELOPE CURVE FOR THE OCCURENCE OF STATIONARY WAVES.

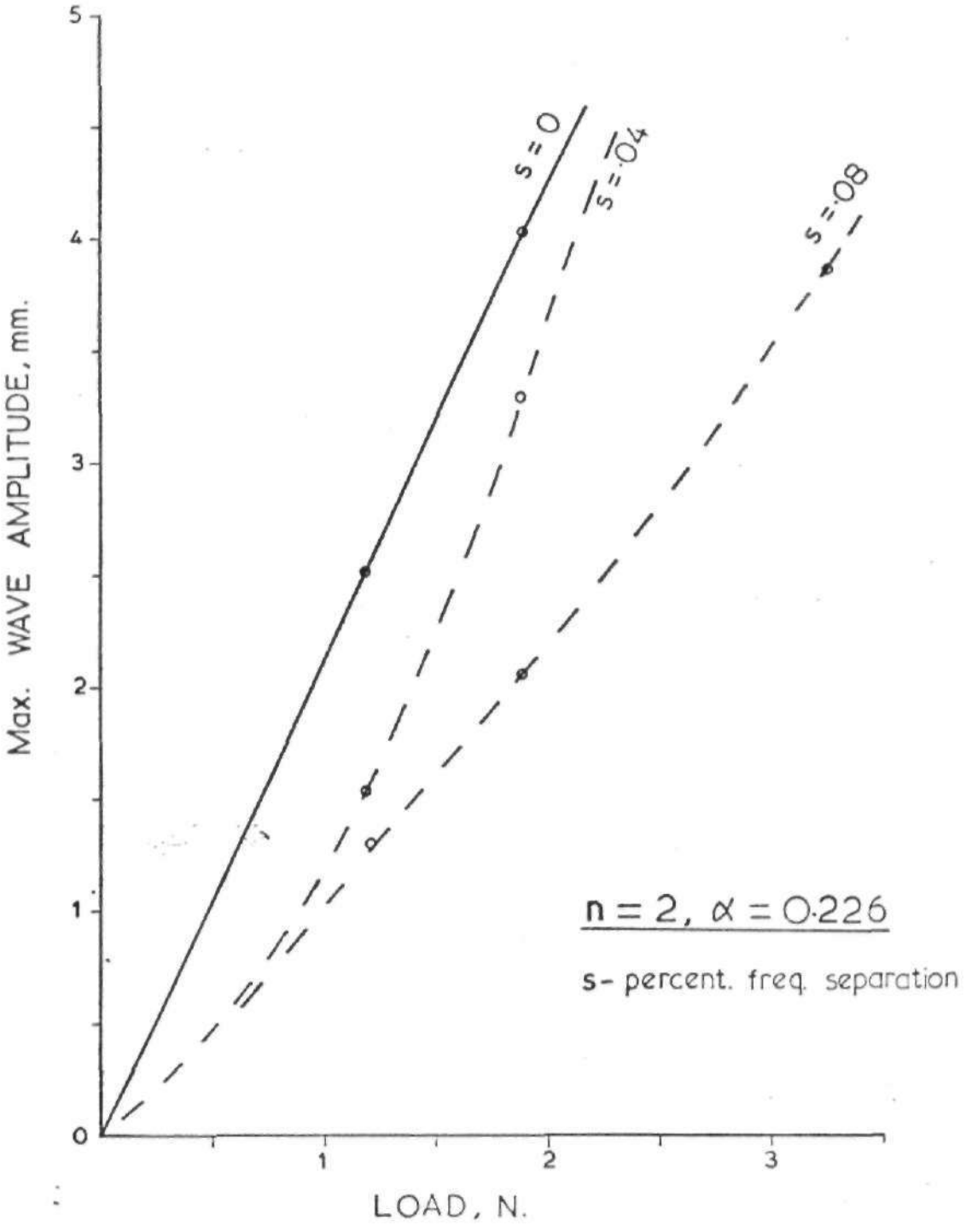


Fig. 4.31 MAXIMUM WAVE AMPLITUDES IN A DISC FOR DIFFERENT VALUES OF PERCENT. FREQUENCY SEPARATION.

Clamping ratio	Nodal diameter	Rayleigh's method	Ritz method (m=0)	Ritz method (m=1)	Exact values (m=0)	Exact values (m=1)
0.1	0	4.24	4.24	25.27	4.24	25.26
0.1	1	3.48	3.48	27.69	3.48	27.67
0.1	2	5.62	5.63	36.97	5.62	36.94
0.1	3	12.45	12.45	53.21	12.45	53.20
0.1	4	21.84	21.84	73.56	21.84	73.56
0.2	0	5.18	5.18	32.29	5.18	32.29
0.2	1	4.81	4.81	34.53	4.81	34.53
0.2	2	6.45	6.45	41.97	6.45	41.96
0.2	3	12.62	12.62	55.42	12.62	55.41
0.2	4	21.86	21.86	74.20	21.86	74.19
0.3	0	6.66	6.66	42.61	6.66	42.61
0.3	1	6.55	6.55	44.63	6.55	44.63
0.3	2	7.96	7.96	50.95	7.96	50.95
0.3	3	13.28	13.28	62.06	13.28	62.05
0.3	4	22.07	22.07	78.12	22.07	78.12
0.4	0	9.02	9.02	58.55	9.02	58.55
0.4	1	9.12	9.12	60.38	9.12	60.38
0.4	2	10.47	10.47	65.95	10.47	65.95
0.4	3	14.97	14.96	75.45	14.96	75.45
0.4	4	22.98	22.98	89.07	22.98	89.07
0.5	0	13.03	13.02	85.03	13.02	85.03
0.5	1	13.30	13.29	86.71	13.29	86.70
0.5	2	14.71	14.70	91.74	14.70	91.74
0.5	3	18.57	18.56	100.17	18.56	100.17
0.5	4	25.60	25.60	112.05	25.60	112.05
0.6	0	20.54	20.52	133.92	20.52	133.91
0.6	1	20.95	20.94	135.46	20.94	135.45
0.6	2	22.52	22.50	140.09	22.50	140.08
0.6	3	26.01	25.98	147.78	25.98	147.76
0.6	4	32.08	32.07	158.50	32.07	158.48

Table 2. NATURAL FREQUENCIES OF DISCS BY EXACT AND THE TWO ENERGY METHOD.

Nodal diameters	Clamping radius ratio, b/a		
	0.1	0.3	0.5
0	4.23	6.66	13.03
1	3.47	6.56	13.31
2	5.62	7.97	14.75
3	12.48	13.31	18.64
4	22.06	22.21	25.73

Table 3. NATURAL FREQUENCIES OF DISCS BY THE FINITE ELEMENT METHOD.

Radius	BESSL			MRAYL			RRITZ		
	w	w_r	w_{rr}	w	w_r	w_{rr}	w	w_r	w_{rr}
0.30	0.00	0.00	12.75	0.00	0.00	12.94	0.00	0.00	12.54
0.40	0.05	0.84	5.60	0.05	0.85	5.61	0.05	0.84	5.59
0.50	0.16	1.27	3.25	0.16	1.27	3.21	0.16	1.27	3.25
0.60	0.30	1.53	2.04	0.30	1.53	2.00	0.30	1.53	2.06
0.70	0.46	1.69	1.25	0.46	1.69	1.22	0.46	1.69	1.23
0.80	0.63	1.79	0.73	0.63	1.78	0.72	0.63	1.79	0.74
0.90	0.81	1.85	0.50	0.81	1.84	0.50	0.81	1.85	0.51
1.00	1.00	1.90	0.63	1.00	1.90	0.63	1.00	1.90	0.68

Table 4. RELATIVE DISPLACEMENT, SLOPE, AND CURVATURE VALUES IN A FREELY VIBRATING DISC ($n = 2, \alpha = 0.3$).

Curvature values for n = 0

Radius	Clamping radius ratio, b/a					
	0.1	0.2	0.3	0.4	0.5	0.6
0.10	11.51	-	-	-	-	-
0.15	6.52	-	-	-	-	-
0.20	4.38	10.76	-	-	-	-
0.25	3.16	7.38	-	-	-	-
0.30	2.34	5.33	11.67	-	-	-
0.35	1.73	3.94	8.61	-	-	-
0.40	1.26	2.92	6.45	13.93	-	-
0.45	0.88	2.14	4.83	10.58	-	-
0.50	0.56	1.51	3.58	8.02	18.18	-
0.55	0.30	1.01	2.57	5.98	13.87	-
0.60	0.09	0.60	1.76	4.33	10.39	26.31
0.65	-0.09	0.27	1.10	2.99	7.53	19.69
0.70	-0.23	0.00	0.56	1.89	5.16	14.15
0.75	-0.33	-0.21	0.14	1.01	3.23	9.52
0.80	-0.40	-0.36	-0.18	0.32	1.68	5.71
0.85	-0.44	-0.45	-0.40	-0.18	0.51	2.72
0.90	-0.44	-0.49	-0.53	-0.50	-0.29	0.58
0.95	-0.42	-0.48	-0.56	-0.64	-0.71	-0.66
1.00	-0.36	-0.42	-0.50	-0.60	-0.75	-0.96

Table 5a.

Curvature values for n = 1

Radius	Clamping radius ratio, b/a					
	0.1	0.2	0.3	0.4	0.5	0.6
0.10	13.49	-	-	-	-	-
0.15	6.34	-	-	-	-	-
0.20	3.95	11.54	-	-	-	-
0.25	2.77	7.27	-	-	-	
0.30	2.05	5.03	12.20	-	-	-
0.35	1.55	3.66	8.56	-	-	-
0.40	1.18	2.72	6.24	14.39	-	-
0.45	0.89	2.04	4.62	10.40	-	-
0.50	0.66	1.51	3.42	7.86	18.62	-
0.55	0.46	1.09	2.50	5.81	13.90	-
0.60	0.31	0.74	1.77	4.21	10.26	26.76
0.65	0.18	0.46	1.18	2.93	7.38	19.72
0.70	0.07	0.24	0.71	1.91	5.05	14.02
0.75	-0.01	0.06	0.33	1.09	3.18	9.37
0.80	-0.07	-0.06	0.05	0.46	1.71	5.62
0.85	-0.11	-0.15	-0.14	0.01	0.61	2.71
0.90	-0.12	-0.19	-0.25	-0.27	-0.12	0.66
0.95	-0.11	-0.19	-0.28	-0.38	-0.48	-0.48
1.00	-0.03	-0.14	-0.21	-0.31	-0.45	-0.66

Table 5b.

Curvature values for n = 2

Radius	Clamping radius ratio, b/a					
	0.1	0.2	0.3	0.4	0.5	0.6
0.10	10.48	-	-	-	-	-
0.15	4.10	-	-	-	-	-
0.20	2.96	11.26	-	-	-	-
0.25	2.57	6.10	-	-	-	-
0.30	2.35	4.16	12.75	-	-	-
0.35	2.17	3.23	8.03	-	-	-
0.40	2.00	2.67	5.60	15.31	-	-
0.45	1.83	2.29	4.19	10.40	-	-
0.50	1.67	1.98	3.25	7.40	19.73	-
0.55	1.50	1.71	2.58	5.42	13.89	-
0.60	1.33	1.46	2.04	3.99	9.89	27.99
0.65	1.18	1.24	1.61	2.92	7.00	19.76
0.70	1.03	1.05	1.25	2.08	4.81	13.66
0.75	0.90	0.88	0.96	1.42	3.13	8.98
0.80	0.80	0.75	0.73	0.92	1.85	5.38
0.85	0.72	0.65	0.58	0.58	0.94	2.70
0.90	0.67	0.61	0.50	0.39	0.38	0.91
0.95	0.67	0.61	0.52	0.38	0.20	0.06
1.00	0.71	0.68	0.63	0.55	0.43	0.23

Table 5c.

Curvature values for n = 3

Radius	Clamping radius ratio, b/a					
	0.1	0.2	0.3	0.4	0.5	0.6
0.10	4.20	-	-	-	-	-
0.15	1.76	-	-	-	-	-
0.20	1.95	8.12	-	-	-	-
0.25	2.30	3.98	-	-	-	-
0.30	2.60	3.11	11.77	-	-	-
0.35	2.82	2.98	6.65	-	-	-
0.40	2.95	3.00	4.71	15.70	-	-
0.45	3.01	3.01	3.87	9.70	-	-
0.50	2.97	2.97	3.42	6.72	20.96	-
0.55	2.87	2.86	3.11	5.05	13.64	-
0.60	2.71	2.69	2.82	3.99	9.34	29.72
0.65	2.50	2.48	2.53	3.22	6.58	19.73
0.70	2.26	2.24	2.24	2.60	4.66	13.12
0.75	2.03	2.01	1.97	2.10	3.25	8.48
0.80	1.83	1.81	1.74	1.71	2.21	5.13
0.85	1.70	1.67	1.58	1.46	1.52	2.78
0.90	1.67	1.64	1.55	1.38	1.18	1.36
0.95	1.77	1.76	1.69	1.53	1.28	0.96
1.00	2.07	2.06	2.04	1.99	1.89	1.71

Table 5d.

Curvature values for n = 4

Radius	Clamping radius ratio, b/a					
	0.1	0.2	0.3	0.4	0.5	0.6
0.10	1.19	-	-	-	-	-
0.15	0.66	-	-	-	-	-
0.20	1.08	4.52	-	-	-	-
0.25	1.61	2.17	-	-	-	-
0.30	2.16	2.21	9.30	-	-	-
0.35	2.69	2.65	4.86	-	-	-
0.40	3.18	3.13	3.82	14.95	-	-
0.45	3.56	3.52	3.71	8.46	-	-
0.50	3.83	3.80	3.82	5.94	21.72	-
0.55	3.96	3.94	3.90	4.88	13.02	-
0.60	3.94	3.92	3.87	4.32	8.69	31.57
0.65	3.78	3.77	3.72	3.90	6.29	19.51
0.70	3.52	3.52	3.47	3.50	4.76	12.47
0.75	3.21	3.20	3.15	3.10	3.66	8.00
0.80	2.91	2.90	2.85	2.73	2.85	4.99
0.85	2.71	2.71	2.66	2.50	2.33	3.02
0.90	2.74	2.73	2.69	2.53	2.21	2.02
0.95	3.13	3.12	3.09	2.97	2.67	2.17
1.00	4.04	4.03	4.03	4.00	3.93	3.78

Table 5e.

Chapter 5

DISCUSSIONS AND CONCLUSIONS

5.1 Membrane Stresses

Membrane stresses have been shown to depend on the square of the transverse deflection of the plate. In the absence of internal stresses, the membrane stresses only contribute to the membrane energy which causes significant nonlinearity in the plate at high deflection amplitudes. Therefore, membrane stresses are not important in initially stress-free disc vibrating with small amplitudes. When internal stresses are present, the interaction between the internal stresses and the membrane stresses produces interaction strain energy. This energy, like the bending strain energy, is proportional to the square of the deflection, and as such, membrane stresses are important in vibrating plates having internal stresses, even when such plates vibrate with small amplitudes.

The membrane stress values given were found by assuming that the mode shape is not significantly affected by the plate amplitude. This assumption, though not strictly correct, was found to be adequate in determining the nonlinear frequencies. The calculation of the harmonic membrane stresses, for the higher modes, involved large

powers of the inverse of the radius; this gave rise to errors, especially when the clamping ratio was small. This is partly why harmonic stress values have not been presented for the plate with clamping ratio of 0.1 and vibrating with 3 and 4 nodal diameters, and for the plate with clamping ratio of 0.3 and vibrating with 4 nodal diameters.

The axisymmetric components of the membrane stresses were found to be more significant than the harmonic components, except for the mode n=1. In circular plates, membrane stresses around the rim make the major contribution to the energy constants, for the higher modes(n>2). For the mode n=0, there is only the symmetric stress function, and the tangential stresses are compressive at the rim. For the mode n=1, the maximum radial component of stress from the harmonic stress function, P, and the symmetric stress function, Q, were found to have the same values over the unclamped region of the plate; and the stresses were tensile. The tangential stresses were compressive at the rim and the maximum value of the harmonic component was equal to the value of the symmetric component at the rim.

For the mode n=2, the tangential stresses from the symmetric function, Q, were tensile at the rim, and the values at the rim were relatively unaffected by the

clamping ratio. The stresses from the harmonic function are relatively small for the smaller clamping ratios($\alpha<0.3$), but for clamping ratio of 0.5 and over, the harmonic stresses are much larger.

For the higher modes($n>3$), the evaluation of the harmonic stresses for plates with small clamping ratios become difficult, as small numerical values have to be raised to high powers. The harmonic stresses are small for plates with smaller clamping ratios, and only become significant in plates with larger clamping ratios. The clamping ratio at which the harmonic stresses become significant is dependent on the mode of vibration; and the clamping ratio giving relatively significant harmonic stresses increases with increase in the number of nodal diameters. The axisymmetric tangential stresses are tensile at the rim, and for each mode the values of the stresses at the rim are relatively unaffected by the clamping ratio.

5.2 Internal Stresses

5.2.1 Rotational Stresses

The effect of the rotational stresses is manifest as the interaction strain energy; this is the energy due to the interaction between the rotational stresses and the membrane stresses. Using a minimising method to derive the energy quantities, it was found that the effect of speed on the mode shape, in a practical situation, is not significant.

Membrane stress values are dependent on vibration amplitude, which affects the mode shape, consequently, the interaction energy is affected by vibration amplitude, although in most practical cases, this effect is not significant.

5.2.2 Initial Stresses

The initial stresses encountered during this study were mainly asymmetric stresses with unknown magnitude and distribution. The effects of initial stresses were more evident in the 1mm and 2mm thick plates. There was frequency separation between the two principal modes, especially for the mode n=2. Without any heat-treatment most of the cold-rolled plates had natural frequencies slightly higher than expected. Heat-treatment brought their natural frequencies closer to the expected values. The 1mm thick plates, even after heat-treatment, had too

much stress and could not be used for most of the tests. The actual stress value was probably the same as in the thicker plates but produced a change in natural frequency proportional to reciprocal thickness squared. The stress relieving method did not significantly reduce the frequency separation between the principal orthogonal modes.

5.3 Natural Frequencies

The natural frequencies for the 3mm thick plates were close to within 2 percent. of the expected theoretical values. The accuracy was much better for the higher modes(n>3). Some of the 2mm thick plates had to be stress-relieved to get the values of the natural frequencies to within 2 percent. of the expected values. The frequency separation of up to 2 percent. that was found in most of the plates for the mode n=2, was not reduced by the heat treatment. This is thought to be due to elastic anisotropy produced by rolling.

It was found that natural frequencies determined using the vibrator were slightly higher, by up to 2 percent., than those determined with the discs excited using the electromagnet. The main differences between the two forms of excitation are (i) in the manner in which the force was transmitted to the discs, and (ii) the area of the disc that the force was acting upon. The second

difference is, perhaps, not very significant as the force required to effect resonance can be relatively small. With the vibrator being used, the mass of the moving coil of the vibrator becomes part of the vibrating disc system, but the spring stiffnes of the moving coil also contributes to the stiffness of the whole system.

The frequency values determined by the various energy methods are seen to compare well with the exact frequency values (table 2). The finite element method was used to derive the natural frequencies of perfect discs in order to determine the accuracy of results obtained when the method is used. Accuracy is improved in the modified Rayleigh method by increasing the number of subdivisions of the plate radius and using the optimum index value for the fifth term in the displacement function. In order to improve the accuracy of the Rayleigh-Ritz method, the number of subdivisions and the number of terms in the displacement function have to be increased, and the choice of admissible displacement function could be improved. In the finite element method, there are more factors that affect the derived frequencies; factors such as the number of elements,the configuration of each element, the assumed interpolation function, the solution routine. To obtain the same degree of accuracy using the three methods, the computing time and space is much larger for the finite

element method than for the other two methods; and that for the Ritz method is more than for the modified Rayleigh method. The use of the finite element method is justified only for the analysis of discs with non-concentric or irregular boundaries. The use of the Ritz method is desirable in the analysis of discs with radius-dependent thickness variation, or if the eigenvalues corresponding to the modes with nodal circles are required.

5.4 Wave Frequencies

The experimental results, generally, agreed well with the theoretical analysis of travelling wave response frequencies. The clamping pressure was found to be important, and inadequate clamping pressure, especially at the higher speeds, led to lower wave frequencies. The interaction energy values were calculated using relations in equation 2.79. An alternative method would be to determine the rotational and membrane stresses and then find the interaction energy between them.

5.5 Frequency Separation

It was found that reasonable frequency separation could be generated by using position-clamping, especially at higher equivalent clamping ratios. Clamping at two discrete positions yields significant frequency separation in the lower modes, but it is impractical in fast spinning discs. Discs with two opposite holes also gave an increasingly large frequency separation at increased clamping ratios. A given area of hole led to higher frequency separations at the higher clamping ratios.

Tests showed that, in position-clamping, the smaller the area of the clamping pad, the larger the amount of frequency separation. Position-clamping changes the mode pattern of the vibrating disc, and a nodal circle often runs through the clamping positions and the nodal lines become curves instead of being straight lines. The change in the mode patterns is usually more obvious at the higher clamping ratios. Discs with holes do not show so much change in their mode patterns. Vibration characteristics are mainly affected by the factors that are prevalent towards the rim of the disc, therefore, changes in mode patterns towards the centre of the disc would not have much effect on the frequency response values of the disc.

With both methods of frequency separation, the location of the clamping positions or the circular holes

often determines the positioning of the nodal lines. The nodal lines, in the modes where there is frequency separation between the orthogonal modes, will be approximately symmetrical about the clamping positions or holes. The effect of the radial location of the holes on the frequency separation was not investigated.

As shown in the results for frequencies of the principal orthogonal modes, position-clamping leads to decrease in the response frequencies, compared to equivalent frequencies in discs with all-round circumferential clamping. However, the higher of the two separate frequencies of the orthogonal modes in plates with holes is usually slightly higher than the equivalent value in a perfect disc. Position-clamping, therefore, leads to greater drop in the response frequencies, and consequently the measured critical speeds of discs with position-clamping are lower than those for discs centrally- clamped and having two opposite holes.

The frequency separation that can be achieved by position-clamping at higher clamping ratios is, usually, much higher than by having holes in the disc. The frequency separation effects possible by the practical position-clamping methods are restricted to particular modes of vibration. This restriction could be overcome by using non-circular flanges, such as rectangular or

elliptic flanges. Such an arrangement will be a compromise between the non-practical 2 position-clamping and all-round clamping, leading to frequency separation in the modes, except for the mode n=0, although the amount of frequency separation will not be as high as in a disc clamped at two discrete positions. An alternative arrangement is to combine the two methods (position-clamping and equi-angularly spaced holes) in a single assembled disc in order to get increased frequency separation.

5.6 Damping Values

The tests showed that various factors could affect the damping present in a vibrating disc. These factors include clamping pressure, clamping material, clamping area, and vibration amplitude. It was difficult, especially for the lower modes($n<2$), to have the damping ratio the same in successive experiments, and the decay pattern was often in beat form, making it difficult to measure the time constants of the decaying oscillation. It was found that the decaying oscillations would appear as beats when the damping in the disc assembly was high. In an attempt to increase the damping in the disc assembly, paper and thin rubber sheets were successively put between the flanges and the thin plates. The damping was increased, and so too was the beating effect in the

decaying oscillation.

In the stationary disc, the following factors were found to lead to an increase in the damping present in the assembled disc.

Vibration amplitude: For the lower modes($n<2$), the vibration amplitude that could be attained was higher than in the higher modes. The fall in oscillation amplitude, immediately the forcing function is removed, shows that the damping at higher amplitudes is more than at lower amplitudes. The higher the initial vibration amplitude, the higher is the damping in the disc at the start of the vibration decay. This effect is due to air damping of the transverse motion of the disc; and the higher the disc amplitude, the higher the air damping.

Clamping area: Damping in the vibrating disc was found to increase with increase in the contact area between the disc and its flanges. Damping in discs with position-clamping was found to be generally lower than for discs with round flanges. Damping was also found to increase with increase in the clamping ratio. An increase in the clamping ratio and therefore the clamping area, leads to an increase in the damping.

The factors described for the stationary disc also affect damping in a rotating disc. The disc, rotating at high speed, generates air currents which increase the

damping. The presence of holes increases these air currents and leads to a further increase in the damping in the rotating disc. The damping tests conducted for stationary discs showed that the damping ratio for small amplitudes is dependent on the mode of vibration being excited. In fast spinning discs, the tests showed that damping is due mainly to the external effects such as the air currents that are set up, and consequently, no significant variation in damping values for the two modes of vibration, n=2 and n=3, were observed.

5.7 Standing Wave Amplitudes

There was reasonably good agreement between the experimental estimates of the amplitudes of standing waves and the theoretical values. In the the experiments, the wave amplitudes at the various speeds found in different tests were consistent but the collapse speeds varied by up to 200rpm. Higher collapse speeds were usually attained by reducing the rate of increase of the speed of the disc. As shown in the results, stationary waves for two or more different modes could be separately maintained over a common speed range. When a stationary wave corresponding to a different mode was to be generated, the wave for the prevailing mode was collapsed by removing the point loading and then re-applying it. This procedure might have to be repeated, at different speeds, until the stationary

wave for the desired mode was set up.

The wave amplitudes and the speed range over which the standing wave for a particular mode could be maintained were found to be influenced mainly by the following factors; (i) damping, (ii) applied force, and (iii) clamping ratio.

Damping: This has more effect on the wave amplitude at collapse than on the speed range, if the nonlinearity in the wave is small. When the generated wave is very nonlinear, minor variation in the damping value has a marked effect on the collapse speed but does not significantly affect the wave amplitude at collapse. In such a situation, a small increase in the damping might cause significant decrease in the collapse speed. This is one of the reasons why random variations could be encountered in the values of collapse speeds of standing waves.

Applied force: The greater the applied force, the greater the wave amplitudes, and an increase in the applied force leads to a small increase in the nonlinearity ratio value. As shown in figs. 4.25 to 4.29, larger values of the force displacement coefficient, y',lead to higher wave amplitude at collapse and greater speed ranges over which the waves are maintained. The effect of the applied force on the wave amplitude is dependent on the mode of the wave set

up, the radial position of application of the loading, and the clamping ratio of the disc. The applied force, in a practical situation, will depend on the side-rubbing force.

Clamping ratio: The value of the force displacement ratio is greatly dependent on the clamping ratio(fig. 4.13). Stationary wave amplitudes are higher in the lower modes(n=2,3) at the lower clamping ratios. Unfortunately, side-rubbing in circular saws is more pronounced at the lower clamping ratios. Therefore, in order not to have large stationary wave amplitudes, which will be maintained over large values of speed ranges, the clamping ratio should be made as high as possible.

5.8 Pulsating Waves

The setting up of stationary waves in discs with frequency splitting is only possible because of the nonlinearity present in the discs when large amplitudes are imposed. The nonlinearity leads to coupling between the wave response characteristics that correspond to the two principal modes. Therefore, applying a large enough force on a dynamically imperfect disc leads to a non-standing wave; this has been termed a pulsating wave. The pulsating wave has been defined as a stationary wave because, at constant disc rotational speed, it does not have relative motion in the direction of the rotation of

the disc. Unlike a standing wave, it has relative motion in the transverse direction with fixed nodes not in the plane of the disc.

The two methods used for generating frequency separation between the principal orthogonal modes were found to lead to reasonable reduction in the maximum wave amplitudes and in the speed range over which the waves were maintained. The theory developed for the forced vibration of circular plates, in section 2.5, while it can be applied effectively in estimating wave amplitudes, phase angles, and speed ranges of a standing stationary wave due to a specified force; it cannot be applied directly in determining the response characteristics of pulsating waves because the value and variation of the damping in the disc is difficult to estimate. The theoretical analysis can, however, still act as a useful basis for estimating the effect of frequency separation on the pulsating stationary waves that are set up.

In the tests, significant amounts of frequency separation led to reduction in the maximum stationary wave amplitudes and speed ranges over which they were maintained; although for small percentage values of frequency separation, s, and with a relatively large force displacement ratio, y, the stationary wave seemed to be "standing". Consequently, the test discs, although in some

cases had up to 2 percent. frequency separation in the mode n=2, did not possess significant pulsating amplitude at the higher wave amplitudes.

The important considerations in determining the effect of frequency separation on the response characteristics of the stationary wave in a disc are (i) the force displacement ratio, (ii) the damping, and (iii) the percentage frequency separation. For particular values of damping and frequency separation, the force displacement ratio has to be below a certain value for there to be significant reduction in the stationary wave amplitudes and speed ranges. In order to estimate the amounts of damping and frequency separation necessary to keep the wave amplitudes and speed ranges below particular levels in a practical situation, reliable values for the maximum possible side-rubbing force have to be known. Fortunately, the modes that have higher values of force displacement ratio can also have higher frequency separation and damping values.

The damping present in a pulsating wave will normally be higher than in a standing wave with the same maximum amplitude, and this helps in reducing the maximum pulsating wave amplitude and speed range. The excess damping will depend on the pulsating amplitude and the pulsating frequency. Spinning discs with eccentric holes

have higher damping than perfect discs. Positioned-clamped discs, because of the smaller clamping area, are subject to lower damping values. Consequently, two discs with the same amount of initial frequency separation by the two methods will have different collapse wave amplitudes, as the discs with holes have higher damping than the disc that is clamped at a number of discrete positions.

5.9 Summary

1. Comparison of the response frequencies determined by the different theoretical methods show that the mode shape is not significantly affected by the rotational speed of the disc or by vibration amplitude, particularly for values of maximum rim displacement less than three times the plate thickness.

2. In centrally-clamped discs, the harmonic membrane stresses are less significant than the axisymmetric membrane stresses, except for the mode n=1.

3. Experimental methods of frequency separation led to reduction in disc response frequencies, and the position-clamping method led to considerably lower frequencies, especially at the higher clamping ratios.

4. Stationary wave effects are greater at the smaller clamping ratios and for the lower modes (n=2,3) of vibration.

5. Small values of percentage frequency separation

(s<0.02) did not significantly affect the stationary wave amplitudes. Frequency separation of up to s=0.06 will be enough, in most practical cases, to lead to reasonable reduction in the wave amplitudes.

6. To obtain reliable experimental values of natural frequencies of thin plates, it was necessary to eliminate residual stresses by heat-treatment. For this purpose a suitable furnace was built. Stress-relieving gave a slight reduction in frequency and closer agreement with the theoretical values.

A physical explanation of the representation of the vibration of rotating discs in terms of travelling waves, along with the effects of stationary waves in high speed circular saws, is given in appendix IV.

REFERENCES

1. Poisson, S. D., "Sur le Mouvement des Corps Elatiques", Mem. Acad. Royale des Sciences de lInstitute de France, 8, 1829.

2. Deresiewicz, H. and Mindlin, R. D., "Axially Symmetric Flexural Vibrations of a Circular Disk", J. Appl. Mech., p. 86, 1954.

3. Kirchoff, G., "Uber das Gleinchgewicht und die Bewegung Einer Elastichen Sichneibe", J. reine angew. Math., 40, 1850.

4. McLeod, A. J. and Bishop, R. E. D., "The Forced Vibration of Circular Flat Plates", Mech. Engng. Sci. Mono., #1, The Inst. Mech. Engnrs., 1965.

5. Mote, C. D., "Free Vibration of Initially Stressed Circular Disks", J. Engng. Ind., Trans. ASME, vol 87, p 258, 1965.

6. Rayleigh, Lord, Theory of Sound, Dover Publications, 1945.

7. Southwell, R. V., "On the Free Vibration of a Uniform Circular Disk Clamped at its Centre; and on the Effects of Rotation", Proc. Roy. Soc. of London, vol. 101, p. 133, 1922.

8. Vogel, S. M. and Skinner, D. W., "Natural Frequencies of Transversely Vibrating Uniform Annular Plates", J. Appl. Mech., vol. 32, p. 926, 1965.

9. Lamb, H. and Southwell, R. V., "The Vibrations of a Spinning Disk", Proc. Roy. Soc. of London, p. 272, 1921.

10. Mote, C. D., "Natural Frequecies in Annuli with Induced Thermal Membrane Stress", Jnl. Engng. Industry, Trans ASME vol. 89, p. 611, 1967.

11. Tobias, S. A. and Arnold, R. N., "The Influence of Dynamical Imperfection on the vibration of Rotating Disks", Proc. Institution of Mech. Engnrs., vol. 171, p. 669, 1957.

12. Dugdale, D. S., "Experimental Analysis of Circular Saw Vibration", 3rd Wood Machining Seminars, Proc, of Forest Products Lab., Richmond, 1973.

13. Dugdale, D. S., "Stiffness of a Spinning Disk Clamped at its Centre", J. Mech. Phys. Solids, vol. 141 p. 349, 1966.

14. Dugdale, D. S., "Measurement of Internal Stress in Discs," Int. J. Engng. Sci., vol. 1, p. 383, 1963.

15. Dugdale,D.S.,"Theory of Circular Saw Tensioning," The Inst. J. Prod. Res., The Inst. of Production Engineers, vol. 4, no. 2, p. 237, 1966.

16. Dugdale, D. S., "Effect of Internal Stress on the Flexural Stiffness of Disc", Int. J. Energy Sci., vol. 1, p. 89, 1963.

17. Dugdale, D. S., "Flexure of Thin Plates Containing Internal Stress", Int. J. Engng. Sci. , vol. 6, p. 239, 1968.

18. Mote, C. D., "Theory of Thermal Natural Frequency Variation in a Disk", Int. J. Mech. Sci., vol. 8, p. 547, 1966.

19. Mote, C. D., "Transient Thermal Stress and Associated Natural Frequency Variations in Circular Disk Elements", J. Engng. Ind., Trans ASME, vol. 89, p. 265, 1967.

20. Mote, C. D., "Unsymmetrical Transient Heat Conduction: Rotating Disk Applications", J. Engng. Ind., Trans ASME vol. 92, p. 181, 1970.

21. Mote, C. D. and Nieh, L. T., "Control of Circular Disk Stability with Membrane Stress", Experimental Mechanics, Nov., 1971.

22. Szymani, R., "Residual Stresses and Tension of Circular Saws for Wood", Univ. of Calif. For Prod. Lab., Service Report 35.01.94, Feb., 1972.

23. Berger, H. M., "A New Approach to the Analysis of Large Deflection of Plates", J. Appl. Mech., Trans ASME, p. 465, 1955.

24. Way, S., "Bending of Circular Plates with Large Deflections", Trans ASME, vol. 56, p. 627, 1934.

25. Dugdale, D. S. and Squires, B. A., "Effect of Residual Load on the Flexural Stiffness of a Thin Disc", J. Mech. Phys. Solids, vol. 13, p. 237, 1965.

26. Dugdale, D. S., "Non-linear Vibration of a Centrally Clamped Rotating Disc", Int. J. Engng. Sci., vol. 17, p. 745, 1979.

27. Battacharya, A. P. and others,"Large Amplitude Vibration of Sectoral Plates", J. Sound & Vibration, vol. 52, p. 137, 1977.

28. Cheng-in, A. and Vinson, J.R., "Influences of Large Amplitudes, Transverse Shear Deformation, and Rotary Intertia on Lateral Vibrations of Transversely Isotropic Plates", J. Appl. Mech., Trans ASME, p. 254, 1969.

29. Wah, J., "Vibration of Circular Plates at Large Amplitude", Pro. ASCE, Engng. Mech. Div., EMS, p. 1, 1965.

30. Tobias, S. A., "Free Undamped Nonlinear Vibrations of Imperfect Cicular Disks", Proc. of Instution of Mech. Engrs., vol.171, p. 691, 1957.

31. Reismann, H., "Forced Vibration of a Circular Plate", Trans ASME, vol. 81 (3) Series E, p. 526, 1959.

32. Dugdale, D. S., "Circular Saw Vibration during Initial Engagement", Pro. 19th. Int. Mach. Tool Des. Res.Conf., Macmillan Press, London, p. 477.

33. Ellis, R. W. and Mote, C. D., "Increased Lateral Saw Stiffness and Vibration Damping with Feedback Control", Wood Science, vol. 11, p. 56, 1978.

34. Zenneck, J., "Uber die Freien Schuwingungen Angenahernd Vollkommerner Kreisformiger Platten", Annalen de Physik, vol. 67, p. 164, 1899.

35. Dugdale, D. S., "Effects of Holes and Slots on Vibration of Circular Saws", Sixth Wood Mach. Seminar, Univ. of Califor. For. Prod. Lab., Richmond, 1979.

36. Mote, C. D., "Stability Control Analysis Of Rotating Plates by Finite Element: Emphasis on Slots and Holes", J. Dynamic Sys., Measurement, and Control, Trans. ASME, 1972.

37. Stephenson, E. and Plank, D., Circular Saws, Thomas Robinson and Son Ltd., 1972.

38. Love, A. H., The Mathematical Theory of Elasticity, 4th Edition, Cambridge Univ. Press, 1934.

39. Langhaar, H. L., Energy Methods in Applied Mechanics, John Wiley and Sons Inc., 1962.

40. Timoshenko, S. and Woinosky-Krieger, S., Theory of Plates and Shells, 2nd Edition, McGraw-Hill Inc., 1959.

41. Weinstock, R. Calculus of Variations, Dover Publication Inc., 1974.

42. Meirovitch, L., Elements of Vibration Analysis, McGraw-Hill Inc., 1975.

43. Martin, H. C. and Carey, G. F., Introduction to the Finite Element Analysis, McGraw-Hill Inc., 1973.

44. Dugdale, D. S., "Internal Stress in Tools", Strain, vol. 3, #4, 1967.

45. Oding, I. A.(ed.), Creep and Stress Relaxation in Metals, Oliver and Boyd Ltd., 1965.

46. Burger, F. K., Design for Welding, Longmans Green, 1948.

47. Baker, W. E., Woolman, W. E. and Young, D., "Air and Internal Damping of Thin Cantilever Beams", Int. J. Mech. Sci., vol. 9, p. 743, 1967.

```
C                *** PROGRAM  BESSL ***
C
      LIBRARY(SUBGROUPNAGF)
      LIBRARY(SUBGROUPNAGG)
      LIBRARY(SUBGROUPNAGH)
      PROGRAM(TEST)
      INPUT 1=CRO
      OUTPUT 2=LPO
      TRACE 2
      END

      MASTER BESSL
C
C**** THIS PROGRAM EVALUATES THE NATURAL FREQUENCY AND MODE SHAPE OF
C**** A FLAT CIRCULAR PLATE USING BESSEL FUNCTIONS.
C
      DIMENSION TITLE(10)
C
C**** READ AND WRITE TITLE
C
      READ(1,101)TITLE
      WRITE(2,201)TITLE
      WRITE(2,202)
C
C**** CALL SUBPROGRAM TO READ PLATE DIMENSIONS AND PROPERTIES.
C
      CALL PDATA
      STOP
  101 FORMAT(10A8)
  201 FORMAT(1H1,8X,9A8)
  202 FORMAT(1H+,8X,80(1H=))
      END

      SUBROUTINE PDATA
C
C**** THIS SUBPROGRAM READS IN THE PLATE DIMENSIONS AND MATERIAL
C**** PROPERTIES.
C
      COMMON/ADATA/N,ALPHA,FC,A(6,6),U(20,4),V(20,4),W(20,4),Z(20,4),PR
     *,B(6,1),C(6,1),R(100),R1(100),R2(100)
C
C**** INPUT AS DATA SOME MATERIAL PROPERTIES.
C
      DIMENSION PR1(10),RHO1(10),YM1(10)
      DATA PR1(1)/0.3/,RHO1(1)/7800./,YM1(1)/210.E9/
C
C**** READ MATERIAL PROPERTIES.IP IS THE PROPERTY NUMBER.
```

```
C
      READ(1,107)IP
      WRITE(2,99)IP
      IF(IP.GT.5)GO TO 11
      PR=PR1(IP)
      RHO=RHO1(IP)
      YM=YM1(IP)
      GO TO 12
   11 READ(1,108)PR,RHO,YM
   12 WRITE(2,208)PR,RHO,YM
C
C**** READ AND WRITE PLATE DIMENSIONS.OUTSIDE RADIUS,RO IN METRES,
C**** CLAMPING RADIUS,RI IN METRES,PLATE THICKNESS,H IN MILLIMETRES.
C
    9 READ(1,106)RO,RI,H,ISTOP
      WRITE(2,206)RO,RI,H
C
C**** CALCULATE THE CLAMPING RATIO,ALPHA.
C
      ALPHA=RI/RO
      WRITE(2,207)ALPHA
C
C**** CALCULATE PLATE FREQUENCY CONSTANT.
C
      H1=H/1000.
      FC=RO**2/H1*SQRT(RHO*12.*(1.-PR**2)/YM)
      WRITE(2,209)FC
C
C**** CALL SUBPROGRAM TO START EVALUATION OF FREQUENCY VALUE.
C
      CALL VALUES1
      WRITE(2,203)
      IF(ISTOP.GT.0)GO TO 9
      RETURN
   99 FORMAT(1HO,8X,18HPROPERTY NUMBER = ,I2)
  106 FORMAT(3F10.6,I5)
  107 FORMAT(I5)
  108 FORMAT(F5.2,F10.3,E14.7)
  203 FORMAT(1HO,4X,72(1H-)//)
  206 FORMAT(1HO,8X,17HOUTSIDE RADIUS = ,F7.4,5HMETRE,//8X,18HCLAMPING
     *RADIUS =,F7.4,5HMETRE,//8X,18HPLATE THICKNESS = ,F8.5,
     *11HMILLIMETRES)
  207 FORMAT(1HO,8X,17HCLAMPING RATIO = ,F5.3)
  208 FORMAT(1HO,8X,17HPOISSONS RATIO = ,F4.2,//8X,16HPLATE DENSITY = ,
     *F8.2,7HKG/M**3,//8X,17HYOUNGS MODULUS = ,E14.7,6HN/M**2)
  209 FORMAT(1HO,8X,27HPLATE FREQUENCY CONSTANT = ,F10.6)
      END
```

```
      SUBROUTINE VALUES1
C
C**** THIS SUBPROGRAM DEFINES THE MODE OF VIBRATION CONSIDERED,THE
C**** FREQUENCY VALUE RANGE.IT OUTLINES THE MRTHOD OF INVERSE LINEAR
C**** INTERPOLATION.
C
      COMMON/ADATA/N,ALPHA,FC,A(6,6),U(20,4),V(20,4),W(20,4),Z(20,4),PR
     *,B(6,1),C(6,1),R(100),R1(100),R2(100)
      REAL DET,WKSPCE(18),X(20),FX(20)
      PI=3.141592654
C
C**** READ AND WRITE MODE NUMBER,N.
C
   10 READ(1,111)N,ISTOP
      WRITE(2,211)N
      EPSO=0.00001
      IMAX=15
C
C**** READ AND WRITE FREQUENCY VALUE RANGE,ERROR MARGIN,MAXIMUM NUMBER
C**** OF ITERATIONS.
C
      I=1
      READ(1,112)XF1,XF2
      WRITE(2,212)XF1,XF2,EPSO
      X(1)=SQRT(XF1*FC*2.*PI)
      WRITE(2,198)I,X(I)
      X(2)=SQRT(XF2*FC*2.*PI)
      CALL BESSEL(X(1))
      IF(N.EQ.0)GO TO 31
      CALL VALUES2(X(1))
   31 CONTINUE
      CALL VALUES3(X(1))
      M=4
      IA=6
      IFAIL=1
      CALL F03AAF(A,IA,M,DET,WKSPCE,IFAIL)
C
C**** NAG LIBRARY ROUTINE TO CALCULATE THE DETERMINANT
C     OF A REAL MATRIX USING THE FACTORISATION METHOD
C     OF CROUT.
C
      FX(1)=DET
      I=2
   13 WRITE(2,198)I,X(I)
      CALL BESSEL(X(I))
      IF(N.EQ.0)GO TO 32
      CALL VALUES2(X(I))
   32 CONTINUE
      CALL VALUES3(X(I))
      M=4
```

```
      IA=6
      IFAIL=1
      CALL F03AAF(A,IA,M,DET,WKSPCE,IFAIL)
      IF(IFAIL.EQ.0)GO TO 33
      WRITE(2,216)IFAIL
      GO TO 34
   33 CONTINUE
      FX(I)=DET
      IF(I.EQ.2)GO TO 41
      FH=FX(1)*FX(I)
      IF(FH.LE.0.)GO TO 41
      X(1)=X(I-1)
      FX(1)=FX(I-1)
   41 X(I+1)=X(I)-(X(I)-X(1))*FX(I)/(FX(I)-FX(1))
      DEL=ABS(X(I+1)-X(I))
      IF(DEL-EPS0)14,14,15
   15 IF(I-IMAX)16,17,17
   16 I=I+1
      GO TO 13
   17 WRITE(2,213)IMAX
      GO TO 14
   14 XP=X(I+1)**2/(FC*2.*PI)
      XK=X(I+1)**2
      WRITE(2,214)XP
      WRITE(2,215)XK
      CALL BESSEL(X(I+1))
      IF(N.EQ.0)GO TO 51
      CALL VALUES2(X(I+1))
    51 CONTINUE
      CALL VALUES3(X(I+1))
      CALL GAUSS
      CALL VALUES4(X(I+1))
      WRITE(2,210)
    34 CONTINUE
      IF(ISTOP.GT.0)GO TO 10
      RETURN
   111 FORMAT(2I5)
   112 FORMAT(2F10.4,F10.8,I5)
   198 FORMAT(1HO,8X,'I =',I2,'X(I) =',F8.4)
   199 FORMAT(1HO,4X,4(4X,E15.7))
   210 FORMAT(1HO,4X,72(1H-))
   211 FORMAT(1HO,8X,33HTHE NUMBER OF NODAL DIAMETER,N = ,I2)
   212 FORMAT(1HO,8X,27HLOWER FREQUENCY VALUE,X1 = ,F8.4,3HC/S,//8X,
     *27HUPPER FREQUENCY VALUE,X2 = ,F8.4,3HC/S,//8X,18HTHE ERROR MARGIN
     * =,E14.7)
   213 FORMAT(1HO,4X,21HFAILS TO CONVERGE IN ,I2,10HITERATIONS)
   214 FORMAT(1HO,8X,30HTHE NATURAL FREQUENCY VALUE = ,F8.4,3HC/S)
   215 FORMAT(1HO,8X,25HTHE FRQUENCY PARAMETER = ,F10.6)
   216 FORMAT(1HO,8X,'IFAIL = ',I2)
      END
```

```
      SUBROUTINE BESSEL(X)
C
C**** THIS SUBPROGRAM EVALUATES THE BESSEL FUNCTION VALUES NECESSARY.
C
      COMMON/ADATA/N,ALPHA,FC,A(6,6),U(20,4),V(20,4),W(20,4),Z(20,4),PR
     *,B(6,1),C(6,1),R(100),R1(100),R2(100)
      DIMENSION Y(2)
      Y(1)=X
      Y(2)=X*ALPHA
      IFAIL=0
      DO 18 I=1,2
      U(1,I)=S17AEF(Y(I),IFAIL)
C
C**** THE NAG LIBRARY ROUTINE RETURNS A VALUE FOR THE
C     BESSEL FUNCTION JO(X).
C
      U(2,I)=S17AFF(Y(I),IFAIL)
C
C**** THE NAG LIBRARY ROUTINE RETURNS A VALUE FOR THE
C     BESSEL FUNCTION J1(X).
C
      V(1,I)=S17ACF(Y(I),IFAIL)
C
C**** THE NAG LIBRARY ROUTINE RETURNS A VALUE FOR THE
C     BESSEL FUNCTION YO(X).
C
      V(2,I)=S17ADF(Y(I),IFAIL)
C
C**** THE NAG LIBRARY ROUTINE RETURNS A VALUE FOR THE
C     BESSEL FUNCTION Y1(X).
C
      W(1,I)=S18AEF(Y(I),IFAIL)
C
C**** THE NAG LIBRARY ROUTINE RETURNS A VALUE FOR THE
C     MODIFIED BESSEL FUNCTION IO(X).
C
      W(2,I)=S18AFF(Y(I),IFAIL)
C
C**** THE NAG LIBRARY ROUTINE RETURNS A VALUE FOR THE
C     MODIFIED BESSEL FUNCTION I1(X).
C
      Z(1,I)=S18ACF(Y(I),IFAIL)
C
C**** THE NAG LIBRARY ROUTINE RETURNS A VALUE FOR THE
C     MODIFIED BESSEL FUNCTION KO(X).
C
      Z(2,I)=S18ADF(Y(I),IFAIL)
C
C**** THE NAG LIBRARY ROUTINE RETURNS A VALUE FOR THE
C     MODIFIED BESSEL FUNCTION K1(X).
```

```
C
   18 CONTINUE
      RETURN
      END

      SUBROUTINE VALUES2(X)
C
C**** THIS SUBPROGRAM EVALUATES THE BESSEL FUNCTION VALUES N AND
C**** (N+1).
C
      COMMON/ADATA/N,ALPHA,FC,A(6,6),U(20,4),V(20,4),W(20,4),Z(20,4),PR
     *,B(6,1),C(6,1),R(100),R1(100),R2(100)
      DIMENSION Y(2)
      Y(1)=X
      Y(2)=X*ALPHA
      DO 20 I=3,N+2
      K=I-2
      DO 19 J=1,2
      U(I,J)=-U((I-2),J)+2.*K/Y(J)*U((I-1),J)
      V(I,J)=-V((I-2),J)+2.*K/Y(J)*V((I-1),J)
      W(I,J)=W((I-2),J)-2.*K/Y(J)*W((I-1),J)
      Z(I,J)=Z((I-2),J)+2.*K/Y(J)*Z((I-1),J)
   19 CONTINUE
   20 CONTINUE
      RETURN
      END

      SUBROUTINE VALUES3(X)
C
C**** THIS SUBPROGRAM EVALUATES THE COMPONENTS OF THE MATRIX WHOSE
C**** DETERMINANT IS TO BE FOUND.
C
      COMMON/ADATA/N,ALPHA,FC,A(6,6),U(20,4),V(20,4),W(20,4),Z(20,4),PR
     *,B(6,1),C(6,1),R(100),R1(100),R2(100)
      DIMENSION Y(2)
      Y(1)=X
      Y(2)=X*ALPHA
      A(1,1)=U((N+1),2)
      A(1,2)=V((N+1),2)
      A(1,3)=W((N+1),2)
      A(1,4)=Z((N+1),2)
      A(2,1)=(N*U((N+1),2)-Y(2)*U((N+2),2))/ALPHA
      A(2,2)=(N*V((N+1),2)-Y(2)*V((N+2),2))/ALPHA
      A(2,3)=(N*W((N+1),2)+Y(2)*W((N+2),2))/ALPHA
      A(2,4)=(N*Z((N+1),2)-Y(2)*Z((N+2),2))/ALPHA
      A(3,1)=(N*(N-1)*(1.-PR)-Y(1)**2)*U((N+1),1)+Y(1)*(1-PR)*U((N+2),1)
      A(3,2)=(N*(N-1)*(1.-PR)-Y(1)**2)*V((N+1),1)+Y(1)*(1-PR)*V((N+2),1)
      A(3,3)=(N*(N-1)*(1.-PR)+Y(1)**2)*W((N+1),1)-Y(1)*(1-PR)*W((N+2),1)
      A(3,4)=(N*(N-1)*(1.-PR)+Y(1)**2)*Z((N+1),1)+Y(1)*(1-PR)*Z((N+2),1)
      A(4,1)=(-N*Y(1)**2+(1.-PR)*(1-N)*N*N)*U((N+1),1)+(Y(1)**3+Y(1)
```

```
     **(1.-PR)*N*N)*U((N+2),1)
      A(4,2)=(-N*Y(1)**2+(1.-PR)*(1-N)*N*N)*V((N+1),1)+(Y(1)**3+Y(1)
     **(1.-PR)*N*N)*V((N+2),1)
      A(4,3)=(+N*Y(1)**2+(1.-PR)*(1-N)*N*N)*W((N+1),1)+(Y(1)**3-Y(1)
     **(1.-PR)*N*N)*W((N+2),1)
      A(4,4)=(+N*Y(1)**2+(1.-PR)*(1-N)*N*N)*Z((N+1),1)+(-Y(1)**3+Y(1)
     **(1.-PR)*N*N)*Z((N+2),1)
      RETURN
      END

      SUBROUTINE GAUSS
C
C**** SUBPROGRAM TO DETERMINE THE MATRIX COEFFICIENTS.
C
      COMMON/ADATA/N,ALPHA,FC,A(6,6),U(20,4),V(20,4),W(20,4),Z(20,4),PR
     *,B(6,1),C(6,1),R(100),R1(100),R2(100)
      REAL WKSPCE(30)
      A(4,1)=U((N+1),1)
      A(4,2)=V((N+1),1)
      A(4,3)=W((N+1),1)
      A(4,4)=Z((N+1),1)
      B(1,1)=0.
      B(2,1)=0.
      B(3,1)=0.
      B(4,1)=1.
      NO=4
      M=1
      IA=6
      IB=6
      IC=6
      IFAIL=1
      CALL F04AAF(A,IA,B,IB,NO,M,C,IC,WKSPCE,IFAIL)
C
C**** THE NAG LIBRARY ROUTINE CALCULATES THE APPROXIMATE
C     SOLUTION OF A SET OF REAL LINEAR EQUATIONS BY
C     CROUT'S FACTORISATION METHOD.
C
      IF(IFAIL.EQ.0)GO TO 20
      WRITE(2,99996)IFAIL
      RETURN
   20 WRITE(2,99995)(C(I,1),I=1,NO)
      RETURN
99995 FORMAT(1HO,4(4X,E14.7))
99996 FORMAT(25HOERROR IN F04AAF IFAIL = ,I2)
      END
```

```
      SUBROUTINE VALUES4(XK)
C
C**** SUBPROGRAM TO DETERMINE PLATE DISPLACEMENT, SLOPE, AND
C     CURVATURE VALUES.
C
      COMMON/ADATA/N,ALPHA,FC,A(6,6),U(20,4),V(20,4),W(20,4),Z(20,4),PR
     *,B(6,1),C(6,1),R(100),R1(100),R2(100)
      DIMENSION X(100)
      WRITE(2,220)
      M=(1.-ALPHA)*20+1
      DO 71 I=1,M
      X(I)=ALPHA+(I-1)/20.
      XY=X(I)*XK
      CALL BESSEL(XY)
      IF(N.EQ.0)GO TO 72
      CALL VALUES2(XY)
   72 CONTINUE
      R(I)=C(1,1)*U((N+1),1)+C(2,1)*V((N+1),1)+C(3,1)*W((N+1),1)+
     *C(4,1)*Z((N+1),1)
      R1(I)=(C(1,1)*(N*U((N+1),1)/XY -U((N+2),1))+C(2,1)*(N*V((N+1),1)
     */XY  -V((N+2),1))+C(3,1)*(N*W((N+1),1)/XY  +W((N+2),1))+
     *C(4,1)*(N*Z((N+1),1)/XY  -Z((N+2),1)))*XK
      IF(N.EQ.0)GO TO 73
      R2(I)=(-C(1,1)*(U(N,1)*XY  +(XY  **2-N*(N+1))*U((N+1),1))-
     *C(2,1)*(V(N,1)*XY  +(XY  **2-N*(N+1))*V((N+1),1))-
     *C(3,1)*(W(N,1)*XY  -(XY  **2+N*(N+1))*W((N+1),1))+
     *C(4,1)*(Z(N,1)*XY  +(XY  **2+N*(N+1))*Z((N+1),1)))/X(I)**2
      GO TO 71
   73 R2(I)=(C(1,1)*(U(2,1)/XY -U(1,1))+C(2,1)*(V(2,1)/XY  -V(1,1))+
     *C(3,1)*(W(1,1)-W(2,1)/XY  )+C(4,1)*(Z(2,1)/XY  +Z(1,1)))*XK**2
   71 WRITE(2,221)X(I),R(I),R1(I),R2(I)
      RETURN
  220 FORMAT(1HO,8X,6HRADIUS,5X,12HDISPLACEMENT,8X,5HSLOPE,13X,
     *9HCURVATURE)
  221 FORMAT(1H+,10X,F4.2,9X,F5.3,10X,F7.4,10X,F8.5)
      END
      FINISH
****
```

```
C                *** PROGRAM  MRAYL ***
C
      LIBRARY(SUBGROUPNAGF)
      LIBRARY(SUBGROUPNAGG)
      LIBRARY(SUBGROUPNAGH)
      PROGRAM(ABCD)
      INPUT 1=CR0
      OUTPUT 2=LP0
      TRACE 2
      END

      MASTER MRAYL
      COMMON /ADATA/N0,ALPHA,A(6,6),B(6,1),C(6,1),R(150),R1(150),R2(150)
     *,P1(150),P2(150),P3(150),Q1(150),S1(150),M0,DELTA
      COMMON/BDATA/W2 ,Y,RS(30),RF1(30),RF2(30)
      COMMON /GDATA/N1
      COMMON /HDATA/W3(20,20)
      DIMENSION X1(20),X2(20),Y1(20),Y2(20),Y3(20)
C
C**** THIS PROGRAM IS A MODIFIED RAYLEIGH METHOD FOR THE ANALYSIS OF
C     VIBRATING CENTRALLY-CLAMPED DISCS.
C
       DO 8 J=1,6
      N0=J-1
      DO 9 I=1,7
C
C**** ALPHA IS THE CLAMPING RATIO.
C
       ALPHA=I/10.
      I2=(1-ALPHA)*100+1
      WRITE(2,103)ALPHA
      WRITE(2,102)N0
      IF(N0.LT.4)M0=6
      IF(N0.EQ.4)M0=7
      IF(N0.GT.4)M0=8
      N1=5
      CALL DIFFERS
      CALL GAUSS
      CALL VALUES1
      CALL VALUES2
      CALL SIMPSON
      CALL ENERGY
      CALL SPEED
      CALL MSTRE
    9 CONTINUE
    8 CONTINUE
      STOP
```

```
   99 FORMAT(1HO,3X,'THE DISPLACEMENT/THICKNESS RATIO DELTA =',F4.2)
  102 FORMAT(1HO,4X,'NO =',I2/)
  103 FORMAT(1HO,4X,'ALPHA =',F4.2)
  104 FORMAT(1H ,F6.2)
      END

      SUBROUTINE DIFFERS
      COMMON /ADATA/NO,ALPHA,A(6,6),B(6,1),C(6,1),R(150),R1(150),R2(150)
     *,P1(150),P2(150),P3(150),Q1(150),S1(150),MO,DELTA
C
C**** SUBROUTINE FOR DERIVING THE MATRIX COEFFICIENTS USING THE
C     BOUNDARY CONDITIONS.
C
       B(1,1)=1.
      DO 51 J=2,5
   51 B(J,1)=0.
      A(2,5)=ALPHA**MO
      A(3,5)=MO*ALPHA**(MO-1)
      A(4,5)=MO*(MO-0.7)-0.3*NO*NO
      A(5,5)=MO*MO*(MO-2.)-NO*NO*(1.7*MO-2.7)
      DO 52 K=1,5
   52 A(1,K)=1.
      IF(NO-1)53,54,55
   53 A(1,3)=0.
      A(1,4)=0.
      A(2,1)=1.
      A(2,2)=ALPHA**2
      A(2,3)=ALOG(ALPHA)
      A(2,4)=ALPHA**2*ALOG(ALPHA)
      A(3,1)=0.
      A(3,2)=2.*ALPHA
      A(3,3)=1./ALPHA
      A(3,4)=ALPHA*(2.*ALOG(ALPHA)+1.)
      A(4,1)=0.
      A(4,2)=2.6
      A(4,3)=-0.7
      A(4,4)=3.3
      A(5,1)=0.
      A(5,2)=0.
      A(5,3)=0.
      A(5,4)=4.
      GO TO 56
   54 A(1,4)=0.
      A(2,1)=ALPHA
      A(2,2)=ALPHA**3
      A(2,3)=1./ALPHA
      A(2,4)=ALPHA*ALOG(ALPHA)
      A(3,1)=1.
      A(3,2)=3.*ALPHA**2
      A(3,3)=-1./ALPHA**2
```

```
      A(3,4)=1.+ALOG(ALPHA)
      A(4,1)=0.
      A(4,2)=6.6
      A(4,3)=1.4
      A(4,4)=1.3
      A(5,1)=0.
      A(5,2)=6.6
      A(5,3)=1.4
      A(5,4)=-2.7
      GO TO 56
   55 A(2,1)=ALPHA**NO
      A(2,2)=ALPHA**(NO+2)
      A(2,3)=1./ALPHA**NO
      A(2,4)=1./ALPHA**(NO-2)
      A(3,1)=NO*ALPHA**(NO-1)
      A(3,2)=(NO+2)*ALPHA**(NO+1)
      A(3,3)=-NO/ALPHA**((NO+1))
      A(3,4)=-(NO-2)/ALPHA**(NO-1)
      A(4,1)=0.7*NO*(NO-1.)
      A(4,2)=0.7*NO*NO+3.3*NO+2.6
      A(4,3)=0.7*NO*(NO+1.)
      A(4,4)=0.7*NO*NO-3.3*NO+2.6
      A(5,1)=0.7*NO*NO*(1.-NO)
      A(5,2)=NO*(4.+3.3*NO-0.7*NO*NO)
      A(5,3)=0.7*NO*NO*(NO+1.)
      A(5,4)=NO*(0.7*NO*NO+3.3*NO-4.)
   56 RETURN
      END

       SUBROUTINE GAUSS
C
C**** SUBROUTINE FOR SOLVING THE SIMULTANEOUS EQUATION.
C
       COMMON /ADATA/NO,ALPHA,A(6,6),B(6,1),C(6,1),R(150),R1(150),R2(150)
     *,P1(150),P2(150),P3(150),Q1(150),S1(150),MO,DELTA
      COMMON /GDATA/N
      REAL WKSPCE(40)
      M=1
      IA=6
      IB=6
      IC=6
      IFAIL=1
      CALL F04AAF(A,IA,B,IB,N,M,C,IC,WKSPCE,IFAIL)
C
C**** THE NAG LIBRARY ROUTINE CALCULATES THE APPROXIMATE
C     SOLUTION OF A SET OF REAL LINEAR EQUATUONS BY
C     CROUT'S FACRORISATION METHOD.
C
      IF(IFAIL.EQ.0)GO TO 20
      WRITE(2,99996)IFAIL
```

```
      RETURN
   20 CONTINUE
      RETURN
99996 FORMAT(25HOERROR IN F04AAF IFAIL = ,I2)
99995 FORMAT(1HO,5(4X,E14.7))
      END

      SUBROUTINE VALUES1
C
C**** SUBROUTINE FOR CALCULATING DISPLACEMENT, SLOPE, AND
C     CURVATURE VALUES.
C
       COMMON /ADATA/NO,ALPHA,A(6,6),B(6,1),C(6,1),R(150),R1(150),R2(150
     *,P1(150),P2(150),P3(150),Q1(150),S1(150),MO,DELTA
      DIMENSION X(150)
      P=C(1,1)
      Q=C(2,1)
      S=C(3,1)
      T=C(4,1)
      U=C(5,1)
      I2=(1-ALPHA)*100+1
      DO 60 I=1,I2
      X(I)=ALPHA+(I-1)/100.
      IF(NO-1)61,62,63
   61 R(I)=P+Q*X(I)**2+S*ALOG(X(I))+T*X(I)**2*ALOG(X(I))+U*X(I)**MO
      R1(I)=2.*Q*X(I)+S/X(I)+T*X(I)*(2.*ALOG(X(I))+1.)+MO*U*X(I)**(MO-1)
      R2(I)=2.*Q-S/X(I)**2+T*(2.*ALOG(X(I))+3.)+MO*(MO-1)*U*X(I)**(MO-2)
      GO TO 70
   62 R(I)=P*X(I)+Q*X(I)**3+S/X(I)+T*X(I)*ALOG(X(I))+U*X(I)**MO
      R1(I)=P+3*Q*X(I)**2-S/X(I)**2+T*(1+ALOG(X(I)))+MO*U*X(I)**(MO-1)
      R2(I)=6*Q*X(I)+2*S/X(I)**3+T/X(I)+MO*(MO-1)*U*X(I)**(MO-2)
      GO TO 70
   63 R(I)=P*X(I)**NO+Q*X(I)**(NO+2)+S/X(I)**NO+T/X(I)**(NO-2)+U*X(I)**
     *MO
      R1(I)=NO*P*X(I)**(NO-1)+(NO+2)*Q*X(I)**(NO+1)-NO*S/X(I)**(NO+1)
     *-(NO-2)*T/X(I)**(NO-1)+MO*U*X(I)**(MO-1)
      R2(I)=NO*(NO-1)*P*X(I)**(NO-2)+(NO+2)*(NO+1)*Q*X(I)**NO+NO*(NO+1)*
     *S/X(I)**(NO+2)+(NO-2)*(NO-1)*T/X(I)**NO+MO*(MO-1)*U*X(I)**(MO-2)
   70 CONTINUE
   60 CONTINUE
      RETURN
99998 FORMAT(1HO,10X,'RADIUS',8X,'DISPLACEMENT',8X,'SLOPE',10X,
     *'CURVATURE')
99999 FORMAT(1H+,12X,F4.2,11X,F6.4,10X,F7.4,10X,F8.4)
      END
```

```
      SUBROUTINE VALUES2
C
C**** SUBROUTINE FOR CALCULATING THE ENERGY DENSITIES.
C
       COMMON /ADATA/NO,ALPHA,A(6,6),B(6,1),C(6,1),R(150),R1(150),R2(150)
     *,P1(150),P2(150),P3(150),Q1(150),S1(150),MO,DELTA
      COMMON /CDATA/STMR1(150),STMR2(150),STMT1(150),STMT2(150),
     *STMRT(150)
      COMMON /DDATA/P5(150),P6(150),P7(150),P8(150)
      COMMON /FDATA/ES(110),E2(110),P4(110)
      DIMENSION X(150)
      F=0.05
      F1=F**2
      A1=3.3*(1.+F1)/8
      A2=3.3*F1/8
      I2=(1-ALPHA)*100+1
      DO 130 I=1,I2
      X(I)=ALPHA+(I-1)/100.
      P1(I)=(R2(I)+R1(I)/X(I)-NO*NO*R(I)/X(I)**2)**2
      P2(I)=R2(I)*(R1(I)/X(I)-NO*NO*R(I)/X(I)**2)-NO*NO*(R1(I)/X(I)-
     *R(I)/X(I)**2)**2
      P4(I)=0.375*1.*(3.0*R1(I)**4+3.0*(NO*R(I)/X(I))**4+2.0*(R(I)*R1(I)
     */X(I))**2)*X(I)/2.
      P3(I)=(P1(I)-1.4*P2(I))*X(I)/2.
      P5(I)=(2.*(STMR1(I)+STMT1(I))**2-2.6*2.0*STMR1(I)*STMT1(I))*X(I)/2
      P6(I)=((STMR2(I)+STMT2(I))**2-2.6*(STMR2(I)*STMT2(I)-STMRT(I)**2))
     **X(I)/4.
      P7(I)=(STMR1(I)*R1(I)**2+STMT1(I)*NO*NO*R(I)**2/X(I)**2)*X(I)/4.
      P8(I)=(STMR2(I)*R1(I)**2-STMT2(I)*NO*NO*R(I)**2/X(I)**2-
     *2*STMRT(I)*R1(I)*R(I)*NO/X(I))*X(I)/8.
      Q1(I)=R(I)**2*X(I)/2.
      Z1=A1-A2/X(I)**2-3.3*X(I)**2/8
      Z2=A1+A2/X(I)**2-1.9*X(I)**2/8
      S1(I)=(Z1*R1(I)**2+NO*NO*R(I)**2/X(I)**2*Z2)*X(I)/2.
      ES(I)=0.49*(STMR1(I)+STMT1(I))**2
      E2(I)=1.69*STMR1(I)*STMT1(I)-0.3*(STMR1(I)+STMT1(I))**2
  130 CONTINUE
      RETURN
      END

      SUBROUTINE SIMPSON
C
C**** SUBROUTINE FOR EVALUATING THE FIRST PART OF THE NUMERICAL
C     INTEGRATION.
C
       COMMON /ADATA/NO,ALPHA,A(6,6),B(6,1),C(6,1),R(150),R1(150),R2(150)
     *,P1(150),P2(150),P3(150),Q1(150),S1(150),MO,DELTA
      COMMON /DDATA/P5(150),P6(150),P7(150),P8(150)
      COMMON /FDATA/ES(110),E2(110),P4(110)
      I2=(1-ALPHA)*100+1
```

```
      DO 64 I=2,(I2-1)
      V=I/2.
      I1=V
      IF(I1.NE.V)GO TO 65
      P3(I)=4.*P3(I)
      P5(I)=4.*P5(I)
      P6(I)=4.*P6(I)
      P7(I)=4.*P7(I)
      P8(I)=4.*P8(I)
      Q1(I)=4.*Q1(I)
      S1(I)=4.*S1(I)
      ES(I)=4.*ES(I)
      E2(I)=4.*E2(I)
      P4(I)=4.*P4(I)
      GO TO 64
   65 P3(I)=2.*P3(I)
      P5(I)=2.*P5(I)
      P6(I)=2.*P6(I)
      P7(I)=2.*P7(I)
      P8(I)=2.*P8(I)
      Q1(I)=2.*Q1(I)
      S1(I)=2.*S1(I)
      ES(I)=2.*ES(I)
      E2(I)=2.*E2(I)
      P4(I)=2.*P4(I)
   64 CONTINUE
      RETURN
      END

      SUBROUTINE ENERGY
C
C**** SUBROUTINE FOR CALCULATING THE ENERGY VALUES.
C
       COMMON /ADATA/NO,ALPHA,A(6,6),B(6,1),C(6,1),R(150),R1(150),R2(150)
     *,P1(150),P2(150),P3(150),Q1(150),S1(150),MO,DELTA
      COMMON/BDATA/W2 ,Y,RS(30),RF1(30),RF2(30)
      COMMON /DDATA/P5(150),P6(150),P7(150),P8(150)
      COMMON /FDATA/ES(110),E2(110),P4(110)
      U1=0.
      T1=0.
      UM1=0.
      UM2=0.
      UM3=0.
      UM
      H1=0.
      H2=0.
      H3=0.
      I2=(1-ALPHA)*100+1
      DO 67 I=1,I2
```

```
      U1=U1+P3(I)/300.
      T1=T1+Q1(I)/300.
      V1=V1+S1(I)/300.
      UM1=UM1+P5(I)/300.
      UM2=UM2+P6(I)/300.
      UM3=UM3+P7(I)/300.
      UM4=UM4+P8(I)/300.
      H1=H1+ES(I)/300.
      H2=H2+E2(I)/300.
      H3=H3+P4(I)/300.
   67 CONTINUE
      W=U1/T1
      W2=SQRT(W)
      Y=V1/U1
      Z1=UM1/U1
      Z2=UM2/U1
      WRITE(2,205)U1,T1,W2,V1,UM1,UM2,UM3,UM4
      WRITE(2,206)H1,H2,H3
      RETURN
  201 FORMAT(1HO,4X,'T1 =',E14.7,4X,'U1 =',E14.7,4X,'W =',E14.7,4X,
     *'W2 =',E14.7,4X,'V1 =',E14.7,4X,'Y =',E14.7)
  202 FORMAT(1H ,E15.7)
  203 FORMAT(1HO,4X,'W2 =',E14.7,4X,'Y =',E14.7,4X,'Z =',E14.7)
  204 FORMAT(1HO,4X,'W2 =',E14.7,'Y =',E14.7,'Z1 =',E14.7,'Z2 =',E14.7)
  205 FORMAT(1HO,2X,'U1 =',E12.5,2X,'T1 =',E12.5,2X,'W2 =',F7.4,2X,
     *'V1 =',E12.5,2X,'UM1 =',E12.5,2X,'UM2 =',E12.5,
     *2X,'UM3 =',E12.5,2X,'UM4 =',E12.5)
  206 FORMAT(1HO,4X,'H1 =',F7.4,4X,'H2 =',F7.4,4X,'H3 =',F7.4)
      END

      SUBROUTINE MSTRE
C
C**** SUBROUTINE FOR CALCULATING THE MEMBRANE STRESSES.
C
       COMMON /ADATA/NO,ALPHA,A(6,6),B(6,1),C(6,1),R(150),R1(150),R2(150)
     *,P1(150),P2(150),P3(150),Q1(150),S1(150),MO,DELTA
      COMMON /CDATA/STMR1(150),STMR2(150),STMT1(150),STMT2(150),
     *STMRT(150)
      DIMENSION F1(110),F2(110),F3(110),G0(110),G1(110),G2(110),G3(110),
     *G4(110),X(150),F4(110),F5(110),G5(110),G6(110),G7(110),G8(110),
     *SMR1(110),SMR2(110),SMT1(110),SMT2(110),SMRT(110),Y(110),H1(110),
     *H2(110),H3(110),H4(110),H5(110),H6(110),RF1(110),RF3(110),Q3(110),
     *Q2(110)
      F2(1)=0.
      F4(1)=0.
      G1(1)=0.
      G3(1)=0.
      G5(1)=0.
      G7(1)=0.
      H1(1)=0.
```

```
      H2(1)=0.
      H3(1)=0.
      H4(1)=0.
      H5(1)=0.
      H6(1)=0.
      N=NO
      MM1=(1-ALPHA)*100+1
      MM2=ALPHA*100
      DO 8 I=1,MM1
    8 STMRT(I)=0.
      DO 71 I=2,MM1
      J=I-1
      DK=0.01
      X(I)=ALPHA+(I-1.)*DK
   74 F1(I)=-(R1(I)**2-N*N*R(I)*(2.*R1(I)-R(I)/X(I))/X(I))/(4.*X(I))
      GO(I)=-(R2(I)*R1(I)/X(I)-N*N*(R2(I)*R(I)-(R1(I)-R(I)/X(I))**2)/
     *X(I)**2)/2./X(I)**(2*N-1)
      DO 75 K=2,I
      J=K-1
      F2(K)=F2(J)+(F1(J)+F1(K))*DK/2.
      G1(K)=G1(J)+(GO(J)+GO(K))*DK/2.
   75 CONTINUE
      F3(I)=F2(I)*X(I)
      G2(I)=G1(I)*X(I)**(4*N-1)
      DO 76 K=2,I
      J=K-1
      F4(K)=F4(J)+(F3(J)+F3(K))*DK/2.
      G3(K)=G3(J)+(G2(J)+G2(K))*DK/2.
   76 CONTINUE
      F5(I)=F4(I)/X(I)
      G4(I)=G3(I)/X(I)**(4*N-1)
      DO 77 K=2,I
      J=K-1
      G5(K)=G5(J)+(G4(J)+G4(K))*DK/2.
   77 CONTINUE
      G6(I)=G5(I)*X(I)**(4*N-1)
      DO 78 K=2,I
      J=K-1
      G7(K)=G7(J)+(G6(J)+G6(K))*DK/2.
   78 CONTINUE
      G8(I)=G7(I)/X(I)**(2*N)
   71 CONTINUE
      FS1=F5(MM1)
      FS2=-2.*N*(1.+2.00*N)*G8(MM1)+G6(MM1)
      FS3=-2.*N*((1.+2.*N)*G8(MM1)-G6(MM1))
      A1=-FS1
      A2=0.
      B1=-(FS2+FS3)*8.*N
      B2=(N*FS2+FS3*(N-1))*2/(2*N-1)
      B3=0.
```

```
      B4=0.
      DO 22 I=1,MM1
      STMR2(I)=0.
      STMT2(I)=0.
      STMRT(I)=0.
      SMR2(I)=0.
      SMT2(I)=0.
      SMRT(I)=0.
   22 CONTINUE
      DO 19 I=1,MM1
      X(I)=ALPHA+(I-1.)*DK
      STMR1(I)=F5(I)/X(I)+A1+A2/X(I)**2
      STMT1(I)=F3(I)/X(I)-F5(I)/X(I)+A1-A2/X(I)**2
      IF(N.EQ.0)GO TO 20
      STMR2(I)=G6(I)/X(I)**(2*N+1)-G8(I)*2.*N*(1.+2.00*N)/X(I)**2
     *+B1*(N+1.-2.*N*N)/(8.*N*(2.*N+1.))*X(I)**(2*N)+B2*(1-2*N)*X(I)
     ***(2*N-2)/2.
     *+B3*(N-1.+2.*N*N)/(X(I)**(2*N)*2.*(2.*N-1.))-2.*N*(1.+2.*N)*B4/
     *X(I)**(2*N+2)
      STMT2(I)=-G6(I)/X(I)**(2*N+1)+G4(I)*X(I)**(2*N-1)+2.*N*(2.*N+1.)
     **G8(I)/X(I)**2+B1*(N+1)*X(I)**(2*N)/(8.*N)+B2*(2.*N-1)*X(I)
     ***(2*N-2)/2.
     *-B3*(N-1.)/(2.*X(I)**(2*N))+2.*N*B4*(2.*N+1.)/X(I)**(2*N+2)
      STMRT(I)=-2.*N*((1.+2.*N)*G8(I)/X(I)**2-G6(I)/X(I)**(2*N+1)-
     *B1*X(I)**(2*N)/(16.*N)-B2*(2.*N-1.)*X(I)**(2*N-2)/(4.*N))
     *+N*B3/(2.*X(I)**(2*N))-2.*N*(2.*N+1.)*B4/X(I)**(2*N+2)
      RF1(I)=-(4.*N*N+1.)*G6(I)/X(I)**(2*N+1)+G4(I)*X(I)**(2*N-1)+
     1B1*(N+1-2*N*N)*X(I)**(2*N)/(8*N)-B2*(2*N-1)**2*X(I)**(2*N-2)/2.
     2+2.*N*(2.*N+1.)**2*G8(I)/X(I)**2
      RF3(I)=2*N*(2*N+1)**2*G8(I)/X(I)**2-4*N*G6(I)/X(I)**(2*N+1)+
     1(2*N+1)*B1*X(I)**(2*N)/8.+(2*N-1)**2*B2*X(I)**(2*N-2)/2.
     2+2.*N*G4(I)*X(I)**(2*N-1)
      Q3(I)=RF1(I)+2*N*STMRT(I)-STMT2(I)
      Q2(I)=RF3(I)-2*N*STMT2(I)+STMRT(I)
   20 CONTINUE
   19 CONTINUE
      WRITE(2,202)
      DO 18 I=1,MM2
      Y(I)=(I-1)*DK
      SMR1(I)=A1
      SMT1(I)=A1
      IF(N.EQ.0)GO TO 18
      IF(N.EQ.1.AND.I.EQ.1)GO TO 18
      SMR2(I)=B1*(N+1.-2.*N*N)/(8.*N*(2.*N+1.))*Y(I)**(2*N)+B2*(1.-2.*N)
     **Y(I)**(2*N-2)/2.
      SMT2(I)=B1*(N+1.)*Y(I)**(2*N)/(8.*N)+B2*(2.*N-1.)*Y(I)**(2*N-2)/2.
      SMRT(I)=B1*Y(I)**(2*N)/8.+B2*(2.*N-1.)*Y(I)**(2*N-2)/2.
   18 CONTINUE
      IB=ALPHA*20
      DO 17 K=1,IB
```

```
      I=K*5-4
   17 WRITE(2,205)Y(I),SMR1(I),SMR2(I),SMT1(I),SMT2(I),SMRT(I)
      IC=(1-ALPHA)*20+1
      DO 21 K=1,IC
      I=K*5-4
   21 WRITE(2,203)X(I),STMR1(I),STMR2(I),STMT1(I),STMT2(I),STMRT(I)
      RETURN
  202 FORMAT(1HO,4X,'RADIAL POSITION',4X,'STMR1',8X,'STMR2',8X,'STMT1',
     *8X,'STMT2',8X,'STMRT')
  203 FORMAT(1HO,5X,F8.2,8X,5(F8.4,5X))
  204 FORMAT(1HO,2X,F5.2,4X,5(E14.7,3X))
  205 FORMAT(1HO,5X,F8.2,8X,5(F8.4,5X))
  207 FORMAT(1HO,8X,F5.2,2(8X,F8.4))
      END

      SUBROUTINE SPEED
C
C**** SUBROUTINE FOR DERIVING THE RESPONSE FREQUENCIES OF THE
C     TRAVELLING WAVES.
C
       COMMON /ADATA/NO,ALPHA,A(6,6),B(6,1),C(6,1),R(150),R1(150),R2(150)
     *,P1(150),P2(150),P3(150),Q1(150),S1(150),MO,DELTA
      COMMON/BDATA/W2 ,Y,RS(30),RF1(30),RF2(30)
      WRITE(2,211)
      DO 68 I=1,21
      RS(I)=(I-1.)/2 .
      C1=W2*SQRT(1.+Y*RS(I)**2)
      C2=RS(I)*NO
      RF1(I)=C1+C2
      RF2(I)=C1-C2
   68 WRITE(2,212)RS(I) ,RF1(I),RF2(I)
      RETURN
  211 FORMAT(1HO,4X,'SPEED RATIO',8X,'FORWARD WAVE',8X,'REVERSE WAVE')
  212 FORMAT(1HO,6X,F5.2,2(12X,F9.4))
      END
      FINISH
```

```
C                *** PROGRAM  RRITZ ***
C
      LIBRARY(SUBGROUPNAGF)
      LIBRARY(SUBGROUPNAGG)
      LIBRARY(SUBGROUPNAGH)
      PROGRAM(ABCD)
      INPUT 1=CR0
      OUTPUT 2=LP0
      TRACE 2
      END

      MASTER RRITZ
C
C
C*****PROGRAM TO EVALUATE FREQUENCY VALUES AND MODE SHAPES OF VIBRATING
C*****ANNULAR PLATES,INNER EDGE CLAMPED,BY THE RITZ METHOD USING
C*****DISPLACEMENT FUNCTIONS (R-B)**(J+1),J=1,NO.
C
C
      COMMON/ADATA/ALPHA,N,NO,W(10,150),WD1(10,150),WD2(10,150),
     *C(150,10,10),D(150,10,10),A(10,10),B(10,10),Z(10,10),SR(10),N1,
     *S1(150),S2(150),VR,PR,GAMMA,FC,F(100,10),G(100,10,10),T1(100),
     *T12(100),R(100),R1(100),R2(100),U(100),U1(100),V(100),V1(100),
     *I2,M2
      NO=7
      CALL INPUT1
      DO 12 J=1,6
      N=J-1
      WRITE(2,101)ALPHA
      WRITE(2,102)N
      CALL DERIVE1
      CALL GROUP1
      CALL SIMPSON1
      CALL SUMM1
      CALL EIGEN
      CALL VALUES1
   12 CONTINUE
      STOP
  100 FORMAT(1HO,//3X,'THE NUMBER OF FUNCTIONS NO =',I2)
  101 FORMAT(1HO,////3X,'THE CLAMPING RATIO ALPHA = ',F4.2)
  102 FORMAT(1HO,///3X,'THE NUMBER OF NODAL DIAMETERS N = ',I2)
  300 FORMAT(1HO,5X,'SPEED(C/S)',6X,'SPEED(REV/MIN)',6X,'FORWARD WAVE
     *FREQUENCY',5X,'REVERSE WAVE FREQUENCY')
      END

      SUBROUTINE INPUT1
      COMMON/ADATA/ALPHA,N,NO,W(10,150),WD1(10,150),WD2(10,150),
```

```
C
C**** SUBPROGRAM FOR DATA INPUT
C
     *C(150,10,10),D(150,10,10),A(10,10),B(10,10),Z(10,10),SR(10),N1,
     *S1(150),S2(150),VR,PR,GAMMA,FC,F(100,10),G(100,10,10),T1(100),
     *T12(100),R(100),R1(100),R2(100),U(100),U1(100),V(100),V1(100),
     *I2,M2
      DIMENSION YS(10),PS(10),RHS(10)
      DATA YS/210.E6/,PS/0.3/,RHS/7.8E-6/
      I2=81
      NO=7
C
C**** NO IS THE NUMBER OF TERMS.
C
      READ(1,89)ISTOP
      IF(ISTOP.LT.0)STOP
      READ(1,91)RADO,RADI,THICK
      WRITE(2,92)RADO,RADI,THICK
      ALPHA=RADI/RADO
      READ(1,93)IP
      WRITE(2,94)IP
      IF(IP.GT.10)GO TO 81
      YM=YS(IP)
      PO=PS(IP)
      RHO=RHS(IP)
      GO TO 82
   81 READ(1,95)YM,PO,RHO
   82 WRITE(2,96)YM,PO,RHO
C     CALCULATE PLATE CONSTANT.
      FC=RADO**2/THICK*SQRT(12.*RHO*(1.-PO**2)/YM)
      RETURN
   89 FORMAT(I2)
   90 FORMAT(/1HO,4X,'CLAMPING RATIO =',F5.2)
   91 FORMAT(3F10.5)
   92 FORMAT(1HO,4X,'OUTSIDE RADIUS =',F7.3,2X,'MILLIMETERS'
     *//5X,'CLAMPING RADIUS =',F7.3,2X,'MILLIMETERS'//5X,'THICKNESS =',
     *F6.3,2X,'MILLIMETERS')
   93 FORMAT(I2)
   94 FORMAT(1HO,4X,'MATERIAL PROPERTY NUMBER =',I3)
   95 FORMAT(3F10.5)
   96 FORMAT(1HO,4X,'YOUNGS MODULUS =',E13.6,2X,'N/MM**2'
     *//5X,'POISSONS RATIO =',F5.3//5X,'DENSITY =',E13.6,2X,'KG/MM**3')
      END

      SUBROUTINE DERIVE1
C
C
C**** THIS SUBPROGRAM DETERMINES THE DISPLACEMENT,SLOPE,AND CURVATURE
C**** VALUES AT SELECTED POINTS FOR TRIAL FUNCTIONS.
C
```

```
C
      COMMON/ADATA/ALPHA,N,NO,W(10,150),WD1(10,150),WD2(10,150),
     *C(150,10,10),D(150,10,10),A(10,10),B(10,10),Z(10,10),SR(10),N1,
     *S1(150),S2(150),VR,PR,GAMMA,FC,F(100,10),G(100,10,10),T1(100),
     *T12(100),R(100),R1(100),R2(100),U(100),U1(100),V(100),V1(100),
     *I2,M2
      DIMENSION X(150)
      DO 13 I=1,I2
      X(I)=ALPHA+(1.-ALPHA)*(I-1)/(I2-1)
      Y=X(I)-ALPHA
      WD2(1,I)=2.
      DO 14 J=1,NO
      W(J,I)=Y**(J+1)
      WD1(J,I)=(J+1.)*Y**J
      IF(J.EQ.1)GO TO 14
      WD2(J,I)=J*(J+1.)*Y**(J-1)
   14 CONTINUE
   13 CONTINUE
      RETURN
      END

      SUBROUTINE SIMPSON1
C
C
C**** THIS SUBPROGRAM IS THE FIRST STAGE OF THE SIMPSON NUMERICAL
C**** INTEGRATION OF THE ENERGY DENSITIES OVER THE RADIAL LENGTH OF THE
C**** PLATE ANNULUS.
C
C
      COMMON/ADATA/ALPHA,N,NO,W(10,150),WD1(10,150),WD2(10,150),
     *C(150,10,10),D(150,10,10),A(10,10),B(10,10),Z(10,10),SR(10),N1,
     *S1(150),S2(150),VR,PR,GAMMA,FC,F(100,10),G(100,10,10),T1(100),
     *T12(100),R(100),R1(100),R2(100),U(100),U1(100),V(100),V1(100),
     *I2,M2
      I3=I2-1
      DO 18 J=1,NO
      DO 19 K=1,NO
      DO 20 I=2,I3
      VT=I/2.
      I1=VT
      IF(I1.NE.VT)GO TO 31
      C(I,J,K)=4.*C(I,J,K)
      D(I,J,K)=4.*D(I,J,K)
      GO TO 20
   31 C(I,J,K)=2.*C(I,J,K)
      D(I,J,K)=2.*D(I,J,K)
   20 CONTINUE
   19 CONTINUE
   18 CONTINUE
      RETURN
```

```
      END

      SUBROUTINE SUMM1
C
C
C**** THIS SUBPROGRAM IS THE SECOND STAGE OF THE SIMPSON INTEGRATION.
C**** IT GIVES THE ENERGY INTEGRALS.
C
C
      COMMON/ADATA/ALPHA,N,NO,W(10,150),WD1(10,150),WD2(10,150),
     *C(150,10,10),D(150,10,10),A(10,10),B(10,10),Z(10,10),SR(10),N1,
     *S1(150),S2(150),VR,PR,GAMMA,FC,F(100,10),G(100,10,10),T1(100),
     *T12(100),R(100),R1(100),R2(100),U(100),U1(100),V(100),V1(100),
     *I2,M2
      DO 21 J=1,NO
      DO 22 K=1,NO
      A(J,K)=0.
   22 B(J,K)=0.
   21 CONTINUE
      DO 23 J=1,NO
      DO 24 K=1,NO
      DO 25 I=1,I2
      A(J,K)=A(J,K)+C(I,J,K)*(1-ALPHA)/(I2-1)/3.
   25 B(J,K)=B(J,K)+D(I,J,K)*(1-ALPHA)/(I2-1)/3.
   24 CONTINUE
   23 CONTINUE
      RETURN
      END

      SUBROUTINE EIGEN
C
C
C**** THIS SUBPROGRAM SOLVES THE EIGENVALUE PROBLEM OF THE TYPE
C**** AX=F.BX,WHERE F IS THE SQUARE OF THE FRQUENCY PARAMETER.A AND B
C**** ARE SQUARE SYMMETRIC MATRICES.THE SUBPROGRAM CALLS NAG LIBRARY
C**** ROUTINES F01AEF,F02ABF,F01AFF.THE SUBPROGRAM OUTPUTS THE FREQUENCY
C**** PARAMETERS AND MODE SHAPES FOR VARIOUS MODES OF VIBRATION
C**** CONSIDERED.
C
C
      COMMON/ADATA/ALPHA,N,NO,W(10,150),WD1(10,150),WD2(10,150),
     *C(150,10,10),D(150,10,10),A(10,10),B(10,10),Z(10,10),SR(10),N1,
     *S1(150),S2(150),VR,PR,GAMMA,FC,F(100,10),G(100,10,10),T1(100),
     *T12(100),R(100),R1(100),R2(100),U(100),U1(100),V(100),V1(100),
     *I2,M2
      REAL DL(10),Y(10),E(10),AA(10,10),BB(10,10)
      DO 31 I=1,NO
      DO 31 J=1,NO
      AA(I,J)=A(I,J)
   31 BB(I,J)=B(I,J)
```

```
      IA=10
      IB=10
      IFAIL=1
      CALL F01AEF(NO,AA,IA,BB,IB,DL,IFAIL)
C
C**** THE NAG LIBRARY ROUTINE REDUCES THE EIGENPROBLEM
C     AX=KBX TO THE STANDARD SYMMETRIC EIGENPROBLEM PZ=KZ.
C
      IF(IFAIL.EQ.0)GO TO 80
      WRITE(2,106)IFAIL
      RETURN
   80 IZ=10
      IFAIL=1
      CALL F02ABF(AA,IA,NO,Y,Z,IZ,E,IFAIL)
C
C**** THE NAG LIBRARY ROUTINE CALCULATES ALL THE EIGENVALUES
C     AND EIGENVECTORS OF A REAL SYMMETRIC MATRIX BY
C     HOUSEHOLDER REDUCTION AND THE QL ALGOFITHM.
C
      IF(IFAIL.EQ.0)GO TO 90
      WRITE(2,107)IFAIL
      RETURN
   90 M1=1
      M2=NO
      CALL F01AFF(NO,M1,M2,BB,IB,DL,Z,IZ)
C
C**** THE NAG LIBRARY ROUTINE DERIVES EIGENVECTORS X OF THE
C     PROBLEM AX=KBX FROM THE CORRESPONDING EIGENVECTORS
C     Z=L'X OF THE DERIVED STANDARD SYMMETRIC EIGENPROBLEM.
C
      DO 91 I=1,NO
   91 SR(I)=SQRT(Y(I))
      WRITE(2,208)SR(1)
      RETURN
  106 FORMAT(25HOERROR IN F01AEF IFAIL = ,I2)
  107 FORMAT(25HOERROR IN F02ABF IFAIL = ,I2)
  108 FORMAT(6X,12HOEIGENVALUES,12(/1H ,4X,E14.7))
  109 FORMAT(1H ,E15.7)
  208 FORMAT(1HO,4X,F7.2)
      END

      SUBROUTINE VALUES1
C
C**** THE SUBPROGRAM CALCULATES THE PLATE DISPLACEMENT, SLOPE
C     AND CURVATURE VALUES.
C
      COMMON/ADATA/ALPHA,N,NO,W(10,150),WD1(10,150),WD2(10,150),
     *C(150,10,10),D(150,10,10),A(10,10),B(10,10),Z(10,10),SR(10),N1,
     *S1(150),S2(150),VR,PR,GAMMA,FC,F(100,10),G(100,10,10),T1(100),
     *T12(100),R(100),R1(100),R2(100),U(100),U1(100),V(100),V1(100),
```

```
      *I2,M2
       DIMENSION X(150)
       DO 79 I=1,I2
       R(I)=0.
       R1(I)=0.
       R2(I)=0.
   79  CONTINUE
       J=1
       DO 80 I=1,I2
       X(I)=ALPHA+(1.-ALPHA)*(I-1)/100.
       DO 82 K=1,NO
       R(I)=R(I)+Z(K,J)*W(K,I)
       R1(I)=R1(I)+Z(K,J)*WD1(K,I)
   82  R2(I)=R2(I)+Z(K,J)*WD2(K,I)
   80  CONTINUE
       DEN=R(I2)
       DO 78 I=1,I2
       R(I)=R(I)/DEN
       R1(I)=R1(I)/DEN
       R2(I)=R2(I)/DEN
   78  CONTINUE
       RETURN
  299  FORMAT(1HO,9X,'RADIUS',8X,'DISPLACEMENT',8X,'SLOPE',9X,'CURVATURE'
      *)
  300  FORMAT(1HO,10X,F4.2,10X,F6.4,10X,F7.4,10X,F8.4)
  301  FORMAT(1H ,F6.2)
       END
       SUBROUTINE FREQV
C
C**** SUBPROGRAM TO EVALUATE THE TRAVELLING WAVE FREQUENCIES.
C
       COMMON/ADATA/ALPHA,N,NO,W(10,150),WD1(10,150),WD2(10,150),
      *C(150,10,10),D(150,10,10),A(10,10),B(10,10),Z(10,10),SR(10),N1,
      *S1(150),S2(150),VR,PR,GAMMA,FC,F(100,10),G(100,10,10),T1(100),
      *T12(100),R(100),R1(100),R2(100),U(100),U1(100),V(100),V1(100),
      *I2,M2
       PI=3.1415962
       FC1=1./(FC*2.*PI)
       J=1
       VC=VR*N
       FV1=SR(J)+VC
       FV2=SR(J)-VC
       VP1=VR*FC1
       VP2=VP1*60.
       FV1=FV1*FC1
       FV2=FV2*FC1
       WRITE(2,302)VP1,VP2,FV1,FV2
       RETURN
  301  FORMAT(1HO,12X,F5.2,18X,F8.4,18X,F8.4)
  302  FORMAT(1HO,8X,F7.2,12X,F8.2,15X,F8.2,15X,F8.2)
```

```
      END
      FINISH
****
```

APPENDIX IV

WAVES IN ROTATING DISCS

1. One-dimensional wave

The surface is initially displaced in the form

$$w = w_1 \cos \frac{2\pi x}{\lambda} \qquad (1)$$

where λ is the wavelength.

This displaced shape moves distance x_1 in the positive x - direction, given by

$$x_1 = ct \qquad (2)$$

where c is the propagation velocity of the wave train (fig. 1).

At this stage, displacement is given by

$$w = w_1 \cos 2\pi \frac{(x-x_1)}{\lambda} \qquad (3)$$

But $\frac{c}{\lambda} = f$, where f is the frequency of oscillation of any chosen point, so a forward-moving wave has the equation

$$w = w_1 \cos 2\pi(\frac{x}{\lambda} - ft) \qquad (4)$$

2. Wave in rim of disc

When there are n complete waves in the rim, and outside radius is R, the wavelength is

$$\lambda = \frac{2\pi R}{n} \tag{5}$$

Also, peripheral distance (fig. 2) is

$$x = R\theta \ , \tag{6}$$

so the equation for a forward-moving wave, moving in the positive θ direction, becomes

$$w = w_1 \cos (n\theta - \omega t) \tag{7}$$

where $\omega = 2\pi f$.

For a reverse-moving wave,

$$w = w_1 \cos (n\theta + \omega t) \tag{8}$$

3. Vibration of stationary disc

The vibration has nodal lines which may be drawn on the disc surface, defining the vibration mode:

$$w = w_1 \cos n\theta \cos \omega t \tag{9}$$

This can be rewritten as

$$w = w_1[\cos (n\theta - \omega t) + \cos (n\theta + \omega t)] \tag{10}$$

This means that the simple vibration of amplitude w_1 is equivalent in every way to the superposition of forward and reverse-travelling waves each of amplitude $\frac{1}{2}w_1$ (see

fig. 3).

4. Vibration of a rotating disc

Let point A on disc be an antinodal point, so that deflection at P (fig. 4) is given by

$$w_p = w_1 \cos n\theta_1 \cos \omega t \qquad (11)$$

Now let the disc rotate at Ω radians/sec. Angle θ is now given by

$$\theta = \theta_1 - \phi \qquad (12)$$

and

$$\phi = \Omega t \qquad (13)$$

so we have deflection at point P fixed in space to be

$$w_p = w_1 \cos n(\theta_1 - \Omega t) \cos \omega t \qquad (14)$$

This is simplified by putting $\theta_1 = 0$ when the above expansion can be written as

$$w_p = \frac{1}{2} w_1 [\cos (\omega + n\Omega)t + \cos (\omega - n\Omega)t] \qquad (15)$$

This means that a stationary probe shows the existence of a single vibration in the form of two waves of equal amplitude and of frequencies $\frac{(\omega + n\Omega)}{2\pi}$ and $\frac{(\omega - n\Omega)}{2\pi}$. This conclusion can be alternatively reached by supposing that the vibration is resolved into two travelling waves. The forward-running wave will give a probe frequency equal to the disc vibration frequency plus the product of the

rotational speed and the number of nodal diameters. The reverse running wave will give probe frequency equal to the disc vibration frequency minus the product of the rotational speed and the number of nodal diameters. When the rotational speed is so increased that

$$n\Omega = \omega \tag{16}$$

we shall have a reverse-travelling wave travelling at its propagation speed in the disc but standing still in space, that is, a standing wave.

5. Disc vibrating in two modes

Exciting a disc at a frequency ω, near the natural frequency of a normal mode, will cause the disc to oscillate. The forced excitation of a rotating disc can be considered as having the disc stationary and the force going round the rim of the disc in the direction opposite to the normal disc rotation. Assume the vibration amplitudes for the two modes are w_1 and w_2. The force which excites the disc at a frequency ω is moved round the rim of the disc in the direction x. If the exciting force is taken as

$$F = F_0 \cos\left(\omega t - \frac{2\pi x}{\lambda}\right) \tag{17}$$

it will be in phase with the disc motion at the antinodal points of both vibrations if displacements are taken as

$$w_A = w_1 \cos \frac{2\pi x}{\lambda} \cos \omega t$$
$$w_B = w_2 \sin \frac{2\pi x}{\lambda} \sin \omega t \qquad (18)$$

Fig. 5 shows the relationship between the position of the force and the disc displacements. In the following analysis, the wave whose frequency is equal to the excitation frequency is termed the excited wave and the other the alternative wave. Suppose motion lags force by phase angle ϕ, where ϕ is between 0 and 180 degrees, the mode displacements become

$$w_A = w_1 \cos \frac{2\pi x}{\lambda} \cos (\omega t - \phi_1)$$
$$w_B = w_2 \sin \frac{2\pi x}{\lambda} \sin (\omega t - \phi_2) \qquad (19)$$

The combined motion is

$$w = w_A + w_B$$
$$= w_1 \cos \frac{2\pi x}{\lambda} [\cos \omega t \cos \phi_1 + \sin \omega t \sin \phi_1] \qquad (20)$$
$$+ w_2 \sin \frac{2\pi x}{\lambda} [\sin \omega t \cos \phi_2 - \cos \omega t \sin \phi_2]$$

or

$$w = \cos\left(\omega t + \frac{2\pi x}{\lambda}\right)\left[\frac{w_1}{2}\cos\phi_1 - \frac{w_2}{2}\cos\phi_2\right]$$
$$+ \sin\left(\omega t + \frac{2\pi x}{\lambda}\right)\left[\frac{w_1}{2}\sin\phi_1 - \frac{w_2}{2}\sin\phi_2\right]$$
$$+ \cos\left(\omega t - \frac{2\pi x}{\lambda}\right)\left[\frac{w_1}{2}\cos\phi_1 + \frac{w_2}{2}\cos\phi_2\right] \qquad (21)$$
$$+ \sin\left(\omega t - \frac{2\pi x}{\lambda}\right)\left[\frac{w_1}{2}\sin\phi_1 + \frac{w_2}{2}\sin\phi_2\right]$$

The above equation can be re-written as

$$w = w_a \cos\left[\left(\omega t + \frac{2\pi x}{\lambda}\right) - \phi_a\right]$$
$$+ w_e \cos\left[\left(\omega t - \frac{2\pi x}{\lambda}\right) - \phi_e\right] \qquad (22)$$

Amplitudes w_e and w_a of the excited and alternative waves are:

$$w_e = \frac{1}{2}\left[(w_1\cos\phi_1 + w_2\cos\phi_2)^2 + (w_1\sin\phi_1 + w_2\sin\phi_2)^2\right]^{1/2} \qquad (23)$$
$$= \frac{1}{2}\left[w_1^2 + w_2^2 + 2w_1w_2\cos(\phi_1 - \phi_2)\right]^{1/2}$$

$$w_a = \frac{1}{2}\left[(w_1\cos\phi_1 - w_2\cos\phi_2)^2 + (w_1\sin\phi_1 - w_2\sin\phi_2)^2\right]^{1/2} \qquad (24)$$
$$= \frac{1}{2}\left[w_1^2 + w_2^2 - 2w_1w_2\cos(\phi_1 - \phi_2)\right]^{1/2}$$

From the above relations, the combined vibrations will yield a pure excited wave when

$$\phi_1 - \phi_2 = 0 \qquad (25)$$

and a pure alternative wave when

$$\phi_1 - \phi_2 = \pi \qquad (26)$$

Fig. 6 shows the amplitude and phase diagrams for two orthogonal modes, in a vibrating disc, using the linear theory of vibrations, i.e. assuming small amplitude vibration. Fig. 6iii shows the amplitudes of the amplitudes of the excited and alternative travelling waves derived from the values in fig. 6i and 6ii. The wave amplitude curves show that at excitation frequencies close to the natural frequencies f_1 and f_2, the wave amplitudes are comparable. The amplitude of the excited wave is larger at frequencies remote from the natural frequencies but the alternative wave is larger when the excitation frequency is intermediate between the two response frequencies.

Each mode contributes a membrane stress varying as deflection squared, giving non-linearity in each mode. The total membrane stress energy depends on the square of the summed contributions from each mode, giving coupling between the two modes. Fig. 7i and 7ii show the amplitude and phase diagrams for two orthogonal modes for a small value of applied force. The amplitudes of the travelling waves corresponding to the vibration characteristics for

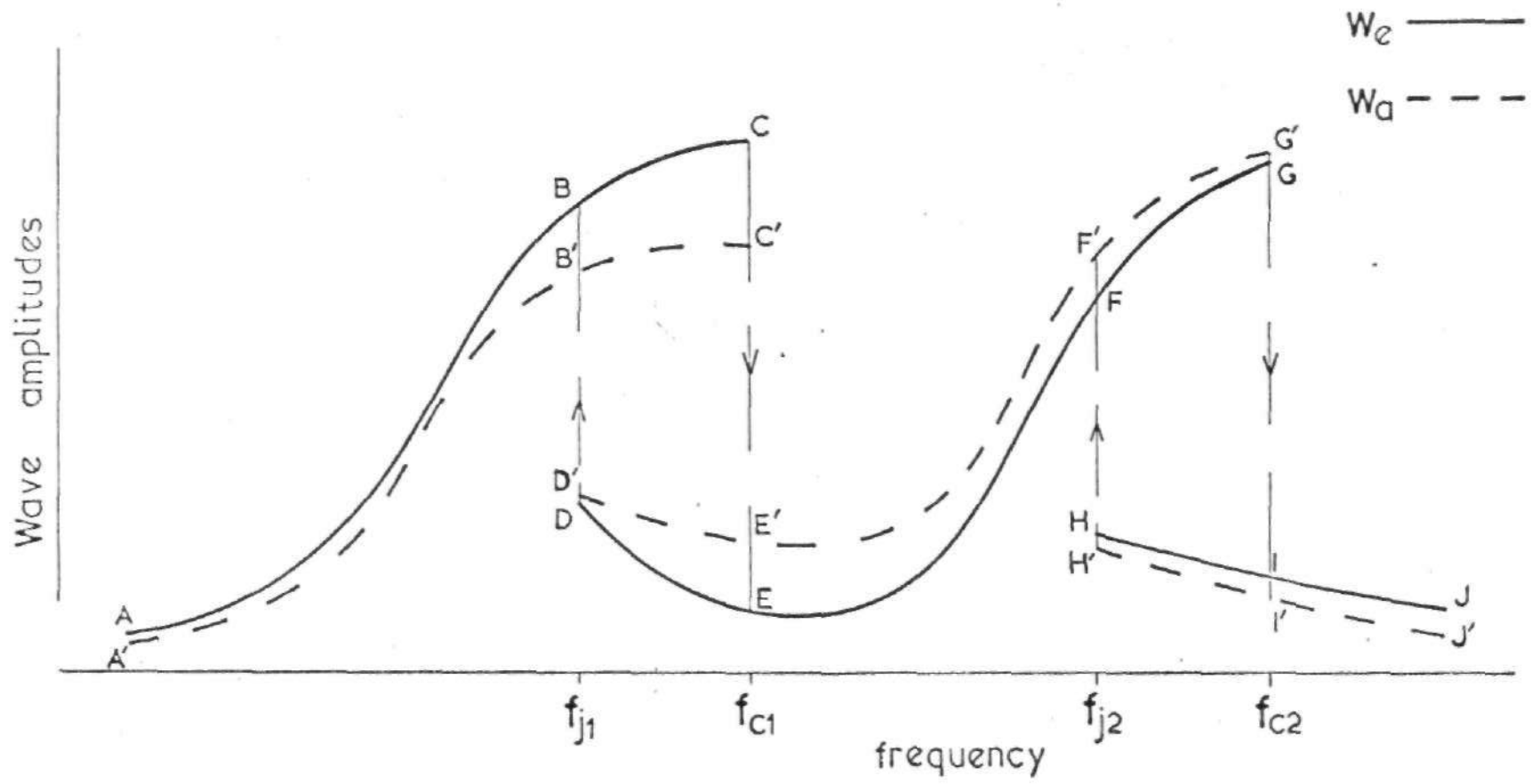


Fig. 8. Wave amplitude curves of fig. 7iii.

the two orthogonal modes are shown in fig. 7iii.

The wave amplitude curves shown in fig. 7iii are enlarged and shown in fig. 8. On increasing excitation frequency, the amplitudes of excited and alternative waves increase along ABC and A'B'C' respectively and, at frequency f_{c1}, collapse to the lower branch. The wave amplitudes then continue along EFG and E'F'G'. At f_{c2}, they collapse from values G and G' to I and I' and continue along IJ and I'J'. On reducing the excitation frequency from an initial value greater than f_{j2}, the excited wave amplitude goes along the curve JIH, jumps to F at f_{j2}, and continues along FED, and then another jump at f_{j1} to B, and continues along BA. The alternative wave amplitude follows the curves in a similar manner to that described for the excited wave but along the dashed lines.

The wave amplitude curves show that the excited wave predominates at the larger amplitudes occuring before f_{c1}. When a large difference occurs between the amplitudes of the travelling waves in a high amplitude region of the response curves, the wave with the higher amplitude will predominate in the disc vibration. In real discs (having some imperfection leading to a frequency separation between two principal orthogonal modes), it is not possible to have just a single wave without the other wave being present. However, as one wave becomes much larger than the other, the disc deflection will be that of the wave with the larger amplitude with the other wave superposed.

APPENDIX IV

In fig. 9, i. and ii. show mode amplitudes and phase angles for two orthogonal modes when a larger force is applied. The corresponding wave amplitude curves are shown in fig. 9iii. The curves show that when a larger force is applied, a relatively pure excited wave is generated. To have a pure excited wave, the frequency separation between the orthogonal modes has to be made as small as possible.

When the speed at which the force is moved round the rim of the disc is given by the relation

$$\Omega = \frac{\omega}{n} \qquad (27)$$

where $\Omega = \frac{x}{Rt}$,

the speed of the excited wave $(\omega - \frac{2\pi x}{\lambda})$ is equal to zero and that of the alternative wave $(\omega + \frac{2\pi x}{\lambda})$ is equal to $\frac{2\omega}{n}$. The excited wave will be stationary in space and the alternative wave will travel round the disc rim. For small values of disc imperfection, only the excited wave amplitude will be of significance, and the waveform around the disc rim will appear, largely, to be standing.

6. Stationary waves in rotating discs

In the analysis given in the previous section, we assume that the disc is stationary and that the force, with a frequency ω, is applied round the edge of the disc. The analysis will hold if the disc is rotated in the direction of negative x at a constant speed Ω. In this case, however, the applied force has to have a frequency of $(\omega - \frac{2\pi x}{\lambda})$ in order to excite a predominant reverse travelling wave. The applied force is represented as

$$F = F_0 \cos (\omega t - n\Omega t) \qquad (28)$$

Similarly, a force with a frequency of $(\omega + \frac{2\pi x}{\lambda})$ will cause the rotating disc to vibrate in the two orthogonal modes and the excited wave will be the forward travelling wave.

When the relation of equation (27) holds, we have a limiting case in which a stationary force in space will cause the disc rotating at a speed of $\frac{\omega}{n}$ to vibrate in the two modes. The "excited" wave, which is the reverse travelling wave, is stationary in space. The "natural frequency" of the rotating disc (i.e. the frequency of free vibration) increases with vibration amplitude as shown in fig. (10). With higher frequency, i.e. higher wave propagation velocity, the disc rotate faster to keep up with the wave.

It is possible to set up a standing wave with large amplitudes in a rotating disc by applying a constant force, if the frequency separation between the orthogonal

modes is small. When there is a significant difference between the frequencies of the orthogonal modes, even when the stationary wave component is predominant, the forward travelling wave will be present making the disc rim to vary from a stationary waveform to an extent depending on the relative magnitudes of the two waves.

7. Energy absorbed by a standing wave

We consider a wave train of n complete waves moving around the rim of a disc. Each part of the disc goes through n cycles of bending stress as the wave train travels over the whole circumference. Energy loss per unit volume due to strain hysteresis in the material of the disc is defined by the hysteresis loop (fig. 11), which becomes wider as stress increases. The stress σ_e to be used for this purpose could be taken as an equivalent shear stress σ_e calculated from the Von Mises function of stress components. Energy loss per unit volume can then be written as

$$\delta U_d = c\sigma_e^{\,m} \qquad (29)$$

It is convenient to assume m=2, though there is evidence that this value may be higher. A volume integral of the bending stresses then gives the energy dissipation rate for the whole disc due to the movement of the wave train relative to the disc. (It is immaterial whether the disc is rotating or not for this purpose.)

$$\dot{U}_d = n\omega c \int \sigma_e^2 d(vol) \qquad (30)$$

All the stress components in a given disc are proportional to wave amplitude w_0, so this integral leads to

$$\dot{U}_d = n\omega C_1 w_0^2 \qquad (31)$$

Additional energy may be absorbed in friction due to imperfect clamping at the central clamping discs, but it is assumed that this is included in the damping constant C_1.

The damping constant C_1 may be obtained theoretically (from a knowledge of the material properties) or directly by experimental measurement of decay time for a given disc. Kinetic and strain energy (which are equal) can also be calculated in terms of the wave amplitude, giving a total, for a linear vibration,

$$U_s = C_2 w_0^2 \qquad (32)$$

Decay of a free vibration is expressed as

$$w = w_0 e^{-(t/t_0)} \quad , \quad \frac{\partial w}{\partial t} = -\frac{w_0}{t_0} e^{-(t/t_0)} \qquad (33)$$

where t_0 is the time constant, and w_0 is the initial amplitude.

Hence the rate of decrease of energy is

$$\dot{U}_s = \frac{\partial U_s}{\partial w}\frac{\partial w}{\partial t}$$

$$= 2C_2 w \frac{\partial w}{\partial t} \qquad (34)$$

$$= -\frac{2C_2}{t_0} w_0^2 \, e^{-(2t/t_0)}$$

At t=0 this is equated to dissipation rate to get

$$C_1 = \frac{2C_2}{n\omega t_0} \qquad (35)$$

Measured decay times are shorter for larger amplitudes, suggesting that m>2.

We suppose that the constant force F is applied to the rim in a frictionless manner, so that it acts normal to the surface of the plate (fig. 12). The stationary wave is described by

$$w = w_0 \sin n\theta \qquad (36)$$

which assumes that as the point of collapse is approached, the force acts at the point of maximum transverse velocity so as to supply the maximum amount of energy. The applied force then has a tangential component αF where

$$\alpha = \frac{1}{R}\frac{\partial w}{\partial \theta} = n\frac{w_0}{R} \qquad (37)$$

As the forces applied to the rotating system by the bearings do no work, the work is supplied by the applied torque T (fig. 12), and the rate of energy input is αFV, where V is the peripheral disc speed, hence

$$\dot{U}_I = \frac{FV}{R} n w_0 = \omega F w_0 \qquad (38)$$

as $\frac{V}{R} = \frac{\omega}{n}$.

On equating the energy input of equation 38 to the dissipation energy rate of equation 31, we get

$$\omega F w_0 = C_1 \omega w_0^2 \qquad (39)$$

so the equilibrium value of wave amplitude as the collapse point is approached is determinate, and is given by

$$w_0 = \frac{F}{nC_1} \qquad (40)$$

This means that it increases in proportion to applied force and is controlled by the damping constant C_1. It should be noted that this condition cannot be attained at single rotational speed. As the wave amplitude increases with increased applied force, the propagation speed of the wave train increases, so the disc speed must be increased to maintain a standing wave.

8. Stationary waves in circular saws

When a circular saw is cutting wood at high speed, it is expected to cut as precisely as possible and to operate without rubbing unduly with the material being cut. (See section 2.6, p. 83). Side-rubbing leads to generation of heat around the rim of the saw. This leads to the setting up of compressive tangential stresses in the plane of the saw disc. Such stresses lead to lowering of the disc stiffness.

APPENDIX IV

When during cutting the saw deflects against a raised spot, the deflection of the disc surface will be localised near the position of the raised spot provided the rotational speed is much lower than the critical speed (fig. 13). Side-rubbing between the saw and the timber at the position of the raised spot will cause heating up of the disc rim. The lowering of the disc stiffness may cause the critical speed of the disc to be reduced and so to approach the speed at which the saw is cutting. When this happens the constant transverse force on the saw due to the side-rubbing between the saw and the raised spot will lead to the excitation of the orthogonal modes of vibration of the disc, resulting in a large amplitude standing wave. The standing wave will lead to large deflection of the disc and the saw will perform a wavy, out-of-line cut.

When significant amounts of frequency separation is present between the orthogonal modes for the mode of vibration excited, the the large amplitude stationary wave will have superposed on it the forward travelling wave with significant amplitude. The deflection of the disc will no longer be stationary in space. The combined waveforms generate higher damping and there is earlier collapse of the disc vibration. The saw under such circumstances, could be used for rough cutting, and because of the pulsating saw edge, there will be sufficient clearance between the saw and the material thereby ensuring that there is no binding between them. It

is estimated that in common wood-sawing applications, values of frequency separation of about 6 percent between the sets of orthogonal frequencies for the modes with 2 and 3 nodal diameters will be adequate in reducing the stationary wave amplitudes sufficiently for the disc to be used around the critical speeds for rough cutting.

APPENDIX IV

LIST OF FIGURES

1. One-dimensional wave.

2. Stationary disc.

3. Vibration of a stationary disc as a combination of two waves.

4. Rotating disc.

5. Displacement of disc vibrating in two orthogonal modes.

6. Linear vibration response curves in disc with frequency separation; (i) Mode amplitudes, (ii) Mode phase angles, (iii) Wave amplitudes.

7. Vibration response curves in disc with frequency separation when a small force is applied; (i) Mode amplitudes, (ii) Mode phase angles, (iii) Wave amplitudes.

8. Wave amplitude curves of fig. 7iii.

9. Vibration response curves in disc with frequency separation when a large force is applied.

10. Variation of response frequency with vibration amplitude.

11. Hysteresis loop.

12. Forces on disc system.

13. Point loading of disc rotating below its critical speed.

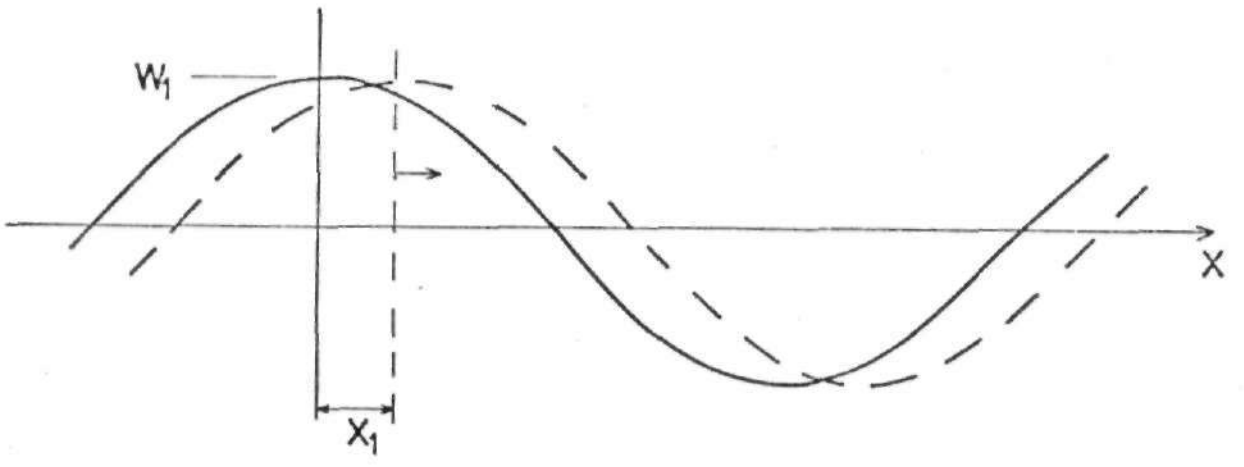


Fig. 1. One - dimensional wave.

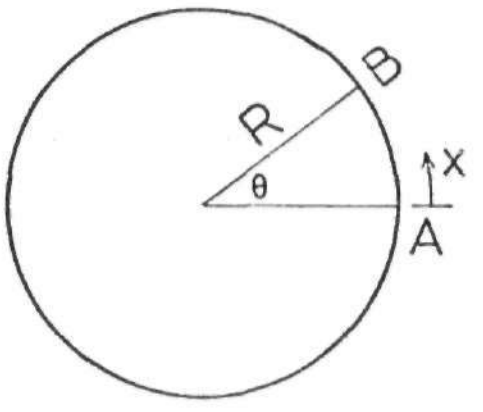


Fig. 2

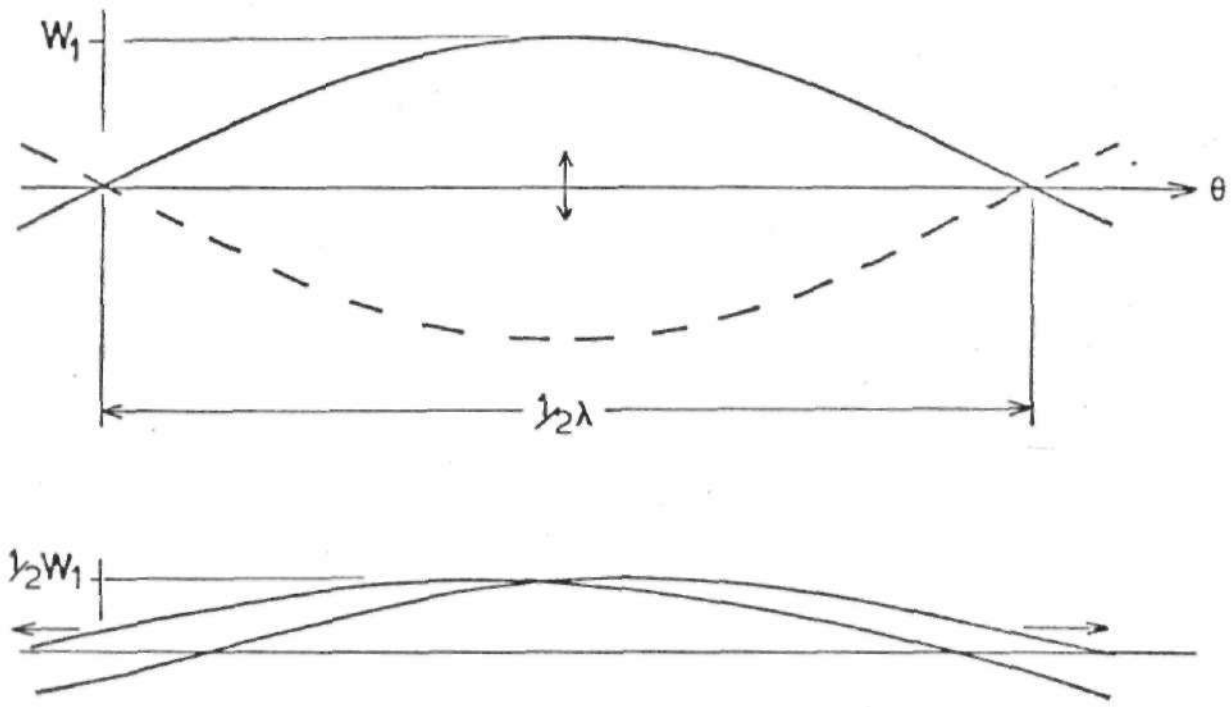


Fig. 3. Vibration of a stationary disc as a combination of two waves.

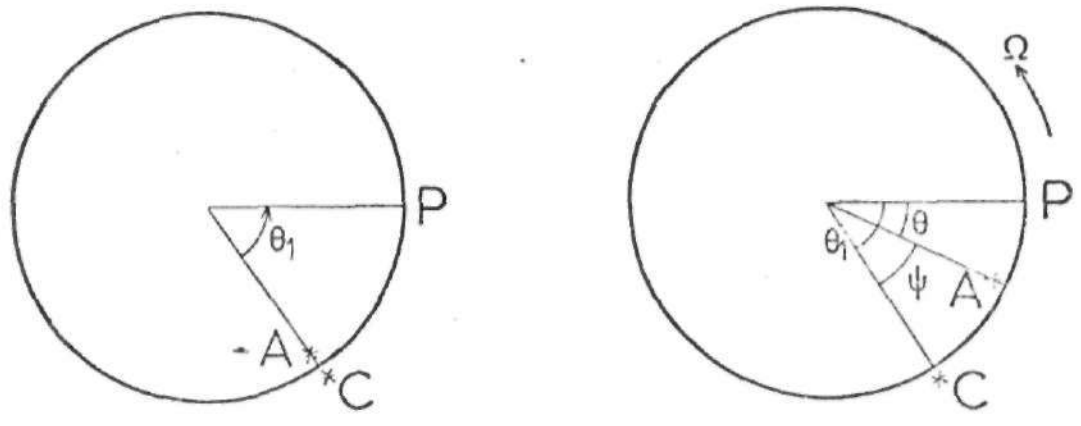


Fig. 4

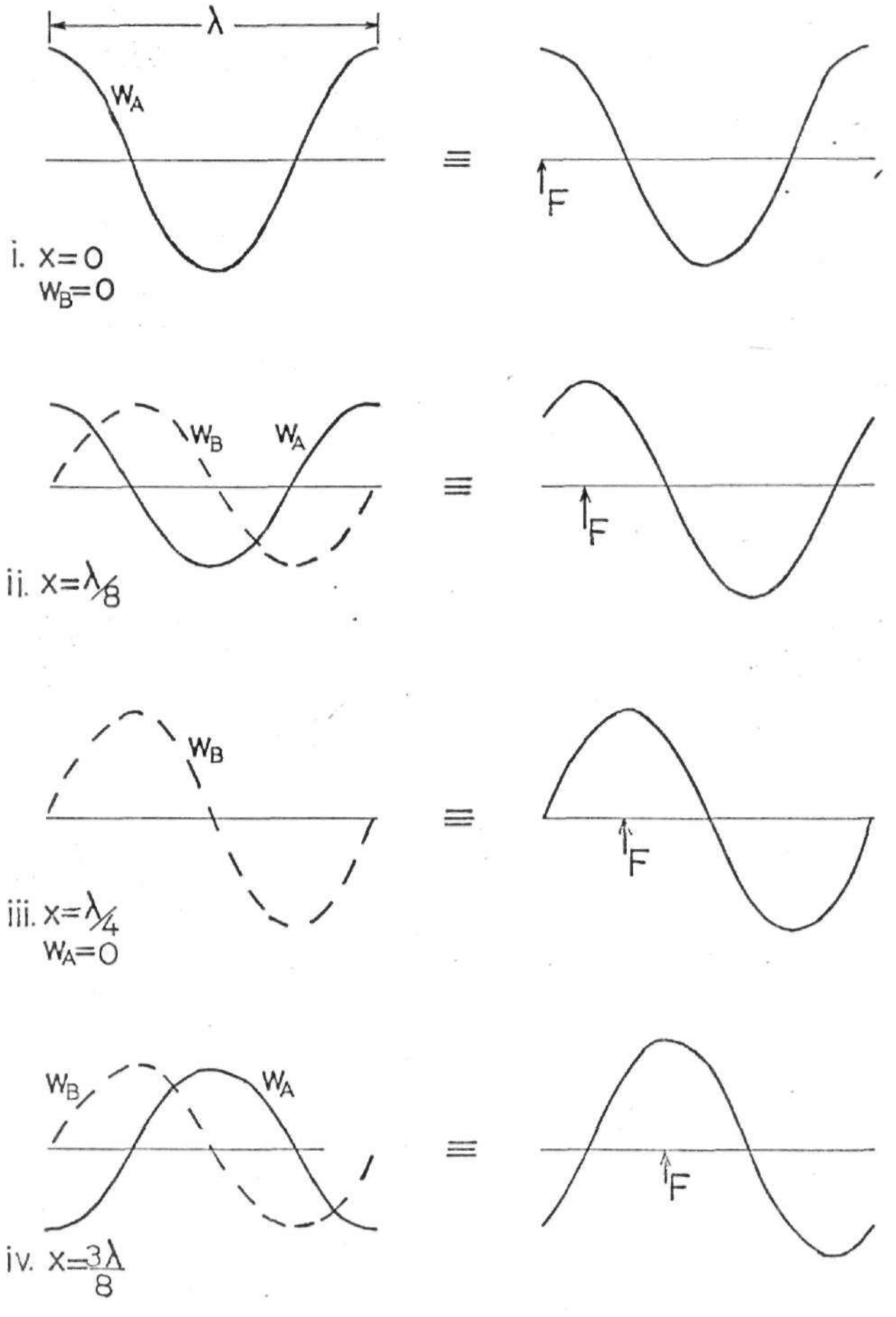
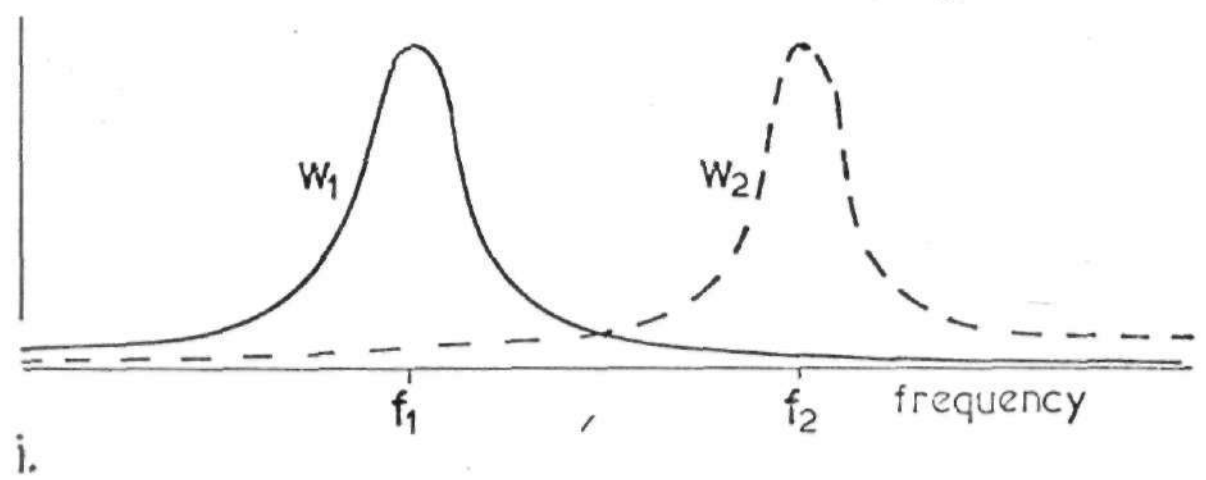
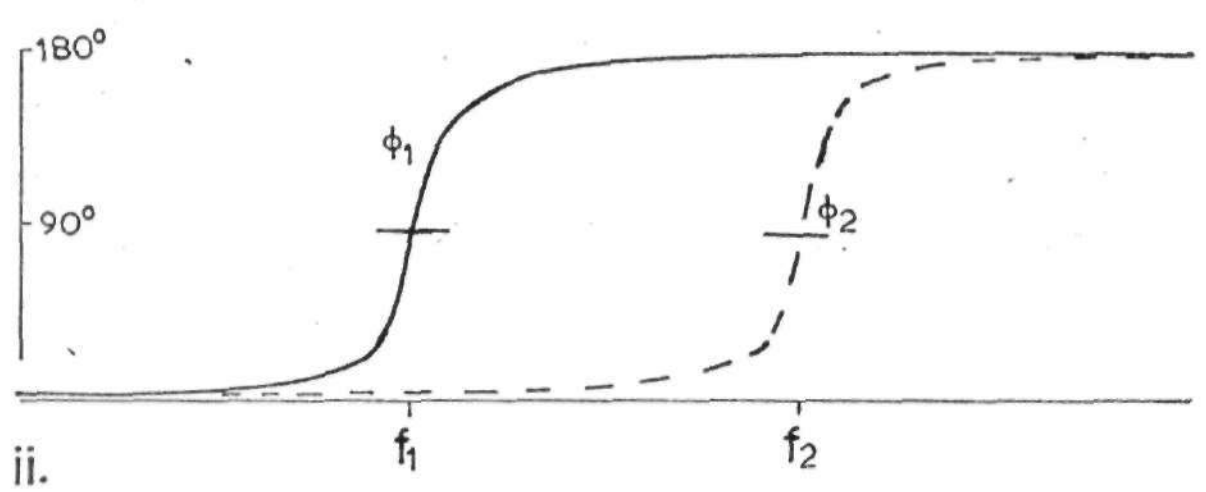


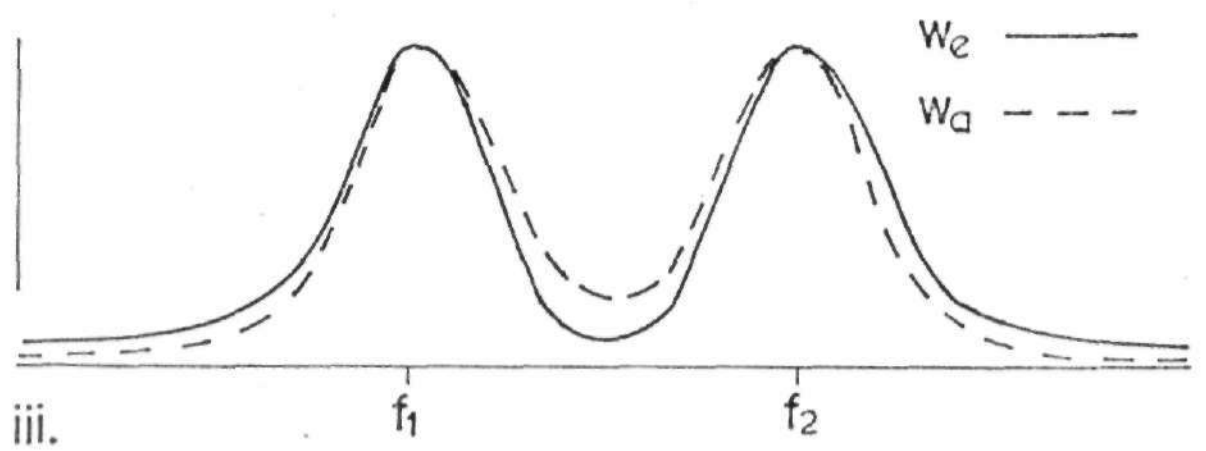
Fig. 5. Displacement due to vibration in two orthogonal modes.



i.

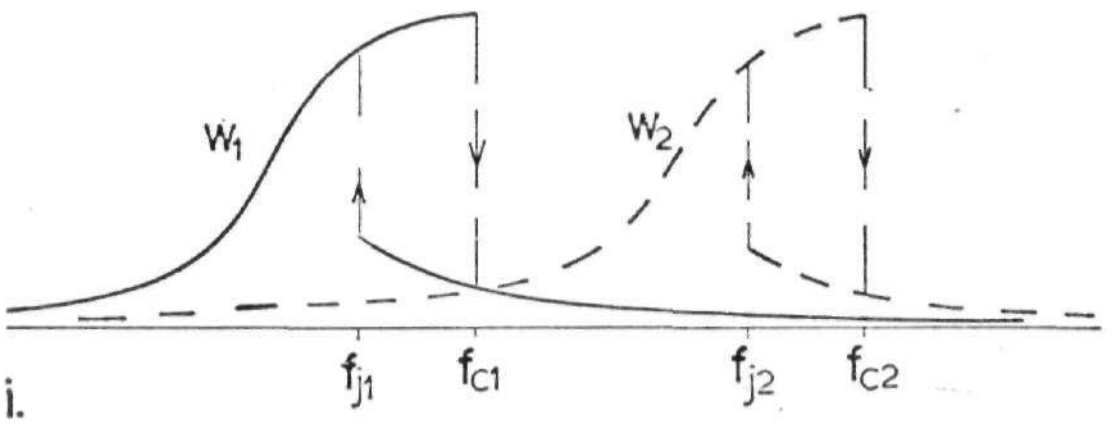


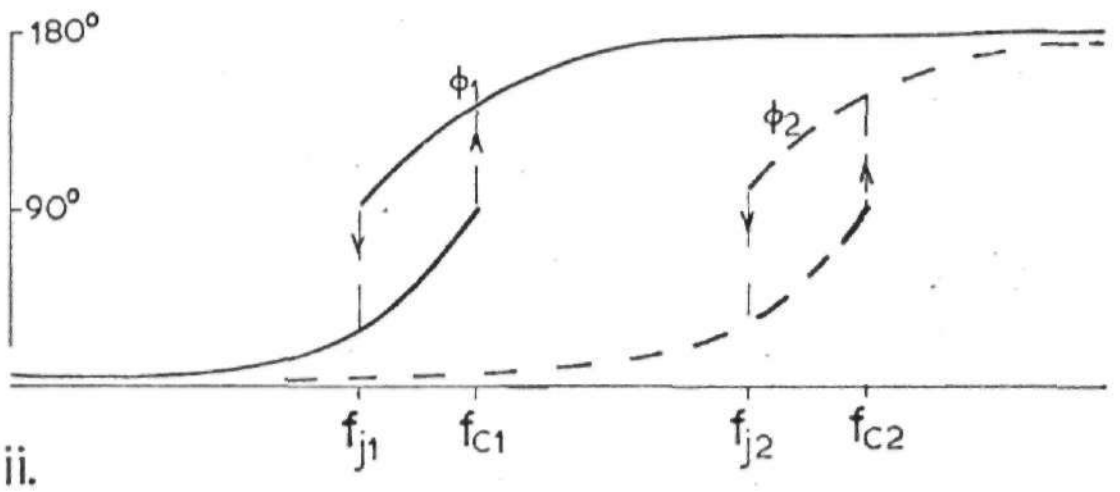
ii.



iii.

Fig. 6. Linear vibration response curves in disc with frequency separation: (i) mode amplitudes, (ii) phase angles, (iii) wave amplitudes.





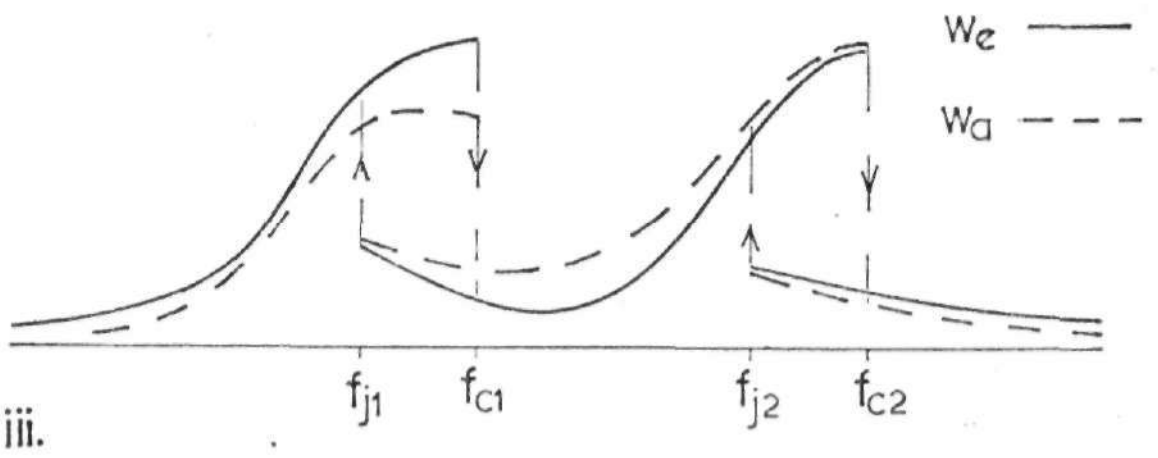
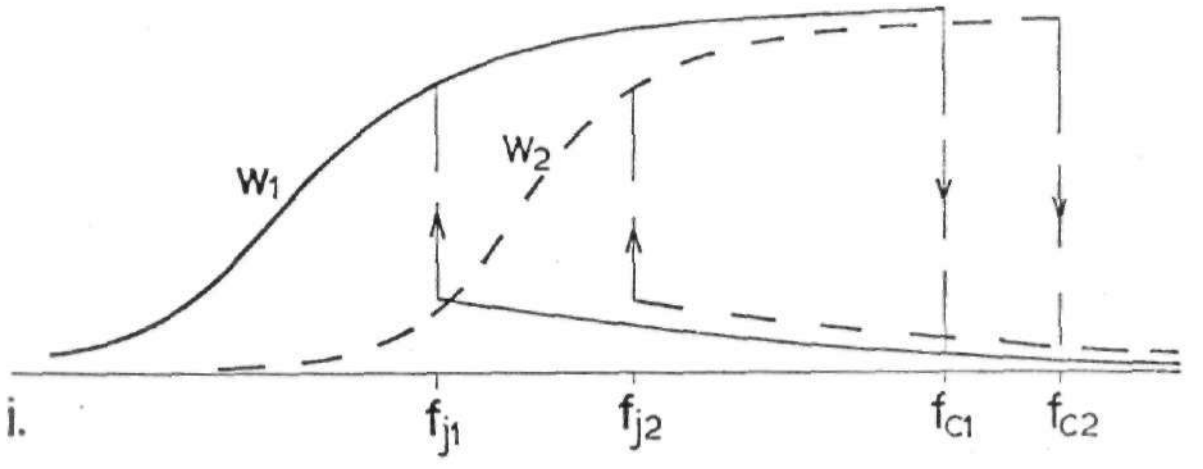
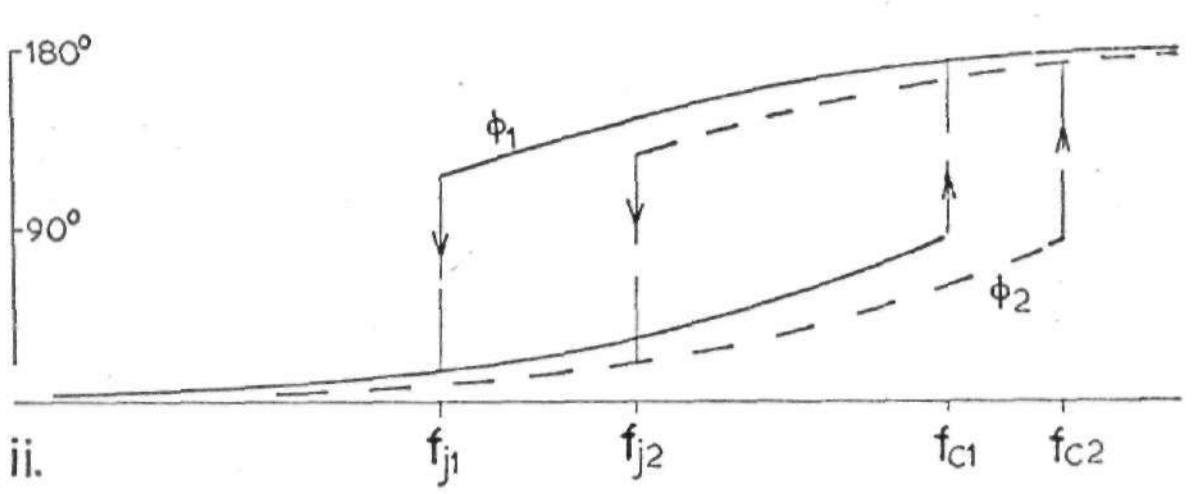


Fig. 7. Vibration response curves in disc with frequency separation, when a small force is applied: (i) mode amplitudes, (ii) phase angles, (iii) wave amplitudes.





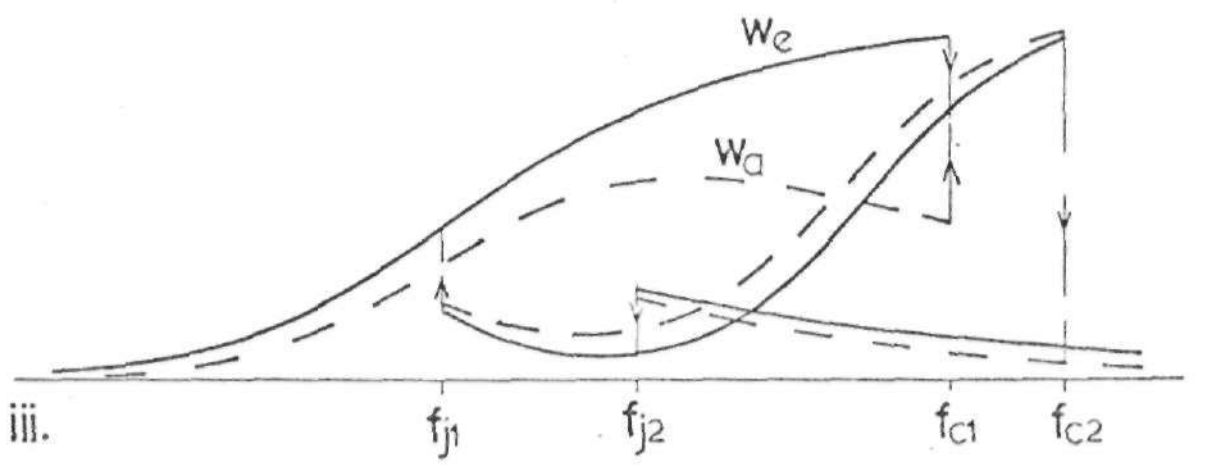


Fig. 9. Vibration response curves in disc with frequency separation, when a large force is applied: (i) mode amplitudes, (ii) phase angles, (iii) wave amplitudes.

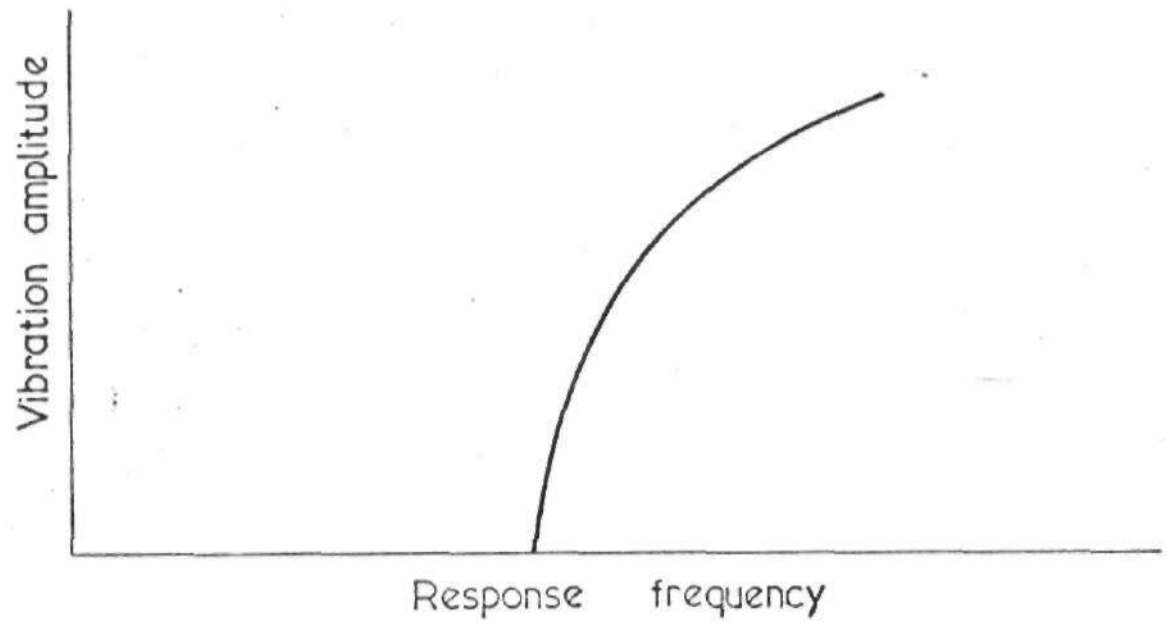


Fig. 10. Variation of response frequency with vibration amplitude.

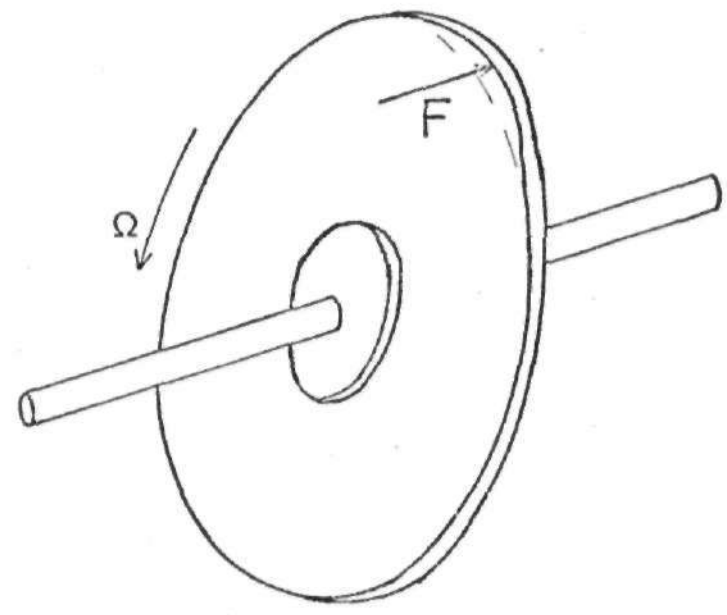


Fig. 13. Point-loading of disc rotating below its critical speed.

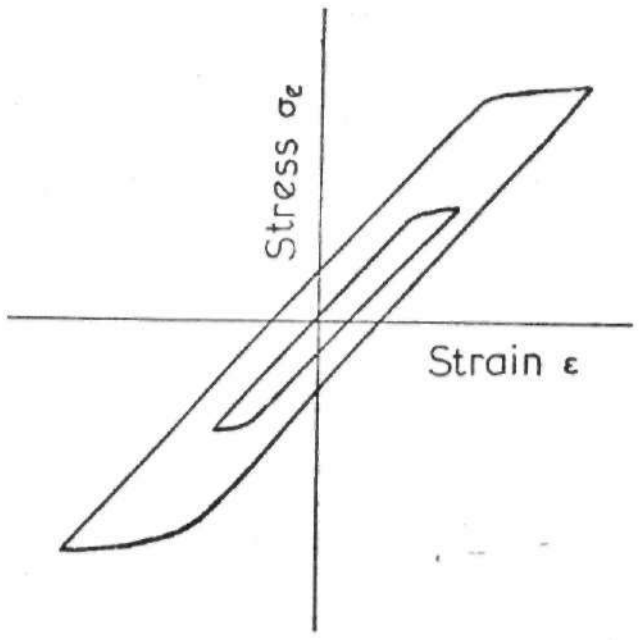


Fig. 11

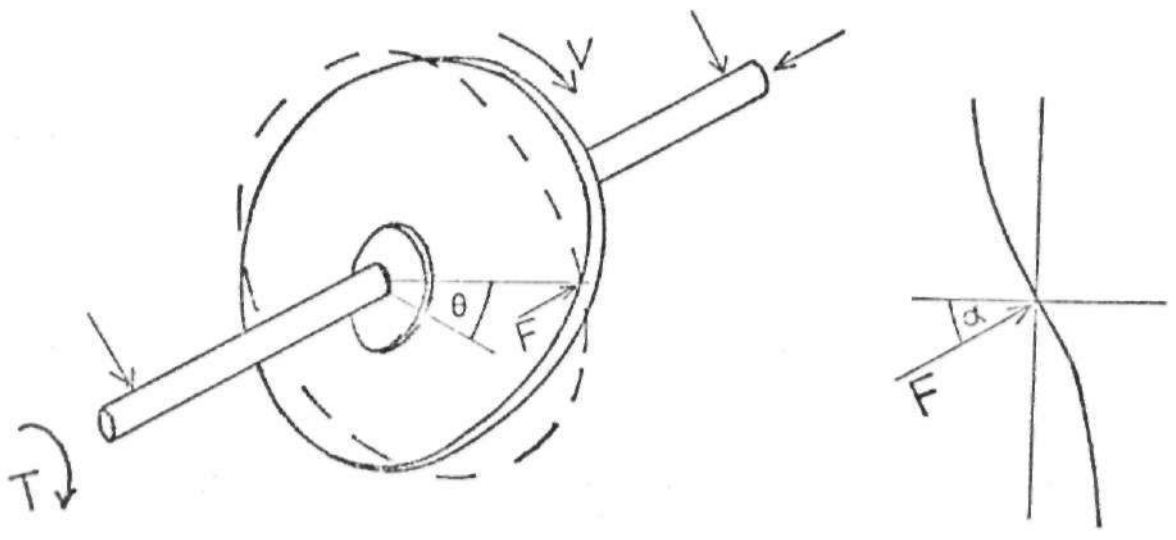


Fig. 12. Forces on disc system.